TECHNISCHE UNIVERSITÄT
MÜNCHEN
Graduate School of Information
Science in Health

Fakultät für Informatik - Lehrstuhl für Informatikanwendungen in der Medizin
Fakultät für Medizin - Nuklearmedizinische Klinik und Poliklinik

Doctoral Thesis

3D intraoperative functional imaging with navigated probes

Thomas Wendler Vidal, M.Sc.

September, 2010

TECHNISCHE UNIVERSITÄT MÜNCHEN

Graduate School of Information Science in Health

Fakultät für Informatik - Lehrstuhl für Informatikanwendungen in der Medizin

Fakultät für Medizin - Nuklearmedizinische Klinik und Poliklinik

3D intraoperative functional imaging with navigated probes

Thomas Wendler Vidal, M.Sc.

Vollständiger Abdruck der von der Fakultät für Informatik der Technischen Universität München zur Erlangung des akademischen Grades eines Doktors der Naturwissenschaften genehmigten Dissertation.

Vorsitzender:		Univ.-Prof. Dr. Klaus A. Kuhn
Prüfer der Dissertation:	1.	Univ.-Prof. Nassir Navab, Ph.D.
	2.	Univ.-Prof. Dr. Markus Schwaiger
	3.	apl. Prof. Dr. Sibylle I. Ziegler

Die Dissertation wurde am 9. September 2010 bei der Technischen Universität München eingereicht und durch die Fakultät für Informatik am 21. September 2010 angenommen.

Ich versichere, daß ich diese Doktorarbeit selbständig verfaßt und nur die angegebenen Quellen und Hilfsmittel verwendet habe.

München, den 5. September 2010 Thomas Wendler Vidal, M.Sc.

Acknowledgments

In the last 3 years I began a trip that started from the pure joy of testing new things (and being sometimes even successful) and ended up shaping most probably the next years of my life and the life of many others around me. Of course, it was not all my fault. I have the clean conscience of not having forced anyone to join us in a journey to a place any of us really knew, but I do carry the weight of pushing people in directions they probably would have never gone. On the way many dreams and plans were abandoned and far too many were doomed to remain an unfulfilled promise. I hope they do not come back to haunt us in future. In summary, I want to be honest and use not only this acknowledgment to say 'thanks', but say also 'I am sorry'... sorry for the time that was lost and the hopes that may not turn to be truth. I can only promise from the deepest of my soul that I will do all what is in my power to lead the ship to a safe and happy port in the years to come.

I want to start with those who suffered probably the most. My family... they had to carry the burden of my absence and my frustrations. It is to them I come when I lose faith; it is them that get the bitter moments, when my humanity gets hold of myself. My little sister I want to thank the uncountable calls to remind me that we are not alone. I want to thank her faith and trust in whatever I do and the honest criticisms when my ego got too far away. If she had not been there I could have not made it the last years and I am sure I will not make it far without her in the future. Our mother I have to thank her constant worries about us reaching happiness. There is no single conversation where she has not tried to remind us that at the end of the day no matter what we do, what matters is to find a little corner where to feel at home and that the only way of getting there is putting not only the others before all, but ourselves too. I do not know anyone who looks so far away in future and at the same sees so deep what is necessary to get there. I am sorry for not listening, I am sorry for not explaining what is behind my crazy acts early enough and

keep the suspense often too long. My father I want to thank the immense trust and hope in me. He is following every single step and enjoying them as if they were his. His optimistic view and his questions made me see with other eyes the track behind. I love you all.

The next two persons who I cannot but thank are Joerg Traub and Tobi Lasser. If there is anything good coming out of the trip, they are responsible of a huge part of it. Joerg I had stolen so many years of life with my inconsistencies and my rebel soul that I will never be able to compensate them. Despite this he has taken the dirty work of generating a basis to build a high building out of my crazy dreams. He has bet on them and although I am sure his investment will be greatly compensated in life. I will go far not to disappoint you, my partner. For Tobi, the story is not too different. If I had made many things possible it was because I have been standing on his shoulders. I have made him take infinite responsibilities, correct thousands of pages and (at the beginning) even make my lousy attempts to programming run (and run fast...). I hope we find a common future to give you back the hand of keeping me (like Joerg) from flying away from Earth and getting lost in the jungle of my dreams. Also you, my friends, thanks a lot.

I want to thank as next my three supervisors, because besides Nassir and Sibylle, I consider also Andreas Buck among the ones that gave shape to this thesis. Nassir I have to thank his blind trust in us. He has opened doors that have let us far and has surprised us once and once again with his impressive eloquence and brightness. Sibylle I have to also thank her trust and wise advice in any moment we needed. If have learned the power of experience and rationality it has been from her. Andreas on the other hand has been my inspirer, there is nothing impossible for him (or almost never). Yet Andreas has taught me that the only way to success is explaining things carefully and simply. All of you I thank your time, patience and guidance throughout excellent years and I hope many more to come.

Nassir always told us, that success in medical technology could only turn truth if it was coming from the hospital itself. I took that advice seriously and essentially never left the Klinikum rechts der Isar till now. On that long time I managed to convince people to believe in the vision of tomorrow's surgery and ended up making them responsible on making it come true... Ken is among them. His incredible karma and sense of efficiency have pushed us towards reality. I really admire his sharp eyes and strong views, I thank him

for being hard when needed and hope not less from him in the road to go. Dr. Andreas Schnelzer I thank him is faith and bravery of willing to be the first to allow our "'TESA Film"' prototypes in the OR. I appreciate also his strong back-up through good and bad times in the path. Marc Martignoni I would like to thank his perseverance in following the innovation in surgery and his patience with this extremely bad planner of me, who still believes the most complicated things can be solved over a weekend. In this part, I want to mention also Dr. Stefan Paepke who tempted me to make a system that would revolutionize surgery, but also who has been extremely honest with constructive criticism. Finally I cannot leave out of this paragraphs the team of Marc and Dr. Schnelzer/Paepke, Alexandra Ehlerding and Jakob Saeckl in particular. They have been the ones taking the hammers and putting the house together from the medical side. Them and the numerous surgeons and gynecologists of my beloved Klinikum that have participated in our research, I thank very much.

Our friends and collaborators in the Policlinico S. Orsola-Malpighi deserve also many thanks here. Ivan Santi and Lorenzo Fantini were the first physicians to take our device in the hand and use them on patients, more patients and every single day more patients. They have been our best source of feedback and have gone so far, that we consider them the first experts in our technologies. Ivan and Lorenzo, as well as the great Stefano Fanti and his team have shown us that doing successful science with friends is possible.

Physicians do not hold however the health systems alone, technicians carry a huge weight. In particular in the last 3 years, I myself have relied on them immensely. I cannot but thank the huge amount of extra hours, patience and good will of Alexandra Bartel in particular, but the complete team under Jutta Graehneis and now Helga Fernolendt... Thanks Alex, Jutta, Helga, Martin Finke, Johanna Häusler... Thank you very much. I hope I can compensate this in future and share with you the fruits hopefully to come.

On the side of technology, little would have been possible with the support of people like Martina Hilla. I cannot remember how many problems you solved for us. José Gardiazabal, my old friend from the UTFSM, was also a constant support and a source of brilliant ideas. I look really forward to join forces in future. Coskun Özgür, my wise companion, as well as, Alexander Hartl, my first student, I thank them their patience, their good mood (I still cannot figure out how they manage to smile always) and wish them all

best wearing my shoes while answering all the open questions I left on the science side. A special thanks also to the amazing Oliver Kutter and Tobias Reichl... Both of you guys, I find simply incredible, as people and scientists.

In the field of industry, I want to thank to Eric Söhngen, the great Eric, he was born for success. I learned a lot from you, old partner. I really look forward to crossing ways in future. Also Ivan Billy taught us so much... I never thought that faith and business could find a place in the same person... admirable, my friend.

At last, but not least, I have to thank all the people that did the real work. Those were my students and co-workers at SurgicEye... Jakub 'Kuba' Bieniarz, Mei-Chuan Chen, Philipp Dressel, Alexandru Duliu, Irène Faure de Pebeyre, Xinxing Feng, Moritz Hoyer, Risto Kojchev, Philipp Matthies, Rebekka Mayr, Asli Okur, Saffiullah Qazi, Asad Safi, Katarzyna 'Kasia' Szajkowska, David Weisgerber, Stefan Wiesner, Xin Xu, Dominik Zäuner, Berenika Zaraska and so many more... I am so sorry for making you wait... I believe it is too late to say it once more, but I owe you far more than you believe. Most of you turned into more than co-workers and students, you turned into people I trust and friends.

For all it remains, to those I forgot in this acknowledgment, but were related... I am sorry for all sorrows I may have caused and I thank you.

Abstract

Innovations in surgery require clear benefits for patients, surgeons and the health care system, as well as perseverance for the scientists and engineers designing and developing such systems. Interest has increased lately to carry on innovations in the field of surgical oncology. One such case is the diagnostic or therapeutic excision of structures like lymph nodes and tumors. These structures have been made visible with the lately introduced pre-operative functional imaging systems in combination with highly specific tracers. However, locating such structures precisely and confirming their complete resection at the time of surgery is impossible due to the lack of proper tools. There is thus a clear potential for innovative solutions with high clinical impact.

In this work, we analyze the needs of intraoperative functional imaging in oncologic surgery. The state-of-the-art is reviewed and a solution based on navigated functional probes is proposed. The essence of the solution is the use of functional probes, from which data is read-out synchronously with its spatial position and orientation. Tailored physical models within a tomographic reconstruction frame are proposed in order to generate 3D images from the acquired data set. Such 3D images would allow to localize marked structures precisely and would also guarantee a complete resection in the operating room.

In order to evaluate this solution, one instance of it is implemented for the particular case of 3D nuclear imaging. In this case, a gamma probe (functional probe) is tracked by an optical tracking system (spatial positioning system), while acquiring synchronously its count rate (read-out). A model of gamma ray dispersion in matter and detection of radiation with that specific gamma probe (physical model) is created. The model is then adapted for its use within an iterative reconstruction framework based on emission tomography algorithms.

In a first phase, the software and hardware implementation is tested on phantoms. Later it is further evaluated in preoperative and intra-operative setup with breast cancer and melanoma patients undergoing sentinel lymph node biopsy. Results show the feasibility of the imaging approach in over 200 patients and a successful introduction in the operative setup in a first cohort of 50 patients. This promising data and the expected advantages for patient, surgeon and health care system speak of an approach that can make it up to the real application. Such application could turn this approach into a potential new tool in surgical oncology and, if followed through perseverance of the research and development team, into an innovation. In summary, this thesis presents the fundamentals of a novel intra-operative navigated functional imaging, its proof of concept, its first clinical deployment and its initial promising outcome.

Zusammenfassung

Die Einführung von präoperativen funktionellen Bildgebungssystemen und hoch spezifischen Tracern hat die Darstellung von millimetrischen Tumoren und Lymphknoten ermöglicht. Dennoch bleiben ihre präzise Lokalisation und die Kontrolle ihrer vollständigen Exzision im Operationssaal aufgrund mangelnder Werkzeuge ausgeschlossen. In dieser Arbeit wird eine neue Strategie zur Bildgebung im OP entwickelt und erprobt, welche auf der synchronen Aufnahme von Messungen von handgeführten funktionellen Sonden und ihrer Position basiert. Massgeschneiderte physikalische Modelle und Filter werden vorgeschlagen, um aus diesen winkelbeschränkten, dünnen und irregulär abgetasteten Datensätzen tomographische Bilder zu rekonstruieren. Eine Instanz dieser Lösung mit Gammasonden wird auch in Hardware und Software implementiert und präoperative sowie intraoperativ bei über 200 Patienten erprobt und in mehreren Iterationen verbessert. Diese Arbeit führt somit einen neuen Ansatz für intraoperative Bildgebung ein, welcher anhand der Daten bei der Instanz von 'Freihand Einzelphotonemissionscomputertomographie' (engl. freehand SPECT) viel versprechende Ergebnisse nachweist.

Contents

Introduction

In 1977 Cabañas [55] proposed a new concept in order to determine the regional invasion of lymph nodes in patients with penile cancer. The idea was to determine which lymph nodes were the first nodes in the drainage of the tumor, extract them and analyze if metastasic infiltration could be found. If the assumption that metastases spread first over the lymphatic system was true[1], this would give a precise staging on the regional nodal involvement thus sparing a radical lymphadenectomy, the standard procedure by that time.

In order to locate these first nodes - which would later receive the name of 'sentinel' lymph nodes - he suggested the use of a technique proposed by Cramer and Karpati [74] in the fifties, the so-called lymphography or lymphoangiography. That technique provided radiographic images where the lymphatic vessels were made visible using X-ray contrast media. The contrast medium was injected in a certain region and flowed from the injection site into the first lymph nodes draining this region. Thus, Cabañas idea was to make a radiogram some time after injection of the contrast medium in the tumor region. This would allow to visualize the sentinel nodes as opaque structures in the X-ray images (figure 0.1).

It was almost 20 years later that the concept of Cabañas made it into the guidelines of malignant melanoma [215] and breast cancer [73]. The idea was essentially the same, but many things had changed:

First, the clinical indication was a different one. The reason for this was mostly that the clinical relevance of the nodal staging in melanoma and breast cancer had a bigger

[1]This assumption takes for granted, that no lymph node can be skipped in the spread.

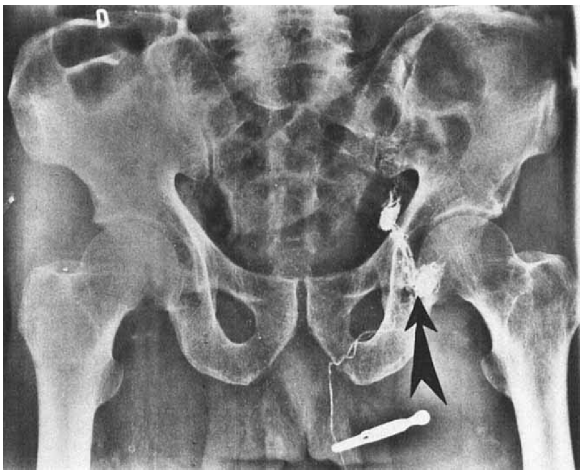

Figure 0.1.: Injection of contrast material in lymphangiogram via dorsal lymphatics of the penis. Arrow indicates SLN. Image taken from [55] and reproduced with authorisation of John Wiley & Sons, Inc.

impact than in penile cancer. Also the difference in the incidence of the diseases played a significant role.

Second, instead of using lymphography the guidelines incorporated the use of lymphoscintigraphy, where instead of an X-ray contrast medium, a radioactive tracer was used.

Third, the surgeon had now the aid of an intra-operative radiation detector capable of detecting the previously injected radioactive tracer and thus allowing a precise localization and the assessment of the resection in the operating room (OR).

Today's medicine speaks of the 'sentinel' concept for melanoma and breast cancer as a success story for the process of bringing innovation into surgery. It took years of clinical studies and optimization for the concept to make it through (for a graphical illustration see figure 0.2). Nevertheless, it brought with it its own technology and tracers, and further its related procedure became a standard of care and it resulted into an important quality criterium for surgical centers in industrialized countries (e.g. in Germany [134, 176], Austria [276, 277], the UK [235, 281], the USA [57, 69, 196], Australia [328, 371], etc.). In other words, the brilliant invention of Cabañas and the effort of the first supporters of that technique became an innovation and changed the standard of treatment in several cancer

types.

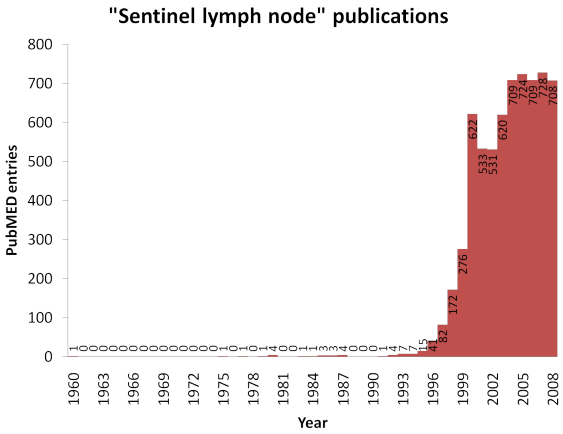

Figure 0.2.: Entries of PubMed for keyword "'sentinel lymph node"' plotted from the oldest in 1960, when the concept was first proposed by Gould et al. in the parotid gland [120], until 2008. The amazing slope in the last years and the immense and stable amounts of publications per year speak for a successful technique.

The process was certainly not easy and shows how carrying out innovations in medicine and in particular in the surgical field requires a long breath and the goal of attacking real problems with clear clinical impact.

The need for perseverance has to do with the evidence-based character and the strong component of standardization of medicine. Switching from one surgical technique to a new one is not something that can be done in a matter of weeks or even months. One fundamental principle of medicine explains this: changes can only be made if it is guaranteed that the risks involved are at least equivalent to the risks of the state-of-the-art procedures. This principle results in the fact that the life of patients cannot be jeopardized and physicians consequently stick to that premise. This requirement has also to do with the fact, that surgery is highly standardized and rigid. Consequently a change will involve deriving the inertia of the so-called standard operating procedures (SOPs).

The necessity for a clear benefit for the patient, the surgeon and the health system is a driving force in innovation. It derives from the fact that at the bitter end, a technology, a technique, a product, ... is only successful if someone is willing to pay for it a fair price.

Thus, a surgical procedure makes only sense if the sum benefit minus investment is *very* positive. This again comes from the inertia of the health system: if the benefit is not big, the cost of changing will not be paid.

Innovations in the medical field carry thus always huge investments or extraordinary inventions, and commonly both. If meant to be successful a medical innovation has to start with a big need. In the sentinel story that was the need to stage the regional lymph nodes in a confident and minimal invasive way. The innovation has further to be based on a sustainable concept. For example, in the case of Cabañas' invention it is the idea of using as staging the status of the first lymph node in the drain of the tumor. Yet the innovation has to be solved with intelligent technology. In the story of sentinel this is the use of radioactive mark for preoperative imaging and intra-operative detection. And most important the innovation has to bring a huge benefit to all involved players. In the example, it is the immense reduction of complications and related costs brought by the sentinel lymph node biopsy.

In this work we describe the steps for shaping a medical innovation in the field of surgical oncology. Of course, it is way beyond the scope of this thesis to go all the way from the design of a technology to the establishment of a standard of care. We are not even sure if our assumptions are true. However the effort is worth the try. The cure for cancer is still not in sight and thus there is a lot of place for improvement in surgical oncology.

Part I.

Motivation, problem definition and state-of-the-art solutions

Chapter 1

Motivation for intra-operative functional imaging

Surgery has experienced radical changes in the last 20 years. This affirmation is particularly true in the field of surgical oncology. There the changes have been on one hand, in the direction of minimizing the impact of the surgical procedure and on the other, towards improving the localization of cancerous tissue and the definition of resection borders.

Minimally invasive surgery is a term that was forged in the nineties and many of its derived surgical procedures have become standards of care for several clinical indications. Its beginning was after the Great War with the availability of proper optics that enabled first endoscopy (e.g. [222, 329]) and then laparoscopy (e.g. [89, 141]). The goal behind it was to reduce the size of scars and allow surgery through natural orifices or several small incisions ('keyhole surgery', name popularized in 1993 [27, 63]). Reducing mortality rates, postoperative complications, hospital stays and costs was the ultimate goal and in several procedures, this goal was indeed reached with even a higher success than expected (e.g. in cholecystectomy [94, 98, 288], see also figure 1.1).

The inclusion of functional information in the recent years has also contributed to minimize the impact of surgery. A good example is the inclusion of fMRI (functional magnetic resonance imaging) for navigation in neurologic interventions (e.g. [201, 294]). In those procedures the complete surgery is guided using preoperative blood oxygenation level dependency (BOLD) MR images as basis for navigation. These images are acquired with

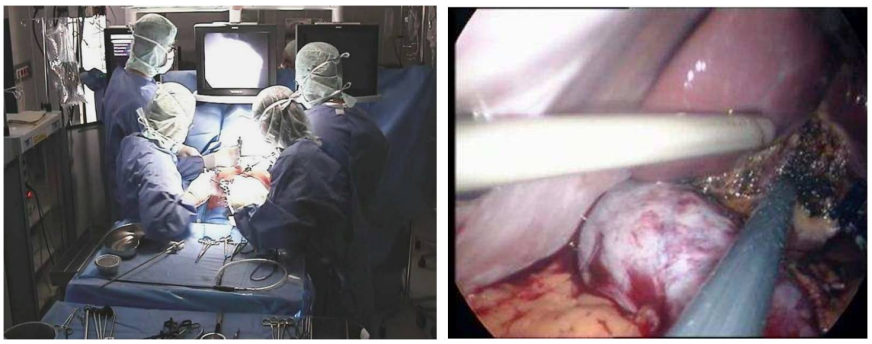

Figure 1.1.: Exemplary setup during laparoscopic surgery and image of laparoscope. Image courtesy of Dr. Nicolas Padoy, John Hopkins University, Baltimore, USA and reproduced with permision of the Association for the Advancement of Artificial Intelligence.

the patient being awake and under the real-time imaging of an MR machine. The patient is asked to perform tasks and the activation patterns of the brain are seen on the screens of the MR. The surgeon may thus proceed taking into account areas of activation and thus may avoid coming close to regions of relevance and is able to minimize morbidity. Groups like the team of Essen have begun exporting the experience into a setup where the imaging is made during the intervention in order to minimize potential misregistration and deformation errors [114] (see also figure 1.2).

Nowadays minimally invasive surgery has been developed further with the inclusion of robotic surgery in the guidelines for prostatectomy [342]. The use of the 'Da Vinci' system of Intuitive Surgical, Sunnyvale, California, USA (cleared for several pathologies by the FDA in April 2004) has allowed shortening postoperative stay (46.4% (n=60) [15]) and sick leave (77.6% (n=127) [139]), as well as reducing complications, like blood loss (75.4% (n=60) [15]), infections (88.9% (n=58) [58]), etc. See figure 1.3.

The second major trend in surgical oncology has been towards improving the localization of tumors and relevant lymph nodes, as well as, the better definition of resection borders. The motivation for these is first the reduction of morbidity by bringing resection to its minimum necessary. Secondly, the aim is to increase the rate of operable tumors and at the same time, reduce the rate of recurrence. Of course if tumors can be better localized and resection borders optimized, the resulting procedure will be minimally invasive and

Figure 1.2.: Left: Exemplary setup during intra-operative MRI system. Intra-operative MRI images a ROI of the brain of the patient on demand. Surgeon can also access the operation situs at the same time. Instruments and MRI scanner are also tracked by an external positioning system allowing navigation based on intra-operative images. Right: Images generated by MRI system before first incision and during operation in 2 exemplary patients. Images reproduced with permision of Medtronic Navigation, Louisville, Colorado, USA.

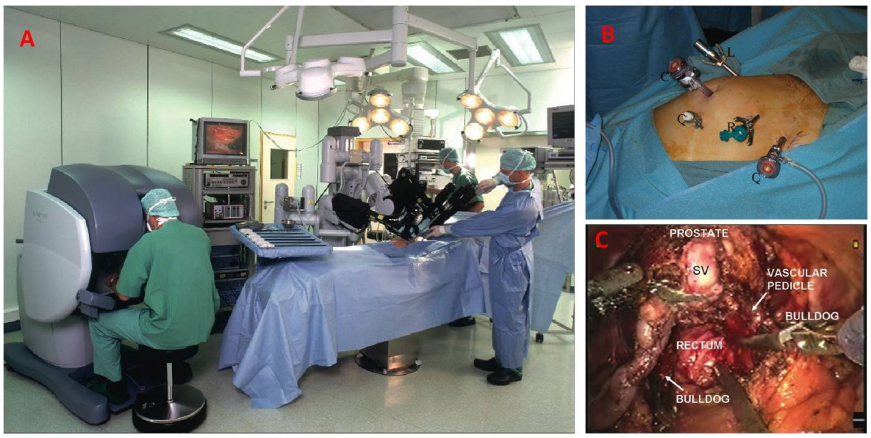

Figure 1.3.: (A) Exemplary setup during robotic prostatectomy. Laparoscopic instruments enter patient through trocars as shown in (B). Laparoscope allows generating images like (C). Images reproduced with permision of the Society of Laparoendoscopic Surgeons.

thus will speak for the previously discussed trend.

Here imaging is playing the most important role. Preoperative imaging modalities have developed in the direction of allowing more than anatomical imaging, but also functional imaging. Functional imaging is defined as generating images of a physiological function of a living being [351]. Classical examples are contrasted imaging modalities like nuclear medicine modalities [366], contrasted ultrasound (US) [111], contrasted X-rays [312] (see also 1.4), etc. Neverthess, slowly also non-contrasted imaging like MR spectroscopy (MRS) [206], elastography [67], etc. have been made commercially available.

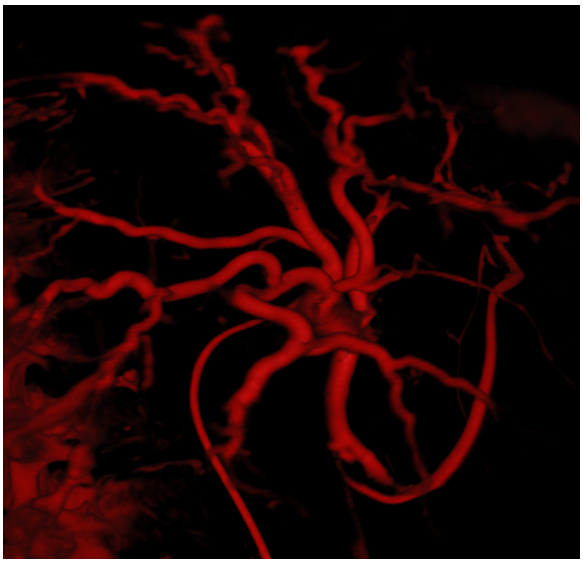

Figure 1.4.: X-ray contrasted image for blood vessels, commonly called X-ray angiography. Through image subtraction contrasted blood vessels become visible. In this particular example, blood vessel tree of liver is visualized in a 3D render mode. Image courtesy of Dr. Martin Groher, Chair for Computer-Aided Medical Procedures, TUM [121].

Essentially preoperative functional imaging allows determining targets for surgery. This can be specially interesting if functional imaging is combined with anatomical imaging ('hybrid imaging'). The best example here is PET/CT (positron emission tomography / x-ray computed tomography) which has replaced almost completely the separated use of PET and CT within less than a decade [80]. In PET/CT, PET contrast media like ^{18}F-FDG, ^{11}C-Choline or ^{68}Ga-DOTATOC enable to image the biodistribution of sugar, choline

and somatostatin receptors, respectively, with millimetric precision [369]. Moreover the functional data can be visualized within the context of the anatomical structures fused with the CT images (see figure 1.5). This information can be used for surgical planning regarding incision planning and definition of resection borders (e.g. in head-neck cancer [228], in melanoma [178], in ovarian cancer [187], etc.).

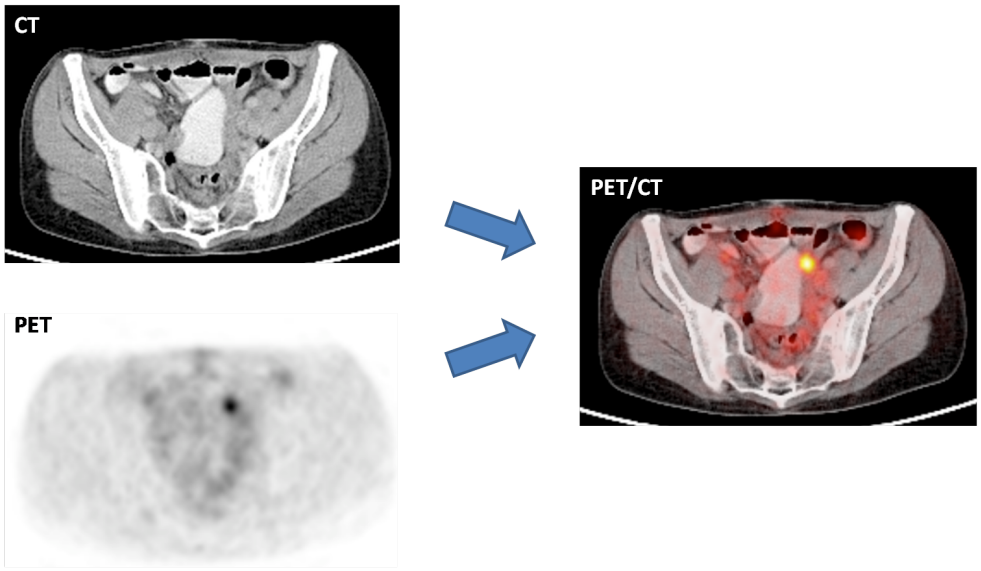

Figure 1.5.: ^{68}Ga-DOTATOC PET/CT image of patient with distant recurrence of neuroendocrine tumor. Local hot spot in the bowel speaks for an operable metastasis. Images were used here for surgical planning. Image courtesy of PD Dr. Andreas Buck, Nuclear Medicine Department, TUM.

There is nevertheless still a major problem when trying to translate preoperative plans in the operating rooms. The imaging data mentioned above is commonly available through the picture archiving and communication system (PACS) - a system that has turned into a standard worldwide (see figure 1.6). However, during the intervention itself these data loose their validity to a large extent, due to changes in anatomy that start with a different patient positioning and extend up to changes due to resection and mobilization of organs (e.g. in the abdomen [33], in the brain [131, 302], in the liver [200], etc.).

In order to account for these, in the field of orthopaedics and neurosurgery so called navigation systems have been proposed [256]. These systems are based on positioning

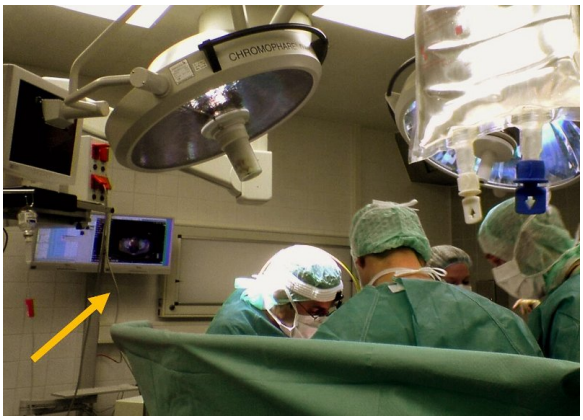

Figure 1.6.: Preoperative PET/CT available over PACS in the operating room during prostatectomy (arrow). Surgeons can always access the preoperative data, however, it is displayed far from the operating scene.

systems that allow determining the position and orientation of surgical instruments in relation to preoperative imaging data. In this way the relative position of the instruments can be displayed and the surgeon can use it for 'navigating' them to the desired position in the anatomy. Navigation systems will be discussed in detail in chapter 5.

In the particular case of surgical oncology this solution is widely used in neurosurgery [100, 156] and to some extent for operable bone cancer (e.g. [374]). They enable precise resection and also optimization of resection borders. The use of these systems has been also proposed for other cancer types in soft tissue (e.g. in lung [180]). However, the problem still remains in how to compensate for deformation and changes in anatomy due to preparation and resection of structures.

An approach that has tried to compensate for this is the use of intra-operative imaging. Intra-operative imaging can in principle exploit all advantages of preoperative imaging and further allow its use during the surgical procedure in order to update plans and verify results after each single step, if necessary (see example in figure 1.7).

The carrying horse of intra-operative imaging for oncologic surgery is intra-operative ultrasound (IOUS, see figure 1.8). IOUS was introduced in 1980 simultaneously by Lane for pancreatic surgery [181] and by Rubin et al. for brain surgery [284]. Its current field of applications has extended widely to anatomies like testicles [20], brain [167], liver [48], etc.

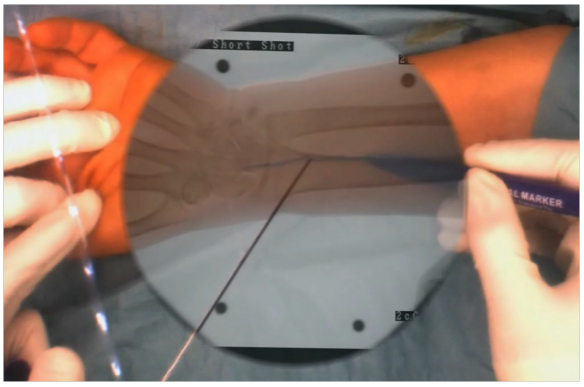

Figure 1.7.: intra-operative combined optical fluoroscopy shot. Surgeon visualizes intra-operative X-ray overlaid on video image in order to place incision correctly. Image courtesy of Lejing Wang, Chair for Computer-Aided Medical Procedures, TUM.

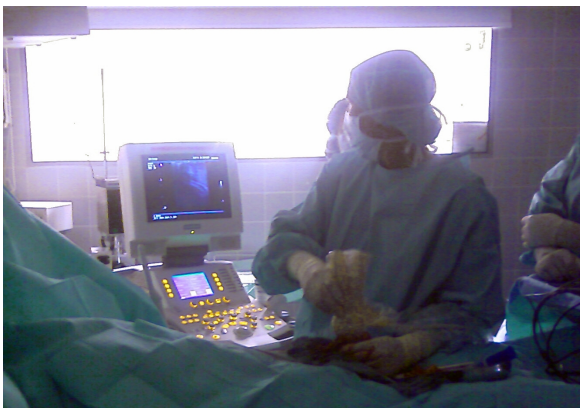

Figure 1.8.: IOUS machine while acquiring image during testicle cancer resection. Physician evaluates dignity of a lesion intra-operatively through analysis of vascularity with Doppler US. The intra-operative information minimizes the risk of misinterpretation or mispositioning of the lesion in the operating situs.

The major lack in IOUS is the missing functional information in most tumor entities. The logical next in order to solve this is bringing functional imaging systems into the OR. Intra-operative functional imagers are however far from being available. Only in particular applications functional systems have made it into the market, being however still far from becoming standards of care. A detailed review on such technologies is chapter 3.

In the end the major issue of surgical oncology can be extracted from the ongoing trends. As stated by Umberto Veronesi, head of the European Institute of Oncology in Milan, Italy and one of the world's most famous oncologic surgeons, during his inaugural talk at the Annual Meeting of the Italian Society of Surgical Oncology (SICO) in June this year [348]: 'the surgical oncologist of today has the responsibility to do as little as needed and at the same time as much as necessary'. Intra-operative functional imaging is one of the tools that are helping in this direction.

Chapter 2

Problem Definition

Shawn Frayne, the president of Humdinger Wind Energy LLC, is only 30 years old. He managed to invent a way of generating energy from wind without the need of any rotating means. In practical words, he extended the domain where wind energy could be useful down to very low power consumption applications and further made it almost independent of maintenance [104]. His invention is most likely to turn into an innovation as it attacks a huge need with a simple solution. It is also in the same line of approaches like the screen technology of the 'one laptop per child' program [146], the engine technology of the Tata Nano (which first unit was delivered on June 17th, 2009) [254], etc. They all have something in common. As said by Frayne during one of his talks in 2007, when you give yourself the most difficult constraints, the resulting solutions are highly likely to become revolutionary inventions [103].

The border conditions applied to intraoperative functional imaging are definitely of this type. It is not by chance that functional imaging technologies have not made it to real applications yet. Constraints for intraoperative imaging are complex and varied as they arise from different sources. Depending on the weighting a possible separation of these sources can be:

1. Functional and workflow constraints: Intrinsic of the procedure, they pose the concrete needs of any improvement to be proposed. They include the protocol of the procedure that is performed, as surgeries follow structured lists of steps and changes in them have to be minimized and well justified, even in case they provide advan-

tages.

2. Regulatory or safety constraints: Regulations of governmental bodies target in general to guarantee the safety of the patient and the medical personnel.

3. Economic constraints: Finally, any improvement has to result in costs that are at most as high as the ones of the standard procedure.

In the following all groups of constraints are discussed for the case of functional imaging in the OR.

2.1. Functional and workflow constraints

Lately John N. Aarsvold, professor at Emory University in Atlanta, Georgia, USA, held a talk about imaging in radio-guided surgery entitled 'Anyone can find a hot node' [12]. In this talk he tried to summarize functional and workflow constraints on this type of imaging. These constraints however apply to the more general case of functional imaging in the OR. He extracted different constraints or boundary to be considered:

1. Context: Depending on the disease to be treated different assumptions are valid. For example, imaging cancerous lymph nodes in the pelvis in case of colon cancer is completely different of imaging lymph nodes in the axilla for breast cancer. The localization of the said structures, the access to them, the surrounding anatomy, their size, the required accuracy for the procedure, etc., they all matter and change dramatically the constraints.

2. Task: As stated in the previous chapter, there are many tasks to be aimed at when incorporating intraoperative imaging into the OR. The tasks can be e.g. in vivo localization of structures (like lymph nodes, metastasis, etc.), ex vivo localization of structures (as in the case of resection borders in radio-guided occult lesion localization), region surveillance (for adjuvant therapy, like radiotherapy of regions structures that could not be resected during surgery), post-excision confirmation (guaranteeing complete resection of all structures meant to be resected), etc.

3. Technology: The technology to be used also plays an important role. This starts with the question if a tracer/contrast media is to be applied, how and where it is applied, what are the characteristics, the dose, the volume, etc. It also incorporates the available detectors like the field of view of the detector, the positioning (how it can be positioned relative to the patient), the re-positioning (if the detector is moved, the precision needed to reposition it), its sensitivity, energy and spatial resolution, etc.

4. Protocol: A procedure done in one institution may be different from the same procedure in another. Guidelines for protocols are not mandatory and accordingly change even between physicians. For radio-guided surgery Aarsvold mentions as example the type of imaging depends on the time it is acquired, i.e. survey imaging, pre-incision/post-excision imaging, time-course imaging, adjunct imaging, etc. Logistics and space play also a relevant role here. The size of the devices and the environment change dramatically depending on the available place, the temperature and lighting conditions, etc.

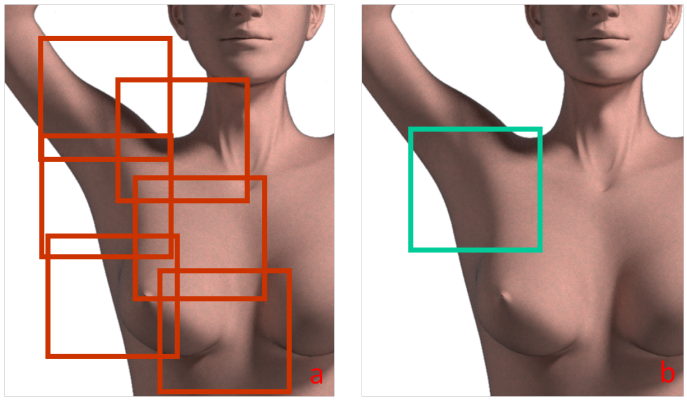

Figure 2.1.: (a) 'Survey imaging' in the case of lymphatic mapping in breast cancer. (b) 'Spot imaging' in the same clinical application. Definitions from [12].

The functional and workflow constraints or border conditions have to be instanced depending on the problem to be solved. Each problem has different constraints. In general a reasonable approach to create these instances is to start with a so called workflow analysis. A surgical workflow is an abstract representation of a SOP. Its grade of detail can be

arbitrary and depends on the steps to be modified and improved. For example in cancer resection a simple workflow could be:

1. Anesthesia
2. First incision
3. Preparation of situs
4. Tumor resection
5. Reconstruction of area of resection
6. Waiting of results of frozen section
7. On cancerous borders, extension of resection in proper direction
8. Sewing

Each step has to be then evaluated in terms of time required. An exemplary result of such time analysis can be seen in figure 2.2.

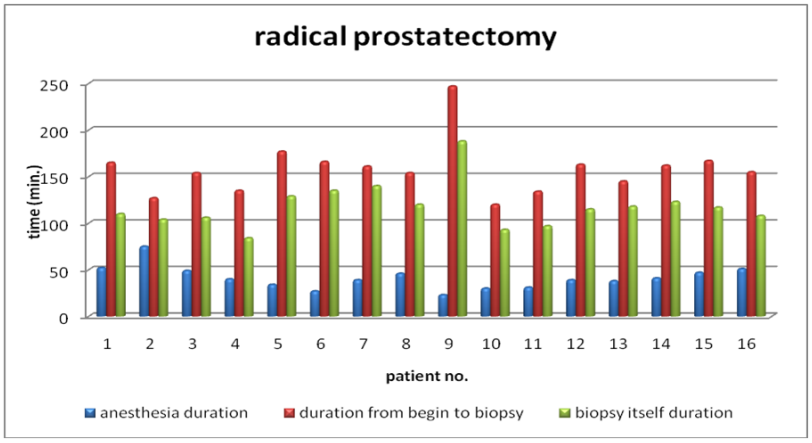

Figure 2.2.: Example of analysis of times for different steps (only relevants for this particular study) of over 16 patients. Stable values for durations of the three steps analyzed show degree of standardization in the procedure. In patient 9, complications and the presence of a novice surgeon resulted in a considerably longer procedure. Graphic taken from [375] by courtesy of Xin Xu, Nuclear Medicine Department, Klinikum rechts der Isar (TUM).

Of course, the problem of defining workflows and times is the fact that in all operations several users are involved. Further the involvement of these multiple users in each step is different according to the task to be solved. In order to model this in a simple way to proceed is to define concrete users with different levels of knowledge and goals with

respect to the system. The definition of users and goals is commonly the first step in the development of new systems according to models like the Capability Maturity Model Integration (CMMI). In the OR commonly at least three users are present: the surgeon, the anaesthesiologist and the circulator. If the procedure is more complex an OR nurse working in the sterile area or further surgeons may assist the procedure. Finally cleaning personnel has to be considered too, as a big part of the preparation of each surgery, as well as the deinstallation of the OR setup is perfomed by them.

Space plays also a very important role in the definition of functional constraints. The patient positioning, the space available around the area, the areas with different levels of steriliy, the available hardware, etc, they all lead to boundary conditions that have to be considered (see figure 2.3). Here interference with other devices and actions taking place during the workflow has to be evaluated.

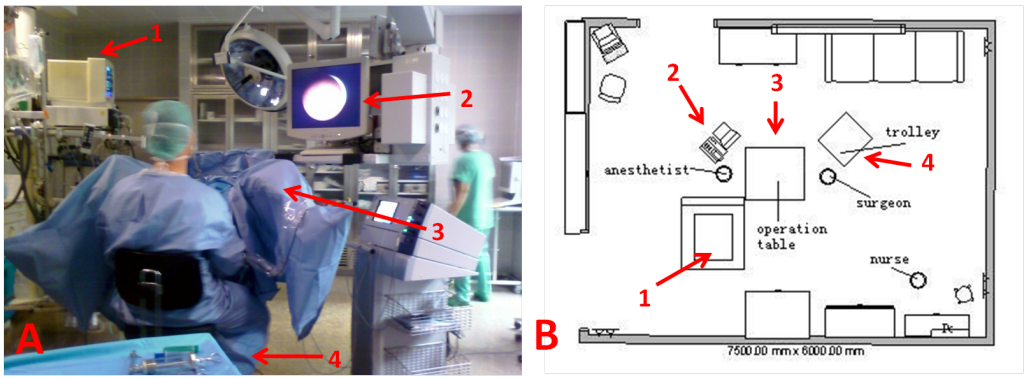

Figure 2.3.: Example of analysis of place in the OR in the particular case of a TUR-B operation (refer also to chapter 3). Surgeon operates only assisted by an anesthesist and a circulator nurse. In (A) a picture during the operation is shown while (B) presents the model defined. (1) is the anesthesy tower, (2) is the endoscope tower, (3) the operating table and (4) the troley with the sterile instrumentation, the surgeon can access any time he/she needs. Images taken from [375] with courtesy of Xin Xu, Nuclear Medicine, TUM

From the latter steps (analysis according to Prof. Aarsvold, workflow analysis, definition of users and goals, as well as definition of space constraints) functional requirements are extracted. Each of them can be stated in terms of a 'wish' or demand and treated almost

independently in the development. An example list can be seen in section 6.

Within the scope of this work, the instance selected to validate the assumptions of the thesis will be a Nuclear Medicine system for 3D intraoperative imaging in the particular context of SLNB in breast cancer and melanoma. This instantiation is meant to validate and concretize the approach for designing 3D functional imaging systems proposed within this thesis. Functional and workflow requirements are very general in nature for this instance. Accordingly its extension to further applications and technologies seems feasible and relatively straight forward.

2.2. Regulatory or safety constraints

Beyond functional and workflow constraints, a major role is played by regulatory and safety constraints. This aspect has increased in importance in the last years due to the trend of guaranteeing quality also in medical procedures. Essentially, the major objective is to make sure that during the complete process of development of medical devices the safety of the patient, the medical personnel and the service personnel is considered. It further includes the considerations made for the traceability of problems in case safety issues are made evident when using the device or from new information available from science or the use of other medical devices. In this way a continuous flow of information on safety can be established and, in case of necessity, measures can be taken to prevent potential dangers from becoming a harm. Of course, this is valid during the complete life cycle of the medical device.

Rather than a recommendation, this quality assurance frame around a medical device is imposed by law in most countries. For example in Germany, the 'Medizinproduktegesetz' (MPG) [8] and the related regulations (like the 'Medizinprodukte-Betreiberverordnung (MPBetreibV)' [9]) stipulate all required documentation and processes inside a medical device manufacturing company, as well as, its providers and the service and maintenance instances related to it.

Although this turns out in country specific laws and ordinances, most countries have adopted harmonized standards as basis of their regulations. The conformity assumption plays here a central role. It states that if a manufacturer is compliant with the relevant har-

monized standards, it is also compliant (in most aspects) with the legal regulations. This implies for a company willing to design a system that can be used in several countries, that the constraints required have to be according to all applicable standards in the target countries. The conformity assumption does not force the manufacturer to follow the standard, but makes the validation easier, as otherwise all aspects of the particular national law have to be proved separately on their own.

In the particular case of Europe, the European Union has defined a directive called the Medical Device Directive (MDD), also known as 93/42EEG directive [7]. This directive has been essentially adopted in every European country and is also sufficient for bringing a medical device into market in several other countries with non or only minor modifications, as it is the case of the Canadian Medical Device Regulation (CDMR).

For the USA similar regulations apply, playing there the most important role the regulations of the Federal Drug Administration (FDA), in particular the Code of Federal Regulations Title 21 (21 CFR) [6], specially in the parts 800 to 900.

In practical terms beyond the administrative and procedural instances around the system, for electrical systems (which is the case in almost all functional imaging devices), a list of so called 'essential requirements' have to be fulfilled. Such requirements are stipulated in the 60601-1 standard (Medical Electrical Equipment - Part 1: General Requirements for Safety) in its different national flavors and iterations (IEC 60601-1, EN 60601-1, etc.). The version of the standard to be used depends consequently on the legal recommendation. For Europe the valid standard is the EN 60601-1 of 2006 [10].

In order to see an analysis of the essential requirements for medical electrical devices in the particular case of functional imaging refer to chapter 11.

For the sake of this work, the risks considered will be the ones of a system based on nuclear medicine principles for imaging aid in SLNB of breast cancer and melanoma patients (selected instance for validation of the approach as mentioned above). Most of the constraints described above apply, making it a good example within functional imaging systems.

2.3. Economic constraints

The final set of constraints comes from the economic side. These constraints are directly related to the price: if the customer (here the hospital) is willing to pay the most a certain amount of money, the design of the system has to be such, that the costs are below that amount.

From the point of view of price, several values are necessary to be considered: the investment, the running costs, the service costs and the maintenance. The first is the one time payment a hospital has to do in order to get the system installed. Normally this price includes the first training session and calibration of the system. The running costs are the operational costs of having the system running. Disposables per use, electricity, supplies, etc. are considered therein. Service and maintenance on the other hand are normally separated from the running costs, although their frequency is not really independent of the use.

Soft values play however also a role in pricing. If a procedure is slightly more expensive, but brings additional values that cannot be quantified easily there is still a chance of getting it through. Evidently the most important of such soft arguments are the non-quantifiable (or hard to quantify) benefits to the patient: comfort, aesthetics, time burden, etc.

For imaging and in particular functional imaging, economic constraints can be complicared. Imaging is essentially a diagnostic tool. Diagnostics in contrast to therapy does not treat, accordingly the only way it will bring an economic benefit is that it makes the treatment better. Better can be faster, cheaper, easier, safer. What 'better' exactly means, is dependent on the application and the costs involved in the current procedures which will be modified or enabled due to the use of the said imaging.

The first step in any economic analysis is to understand the cost structure of the state-of-art procedure. For example in Germany most procedures are reimbursed within the standard packages for treatment of a particular indication. Indications on their own are classified according to standardized codes, commonly known as international classification of disease codes or short ICG. Such packages are contained within a so called diagnosis related group (DRG) (see for example German regulation in [5]). The amount of money within a DRG has to cover for the complete procedure including drugs, personnel,

hospitalization, etc.

In order to give some place for innovation, new procedures can receive a higher reimbursement. Such tools are available for example in Germany and are known as 'neue Untersuchungs- und Behandlungsmethoden' (in English: new examination and treatment method, NUB). In order to be able to get that said reimbursement the hospital planning to apply the new method has to apply for them showing clinical trial data supporting the clinical avantages of the method in comparison with the standard of care. The amount of patients has to be also fixed.

From side of investment, the health system often counts on funds for renewing facilities or implanting new procedures with proven patient and cost improvement. Such funds are however not available at any time and may vary depending on the planification of the hospital. Potential money from research projects and extraordinary substitution of devices due to failures may be also be available, but is not the standard case.

Given the information above, an estimation of investment and running costs may be done. Here in the case of the development of new machinery the advantages are not known and have to be estimated. The final calculation is then simple, as shown in figure 2.4.

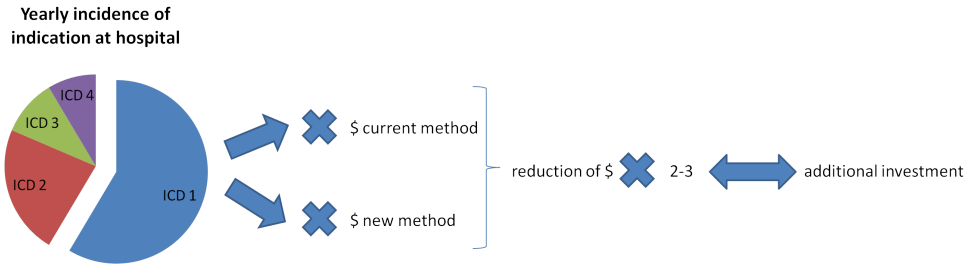

Figure 2.4.: Calculation of budget for investment and running costs for new device. The cost ($) reduction with a new procedure typically has to cover the additional investment due to the new technology in a horizon of less than three years (additional investment understood as difference between planned investment on current technology, like replacements, maintenance, etc. and the investment and maintenance cost of the new device).

Such a calculation does not have to be trivial and may include different indications and the information previously discussed on DRGs, NUBs and planned investment costs. The resulting values for running costs and investment may at the end be put in a plausible frame and thus avoid developing technology that may well solve the problem, but that would not be bearable in the routine.

2.4. Summary

In the last sections different constraints were analysed for the particular case of functional imaging. Examples were also given in the particular case of lymphatic mapping in the OR for breast cancer. The degree of complexity included is minimal and can be extended ad nauseam. However, this brief overview shows the difficulty of the contraints that burden the development of new medical technology and correspondent medical techniques.

In the case of functional imaging, any breakthrough has to start from such an analysis of boundary conditions in order not to remain on the road. In that sense and following Shawn Frayne's view, the only way of finding a revolutionary solution for a problem is giving oneself hard constraints and standing a little aside from conventional assumptions.

Chapter 3

State-of-the-art

Intraoperative imaging in the OR has been a keyword in the innovative circles of surgery over the last decades. Several systems are commercially available and have made it to become standards of care in particular applications. Even some functional imaging devices have made the step into the operating room.

In order to review the different systems, it is best to divide them according to application rather than modality. This segmentation has the advantage of making evident competing and complementary technologies.

Essentially there are three major areas, in which intraoperative imaging has been used for imaging functions: lymphatic mapping, blood vessel mapping and tumor localization / tumor bed control.

3.1. Intraoperative imaging systems for lymphatic mapping

Imaging of lymphatic vessels is the field that has brought functional imaging in the OR the farthest. The need for this comes mainly from oncology and in particular the sentinel lymph strategy: to determine the lymph nodes in the drain of a tumor. There are however other techniques that require it, like the lately introduced surgical technique of axillary reverse mapping (ARM) [45].

In order to accomplish lymphatic mapping several technologies have offered solutions with advantages and disadvantages. Essentially in all of them the modus operandi consists

of injecting a tracer (of whatever nature it may be) either in the anatomic structure of interest and/or in proximity to it and letting it be transported by the lymphatic system. Monitored by an imaging modality the tracer can then be found in the lymph nodes of interest. In almost all approaches the tracer is chosen to be a large particle size colloid or equivalent that is not transported by blood vessels, but can be transported by lymph vessels and ideally get stuck in the lymph nodes making them 'hot spots' of the utilized tracer.

Depending on the type of tracer used (for review of possibilities see [148]), different technologies can be used.

3.1.1. Radionuclide tracers

The most common type of tracer for lymphatic mapping is ^{99m}Tc bond to a colloid. Different commercial colloids are available like nanocoll ® [119], but also other agents like lymphoseek ® [354] have made it to the market with good imaging times (commonly imaging possible 5-120min after injection), low patient dose (<0.4mSv) and washout values (normally within 24h-36h). In all the cases the used radionuclide is ^{99m}Tc (half life 6.01h). Accordingly the devices meant to image it have to be systems that detect gamma radiation in the range of 140.51keV (^{99m}Tc's 89% of decays are gamma rays with such energy).

For non-imaging localization of such tracers, gamma probes have been developed [138] and up to 20 different companies produce them nowadays [13]. The market of gamma probes is estimated in over 20.000 devices and they are a standard tool in SLNB. Their specifications have been brought to their limits pushed by competition: with only 100-200g, acquisition times ranging from 0.1-1s they allow localization of structures as deep as 7cm with an accuracy that is essentially given by the distance to the radioactive structure (5-20mm in conventional cases).

The intra-operative use of gamma cameras was introduced in the pioneer work of Gitsch et al [117]. The idea of the Austrian group was to take a conventional gamma camera and use it as operating table (see figure 3.1). Accordingly during the operation, the surgeon would always be able to check the AP scintigraphy of the patient. Unfortunately this brilliant idea did not come into consideration due to logistic reasons until the introduction

of so called mini gamma cameras.

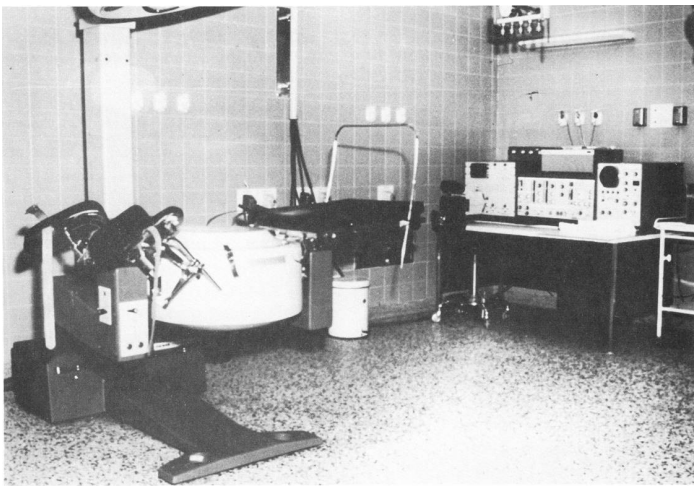

Figure 3.1.: Image of gamma camera used by Gitsch et al. for lymphatic mapping of cervical cancer using ^{99m}Tc colloids in the eighties [117].

In the last decades some commercial light and even hand-held gamma cameras have been made available. The first group to introduce them was the group of Hartsough, Barber, Woolfenden, Barrett and collaborators in 1989 [130]. Since then several groups have developed prototypes in academia (e.g. [29, 208]), but also in industry (e.g. [1, 2, 4]). According to John Aarsvold up to date there are nine companies producing small field of view gamma imagers that can potentially be used in the OR and seven hand-held gamma cameras meant for intraoperative use [13].

Mini gamma cameras allow generating 2D images of resolutions up to 4mm at 5cm distance from the object of interest for acquisition times in the order of 20s (shorter acquisition times yield lower resolution) [39]. Their field of view varies from 4x4cm2 [1, 2] up to 20x20cm2 [4] depending if they use either big parallel hole collimators or pinhole geometries. The increased field diminishes either sensitivity or resolution [39].

Small field of view systems often include a cart that holds the heavy detector and allows positioning the camera statically in relation to the patient in order to integrate readings over a longer time. Unfortunately this reduces the flexibility of their use in the OR. The most spread solution is probably the one proposed by the group of José María Benlloch and the company Oncovision (Valencia, Spain). They propose the use of a very small camera

hanging from an arm that can be covered by a sterile foil (figure 3.2). Flexibility is thus kept within a level and still images can be generated. Their approach is particularly interesting for laparoscopic procedures as shown by Lenka Vermeeren from the group around Renato Valdés Olmos [346, 347].

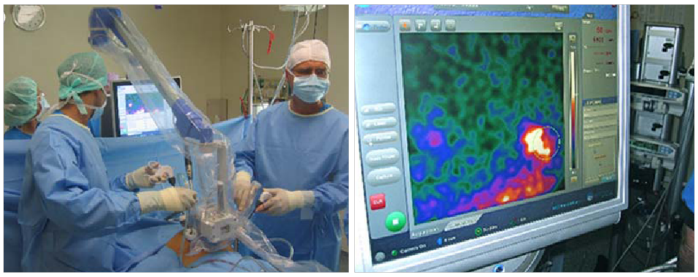

Figure 3.2.: Mini gamma camera as used during laparoscopic SLNB as shown in [347]. Camera is covered by sterile sheath and placed over patient. Images are visualized on line. Image reproduced with permission of Springer.

Purely hand-held cameras have also been proposed and are provided by at least four companies (figure 3.3). They have flexibility, but require holding the camera still during the acquisition in order to generate valid images. Further, ergonomics is an issue as the weight of the device itself can be between 1,2 kg for high-resolution devices and to 800 g for lower resolution devices [29].

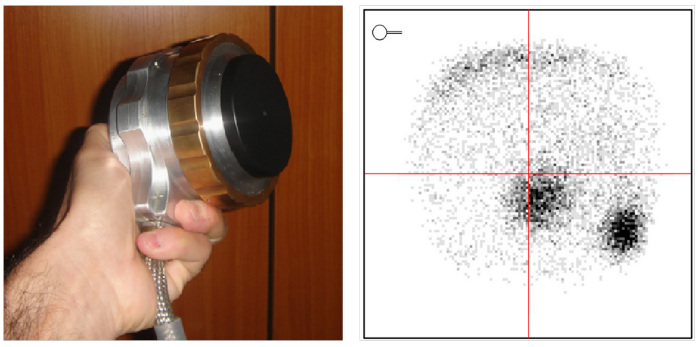

Figure 3.3.: Hand-held mini gamma camera and image of 2 axillary sentinel nodes in breast cancer patient [29]. Image reproduced with permission of Elsevier.

In general both approaches present a major lack when putting the generated images in relation with anatomic information (physicians require to put the images in relation

with the anatomy and the operation situ in their heads). Interesting solutions have been proposed by the group around Benlloch, like the inclusion of a laser pointer or the use of a radioactive pen to have a reference between anatomy and gamma camera image. Also worth mentioning is the approach of Sergei Vidal-Sicart, where a radioactive seed is put on the tip of a gamma probe or a surgical instrument respectively [250, 347].

Further problems not completely attacked by 2D radioactive imagers are the effects of shadowing and shine-through. These together with the cost compared to gamma-probes (factor 3 to 7 depending on the probe and the mini camera to be compared) have prevented a successful entrance of this technology into clinical practice.

3.1.2. Magnetic tracers

Lately several groups have introduced a new approach for lymphatic mapping (e.g. [162, 168, 269, 376]). Instead of using radioactive colloids, they have proposed using magnetic particles. Magnetic particles are potentially an excellent contrast medium for MRI devices. Of particular interest is their non-radioactive nature, their good imaging time (images possible 15-60min after injection) and their washout time (considerably longer than 24h).

The initial work of the groups of Suga and Kobayashi [169, 315] have shown that paramagnetic contrast agents produce good results in mice and are an alternative solution for a good visualization of nodes and lymphatic vessels [173].

If meant to be used in the operating room these tracers would require the use of intraoperative MRI. As mentioned in the introduction, intraoperative MRI is available. Nevertheless logistic issues have constrained its use to extremely complex procedures where the intraoperative availability of MRI changes dramatically the outcome of the patient [248]. Such is the case of neurosurgical procedures, but definitely not of lymphatic mapping in oncology.

Technical specifications are essentially the same of MRI: sub millimeter resolution, acquisition times in the range of 2min, penetration down to 20cm, etc.

A recent development by the British company Endomagnetics (London, UK) under the technical lead of Quentin Pankhurst will however allow hand-held (100-200g) fast (0.1-1s) one dimensional detection of magnetic tracers in a SLN setup with a similar accuracy

as gamma probes [3]. This promising non-imaging approach may slowly displace the radioactive approach in future.

Imaging developments in this direction have been also published by the group of Prof. Buzug. His group is developing open-coil geometries that could allow 2D magnetic particle imaging towards intraoperative applications [289].

3.1.3. X-ray tracers

X-ray contrast media have also been proposed for lymphatic mapping. Actually, the origins of lymphatic mapping are the so called lymphography introduced in Munich in the fifties [74].

In the early 2000s some groups gave a rebirth to the development of contrast agents for CT lymphoangiography aiming at SLN [214, 316]. In this technique an X-ray contrast agent like undiluted iopamidol is injected peritumorally. Intra-operatively a fluoro CT, a fluoroscopy device or a C-arm based cone-beam CT may be used to image the contrast media and guide thus the surgeon.

The major advantage of this technique is the fact that the image incorporates both functional and anatomical information and it can also be performed in 3D mode (figure 3.4).

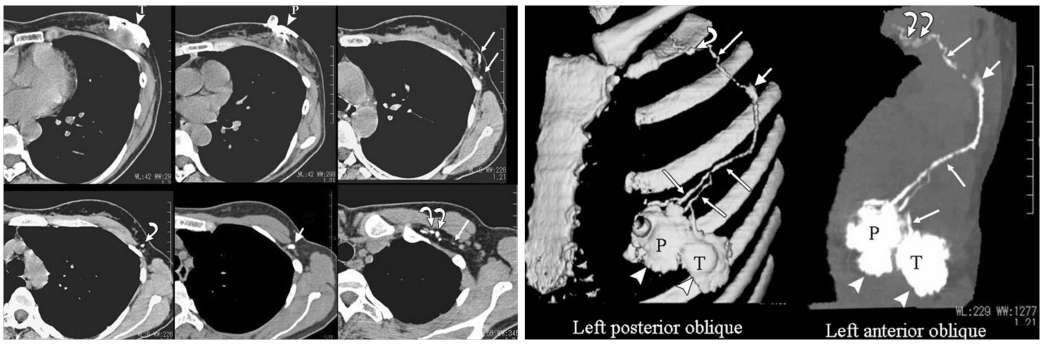

Figure 3.4.: Example of contrast enhanced CT for lymphatic mapping. On the left slices show the lymph nodes on the thoracic wall. On the right rendering of the injection site, the lymphatic drain and SLNs is shown [316]. Image reproduced with permission of the Radiological Society of North America.

On the side of the tracer itself, washout has not been reported, but imaging can be done

already 5-15min after injection.

Currently the experimentation has been restricted to preoperative imaging with high resolution CT. Technical specifications are very interesting: penetration up to 20cm, sub millimetric resolution, extremely fast imaging (<2s). There is, however, up to date no data showing that fluoro-CT or C-arm based cone-beam CT can achieve such high quality images.

Radiation dose for the patient is also an issue [314]. This technique would require per scan a dose 25 times higher than the complete dose of the radioisotope approach (0.2 vs. 4mSv, dose of conventional SLNB versus dose of contrast high-resolution CT of the thorax) [183, 373].

In that sense, there is no easy entrance in the market for these techniques at least in short/mid term.

3.1.4. Colored tracers

Vital blue-dye (1% isosulfane blue dye solution) was introduced in the pioneer work of Morton as intra-operative marker for SLNB in malignant melanoma [224]. Vital blue-dye enables to highlight the lymphatic drain of the tumor for visual evaluation and thus enables to find the SLN by following the blue-marked lymphatic vessels towards a blue spot in the lymph basin (see figure 3.5). The major advantage is of course the possibility of using the bare eye to visualize the tracer without the need of an imaging system. This includes the possibility of using the lymphatic vessels that are also marked as 'road-map' to the node.

Blue-dye has big advantages: it does not include radiation; it can be seen with the bare eye (sub millimetric resolution); it can taint the SLNs in 5-15min; washout is much more than a day; etc.

There are, however, major drawbacks related to the isosulfane solution itself. Isosulfane presents a degree of toxicity, allergenicity and a slow resorption. The first produces local necroses if applied in concentration over 3 %. Far more important is the risk of anaphylaxis reported in about 1 % of the patients [34, 72, 165, 188]. As the injection of isosulfane is normally around the tumor, the blue color makes the excision of the main tumor dif-

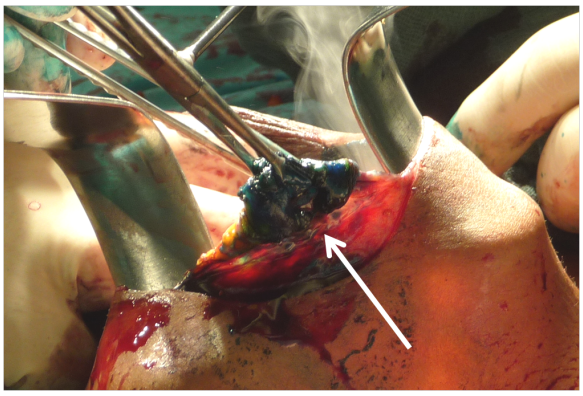

Figure 3.5.: SLN conglomerate showing clear blue coloring during blue dye guided SLNB in breast cancer.

ficult and can even lead to insufficient or exaggerated resections due to the difficulty of distinguishing the tumor borders clearly. Regarding the resorption, the blue color remains visible in the injection place as well as in the urine and stool for months [173]. All of these issues are fundamental problems and little can be done to overcome them.

Alternative dyes have been also proposed. An example is indocyanin green dye (ICG) which was evaluated in breast cancer by the group of Motomura already in the nineties [225]. ICG has the advantage that besides being green (easier to tell apart from human tissue), that it has a fluorescent component (see next section). ICG can be imaged already 5-15min after injection, but at most for 30min until washout is evident. This burdens this tracer as it creates unnecessary stress on the surgical procedure.

One particular development related to blue dye is worth being mentioned. The company Eurorad has lately introduced as investigational device, a combined optical-gamma probe system [2]. Such system allows detecting blue dye with higher sensitivity than with the bare eye. Although not being an imaging system, this combination should be considered in future for example for the combined use of fluorescent tracers and radioactive ones. The probe is essentially as light as a gamma probe with similar acquisition times and has increased spatial resolution (down to 0.1mm) due to the optical detector.

3.1.5. Fluorescent tracers

Very interesting is also the use of fluorescent tracers. Fluorescent tracers have the major advantage of basing on non-ionizing radiation and being capable of being detected with high resolution (0.2-2mm) and relatively 'small' systems.

There are several approaches for using optical tracers for lymphatic mapping. In all of them, again a contrast medium and camera systems with proper filter systems are used. The way the illumination is dealt with and the processing of the acquired images are different.

The first reports were by the group of McGreevy in 2003 [209]. There they used an IR microscope and a fluorescent vitamin for lymphatic mapping in a pig setup. Some years later the group of Kitai introduced for the first time a handheld intraoperative device for breast cancer [166] and the use of ICG as tracer. In those preliminary work a handheld camera (200-400g) was added LEDs in the range of 760nm for excitation of the ICG fluorescent component with highest absorption at 765nm. The camera was also added a low pass filter at 820nm to avoid non-fluorescent light to be detected (peak of ICG's fluorescent emission is at 840nm). Acquisition time was between 1-10s.

Beyond the good results of the group of Kitai, depth penetration is an issue with ICG. In a phantom setup, Kitai et al managed to detect ICG up to 1cm in depth (phantom of human like tissue). This is not sufficient for percutaneous imaging, but is for intraoperative imaging in situ. As a matter of fact the technology is showing a boost in open surgery applications. Groups in Japan and Germany are publishing applications of SLNB in anal/rectal cancer [137, 233], gastric cancer [179, 320, 321], as well as superficial lymphatic basins like in breast cancer [227] or skin cancer [339], among others...

A rather more sophisticated approach is the one of the group of John Frangioni and their device 'FLARE' [337] (see figure 3.7). There they completely replace the OR lamps with a illumination system that excites the fluorophores used and at the same time generates the required light for the operation. In the illumination system they include a camera system with filters for different wavelengths in order to generate images in different bands.

Probably the most promising approach is the one of George Themelis of the group of Vasilis Ntziachristos [326]. There a three camera system is used to obtain multi spectral

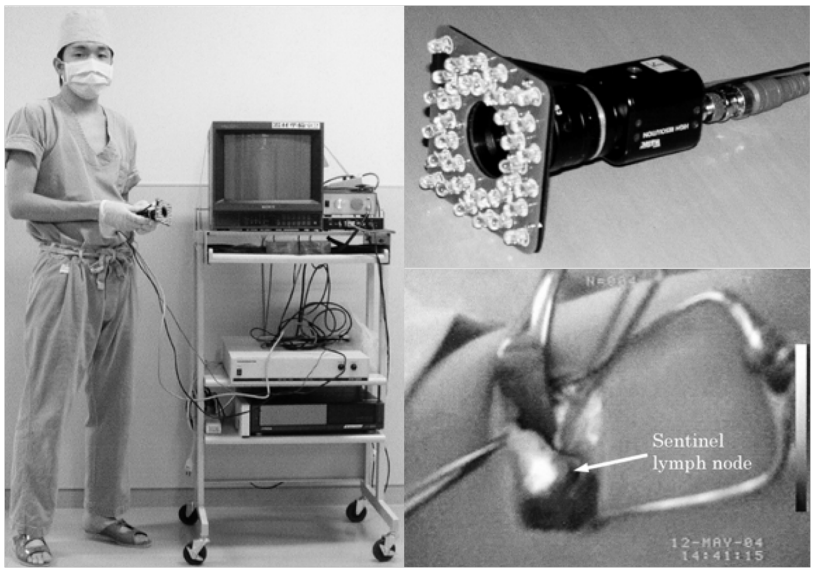

Figure 3.6.: Initial system for fluorescent lymphatic mapping by the group of Kitai in 2005 [166]. Hand-held camera is extended by 760nm LEDs and 820nm low pass filter. Sentinel node can be made 'visible' when opening the axilla. Image reproduced with permission of the Japan Science and Technology Agency.

imaging by using a very intelligent combination of narrow band optical filters and image composing. The major advantage is the possibility of making a compact solution which allows using a less complex system than FLARE and minimize the changes in the workflow.

All mentioned systems suffer the major disadvantage of optical systems: depth penetration. Despite amazing improvements in sensitivity, the fact that light penetrates only some millimeters in tissue avoids making visible structures deeper than 2-3cm. Approaches using lower frequency light in the near-infrared may improve this, however there is still considerable work to do.

A combination of optical tracers with other tracers for deeper penetration is promising, but will require more work on the side of clearance for human use (see as example [173] or [237]).

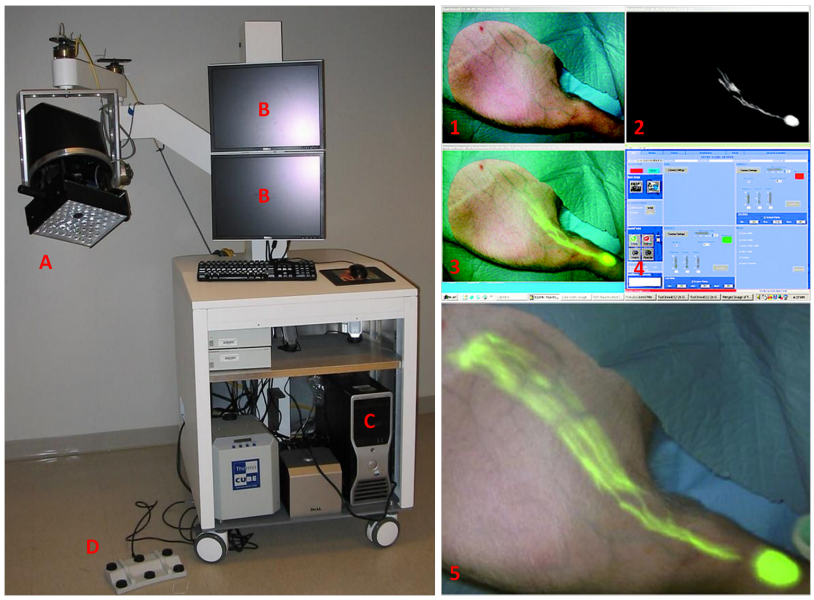

Figure 3.7.: Fluorescence-assisted resection and exploration (FLARE) system by the group of John Frangioni. System comprises several parts: (A) a camera/illumination head for replacing the OR lamps and illuminating the surgical situs with proper frequencies for fluorescence and normal visualization, as well as acquiring light and fluorescent images; (B) monitors for display of images in fluorescence images and combined light and fluorescent images; (C) a data processing unit for merging images; (D) a user interface in the pedal to switch modes of visualization. On the left, screenshots of system are shown. User interface shows light image (1), fluorescent image (2), merged image in small (3) and zoomed in (5), as well as controls (4).

3.1.6. Micro bubbles and ultrasound contrast tracers

Ultrasound contrast agents were introduced lately as a non-ionizing radiation alternative for enhancing structures and visualizing them using sonographic techniques [367]. The idea is in general to use agents that behave considerably different than human tissue when imaged with ultrasound. An example is micro bubbles. Micro bubbles can be designed in a way to have dimensions such that ultrasound waves make them resonate. The resonance of them generates echoes that are considerably higher in intensity than the echoes of tissue. Accordingly, they present enhancement in the ultrasound images.

Such bubbles and similar contrast agents have been coupled to different biomolecules making sonographic tracers out of them. In the case of lymphatic mapping, the use of such agents results in the so called lymphosonography (see example in [118]). Their use in humans for lymphatic mapping has only been published lately by the group of Ali Sever et al. [300] (see figure 3.8). From the point of view of the tracers, they are of course non-radioactive, require 5-30min to be imaged after injection and unfortunately present a very fast washout (<5min). On the side of the imaging CE US systems allow detecting lymph nodes as deep as 7cm with resolutions in the range of 0.2-2mm. The sonographic probes weight in the range of 100-200g.

Their intraoperative use is yet unclear, but as the group of Sever showed by using it for placing of wires (which can be used then as guidance in the OR) the approach seems feasible.

3.1.7. Summary

In the last subsections several tracers and the correspondent technologies have been described. The following table (table 3.9) summarizes the overall properties of the different approaches.

Evidently each tracer and the related technologies has advantages and disadvantages. The decision of what tracer would be used is then in the hands of the surgeon and his/her infrastructure as well as financial situation.

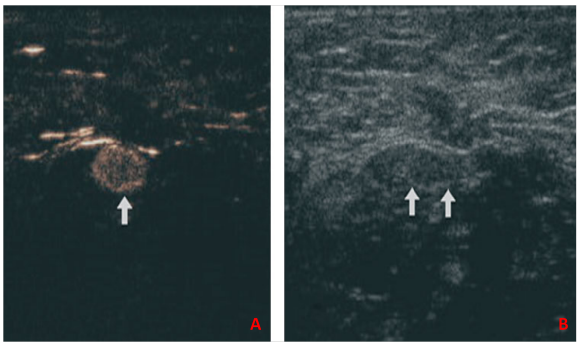

Figure 3.8.: Example of lymphatic mapping with contrast-enhanced ultrasound. (A) Image of axilla showing lymphatics and a sentinel lymph node (arrow). Image was captured in special ultrasound modality called contrast pulse sequencing that allows enhancement of contrast-media. (B) B-mode ultrasound image shows a lymph node (arrows) in the area of major contrast confirming that the contrast-agent accumulation succeeds in such. Image reproduced with permission of John Wiley and Sons Ltd from [300].

3.2. Intraoperative imaging systems for angiography

Angiography is one of the earliest functional imaging modalities. It was introduced in the twenties by Egas Moniz, the first Portuguese Nobel price holder [84]. In it the aim is to visualize the physiological function of blood flow in order to diagnose disorders. Its most common realization is through the use of contrast media injected to the blood vessels, but lately also non-contrasted solutions have been proposed using the intrinsic properties of blood or the vessels.

Making blood vessels visible has a big importance in surgery and in particular in the view of trends towards minimal invasion (e.g. [21, 303]) and quality assessment (e.g. [197, 303]).

Intraoperative systems for angiography were introduced in the late sixties by Bruecke and Piza [50] as a way to solve the problem of transporting preoperative images into the OR. The most important representatives are reviewed in the following paragraphs.

	Property	Unit	Gamma Probe	Magnetic Probe	Opto-gamma Probe	Colored Tracers	CE US	Gamma Camera	Arm-mounted gamma camera	CE Fluoroscopy	Fluorescent Camera	Arm-mounted fluorescent camera	CE IO MRI	CE IO CT
Device	Radiation	[mSv]	<0.4	0	<0.4	0	0	<0.4	<0.4	<1	0	0	0	<10
	Penetration*	[mm]	<70	<30	<70	<1	<70	<100	<100	<200	<20	<20	<200	<200
	Acquisition time	[s]	0.1-1	0.1-1	0.1-1	0	<1	10-30	10-30	0.1	1-10	1-10	120	<2
	Weight	[g]	100-200	100-200	100-200	n/a	100-200	1500-4000	n/a	n/a	200-400	n/a	n/a	n/a
	Flexible movement		yes	yes	yes	yes	yes	no	no	no	yes	no	no	no
	Accuracy	[mm]	5-20	5-20	0.1-20	0.1	0.2-2	5-20	5-20	0.1-0.2	0.2-2	0.1-2	0.1-2	0.05-0.5
	Dimensions		1D	1D	1D	2D	2D/3D	2D	2D	2D	2D	2D	3D	3D
	Wire		yes/no	yes	yes	n/a	yes	yes	n/a	n/a	yes	n/a	n/a	n/a
	Investment	[kEUR]	10-40	30-40	25-40	0	70-130	50-70	70-100	100-200	30-60	60-120	1000-2000	300-400
Tracer	Tracer		Tc99m-colloid	Iron nano-particles	Tc99m-colloid + blue dye	Blue dye	Micro-bubbles	Tc99m-colloid	Tc99m-colloid	Iodine-contrast media	ICG	ICG	Iron nano-particles	Iodine-contrast media
	Visible bare-eye		no	yes	yes	yes	no	no	no	no	no	no	no	no
	Injection	[min]	5-120	15-60	5-120	5-15	5-30	5-120	5-120	5-15	5-15	5-15	15-60	5-15
	Wash out		>24h	>24h	>24h	>24h	<5min	>24h	>24h	n/a	<30min	<30min	>24h	n/a
Misc.	Cost p. pt.	[EUR]	~25	~400	~35	~10	~60	~25	~25	~25	~90	~90	~1000	~400
	Clinical acceptance		standard	in trial	in trial	standard	in trial	initial	in trial	hypothetical	initial	initial	in trial	in trial

Figure 3.9.: Summary of approaches for intraoperative lymphatic mapping. The prices of the devices are estimated at the time of putting the table together, based on the available commercial systems. Running costs included many disposables required as well as the cost of the tracer itself.

3.2.1. X-ray angiography

X-ray contrasted angiography is probably the most extended of all imaging approaches for blood vessels. It was introduced in 1927 by Egas Moniz [84] in order to image blood vessels in the human brain. The concept is based on the injection of X-ray opaque contrast media in the blood vessels of interest. As a result, blood vessels, that do not present a significant contrast in X-ray images turn clearly visible. Further, if images are generated before the injection of the contrast medium, the subtraction of the contrasted images and the ones without contrast results in clear images of the blood vessels (see figure 3.10). This is often called subtraction angiography.

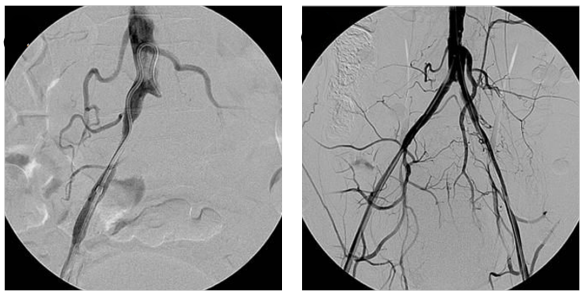

Figure 3.10.: Intraoperative angiograms at two different times during an operation in the pelvis. Image taken from [82] and reproduced with permission of Elsevier.

In the operating room X-ray angiography can be performed using C-arms [49], fluoroscopic systems [191] or fluoro-CT [231]. An interesting implementation is the novel robotic motorized angiography suite of Siemens [11]. In it a C-arm is mounted on a robot allowing fast and precise positioning of it and also high resolution cone-beam CT reconstructions, allowing also 3D angiography in the OR.

Resolution is sub millimetric and penetration above several centimeters. Regarding the contrast used, normally it is injected on need and gets diluted (washed out) in the range of a minute, making the use of large amounts of contrast medium necessary.

In general X-ray angiography has the disadvantage related to the radiation exposure (up to 20mSv at 1fps in the pelvic area or brain, lower in other anatomies [253,287]) and has had a very slow movement from the interventional world to surgery. Preliminary it has only been established in the field of vascular surgery (e.g. [383]) and of neurosurgery (e.g. [83]),

where the radiation exposure is negligible in contrast to the advantage the information on the vessels brings to the outcome of surgery.

3.2.2. Intraoperative MR angiography

Similar to X-ray angiography MRI can also be used to depict blood vessels. In this case there is no need of contrast media, as blood vessels present sufficient contrast in several MRI sequences (i.e. [82]). Intraoperative use has been essentially restricted here to vascular surgery.

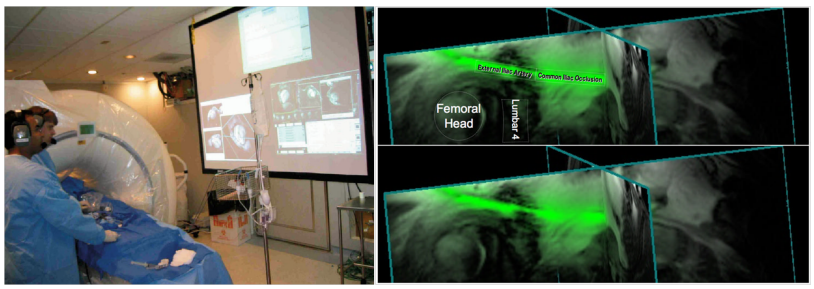

Figure 3.11.: Example of intraoperative MRI angiography: setup and exemplary image showing 2 MRI slices rendered and a vessel highlighted in green. Pictures taken from [82] and reproduced with permission of Elsevier.

Resolution is in the same range of conventional MR (0.1-2mm). Similar is the case of acquisition times (1-120s), which increases depending if 3D images are needed or which spatial resolution is desired.

Despite the amazing performance of such systems the requirements on logistics are immense (see figure 3.11), making its use beyond 'quasi'-interventional very restrictive.

3.2.3. US angiography

Ultrasound is an inexpensive flexible and harmless imaging modality. Accordingly its use for angiography makes it extremely interesting. There are essentially two ways of generating angiographic images using ultrasound: using contrast or using the fact that the blood flows.

In the first approach, as in the case of lymphosonography, research has been done in the

direction of using contrast media to enhance blood vessels (e.g. [47,386]). Its application in an intraoperative setup has not been completely established yet, but there are initial works (e.g. [172]). The advantage of such an approach is the easier interpretation and the lack of movement artifacts in comparison to the other approach.

Minimal changes in the reflected frequency of ultrasound waves has been studied in details since the sixties (e.g. [102,381]). These changes are essentially due to the well-known Doppler effect which explains that moving objects reflect incoming waves at a shifted frequency. The relation between the shift in the frequency allows calculating very precisely the relative speed of the moving object in the perpendicular direction. This speed can then be calculated for every point of a region of interest of the B-plane image and then overlaid on it as color image (see 3.12).

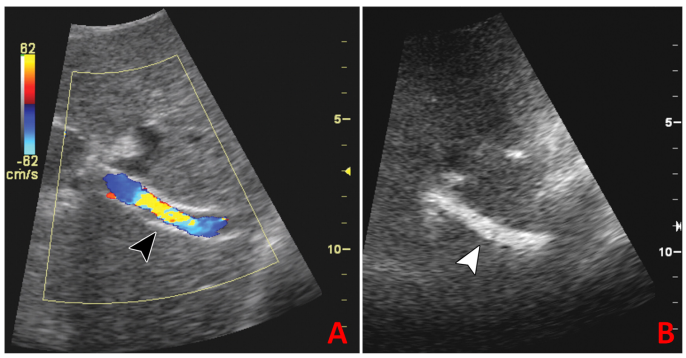

Figure 3.12.: Example of Doppler ultrasound for vessel visualization in liver: (A) Overlay of speed map calculated in region of interest surrounded in yellow show stenosis on the arrow (turbulences produce blood flow in several directions which are shown in colorful area). (B) As comparison the same slice is shown only in B-mode ultrasound, where vessel can be seen, but functional behavior is not visible. Image from [353] and reproduced with permission of the American Roentgen Ray Society.

Its first use was evidently angiography, having become now-a-days a standard-of-care in several applications (e.g. [93,144]).

Its intra-operative use for angiography has been mostly in the evaluation of the flow patterns in vascular surgery (e.g. [307]) and in order to characterize the vascularity of tumors

(e.g. [152]) or provide context information of vessels (e.g. [379]) in oncologic surgery.

In general, if contrasted or not, US angiography may achieve sub millimetric spatial resolution and real time imaging. The possibility of using 3D US probes or tracked US probes to generate 3D US images is also available here since the early nineties [331].

3.2.4. Narrow band imaging-based endoluminal superficial vessel visualization

One quite innovative solution for imaging superficial blood vessels is the one proposed by narrow band endoscopy. In that approach a conventional endoscope is modified such that the light used for illumination is filtered by narrow band optical filters (commonly one filter at 415nm and one at 540nm with bandwidths of 30nm and 20nm respectively) [310]. Interestingly in these two light bands blood vessels present a big contrast to tissue predominantly due to hemoglobin.

Hemoglobin is responsible for the red color of blood, as it is the main pigment of red blood cells. Its concentration outside blood vessels is minimal. It presents also an absorption profile with clear peaks at 415nm and 540nm.

When illuminating tissue with such light, the 415nm component gets strongly absorbed by hemoglobin in mucosal capillaries while being reflected in normal tissue. The 540nm band has a higher penetration reaching lower layers before being absorbed by blood of deeper mucosal and submucosal vessels or reflected by tissue (i.e. it has a very high spatial resolution down in the micron range, but only penetrates few millimeters). Accordingly blood vessels and to some extent their depth become visible in the endoscopic images (figure 3.13).

Beyond diagnostics this technology has been used intra-operatively in colon malignancies [282], bladder cancer [61], Barrett's esophagus disease [327], among others.

Despite the promising results, the method is applicable only under controlled conditions of illumination, as it is the case of endoscopy. The blood vessels visualized are also very superficial, as the light used only penetrates few millimeters in tissue.

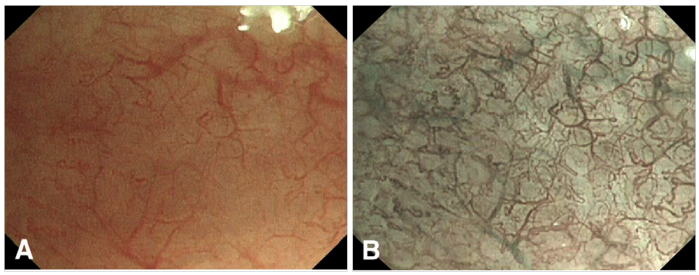

Figure 3.13.: Example of difference between light image (A) and narrow band image (B) of endoscope in Barrett's esophagus patient. Capillaries appear in brown and deeper lying vessels in cyan. Image taken from [310] and reproduced with permission of Elsevier.

3.2.5. Fluorescence-based superficial vessel visualization

The use of fluorescence tracers is also possible in order to visualize blood vessels intraoperatively. The technology needed for this is essentially the same discussed in the section on lymphatic mapping, however its applications are mostly in neurosurgery. There the operative microscopes are commonly used. Those microscopes have been modified to include illumination in the desired range of fluorescence. An exemplary use is depicted in [127], where the fluorescent tracer applied is ICG (see figure 3.14).

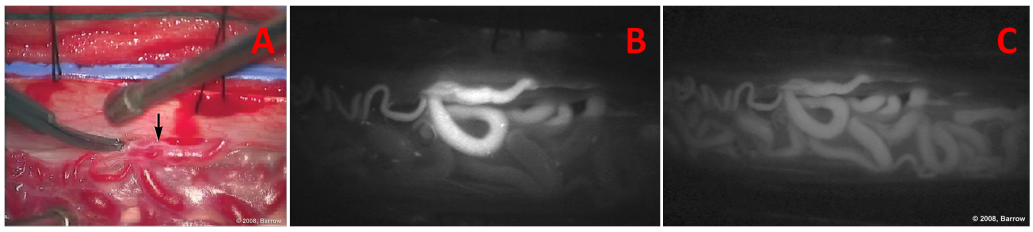

Figure 3.14.: Example of microscopy images in white-light and fluorescence for contrast enhanced blood vessels. (A) White light image showing vessels and surgical instruments. (B) and (C) fluorescence images at different time points showing the dynamics of the contrast media. Image from [127] and reproduced with permission of the Wolters Kluwer Health.

The system of the group of Prof. Frangioni has also been used lately in similar approaches in preclinical ORs [322], an example is shown in figure 3.15.

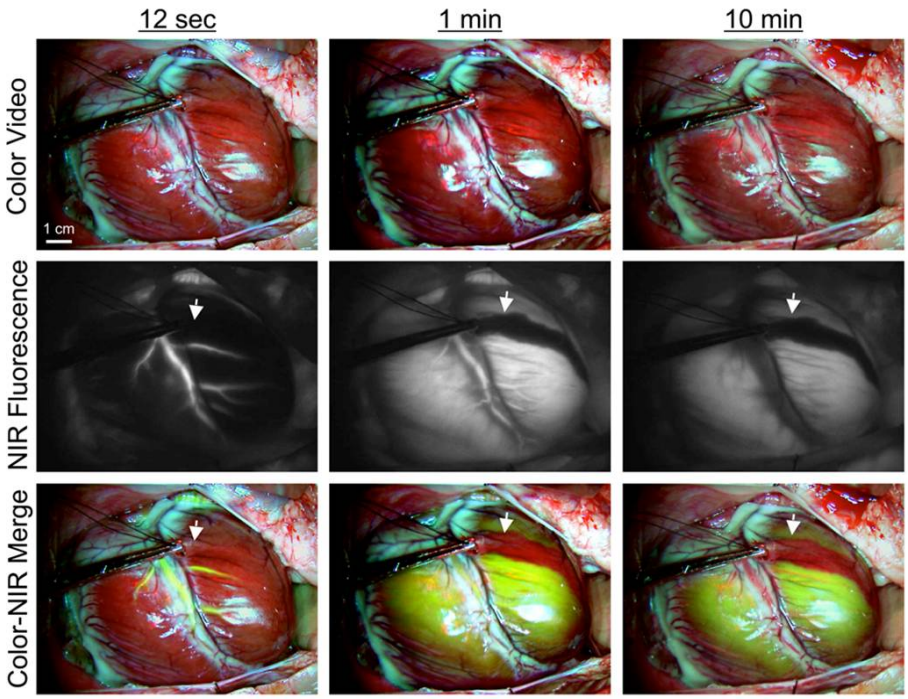

Figure 3.15.: Arterial phase (12 sec), venous phase (1 min), and late phase (10 min) of a pig's heart after intravenous injection of methylene-blue. Arrows show perfusion in a clamped branch of an artery. NIR fluorescence images were acquired with a 100msec exposure time. Figure reproduced from [322] with permission of Elsevier.

Although in a preliminary phase, this technique may open possibilities of imaging down to 1cm of depth with sub millimetric resolution and fast acquisition times (0.1-2s). Even the possibility of using handheld fluorescence cameras for these means may be possible. The need of constantly injecting contrast media however, as in the case of x-ray angiographic systems, is an important issue that has to be considered.

3.2.6. Thermography-based superficial vessel visualization

In the fifties, Lawson introduced the concept of thermal imaging in medicine [184]. Thermography was a technique to estimate temperature from images based on the black body radiation relation to temperature. In other words, from properly calibrated infrared images it was possible to 'see' the surface temperature of objects. Initially it was used for diagnosing breast lesion like in [185, 350]. The concept behind was that if the nude breast was kept in a cold room for 10-15 minutes, the temperature distribution in it would be correlated to the vascularity, which could then reveal vascularized lesions.

Thus differences in temperature between blood vessels and normal tissue could allow visualization of them in an intraoperative setup. In the last years such approaches have become common in cardiac surgery (i.e. [308]) presenting enhanced contrast in a couple of millimeters with good refresh rates and spatial resolution (see figure 3.16).

Such images are very interesting as they do not rely on tracers, however, they are not completely reliable due to sources of heat in the OR and even physiological variations in temperature.

3.2.7. Summary

In the previous subsections different approaches for imaging blood vessels were reviewed and their specifications mentioned. Table 3.17 summarizes the discussed technologies in terms of the technical data including logistics and also costs.

There are surely other approaches that a person working in the field can make use of. Examples could be the use of diffusion tensor MR, radioactive tracers (like ^{15}O-water), etc. As in the case of lymphography, the decision on the system to use depends strongly on the target application and boundary conditions of it (see chapter 2).

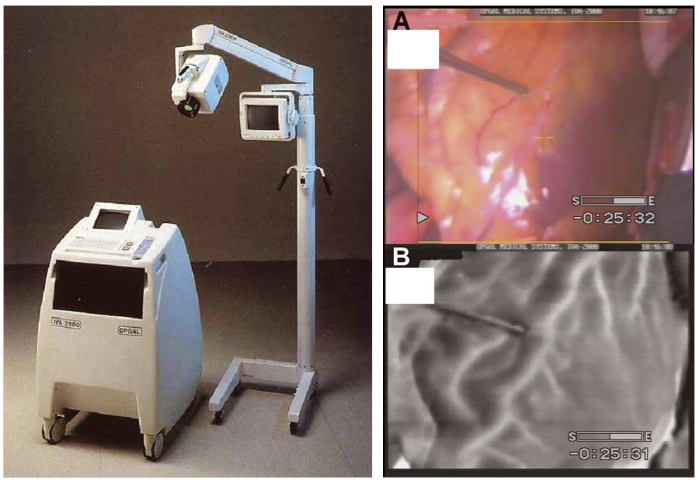

Figure 3.16.: Example of system for thermography and images of a coronary artery evaluation in the OR. (A) shows the white light image of the myocardium and (B) the thermal image where the coronary arteries can be clearly depicted and obstructions evaluated as done here. Pictures taken from [308] and reproduced with permission of the European Association for Cardio-Thoracic Surgery.

3.3. Intraoperative imaging systems for localization of primary tumors

The strong trend of cancer screening, as well as the increasing conscience of the public have resulted in the detection of tumor in very early stages for a variety of cancer types. The overwhelming advantages in functional imaging and in particular in hybrid imaging have made sub millimetric focii of tumor visible. As a result the surgical world has been confronted with the necessity of finding ways of intra-operatively localizing such structures with precision.

In this sense, intraoperative imaging and navigation systems have been posed the challenge of enabling accuracies and sensitivities equivalent to the ones of the big preoperative imaging devices. Three different approaches have be developed for localization: intrinsic property-based localization, systemic labeling-based localization and marker-aided localization.

In the localization based on intrinsic properties, the properties of the tumor or of the

	Property	Unit	X-ray	MR	Doppler US	CE US	Narrow band	Fluorescence camera	Arm-mounted fluorescent camera	Thermal
Device	Radiation	[mSv]	<20	0	0	0	0	0	0	0
	Penetration*	[mm]	<200	<200	<70	<70	<3	<20	<20	<3
	Acquisition time	[s]	<0.1	<120	<1	<1	<0.1	<0.1	1-10	<1
	Weight	[g]	n/a	n/a	100-200	100-200	400-600	200-400	n/a	400-600
	Flexible movement		no	no	yes	yes	yes	yes	no	yes
	Accuracy	[mm]	0.1-0.2	0.1-2	0.2-2	0.2-2	0.01-0.1	0.2-2	0.1-2	0.2-2
	Field of view	[cm2]	20x20	20x20	7x7	7x7	2x2	5x5	10x10	10x10
	Dimensions		2D/3D	2D/3D	2D/3D	2D/3D	2D	2D	2D	2D
	Wire		n/a	n/a	yes	yes	yes	yes	n/a	yes
	Investment	[kEUR]	100-1000	1000-2000	30-130	70-130	50-100	30-60	60-120	30-50
Tracer	Tracer		X-ray-contrast media	None	None	Microbubbles	None	ICG	ICG	None
	Visible bare-eye		no	no	no	no	no	no	no	no
	Injection	[min]	<0.1	n/a	n/a	<5	n/a	<0.1	<0.1	n/a
	Wash out		<1	n/a	n/a	<5	n/a	<1	<1	n/a
Misc.	Cost p. pt.	[EUR]	~200	~1000	0	~60	0	~200	~200	0
	Clinical acceptance		specific applications	trials	specific applications	trials	specific applications	hypothetical	initial	trials

* for standard uptake in case of tracers

Figure 3.17.: Summary of approaches for intraoperative angiography. The prices of the devices are estimated at the time of preparing the table from data available on the Internet. Running costs included essentially costs for operation and the cost of the tracer itself if applicable.

metastases themselves are used to make it visible. These distinguishable properties from normal tissue are detected directly by the imaging system on its own. An example is the case of functional processes in liver metastases that lead to changes in echogenecity between tumorous tissue in comparison to healthy one, which make a visualization possible using ultrasound without any tracer.

In the localization based on systemic labeling, also a property intrinsic to the tumor is exploited. However, this property is made distinguishable through a tracer that gets accumulated in the tumorous tissue or its immediate neighborhood (or shows no uptake in the tumor). A classic example is the labeling of high metabolism tumors with radioactive labeled sugar. This makes the localization of the cancerous tissue equivalent to the localization of radioactive focii.

Finally the localization through markers uses the concept of landmarks. In it the target area is detected in one imaging modality and then 'tagged' with a marker that can be easily localized in surgery. This is extremely useful for impalpable tumors or tumors that could not be detected otherwise by the other approaches in the OR ('occult lesions') or where the possibility of taking the wrong structure out is high (e.g. when 'fishing lymph nodes'). The concept was introduced in the early eighties for non-palpable breast cancer lesions [352]. In that time Voss used a thin flexible wire to mark tiny non-palpable breast lesions using as guidance the images of x-ray mammography. Nowadays such techniques have been modified to millimetric precise marking using stereotactics systems or image-guided marking with US or MR.

Depending on the tumor entity the choice of the approach to be used is accordingly different. Several options have been available at both academic and commercial level. In the following the most relevant in terms of clinical acceptance and relevance will be discussed.

3.3.1. Sugar metabolism

Cancerous tissue usually presents a higher metabolic activity than surrounding tissue. This fact can be exploited for intraoperative localization. Most of the approaches for imaging increased metabolic activity are based on tracers.

One of the first signs of malignancy is an accelerated glucose metabolism, both in terms of transport and utilization [211, 356]. This fact was used first by Som et al. in the early eighties to diagnose tumor [309] using ^{18}F-2-fluoro-2-deoxy-D-glucose, also known as ^{18}F-FDG or FDG. FDG is a radio-tracer including a ^{18}F atom, which emits positrons and indirectly is thus a source of annihilation photons. FDG is incorporated by cells like glucose by active transport proteins (GLUT) and gets processed by hexokinase into FDG-6-phosphate, which is not further processed and remains trapped in the cell [53, 113, 252].

Today the use of FDG for tumor diagnosis represents 80% of all PET examinations worldwide. Accordingly its use for radio-guided surgery has been in the wish list of many surgeons for many years now [123, 317].

^{18}F emits 97% of its emissions as positrons with a maximum energy of 635keV. These positrons penetrate tissue only a couple of millimeters [66] until they meet an electron and annihilate into two 511keV photons in opposite directions. Accordingly in order to detect FDG, either high-energy annihilation photon detection or direct beta detection is possible. Many scientific and industrial groups have pushed mostly the development on non-imaging probes for both detection types.

High-energy gamma-probes (also known as PET gamma probes) have been developed for general localization of radioactive hot spots. However, their utilization is restricted by spatial accuracy when used for control of residual cancerous tissue [123, 262] (spatial resolution in the range of a centimeter).

In order to improve the spatial resolution of non-imaging probes, the detection of the positrons themselves was introduced for intra-operative use in the late eighties and early nineties [75, 273]. The integration of positron detection by means of semiconductors and scintillator crystals in intra-operative hand held probes (commonly known as beta probes or positron probes) resulted in further improvements to the location of tumor cells [75, 193, 271–273, 359, 385].

Going to imaging, only little has been done towards 'FDG cameras'. To date no group has put a high energy camera meant for intra-operative use. Only few examples, known as beta cameras or positron cameras, are available [332] (see also figure 3.18).

In order to be able to use the technologies developed for low energy tracers, Yang et al. have worked on labeling sugar with ^{99m}Tc [377]. Such tracer would essentially allow

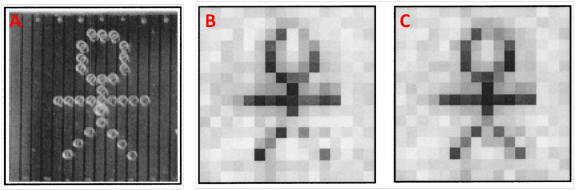

Figure 3.18.: Example of results of beta camera imaging of system described in [332]. (A) shows phantom directly on the camera. (B) is the raw data generated and (C) the corrected image. Pictures reproduced with permission of the American Association of Physicists in Medicine.

imaging with almost half of the dose necessary for FDG (3mSv vs. 7mSv) with better logistics (detection already 30min after injection vs. 45min for FDG and up to 24h later vs. a maximum of 6h for FDG). The results are promising, however the success of FDG is simply too bright in terms of installed infrastructure, quantification, timing, etc. to allow these tracers to get enough attention yet.

As nuclear imaging has not provided a good solution initial efforts have been done towards the development of fluorophore labeled sugar analogues (e.g. [65, 387], see also figure 3.19). These approaches however are still in a very preliminary phase, as the molecular size of the fluorophores allow only a minimal transport of the tracer into cells. Still with good imaging quality after several hours and a slow wash-out, no radiation dose and potentially cheap production, they may open new ways in future.

3.3.2. Energy production

Increased metabolism in general results in increased needs of energy and accordingly of infrastructure for energy generation, which in the case of cells are mitochondrias. Mitochondrias normally have a negative membrane potential which would make cations potential markers for them. In particular the tracer for vitality of heart, ^{99m}Tc-2-methoxy-2-methylpropylisonitrile, also known as ^{99m}Tc-sestamibi, ^{99m}Tc-MIBI or simply MIBI has shown good results.

Already in the nineties Carpentier et al. showed an increased concentration in oxyphil cells in parathyroid adenoma, a degeneration of the parathyroid glands [59]. This was

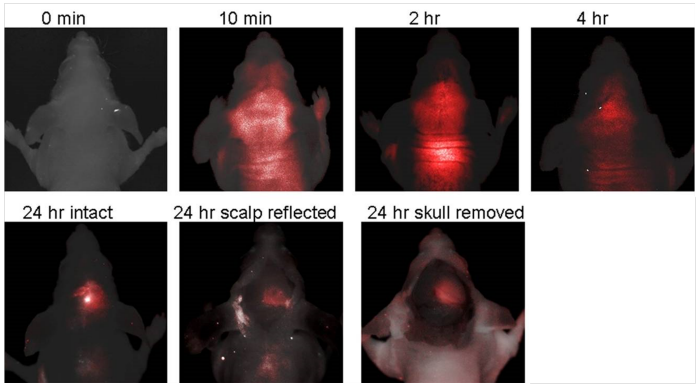

Figure 3.19.: Example from [387] on fluorescent image of glucose analogue tagged with fluorophore in brain tumor of a mouse. Tumor to background is optimal at 24 hours and shows clearly the tumor. Image reproduced according to the terms of the Creative Commons Attribution License.

used later on as basis for radio-guided resection of such adenomas in the case of primary hyperparathyroidism [205]. Original works of the group of Ubhi et al. used ^{201}Tl-chloride [340], but later on it was popularized by the group of Norman in the University of Miami [232].

As explained in [344], the major issues in the uptake of MIBI are the mitochondrial density and the membrane permeability. This is true in several tumors including breast cancer [344], brain tumors [26], etc.

The use of imaging devices for functional image guidance based on MIBI is also a growing field. Groups have used mini gamma cameras in brain [170] and parathyroid [95]. In such cases mini gamma cameras allow producing images in the range of 10-20s with resolutions under 5mm in areas of 5x5cm^2. See also section on lymphatic mapping for more details on those imaging devices.

High mitochondrial activity results in changes in the temperature of the cell. Temperature distribution in the body is a complex function of heat exchange processes with the environment, the metabolic activity, the vascularity, the circadian rhythm, as well as the nervous activity meant to achieve temperature and chemical stability of the body. In the presence of tumors all these factors are influenced, being the own energy production among the most important. The result is the departure of the tumor from the temperature

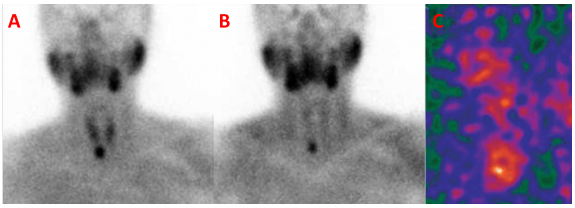

Figure 3.20.: Example of a parathyroidectomy guided with an intra-operative gamma camera. (A) shows the preoperative scintigraphy during the early phase of MIBI. In (B) the parathyroid adenoma becomes clearly visible. (C) intra-operatively the adenoma can be visualized as hot spot below the thyroid [95]. Figure reproduced with permission from Elsevier.

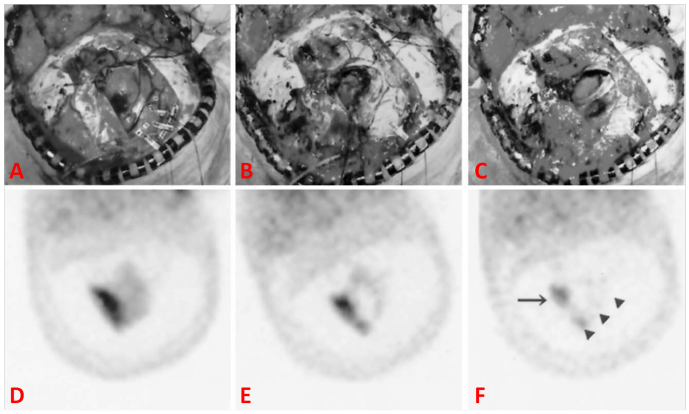

Figure 3.21.: Example of a brain surgery using the aid of an intra-operative gamma camera and MIBI systemic labeling. (A) and (D) show the tumor situs and the intra-operative scintigraphy before the operation. (B) and (E) show the image during the procedure and (C) and (F) the final status, where still tumor tissue remains on the borders of the resection (arrows). Figure taken from [170] and reproduced with permission from Elsevier.

surrounding healthy tissue. This fact has been known since the time of Hypocrates.

The use of thermography was already mentioned in the previous section for imaging blood vessels. Its principle is essentially the same in tumor imaging. Although not widely extended infrared thermography has been even proposed for intra-operative use (e.g. [154], see also 3.22).

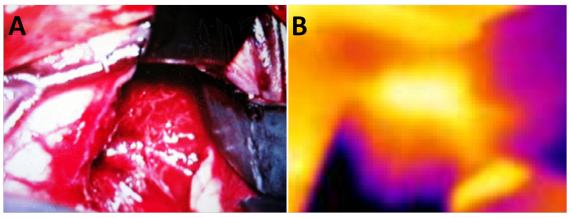

Figure 3.22.: White light image (A) of brain tumor and corresponding themogram (B) showing a difference of almost 2 deg C between tumor and surroundings. Figures from [154] reproduced with permission of Elsevier.

Despite the good spatial resolution of current systems (down to several microns), as well as temperature resolution (down to 0.06 deg C), this technology is very dependent on the shape and material of the surfaces and has a minimal penetration, which has kept it away from most potential applications.

3.3.3. Iodine metabolism

Iodine in the human body is an essential nutrient as constituent part of the thyroid hormones thyroxine (T4) and triiodothyronine (T3). Accordingly the thyroid absorbs actively iodine from blood and stores it. As a result the iodine distribution in the body is essentially proportional to the blood distribution, but in the thyroid where it presents an uptake up to 10.000 higher [126].

This fact has been used to localize thyroid cancer. Commonly thyroid cancer cells retain the absorption and storage nature of normal thyroid tissue. If thyroid cancer cells should exist beyond the thyroid, they would result in a focal uptake of iodine and thus a good target for surgery.

Early in the forties the first experiments were realized where radioactive isotopes of iodine where given to animals in the search of using them [126] for treating thyroid ma-

lignancy and detecting metastases. First results with patients follow from the group of Seidlin et al. [298,299].

The intra-operative detection of thyroid cancer metastases using non-imaging probes has been proposed by several groups with different isotopes of iodine, e.g. [159,230], however, intra-operative gamma cameras have not yet been tried for the detection of such metastases, but have huge potential in functional image-guided surgery.

There are essentially two radioactive isotopes that may be used: ^{123}I and ^{131}I. ^{123}I is a gamma emitter with more than 50 emission energies, being however 83% of the decays at 158.97keV. It can be then detected easily using the technology of ^{99m}Tc-detectors, showing almost identical specifications. Biologically ^{123}I can be imaged already half a day after administration for two days (half life 13.27h) and implies a dose below 1mSv for the patient.

^{131}I on the other hand emits at a significantly higher energy (81.7% at 364.49keV and 6.14% at 284.30keV). Accordingly conventional gamma detectors for ^{99m}Tc cannot be used. ^{131}I-gamma probes have been made available for intraoperative use too. Their performance is diminished in comparison to ^{99m}Tc-probes (spatial resolution only in the range of 7mm and increased diameter and weight >200g). Gamma cameras can be used to image ^{131}I, but to date no developments for intra-operative imaging are done. Due to the long half life of 8.02d, images can be performed long time after injection, approximately 2 days for proper tumor to background. The radiation dose can be as high as 15mSv.

3.3.4. Osteogenesis

In the case of cancer types concerning bones, the creating of new bone structures may also be a good marker for malignancy. Since the fifties Leblond et al. have studied bone growth using radioactive tracers [186]. Nowadays so called 'bone scans' are a standard procedure to visualize fractures and look for bone metastases.

Tracers like ^{99m}Tc-hydromethane diphosphonate (known as ^{99m}Tc-HDP), ^{99m}Tc-methylene-diphosphonate (commonly known as ^{99m}Tc-MDP) and ^{99m}Tc-2,3-dicarboxypropane-1,1-diphosphonate (also known as ^{99m}Tc-DPD) are administered to patients and accumulate in regions with calcium content and in particular in areas with high levels of osteogenesis [107].

The use of such techniques for intra-operative image-guidance are initial besides experiences over 20 years, but show potential (e.g. [241, 323]). Technically due to the use of ^{99m}Tc, the performances are similar to the ones for MIBI. The logistics are good for the intra-operative use: imaging can be done already 3h after injection. Further good images can be acquired as late as 24h after injection.

3.3.5. Haem production

One of the most successful examples of functional imaging in the OR is the combination of fluorescence transurethral optical imaging systems (fluorescence cystoscopy) and contrast media like HexVix ® [151]. This method is used for the detection of bladder cancer. The tracer used here is HexVix ®, a derivate of 5-ALA. Its chemical name is hexyl aminolevulinate, 5-ALA hexylester, 5-ALA hexylesther, aminolevulinic acid hexyl ester, hexaminolevulinate or hexyl 5-aminolevulinate. HexVix ®is an amino acid that presents a higher accumulation in bladder cancer cells than in healthy bladder tissue [149]. 5-ALA is the starting point in the normal biosynthesis of haem in human cells. Within the pathway of haem, the substance immediately before haem is protoporphyrin IX (PPIX). This molecule is fluorescent and can be excited with light of 375-440 nm (blue) emitting in the range of 628-644 nm (red) [199]. PPIX substance seems to be processed also slower to haem in bladder cancer cells increasing thus the relative fluorescence of these in relation to healthy cells [149]. In clinical use, a cystoscope equipped with the proper illumination light and filter system is capable of imaging PPIX. As a result tumor cells can be made visible in the bladder and can be resected directly using the resection sling included in most cystoscopes.

In this particular case, despite the promising results, there is still some perseverance needed. HexVix ®has not made it yet through the clearance of the U.S. Federal Drug Administration (FDA), being thus only applied in Europe [25] (see latest FDA report [71]).

The 5-ALA approach can also be used in brain surgery where successes are considerable beyond cost issues (e.g. [70, 218, 372], see also figure 3.24).

The hardware required for imaging 5-ALA is essentially equivalent to the one introduced for fluorescence imaging in SLNB. Accordingly its real-time nature can be a highly attractive point, whereas the reduced penetration is its bigger restriction.

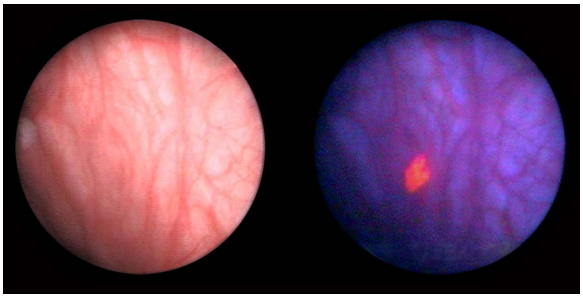

Figure 3.23.: White light versus fluorescence image. Bladder carcinoma in situ becomes visible (red spot) over healthy tissue (blue). Image by Patrice Jichlinski of CHUV Lausanne.

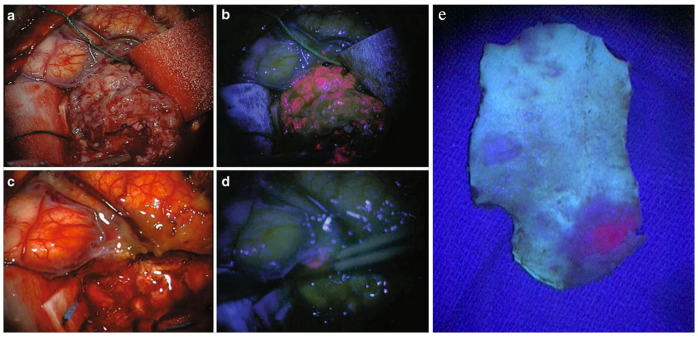

Figure 3.24.: Images from [70] showing meningioma marked with 5-ALA. In (a) tumor is visible with bare eye and fluorescence image confirms it (b). Note that blood covered areas of tumor are not visible in fluorescence mode. After resection in (c) no visible tumor is found, however fluorescence shows a spot that proved to be meningioma. In (e) in a further patient 5-ALA shows infiltration of tumor in bone. Figures reproduced with permission of Springer Verlag.

3.3.6. Calcification

Processes involving calcification in tumors result in changes in the X-ray absorption in relation with the surrounding healthy tissue.

The histologic importance of calcifications in breast cancer is known since the fifties (e.g. [99]). There are two major mechanisms that explain calcification in breast cancer: secretion and necrosis. In the first, tumor cells start producing secretory vesicles with significantly higher rates than normal tissue. They discharge in the extracellular matrix forming thus calcifications in their surroundings. In the case of necrosis the calcification happens in the debris of the dead cells passively [338].

X-ray imaging has been used to detect such calcifications for almost 50 years. If meant to be used in the OR, the X-ray images have to be acquired intra-operatively, which can be theoretically done using C-arm based systems (fluoroscopes) or directly intra-operative CTs. Although both options are possible, there are two major problems: the logistics of using such devices in the OR and the necessity for surgeons of having a radiologic training.

A common approach to avoid both problems is putting a marking in the lesion detected. This approach was shortly mentioned in the beginning of these chapter recalling the technique of Voss [352] to fix a wire to the lesion seen in a further modality. Such technique has now become standard and it is known as wire-guide localization (WGL) [171].

A very interesting alternative was proposed by the group of the European Institute of Oncology in Milan. There a technique called radio-guided occult lesion localization (in short ROLL) was developed [246]. There lesions with suspicious echogenecity and of non-palpable nature are marked with a small amount of radioactivity and then they are localized using a gamma detector or a gamma camera [250] (see also figure 3.25).

The technical specifications for such approaches are essentially the same as the ones for MIBI-guided surgery or radio-guided SLNB, however there is a significant difference. The radio-isotope concentration can be lowered by a factor of 100, as the tumor is marked directly. This results in considerably lowered patient and personnel doses ($<$0.2mSv patient doses, $<0.1\mu$Sv surgeon doses per operation).

Disorders in the calcification are also present in bone malignancies (e.g. [157, 268], see figure 3.26). The use of intra-operative imaging is mainly done using fluoroscopy, but

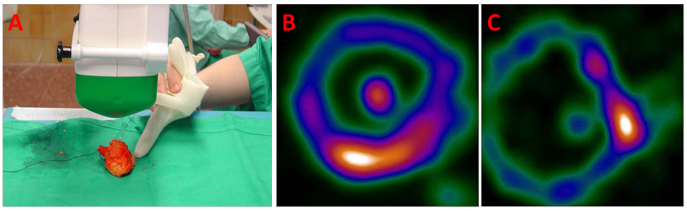

Figure 3.25.: Example of ROLL technique with intra-operative gamma camera [250]. (A) shows gamma camera on top of resected tissue. (B) shows lesion removed in the center and a trace of the movement of a radioactive pointer around the specimen. (C) shows a different case where the lesion is close to the border of the specimen. Image reproduced with permission of Springer.

also 3D approaches are under development in particular with the new C-arm flat panel detector technology which is allowing high quality images which can be then used for 3D reconstruction (e.g. [76]).

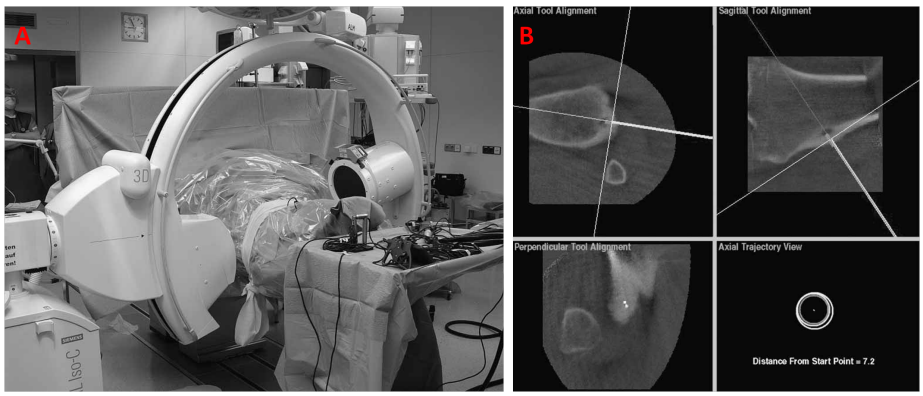

Figure 3.26.: Images from [157] to illustrate use of C-arm for imaging tumor with different X-ray absorption than normal tissue. (A) C-arm used to produce 3D images by rotating around anatomy of interest. (B) intra-operative images show osteoma and position of a tracked instrument. Pictures reproduced with permission of Informa Healthcare.

Intra-operative fluoroscopy systems produce fast images (<0.1s) with high resolution (<0.1mm), but produce a patient dose of up to 1mSv per procedure.

3.3.7. Blood utilization and leakage

Increased blood utilization is one of the further characteristics of cancerous degeneration. The faster metabolic activity of tumor cells results in the growth of first capillaries and later bigger blood vessels to tumors. Similarly blood vessels show a bigger amount of leaking in the proximity of tumors, making their detection easier based on the blood distribution.

In the previous section many methodologies for imaging blood vessels have been explained. Narrow band endoscopy, thermography, fluorescent imaging and Doppler ultrasound for example can be used to image blood vessels showing unusual placement and structure.

In particular the leaking of blood in tumors is used in intra-operative imaging of gliomas (e.g. [101]). The contrast medium used in that case is commonly gadopentetate dimeglumine (also known as Gd-DTPA). This contrast medium is based on Gadolinium ions which are toxic to humans, but are protected by a complex of diethylenetriamine pentaacetic acid. Gadolinium on its own reduces the spin relaxation time of the surrounding tissue due to its paramagnetic nature.

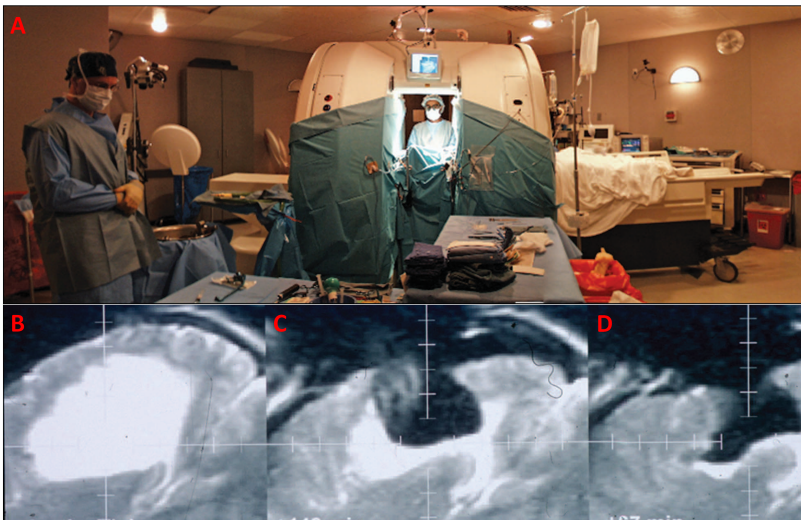

Figure 3.27.: Images from [101] show the first designed intra-operative MRI in 1994 (A) and exemplary images of a glioma contrasted with Gd-DPTA in three different stages of a surgery (B-D). Figures reproduced with permission of Taylor and Francis.

3.3.8. Receptor expression

Receptors are protein molecules embedded in the cell membranes of cells or free in the cytoplasm. They are 'docking' stations of signaling molecules and contribute thus to the cell communication process. Several receptors are over expressed in tumors. Among them somatostatin, gastrin, bombesin, gastrin-releasing peptide, neurotensin, or neuropeptide Y have been discussed in the literature [278]. They are also excellent targets to make cancerous processes visible.

In particular the somatostatin receptor has been widely explored for neuroendocrine tumors. Several tracers are available for it including the somatostatin analogue octreotid (D-Phe-c[Cys-Phe-D-Trp-Lys-Thr-Cys]-Thr(ol)). This analogue can be combined with 1,4,7,10-tetraazacyclododecane-1,4,7,10-tetraacetic acid (also known as DOTA) in order to create complexes that include radioactive isotopes like ^{68}Ga resulting in ^{68}Ga-(DOTA(0)-Phe(1)-Tyr(3))octreotid (or simply ^{68}Ga-DOTATOC). ^{68}Ga is a very interesting isotope which can be produced in Ga-Ge-generators and emitts positrons with an end-point energy of 1899.1keV (88% of the decays). Accordingly, the penetration in tissue may be up to 9mm. The half life of 67.63min of ^{68}Ga allows only a short time for intra-operative use of ^{68}Ga-DOTATOC being images made 30min after injections for up to 4h. The short half time of the isotope results however in a reduced radiation dose in the range of 3mSv. Initial data has been made available to the public by high-energy probe providers on the use of ^{68}Ga-DOTATOC in radio-guided surgery, but no major publication included those cases yet.

In the field of low energy emitters, ^{111}In has also be linked to constructions similar to ^{68}Ga-DOTATOC. Such is the case of ^{111}In-diethylenetriamine pentaacetic acid-D-[Phe1]-octreotid (also known as ^{111}In-DPTA-D-[Phe1]-octreotid, ^{111}In-DPTA-octreotid or simply ^{111}In-octreotid) or In-octreotide [87]. ^{111}In decays with an interesting gamma emission at 171.3keV (90%) and a half life of 2.80d. Biologically imaging of ^{111}In-octreotid is optimal after 24h and can be repeated for some days. In radio-guided surgery early works like the one of Oehrvall et al. [234] showed the feasibility of using unmodified ^{99m}Tc-non-imaging detectors in combination with ^{111}In-octreotid. Currently gamma probes are used in several institutions to locate such tumors [124], however, imaging technologies have not

yet been applied.

3.3.9. Structural changes

Beyond the processes mentioned in the sections above further more complex metabolic pathways may be altered due to cancer. In particular some of them can be put together under the title of processes resulting in structural changes. The most relevant of these approaches are briefly reviewed in the following.

Echogenecity

Ultrasound imaging of echogenecity has been used to tell apart tumor from normal tissue since the very early times of the technique. Changes in echogenecity are complex to be explained and have to be determined from comparison with normal anatomy. Interesting studies like the one of Mauerer et al. [198] have taken systematic approaches to filter out characteristics. The problem in the end is that the surgeon is then obliged to become a good radiologist and make decisions fast (see figure 3.28). Despite this, ultrasound use in the OR is a standard of care in breast cancer, urological malignancies, etc.

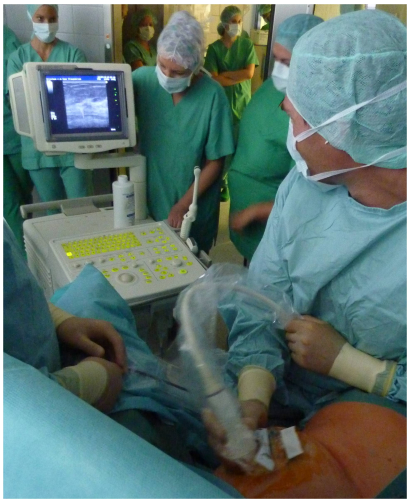

Figure 3.28.: Ultrasonographic analysis of echogenecity of lesion in breast. Patient had next to a biopsy proven breast tumor, two close fibroblastomas. Surgeon used image to clarify the position of tumor relative to the same benignant structures.

As in the case of calcifications, the problem of surgeons requiring a good training in radiology has also been solved by means of the WGL and the ROLL technique. In the particular case that the structure to be marked is a lymph node and the modality used is US, the ROLL technique is called radio-guided ultrasound lymph node localization (RULL) [324].

Elastic properties

Besides echogenecity, ultrasound however can be also used for elastography a further way to visualize changes in structural changes resulting in elastic properties. Making elastography from ultrasound is a relatively new procedure introduced only in the beginning of the nineties (e.g. [239]) and has generated up to date over 1800 hits in PubMed. The concept behind is the fact that ultrasound waves generate tissue compression. This compression produces strain (displacement) in the tissue. The strain on the other hand is a function of the elastic properties of the tissue. In this way, an ultrasound device is capable of imaging strain along the axis of insonation, by analyzing the non-linear component of the backscattered waves a good estimation on the strain can be done [286].

The application of ultrasound elastography in the OR is only in an early stage. Kato et al. [155] or Schloz et al. [293] have introduced this technique intra-operatively in liver and brain surgery.

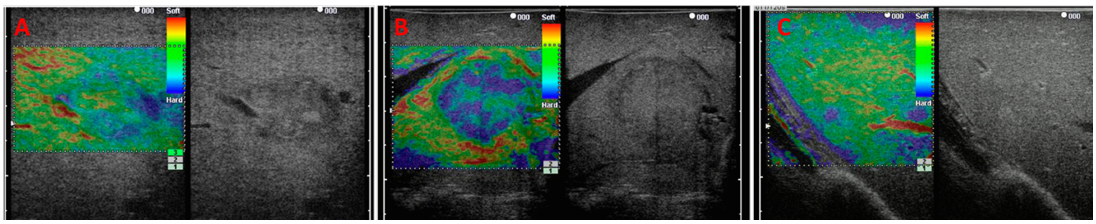

Figure 3.29.: Example of intra-operative elastography of liver. (A) shows elastogram and B-mode ultrasound of a lesion of type 3 showing a mosaic pattern with dominant green areas. (B) shows a tumor with mosaic pattern with dominant blue areas. (C) shows a blue homogeneous lesion with a obscure high-echo in the B-mode scan [155]. Images reproduced with permission of John Wiley and Sons.

There is also some work on other types of elastography for example MR elastography

[142]. There the elastic properties of tissue are also obtained from mechanical vibrations induced by the MR device and analysis of the wave propagation from the imaging data. There is up to date no reference of the use of this technique in an intra-operative setup although it is potentially applicable.

Magnetic spin relaxation

Among the magnetic properties of a given material magnetic spin relaxation plays a fundamental role in magnetic resonance imaging. The magnetic spin relaxation of a given tissue depends on the chemical composition of it, being thus the source of contrast in normal weighted MR images. In oncologic questions, MRI has been used for detection of tumors since the very first human image [77].

In the OR MRI has been used mainly for image-guided resection of brain tumors (e.g. [101, 110]), however some groups have proposed also its use for other pathologies like liver metastases [203] and head and neck cancer [105], in both cases however rather in an interventional setup.

Here the problem of a radiologic training for the surgeon arises, accordingly the WGL and ROLL techniques are also standard since the nineties [306].

Auto-fluorescence

A further example of such abnormal processes is the modification in the amount and distribution of endogenous fluorophores in cancerous cells in relation to healthy tissue. These changes may be used with the aid of proper fluorescent devices to create images where cancerous tissue may be highlighted from normal tissue based on their auto-fluorescence.

The list of fluorophores that play a role in tissue auto-fluorescence includes collagen, elastin, fibrillin, flavin, indolamine (as monomer, dimer and trimer), lipofuscin, NADH (reduced form only) and tryptophan [220].

The use of autofluorescence for intra-operative aid has essentially been restricted to endoscopic procedures (e.g. [161] and figure 3.30), but it is a very active field where also the image processing community has put immense efforts.

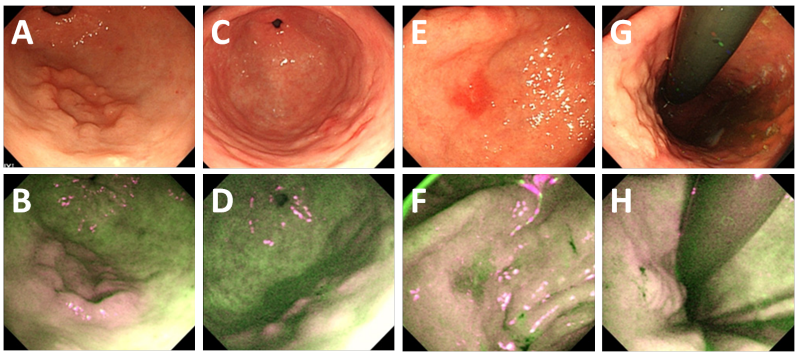

Figure 3.30.: Different patterns of lesions see with white light and autofluorescence false colors. (A) and (B) show a lesion with pink color over green background. (C) and (D) show a pink-greenish lesion over green background. (E) and (F) show a pink-greenish lesion over purple background and finally (G) and (H) a diffuse lesion over purple background. All four patterns cover almost 90 % of all lesions as stated by the authors. Pictures taken from [161] and reproduced with permission of Gut and Liver.

3.3.10. Future applications

Besides the list discussed in the past sections, there are important developments in labeling other functional processes in cancer. Some of them could be used with the current technology for initial testing. In the following some of them will be mentioned together with their biological rationale.

Protein synthesis

Metabolic active cells, as cancerous cells, show also commonly an increased protein synthesis. Especially interesting are essential amino acids or amino acids that are extracted mainly from food. One example of each of them are methionine and tyrosine respectively.

Nuclear medicine approaches to mark these amino acids have resulted in O-(2-^{18}F-fluoroethyl)-L-tyrosine (also known as ^{18}F-FET or simply FET) [370] and [^{11}C-methyl]-L-methionine (also known as ^{11}C-MET or MET) [292]. These tracers have had success mainly in brain tumors as well as head and neck malignancies [251, 357].

Fatty acid metabolism

Following with the major components of cells, fat is a further candidate to visualize abnormal growth. In deed there are sufficient indications that there is an increased metabolism of fatty acids in tumor cells. The major sign is the over expression of fatty acid synthase a key player in the process. This enzyme is over expressed in a variety of tumors, such as breast cancer [18], gastrointestinal stromal tumors [283], melanoma [145], head and neck [304] or prostate cancer [90].

In consequence to this and taking into account the fact that acetate has been shown incorporated in the cellular lipid pool of cancerous cells with increased fat synthesis [318], makes acetate based tracers like ^{11}C-acetate good markers for such metabolic disregulation (e.g. [242]).

Choline metabolism

Choline is a salt that belongs to the essential nutrients for humans. Choline and its metabolites are needed for (a) structural integrity and signaling in cell membranes, (b) neurotransmission and (c) as source for methyl groups in the synthesis of S-adenosylmethionine.

An increased choline concentration in tumor cells has been observed in particular in cancer types like prostatic cancer [133], where sugar metabolism and proliferation are not high. This has resulted in many groups making use of this fact for imaging. Examples are the nuclear tracers ^{11}C-choline [260, 275], ^{18}F-fluoromethyl-choline, and ^{18}F-fluoroethyl-choline [79, 264]. The intra-operative application of such tracers represents an interesting potential, in particular in the detection of metastases.

The choline concentration however can be also imaged from its characteristic peak in MR spectroscopy (MRS). In the case of prostate cancer this has become slowly a standard of care in diagnostics (e.g. [345]). Initial work has been done to perform MRS in the OR [125]. Due to the big logistic issues, this however makes its use restrictive [247].

Hormone production

Hormone producing cells that degenerate to cancer often retain their character and even over express it. Such is the case of catecholamines hormone active tumors.

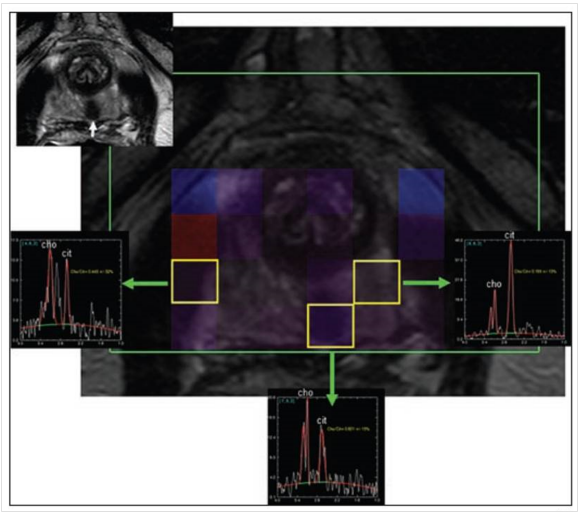

Figure 3.31.: Example of an MR spectroscopic image in prostate cancer from [345]. Depending on the choline to citrate ratio and information on the fat content the choline can be used to localize suspicious regions. Figure reproduced with permission of American Roentgen Ray Society.

Cathecolamines are neurotransmitters like dopamine, norepinephrine (noradrenaline), and epinephrine (adrenaline). Molecules in that pathway have been used in the past in order to visualize this tumors in nuclear medicine. There essentially ^{18}F-L-Dihydroxyphenylalanine (also known as ^{18}F-L-DOPA or FDOPA), ^{131}I-meta-iodobenzylguanidine (also known as ^{131}I-MIBG) and ^{123}I-meta-iodobenzylguanidine (also known as ^{123}I-MIBG play the major role [132].

L-Dihydroxyphenylalanine (L-DOPA) is a precursor of catecholamines on its own [195] while the MIBG compounds are catecholamine analogues that utilize the amine precursor uptake mechanism of such cells and end up being incorporated into vesicles or neurosecretory granules in the cytoplasm [38].

The use of such tracers in the OR has been restricted to radio-guided surgery with non-imaging probes (e.g. [143]).

DNA replication

Uncontrolled growth is found among the symptoms of malignancy. Accordingly labeling tissue growth or consequently cell divisions (cell proliferation) results in a strong tool for localizing tumors in areas with low or controlled growth like the brain. As a pure functional property, the most successful approaches also come from the side of the nuclear medicine on the hand of 3-^{18}F-fluoro-3-deoxy-thymidine (abbreviated as ^{18}F-FLT or simply FLT).

FLT is an analogue of thymidine, one of the four bases of the deoxyribonucleic acid (DNA). Accordingly it is incorporated by cells undergoing DNA replication, fundamental step for cell proliferation [54]. To date FLT has proven to be an excellent tracer for early detection of relapses in several cancer types including lymphoma [51], lung cancer [52], etc.

Angiogenesis

A further potential marker for malignancy is angiogenesis, i.e. the growth of blood vessels. Many particular biochemical conditions can be found in areas where blood vessels are being created or repaired and this is the base for imaging them. Work has been done to define molecules involved in the process. The best results come from the tripeptide ^{18}F-Galacto-RGD. This tracer images the expression of $\alpha_v\beta_3$-integrin [37]. It is expressed on activated endothelial cells as well as some tumor cells. As a result this is in a good marker for angiogenesis.

The group of Beer et al. has shown the usefulness of the tracer in a variety of cancer types including brain tumor [291], breast cancer [36], head and neck cancer [35], etc. However here also a use in the OR has not been reported yet. The possibility of using also low energy tracers like ^{125}I-Gluco-RGD [259] could open doors to intra-operative imaging.

Hypoxia

The increased metabolism often results in lack of oxygen in tumor cells. This fact can also be used as a potential way of localizing tumors. Under hypoxic conditions (lack of oxygen), radicals of nitroimidazoles cannot be re oxidized, which results in a binding of these

to intracellular macromolecules. This prevents the back diffusion across the cell membrane and results in an accumulation [243, 244].

Radioactively labeled nitroimidazoles can be for example ^{18}F-fluoromisonidazole (also called ^{18}F-MISO or simply FMISO) or ^{18}F-fluoroazomycin arabinoside (known also as ^{18}F-FAZA or simply FAZA) [150, 261]. They have shown good results imaging hypoxia in head and neck cancer [175, 311], brain tumors [319], lung cancer [112], etc. A similar approach is the one of ^{64}Cu-Cu(II)-diacetyl-bis(N4-methylthiosemicarbazone) (^{64}Cu-ATSM or Cu-ATSM) and relative biomolecules [109, 140].

A different approach to image oxygenation of tissue is using the so called blood oxygen level-dependent (BOLD) MRI. In BOLD MRI, a type of functional MRI imaging introduced in the early nineties [236], changes in the amount of oxygen that is bound to hemoglobin molecules in tissue is measured.

Liu et al have used this techniques for intra-operative guidance of operations, but there rather to visualize the active areas of the motor cortex that should be kept from harm in neurosurgery [194]. Although not used as method for localizing tumors, it is thinkable to go for hypoxia imaging during interventions in the tumor types mentioned before.

3.3.11. Summary

In the last subsections several approaches for making cancer visible in the OR were presented and potential extensions were discussed. Table 3.32 summarizes the approaches that are being used in the OR at different levels.

	Tracer			Technology										General		
Process	Name	Injection [min]	Wash out [h]	Name	Resolution [mm]	Penetration [mm]	Field of view [cm2]	Dimensions	Acquisition time [s]	Radiation [mSv]	Weight [g]	Flexible movement	Wire	Investment [kEUR]	Cost p.pt. [EUR]	Clinical acceptance
Sugar metabolism	FDG	>45	<6	Beta probe	<5	<2	1x1	1D	<1	<7	100-200	Yes	Yes/No	10-40	~500	Initial
	FDG	>45	<6	Beta camera	<5	<2	3x3	2D	<5	<7	150-300	Yes	Yes	30-60	~500	Trial
	FDG	>45	<6	PET gamma probe	<10	<500	1x1	1D	<1	<7	200-400	Yes	Yes/No	15-40	~500	Initial
	Tc99m-ECDG	>30	>24	Gamma probe	<5	<70	1x1	1D	<1	<3	100-200	Yes	Yes/No	10-40	?	Trial
	Tc99m-ECDG	>30	>24	Gamma camera	<5	<100	5x5*	2D	<20	<3	1500-4000	Yes/No+	Yes	50-70	?	Hypothetical
	NIR-DG	>1000	>24	Fluorescence camera	<1	<20	5x5*	2D	<2	0	200-400	Yes/No+	Yes	30-100	?	Trial
Mitochondrial activity	None	n/a	n/a	Thermal camera	<2	<3	5x5*	2D	<1	0	200-400	Yes/No+	Yes	30-50	0	Trial
	MIBI	>180	>24	Gamma probe	<5	<70	1x1	1D	<1	<7	100-200	Yes	Yes/No	10-40	~200	Standard
	MIBI	>180	>24	Gamma camera	<5	<100	5x5*	2D	<20	<7	1500-4000	Yes/No+	Yes	50-70	~200	Trial
Iodine metabolism	I123	>1000	>48	Gamma probe	<5	<70	1x1	1D	<1	<1	100-200	Yes	Yes/No	10-40	?	Trial
	I123	>1000	>48	Gamma camera	<5	<100	5x5*	2D	<20	<1	1500-4000	Yes/No+	Yes	50-70	?	Hypothetical
	I131	>3000	>72	I131 gamma probe	<7	<300	1x1	1D	<1	<15	150-300	Yes	Yes/No	15-40	?	Initial
Osteogenesis	Tc99m-HDP,-DPD or -MDP	>180	>24	Gamma probe	<5	<70	1x1	1D	<1	<3	100-200	Yes	Yes/No	10-40	~100	Initial
	Tc99m-HDP,-DPD or -MDP	>180	>24	Gamma camera	<5	<100	5x5*	2D	<20	<3	1500-4000	Yes/No+	Yes	50-70	~100	Trial
Haem production	5-ALA	>180	>5	Fluorescence camera	<1	<5	5x5*	2D	<1	0	200-400	Yes/No+	Yes	30-100	~300	Extended
Calcification	None	n/a	n/a	Fluoroscopy	<1	<200	20x20	2D	<0.1	0	n/a	No	n/a	100-200	0	Initial
	None	n/a	n/a	IO CT	<1	<200	20x20	3D	<2	0	n/a	No	n/a	300-400	~200	Trial
	Tc99m-colloid (ROLL)	<5	>24	Gamma probe	<5	<70	1x1	1D	<1	<0.2	100-200	Yes	Yes/No	10-40	~200	Extended
	Tc99m-colloid (ROLL)	<5	>24	Gamma camera	<5	<100	5x5*	2D	<10	<0.2	1500-4000	Yes/No+	Yes	50-70	~200	Initial
Blood utilization	None	n/a	n/a	Narrow band imaging	<1	<1	2x2	2D	<1	0	400-600	Yes	Yes	50-100	0	Initial
	None	n/a	n/a	IO Doppler US	<1	<70	7x7	2D/3D	<1	0	100-200	Yes	Yes	70-130	0	Initial
	None	n/a	n/a	Thermal camera	<2	<3	5x5*	2D	<1	0	200-400	Yes/No+	Yes	30-50	0	Trial
	Microbubbles	<5	<0.1	IO US	<1	<70	7x7	2D/3D	<1	0	100-200	Yes	Yes	70-130	0	Trial
	ICG	<0.1	<1	Fluorescence camera	<1	<20	5x5*	2D	<1	0	200-400	Yes/No+	Yes	30-100	~90	Trial
Somatostatin expression	Ga68-DOTATOC	>30	<4	PET gamma probe	<10	<500	1x1	1D	<1	<3	200-400	Yes	Yes/No	15-40	?	Hypothetical
	Ga68-DOTATOC	>30	<4	Beta camera	<5	<2	3x3	2D	<1	<3	150-300	Yes	Yes	30-60	?	Hypothetical
	In111-octreotid	>1000	>24	Gamma probe	<5	<70	1x1	1D	<1	<7	100-200	Yes	Yes/No	10-40	~600	Extended
	In111-octreotid	>1000	>24	Gamma camera	<5	<100	5x5*	2D	<20	<7	1500-4000	Yes/No+	Yes	50-70	~600	Hypothetical
Blood leak	Gd-DPTA	>10	<2	IO MR	<1	<200	20x20	3D	<120	0	n/a	No	n/a	1000-2000	~1000	Initial
Structural changes (autofluorescence)	None	n/a	n/a	Fluorescence camera	<1	<1	5x5*	2D	<1	0	200-400	Yes/No+	Yes	30-100	0	Extended
Structural changes (echogenecity)	None	n/a	n/a	IO US	<1	<70	7x7	2D/3D	<1	0	100-200	Yes	Yes	70-130	0	Standard
	Tc99m-colloid (ROLL/RULL)	<5	>24	Gamma probe	<5	<70	1x1	1D	<1	<0.2	100-200	Yes	Yes/No	10-40	~100	Extended
	Tc99m-colloid (ROLL/RULL)	<5	>24	Gamma camera	<5	<100	5x5*	2D	<10	<0.2	1500-4000	Yes/No+	Yes	50-70	~100	Initial
Structural changes (magnetic spin relaxation)	None	n/a	n/a	IO MR	<1	<200	20x20	3D	<120	0	n/a	No	n/a	1000-2000	~1000	Trial
	Tc99m-colloid (ROLL)	<5	>24	Gamma probe	<5	<70	1x1	1D	<1	<0.2	100-200	Yes	Yes/No	10-40	~500	Extended
	Tc99m-colloid (ROLL)	<5	>24	Gamma camera	<5	<100	5x5*	2D	<10	<0.2	1500-4000	Yes/No+	Yes	50-70	~500	Initial

* Arm-mounted solution may achieve easily fields of view of 10x10 cm2

+ Arm-mounted solution cannot be considered for handheld use

Figure 3.32.: Summary of approaches for intra-operative tumor and metastasis imaging. Technologies, prices, etc. are estimated from the results of searches in PubMed and commercial companies at the date of creation of the table. Running costs are essentially the costs for the tracers and the requirements of the equipment.

Part II.

Proposed solution and used technology and methods

Chapter 4

Proposed solution

Intraoperative functional imaging is in its baby shoes and constraints on it are not minimal. Nevertheless the conventional approach does not have to be the only one. Solutions and in particular innovative solutions come often from combination of previously not combined technologies or from porting solutions from different fields.

4.1. Introduction

Intuition brings often surprises with it, but it requires also a good deal of perseverance to become successful. Back in 2004 that was actually the case. Prof. Nassir Navab had been recently appointed Professor at the Technische Universität (TUM) and he was interested in intraoperative applications. As Prof. Markus Schwaiger, from the Nuclear Medicine Department of TUM, was involved in that appointment, Prof. Navab ended up discussing with the Nuclear Medicine people and in particular with Dr. Sibylle Ziegler (now also Professor), Dr. Maria Burian (Department of Surgery), Dr. Guenter Meissetschlaeger and Dr. Morand Piert who were involved then in the evaluation of beta probes for control of resection borders in cancer surgery .

The topic was tempting and promising. First, cancer was the number two killing cause in developed countries. Second, beta probes were a novel intersting and elegant instrument. The concept behind them was extremely straight forward. Tumors have a higher metabolic activity than most healthy tissue and metabolize accordingly more sugar [309]. Sugar on

the other hand could be made radioactive and one particular radioactive sugar, FDG had shown an impressive uptake and excellent tumor to background ratio in almost every cancer type [113, 257]. If this radioactive sugar could be then detected intraoperatively, tumor surgery could be performed guided with functional information.

As described in chapter 3, beta probes were especially designed for such means. The major problem of these devices was however, the one dimensional nature of the data provided and the resulting difficulty to evaluate the readings in a wider context and without the need of a 'good' spatial memory.

For our group the solution to such problems was clear. The use of tracking systems for acquiring the position and orientation of the beta probes during the border control could be used to generate an intraoperative distribution of activity on the scanned surface. This distribution could then be superimposed onto the view of the surgical scene and thus be used to guide the surgeon in the task of detecting the cancer cells with high FDG and thus high metabolic activity uptake.

The implementation of such project was handed to Joerg Traub (now PhD) and me (both members of the group at the Faculty of Computer Science) by the beginning of 2005. By February 2006 a system combining beta probes and tracking was running. The device allowed imaging radioactive surfaces and visualize them overlaid on the video of a tracked camera (see figure 4.1 and [364]).

It was at that time that Prof. Navab met Dr. Farhad Daghighian (IntraMedical Imaging, LLC, Los Angeles, California, USA) in Palm Springs and they came to the idea of testing the combination of gamma probes and tracking in order to generate 3D nuclear images in the OR. The idea was old in deed, since 1989, people had already proposed using radioactive detectors and navigation systems [130]. It was probably however Dr. Irving Weinberg (PEM Technologies Inc., Rockville, Maryland, USA) who first drafted the concept of doing imaging using tracked radiation detectors [358] (see figure 4.2), being by far the first implementation by the group of Prof. José María Benlloch (Instituto de Física Corpuscular, Valencia, Spain) shortly after [39]. Prof. Benlloch's concept was directly derived from Computer Vision. His team had an operational mini gamma camera, which he added tracking markers in order to position it at particular orientations from an object. The images generated by the camera in each position and the information on the position itself

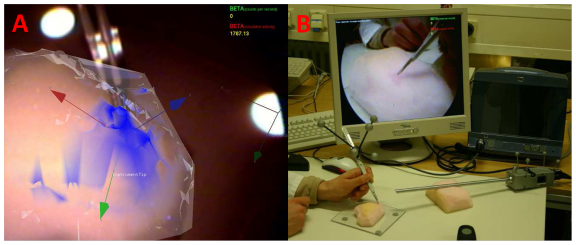

Figure 4.1.: Augmented reality visualization of the acquired activity of a phantom's surface beta activity. Blue is high measured activity, white is low. The upper number shows the measures of the real beta probe (which was turned off after acquisition), the lower number shows the simulated activity at the tip of the instrument. On the right side the same scene as on the left is seen from outside showing the simulated activity with the beta probe control unit turned off [364].

was then used to find correspondences between hot spots and calculate the 3D position of these by triangulation. The results ended up in two Spanish patents and a paper, but was abandoned then.

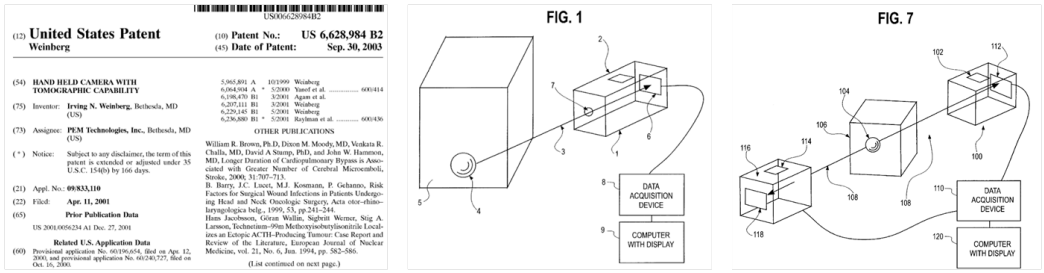

Figure 4.2.: Patent by Dr. Irving Weinberg as published back in 2003 showing tracked gamma hand held cameras for 3D reconstruction, both in a single photon setup (fig.1) as well as in a coincidence imaging setup (fig.7) [358].

The idea of Dr. Daghighian and Prof. Navab was however slightly different from the implementation of Prof. Benlloch. They considered using the readings of a tracked gamma probe moved with the freehand, instead of gamma cameras, in order to generate an image. As they did not believe that this could be possible, due to the ill-posedness of the approach, Nassir recommended using the readings not for reconstruction, but rather for registration

of intraoperative readings of a gamma probe and preoperative images.

Registration of preoperative images with gamma probe readings was a complex problem on its own. Following the conventional approach used in X-ray/CT registration, the way to go would be to (a) project the 3D preoperative image in order to generate 'virtual' readings of a gamma probe, and then (b) minimize the distance between real and virtual readings by changing a transformation between the coordinate system of the image and the one of the tracking system (figure 4.3).

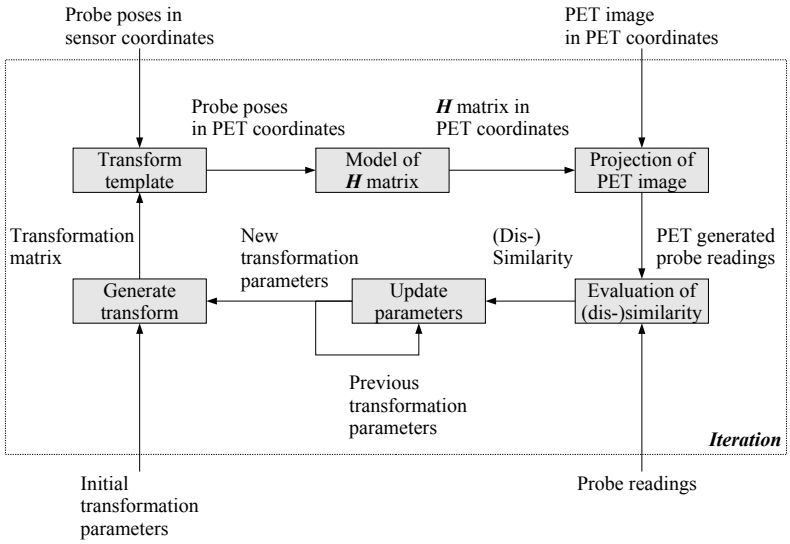

Figure 4.3.: Registration of tracked gamma probe readings with preoperative images (here PET images). As the images used are PET images, the gamma probe to be used is a high energy gamma probe. Figure taken from [361]

Another approach for the registration was to perform it completely in 3D. In that case the tracked gamma probe readings were meant to be reconstructed into a 3D image, which then be registered with the preoperative image. Actually nobody believed such approach would have a chance, but it was then that the spark of inspiration shined. Why not try it at least?

It took a couple of dark months to have the first implementation running. By December 2006 the first images were there, yet not really clear enough to speak of success, but there. In March 2007 within the last two weeks before the deadline of MICCAI 2007, a conference

to be hosted in Brisbane, Australia, and with the help of Tobias Lasser, finally 4 hot spots of radioactivity shined on the monitor of the system, the first evidently correct images of what would be later called freehand SPECT were there (see figure 4.4 and [362]).

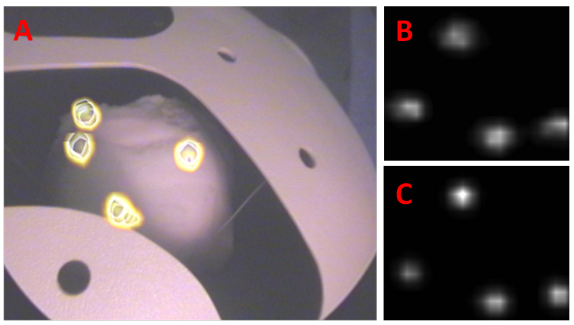

Figure 4.4.: (A) First reconstructed 4 hot spots using freehand SPECT overlaid on the video image of a tracked laparoscope. (B) reconstructed slice using freehand SPECT concept vs. (C) corresponding PET slice [362]. The spots were double marked with ^{99m}Tc and ^{18}F allowing to validate the low energy spots reconstructed with freehand SPECT with PET.

4.2. Image generation in 3D preoperative imaging

Freehand SPECT is only one example of a completely new approach of 3D functional imaging. Such imaging combines all advantages of preoperative 3D imaging and non-imaging or 2D intraoperative probes. It also fulfills intrinsically many of the constraints analyzed during the last chapters.

The key for such an imaging approach lies within the way of generating fully tomographic data sets from projections. Tomography in medical imaging has been exploited widely in the past. X-ray computed tomography (CT) for example uses a full set of 2D X-ray projections acquired around the object of interest. This set of projections is then 'back projected' in order to generate 3D images. Similar is the approach used in SPECT imaging. There the projections are planar scintigraphic images and commonly the algorithms used are more sophisticated than the back projection methods used in CT. The reason for the need of more complex algorithms to generate 3D images from a set of 2D scintigra-

phies comes from the fact that the mathematical assumptions on the projections diverge too much from the ones valid in most cases in reality, besides perhaps in the case of CT.

Algorithms meant to generate 3D images from projections are often referred to as reconstruction algorithms. The problem to be solved by those algorithms in mathematical terms is the determination of a function f in 3D given a set of projections functions g_T in 2D. f is normally a scalar function of space ($f(\vec{p})$), g_T is on its own a function of two parameters (x, y) and of course on the relative position it was acquired from T in relation to the coordinate system used for f. Typical functions f can be the X-ray attenuation, the radioactivity concentration, the echogenecity distribution, the fluorescence density, etc. The images g_T are directly related to f being for the latter examples 2D images of the transmitted X-rays, the detected radioactive emissions, the reflected echo or the emitted fluorescent light.

Finally reconstruction algorithms can be stated as problems where the equation

$$g_T(x, y) = h(f(T(\vec{p}))) \tag{4.1}$$

has to be inverted. The mapping h tells the way the desired function $f(\vec{p})$ has an influence on the detected signal g_T. In mathematical terms the mapping h takes a volume of interest in space $ROI \subset \Re^3$ and brings it to 2D projections, i.e. $\Re_0^+ \times \Re_0^+$:

$$h : ROI \mapsto \Re_0^+ \times \Re_0^+ \tag{4.2}$$

Accordingly it is strongly dependent on the modality to be considered: the detection process, the signal propagation, the interaction of the signal with the body, etc. In order to give an example a fairly good model for the mapping of the X-ray attenuation distribution inside a body generated by a point source X-ray is given by:

$$g_T(x, y) = I_0 \exp\left\{-\int_{S(x,y)} f(T(\vec{p}))ds\right\} \tag{4.3}$$

where $S(x, y)$ is the line from the emission source and the detector element (x, y), I_0 is the intensity of the X-ray source and $f(T(\vec{p}))$ is the X-ray attenuation in the coordinate system of the detector.

In preoperative imaging, depending on the type of acquisition, two radical different approaches are available for inverting such mappings from a set of 2D images $\{g_i\}$: analytic

and iterative reconstructions. The first is fundamentally used in cases when the projection set is a complete and dense set as they base on geometry. The back projection algorithm is a classical example of it. For the given X-ray point source imaging case mentioned above, the inversion of the given mapping is given by:

$$f(\vec{p}) = \iint_{\Omega(\vec{p})} \left\{ \ln\left(-\frac{g_{T(\omega)}(x,y)}{I_0} \right) d^2\vec{\omega} \right\} \tag{4.4}$$

where $\Omega(\vec{p})$ is a the half sphere around point $\vec{p}$ and $g_T(\omega)$ are 2D projections on the said half sphere.

In contrast to analytic reconstruction methods, iterative reconstruction methods allow more flexibility with worse performance in terms of computational burden. They require a discrete problem statement. In practical terms, since the projections are in general acquired by array sensors, the functions g_T are discrete functions defined only in a finite number of points, i.e. g_i for a finite set of i. For the function to be reconstructed f, a basis function ϕ is used to discretize the problem. The discrete values of f at position $\vec{p}_j$, denominated f_j can be interpreted as

$$f_j = \int \phi(\vec{p} - \vec{p}_j) f(\vec{p}) d^3\vec{p}. \tag{4.5}$$

Figure 4.5 shows such a discretization using a pulse function for ϕ.

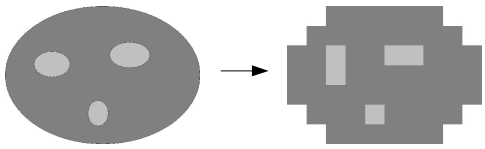

Figure 4.5.: Discretization of the volume distribution to be determined, here a 2D example.

Given this discretization and assuming a linear relation between the reconstructed volume and the projections, the problem of reconstructing an image from projections can be stated in terms of

$$\vec{g} = \mathbf{H}\vec{f}, \tag{4.6}$$

where all variables are vectors or matrices. In particular, $\vec{g}$ orders in one vector all N_{meas} values of all projections g_i[1], $\vec{f}$ groups all N_{pos} values f_j of the volume to be reconstructed (as shown in figure 4.6) and **H** is the so called system matrix of the acquisition system of dimension $N_{meas} \times N_{pos}$. Each element of the system matrix describes the linear contribution of each volume element to each projection element.

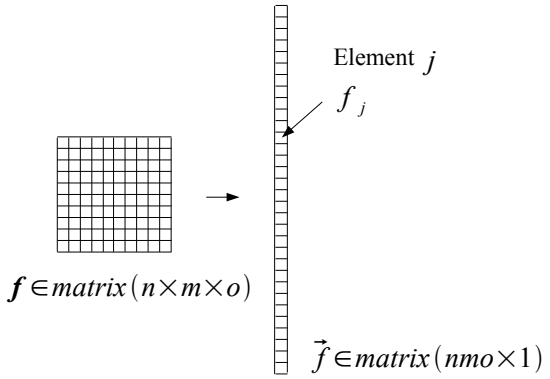

Figure 4.6.: Reshaping of volume into a vector. Here $nmo = N_{pos}$.

The reconstruction problem is then, as posed above, the problem of solving a linear equation system and it is here were iterative reconstruction algorithms can offer solutions. For the sake of discretization the problem is stated as a set of equations:

$$g_i = H_{i,j} f_j. \tag{4.7}$$

Probably the most well known iterative reconstruction algorithm is the algebraic reconstruction technique (ART). There the algorithm of reconstruction considers every projection as a constrain to the set of possible solution and modifies it in order to satisfy the said constraint. In the absence of errors and noise, the use of every projection on the previously modified solution iteratively converges to a solution where all constraints are satisfied. Figure 4.7 shows this for a two projection case.

In practical terms the ART reconstruction reduces to an iterative formula where the update of the solution is done by adding a term proportional to the subtractive error for each

[1] N_{meas} is the multiplication of the number of projections times the amount of pixels/projection elements of them.

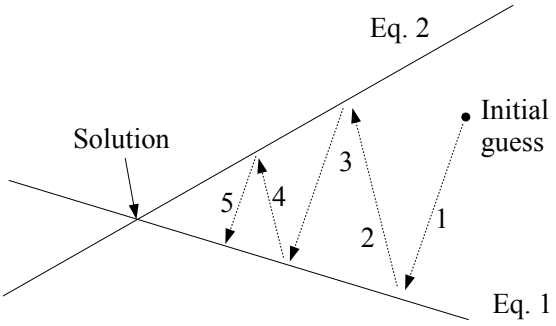

Figure 4.7.: Algebraic reconstruction technique (ART). Each projection implies a constraint, here shown by an equation. The solution is when both equations are satisfied. Starting with an initial guess the algorithm moves the solution to satisfy equation 1. Then it moves to fit equation 2 and so iteratively until the solution is met.

projection in each iteration. One has

$$f_j^{(n+1)} = f_j^{(n)} + H_{i,j}\left(g_i - \eta(n)\sum_k H_{i,k} f_k^{(n)}\right)\left(\sum_k H_{i,k}^2\right)^{-1}, \tag{4.8}$$

where $H_{i,j}$ is the entry at row i and column j of $\mathbf{H}$ and η is a so called relaxation factor that commonly is reduced for increasing iteration number, i.e. $\eta(n)$ is a monotonically decreasing positive function. $f_j^{(n)}$ is the value of f_j as calculated by the algorithm in iteration n. In the case of ART, all voxels are updated simultaneously with each projection.

Both analytic and iterative reconstruction problems however are as inversion techniques dependent on a proper sampling and suceptible to noise. In preoperative imaging this problem is attacked from different sides: the acquisition, the model and the reconstruction algorithm.

On the side of the acquisition, the best way of guaranteeing a proper reconstruction is providing a full set of projections. In the case of axial CT for example projections are acquired covering 180 degrees in equidistant steps of a circular trajectory. In SPECT up to three planar gamma cameras allow acquiring also projections covering 360 degrees in constant steps [366]. The technical implementation relies on gantries along which the detectors rotate.

Is such an acquisition not possible, then one speaks of limited-angle tomography, where projections are missing and some prior information is needed to avoid artifacts [30, 147]. Yet in those approaches the images are commonly acquired in equidistant steps and following a symmetric trajectory using specialized gantries.

More interesting is the case of non-circular trajectories used in state-of-the-art SPECT devices. In those cases, for each step the detector is placed as close to the object of interest as possible. The resulting trajectory is similar to an ellipse, but might not necessarily be one [14, 330]. Further interesting approaches are the ones of the company Spectrum Dynamics, Haifa, Israel, where small gamma cameras sweep over the heart of a patient and generate 3D images of it from a quasi-symmetric set.

Longer, homogeneous or denser sampled acquisitions are also a proper approach to improve the quality of reconstructions as seen in clinical protocols of PET and SPECT, where the acquisition time is a function of the expected uptake and the desired signal to noise ratio. All these result, however, in additional time which plays a negative role in terms of motion artifacts and logistics.

The use of gantries brings in it a further advantage, the region to be reconstructed can be easily defined. For most preoperative systems the region to be reconstructed is merely a cylinder with the radius of the accessible space of the gantry and a length which is selected by the operator of the device depending on the anatomy to be scanned. Some systems include a 'topographic' image (i.e. image for means of orientation in relation to the topography patient) to help on the latter selection. That image is a very fast 2D anatomical image (for example in CT or MR devices) used to select the region to be reconstructed before a time consuming or radiation involving 3D acquisition.

On the side of the model, as normally the reconstruction problem represents an ill posed problem, it is of fundamental importance that the information provided in the system matrix is sufficient for a valid reconstruction (for example on effect of errors in modeling on reconstruction see [266]), the geometry of the detectors (e.g. [189, 258, 267]), the detection process (e.g. [189, 313]) and the interactions of the gamma rays with the body can be modeled analytically [219, 240, 343] or simply acquired point-by-point (e.g. [249]).

Finally the reconstruction algorithm can be used to improve quality too. The more additional information on the object or the physical process to be reconstructed is added,

the better the results are. For example if a nuclear image is to be reconstructed with an iterative method, generally the maximum-likelihood estimation maximization (ML-EM) would perform better than merely algebraic methods like ART as it includes information on the Poisson nature of the detection process [343].

Another strategy is to include information on the anatomy. This was the case in old PET or SPECT devices which used a so called transmission scan introduced in the fifties for SPECT [177]. Current PET/CT and SPECT/CT use the CT for attenuation correction and constraining the reconstructed images as proposed already for the first hybrid imagers [163].

4.3. From preoperative to intraoperative 3D imaging

The reconstruction approach presented before is essentially general. Adapting it to the constraints of intraoperative functional imaging would yield an intraoperative 3D functional imaging system.

The major constraint and resulting change comes from logistics. As described in details in chapter 2 workflow changes are hard to carry out and result in dead ends for innovation. In that sense approaches involving big hardware and changing the access of the surgeon to the patient are unlikely to be successfully integrated in the OR. From the analysis in the state-of-the-art chapter the technologies that fulfill this constraint are either hand held or arm-mounted devices. The use of those technologies for 3D imaging, however brings with it a major issue if meant to be used for OR: there is no gantry. Accordingly it is not possible without further hardware to determine the relative position of the projections to the region to be reconstructed. Moreover and more important it is complicated if not completely impossible to obtain symmetric and complete sets of projections (see figure 4.8).

In order to solve this issue the approach of our group in 2004 could be used. A positioning sensor could be fixed to the detector and its position could be acquired simultaneously with its reading. In the case of arm mounted systems, even a robotic solution could be an option. In any of both cases, a proper synchronization between positioning information and read-out is of course of major relevance.

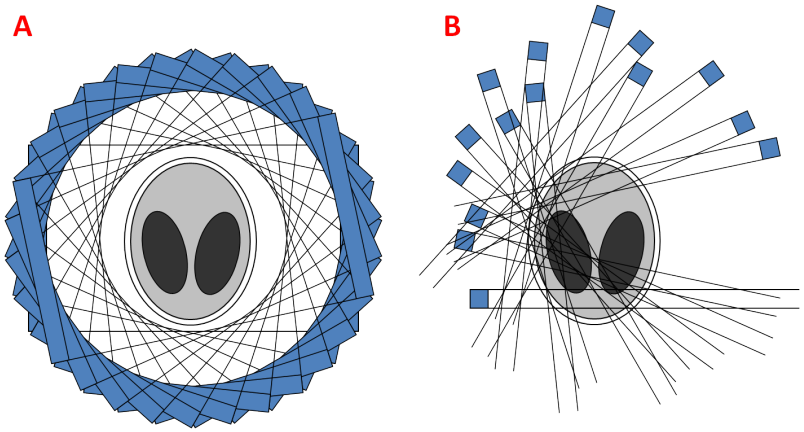

Figure 4.8.: Comparison of projections for a gantry based system (A) and a 'freehand' acquisition system (B), i.e. arm-mounted systems or hand-held systems. Normally gantry systems have a big field of view, allow the acquisition of a complete set of projections, however cannot come too close to anatomy. In contrast, in a 'freehand' acquisition system the field of view of the detector is small, the projections are far from symmetric however can be taken very close to the anatomy.

The loss of symmetry automatically makes it probably impossible to use analytic approaches for reconstruction. The problem is however that iterative methods cannot be applied directly as it becomes very hard to precompute entries of the system matrix as the relative position of the region to be reconstructed and the detector is not known before the acquisition starts.

Leaving out the gantry implies also changes in the used detectors. If the detectors are meant to be hand-held a maximum weight of 500g is tolerable. In the case of arm mounted systems a maximum weight could be in the range of 5 to 10kg. Changes in weight imply changes in size and with it the possibility of coming closer to the anatomy of interest and the reduction of the field of view, what at the end also reduces the amount of acquired information.

In summary the changes resulting from abandoning the gantry concept are displayed in table 4.1.

In the following only the hand-held devices will be considered for 3D functional imaging in the OR as they are the main topic of this thesis. The reason is that they are farther away from conventional preoperative functional imaging. The constraints for them are significantly harder, than the ones of arm-mounted systems. From tables 3.9, 3.17 and 3.32 the available hand-held technologies can be seen in figure 4.9.

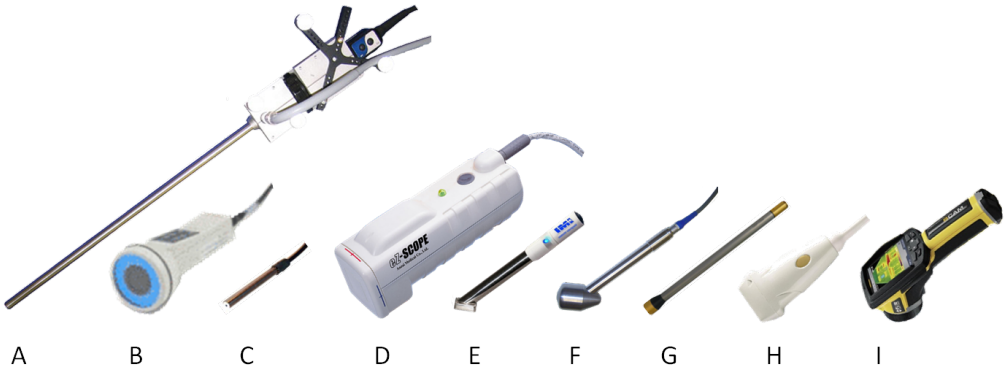

Figure 4.9.: Commercially available hand-held systems for intraoperative use: (A) optical camera, capable of narrow band imaging, (B) fluorescence camera, (C) optical spectrometer, (D) mini gamma camera, (E) beta camera, (F) gamma probe, (G) beta probe, (H) ultrasound probe and (I) thermal camera.

Property	Gantry-based imaging	Arm-mounted imaging	Hand-held imaging
Angle coverage of projections	Full angle	Limited angle	Limited angle
Symmetry of projections	Per construction	Only if robotized	Impossible
Calculation of relative position of projections	Per construction	Using tracking	Using tracking
Weight of detector	Irrelevant	<5kg	<500g
Applicable reconstruction algorithm	Analytic or iterative	Iterative	Iterative
Definition of region to be reconstructed	Simple, based on bed length or topogram	Depends on acquisition	Depends on acquisition
Precomputation of system matrix for iterative reconstruction	Possible	Only if robotized	Impossible
Field of view of detector	normally 20x20cm^2	max. 10x10cm^2	max. 5x5cm^2
Statistics of acquired data	High	Medium	Low
Distance between detector and anatomy	Far	Close	Close or Invasive
Dimensionality of detector	3D	3D* or 2D	3D*, 2D or 1D

Table 4.1.: Comparison of properties between gantry based intraoperative imaging systems, arm-mounted systems and hand-held systems. (*) 3D systems that are arm-mounted or hand held are rare. An example would be 3D US or aperture coded gamma cameras.

4.4. 3D functional imaging with tracked probes

In the last section the gantry of conventional 3D imaging systems was abandoned in order to enable workflow integrated intraoperative imaging. In this section the different steps of image reconstruction are considered given the starting point that the detectors used are hand-held.

4.4.1. System architecture

The combination of tracking technologies and hand-held detectors for 3D imaging results in changes in the system architecture of the 3D imaging system. The components proposed by our group were a hand held detector with means for being detected, a tracking system capable of determining the position of a hand held detector, a data processing unit capable of collecting the read-out of the detector and the tracking system, process it and generate an image to be visualized in a display unit (see figure 4.10).

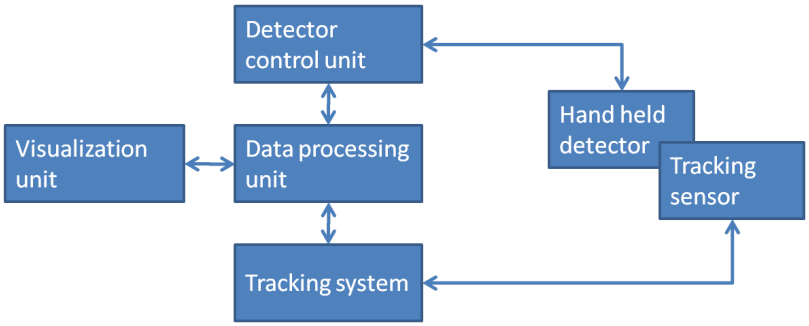

Figure 4.10.: Architecture for 3D functional imaging with hand held detectors as proposed in this work.

Clearly the hand-held detector does not need to have a proper sensor as such if the tracking system is capable of figuring out its position by other means, like for example from image recognition if the used tracking system is based on optical cameras. Nevertheless in most cases, the existance of a tracking sensor would be given.

4.4.2. Dimensionality of the problem

From the discussions above the options for image reconstruction are restricted to iterative reconstruction approaches. The reconstruction problem is then stated accordingly to equation 4.7. In case of 1D detectors g_i is a single value, and i is an integer related to a time t_i. As a result **H** has a row for each acquisition (N_{meas} measurements) and a column for each voxel (N_{pos}) in space to be reconstructed (see figure 4.11).

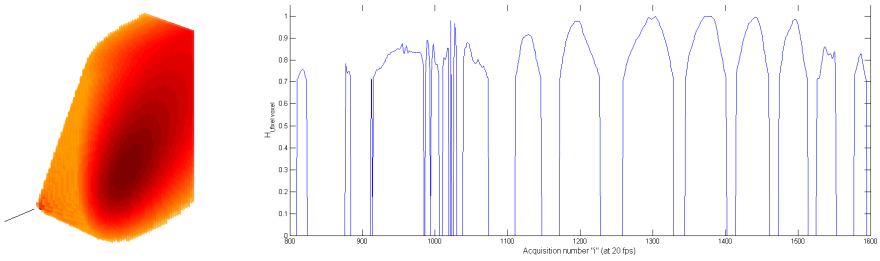

Figure 4.11.: Left: Single row of a system matrix for a nuclear probe. The line is meant to symbolize the position of the gamma probe. The color gives the value of the $H_{i,j}$: darker means higher value and lighter less. Discretization used is 5mm in a volume of 300x300x300mm^3. Right: Column of same system matrix for 800 measurements at 20fps. Sharp drops of signal have to do with the total absorption of collimator.

In case of 2D detectors g_i is an image of $S_x \times S_y$ in 2D acquired at time t_i. The system matrix has then $S_x S_y \times N_{meas}$ rows and N_{pos} columns.

4.4.3. Definition of region to be reconstructed

One aspect mentioned during the analysis of the difference between gantry-based and freehand systems was the fact that the region to be reconstructed is not trivially defined. The problem has its origin it the lack of a natural origin for space coordinates. Ideally such origin would be the patient, but even in case the patient is tracked using tracking sensors, the relation between the positioning sensor and the region to be reconstructed in the patient has to be defined.

There are many approaches to solve this issue. The first and most trivial is the fixation of the positioning sensor at a known position relative to the anatomy. This solution despite

being simple and easily applicable is very suceptible to user errors. Placing the tracking sensor slightly tilted would tilt the complete region to be reconstructed in relation to the real anatomy.

A better solution is the 'calibration' of the volume of interest. This can be done by touching with a tracked pointer on anatomical points on the body of the patient and then calculating from the 3D coordinates of those points the region to be reconstructed. An example of that implementation was used during the major part of this work (e.g. figure 4.12).

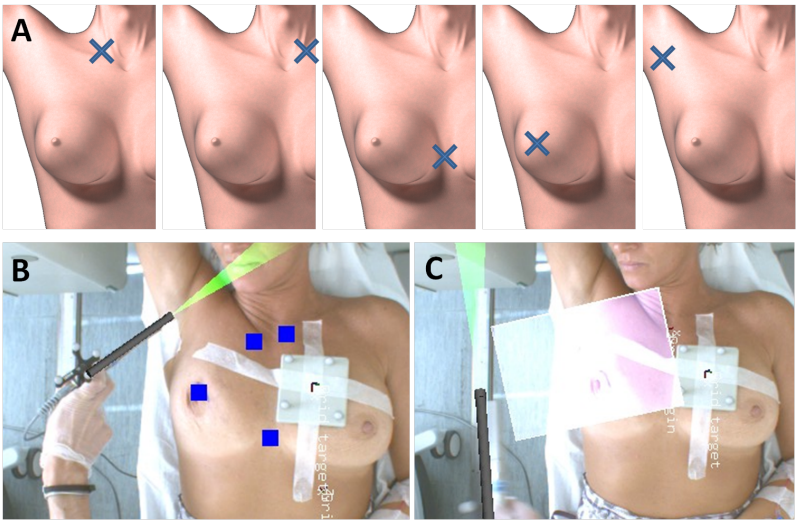

Figure 4.12.: (A) shows landmark points used for the definition of a region to be reconstructed for SLNB in breast cancer. (B) shows the procedure of clicking on a patient with a tracked pointer, here a gamma probe (blue points) and (C) the resulting region to be reconstructed overlaid on the video image.

A more intelligent solution for defining the volume of interest is to use a measure to rate the amount of information collected while scanning for a region in space. The volume of interest would then be the area having a minimal amount of information in terms of $||H||_2$. A possible implementation for a rectangular volume of interest is shown in figure 4.13.

Such idea can be extended to non-rectangular regions of interest by defining the volume of interest as a list with positions in space where the information amount is above a threshold. The threshold will be of course highly dependent on the type of information collected.

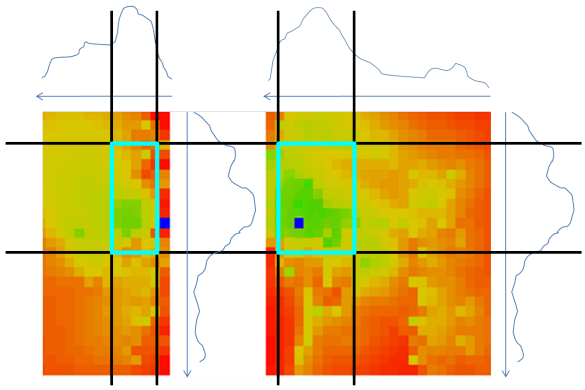

Figure 4.13.: Automatic calculation of rectangular volume of interest from information collected during a freehand scan. Images show the collected information as scalar value, being green areas with high amount of information and red areas with little or no information. By projecting this information in each axis and applying a threshold, a rectangle in cyan can be selected as area of interest.

There are however problems hidden in this approach. The reasoning behind it is that regions with little information are not of interest and do not have to be considered for imaging. However, if an unexperienced user does not cover the region of real interest, such will not be considered. Also artifacts may arise if the region scanned does not contain the source of the detected signal. These issues will be discussed in the exemplary implementation of the proposed 3D functional imaging approach in Part III.

4.4.4. Calculation of the system matrix

As stated in the last section, for hand held detectors, it is not possible to precalculate the system matrix. The reason is quite logic: the movement is freehand and cannot be predicted. As a result a 3D imaging system as described here has to be able to calculate its system matrix 'on the fly'.

As the system matrix plays an extremely relevant role on the result, the calculation of system matrices on the fly has to be as precise as possible and include as much information as available, while at the same time being simple and fast. There are essentially two options to attack such problem: through look-up tables and interpolations or through physical models. In the first a black-box approach can be used where each entry $H_{i,j}$ of the system

matrix is interpolated from the relative position and orientation of the detector at t_i to the given voxel j and a previously acquired set of data comprising the sensitivity of the used response in space from a unitary point source of the signal to be detected. Such an approach is also used in preoperative imaging (e.g. [249]). An implementation for non-imaging probes can be seen in figure 4.14.

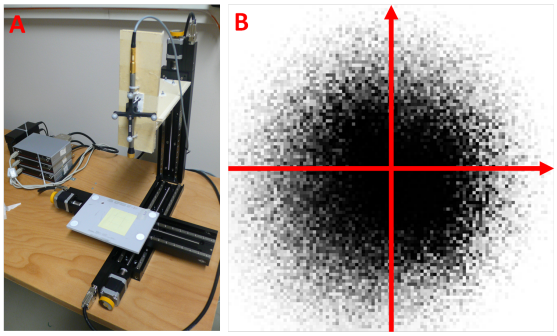

Figure 4.14.: (A) shows an example of a positioning table used to generate the readings needed for producing the look-up table for a hand held beta probe. (B) is an exemplary set of data produced by the said positioning table at a constant height. The red axis show two of the coordinates in the look-up table.

The second approach involves developing physical models that model well enough the detection process, as well as include some knowledge on potential effects due to the transfer of the detected signals through different media. In other words, what is needed is a model of the mapping h discussed in the latter sections. A very simple example would be the case of a 1D beta detector. There h maps to $\Re_0^+$. A very simple model for h would then be:

$$h(d,\alpha) = \frac{S\cos\alpha}{2}\left\{1 - \frac{1}{\sqrt{\frac{D^2}{4d^2}+1}}\right\}, \tag{4.9}$$

where d, D and α are defined as in 4.15 and S is a constant indicating the intrinsic sensitivity of the probe in cps/Bq. Such model can be then used to fill a system matrix if $d(i,j)$ and $\alpha(i,j)$ are known.

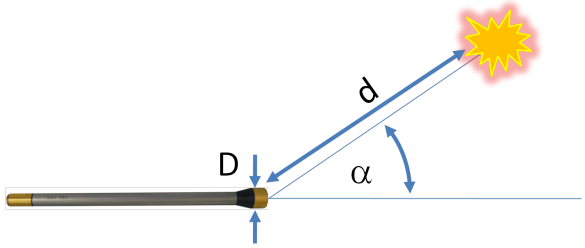

Figure 4.15.: Very simple model for beta detection considering only geometric effects.

4.4.5. Positioning of detector and patient

The idea of our group included the use of a tracking system in order to get the position and orientation of the detector for each acquired read-out. In practice, most of the implementations for tracking systems base on the use of tracking sensors in general terms which are placed on the object to be tracked. These sensors have to be fixed if possible to the tracked object and have to be able to be used in the OR. This is a non-trivial step, as there are major constraints on sterility, electrical compatibility, as well as performance for the tracking systems that may increase the complexity of the 3D functional imaging solution.

On the side of medically applicable tracking systems, essentially two technologies have made it to series: infrared optical tracking and electromagnetical tracking. Both technologies perform fairly well in terms of accuracy (range of 0.2-2mm), refresh rate (range 20-80fps), tracking volume (range of 50x50x50cm^3), etc. and are used in uncountable applications in surgical navigation.

In the case of the first (to be described in details in chapter 5) a so called tracking target has to be attached to the instrument to be tracked, here the hand held detector. Such tracking targets commonly cannot be used under standard sterile covers and have to be clipped or fixed at the beginning of every use to the detector to be used. Accordingly they have to fulfill requirements on sterility. In the case of optical tracking, it is important to consider also the fact that the line of sight between tracking target and the tracking system has to be gived. So handling of the detector has to be considered seriously, as well as the positioning of the tracking system.

On side of electromagnetical tracking, normally small wired sensors are placed on the tracked instruments. Those sensors do not require a line of sight like the optical system and

can be thus placed below any needed sterile cover. Nevertheless the volume of tracking is reduced and special care has to be taken on potential disturbances by metallic materials and electromagnetical fields.

Having the position and orientation of the used detector is not all what is needed. As described above the position of the volume of interest has to be known, as the relative position between detector and region to be reconstructed is needed for the calculation of the system matrix. This can be solved by considering also a tracking target or sensor on the patient. The position of it in relation to anatomy has to be such, that the surgery can be performed without disturbances, but yet to be as close to the operating situs as possible to avoid deformation.

Finally with proper target definition readings of the used detector and volume of interest can be put in the same coordinate system (see also figure 4.16).

4.4.6. Calibration of detector

Placing a tracking target or a tracking sensor on a hand-held detector does not fulfill the complete task of getting the detector readings in the same coordinate system with the volume of interest. Depending on the detector to be used the process of calculating such transformation, commonly known as calibration, differs.

For 1D sensors like nuclear probes, optical probes or magnetic probes essentially the calibration requires the localization of the sensing part of the probe in relation with the tracking target. Figure 4.17 taken from [361] shows the process in an image.

In the case of 2D sensors, the process of calibration is slightly harder. There not only the position of the sensor has to be determined in the coordinates of the tracking system, but also the transformation between this and the plane of imaging is needed.

For systems like optical cameras (potentially also thermal cameras, gamma cameras and fluorescent cameras) a standard camera calibration procedure can be used. In it a known 2D pattern, for example a chessboard pattern of known size can be used to determine the intrinsic parameters of the camera from a set of $n > 10$ frames using a standard algorithm for camera calibration [129] (see figure 4.18). From this procedure the projection matrix P to map three dimensional points onto the image plane can be estimated.

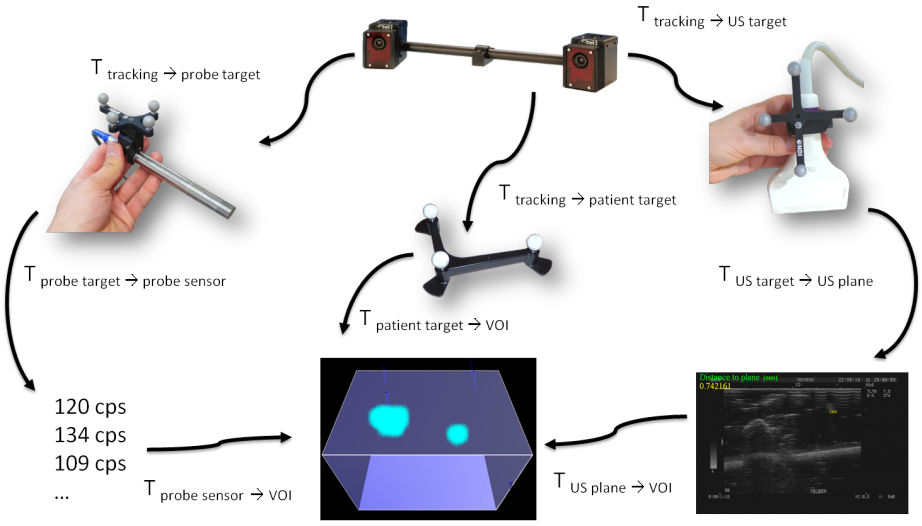

Figure 4.16.: Needed transformation in order to place readings of a hand held detector (here gamma probe or ultrasound probe) in the same coordinate as the volume of interest. The transformations from the tracking system (in this example an optical system) to the tracking targets of both detectors, as well as the transformation to the patient target is provided on real-time by the tracking system. The transformation between the patient target and the volume of interest was discussed in section 4.4.4, while the calculation of the transformations from the tracking targets of the detectors to the sensor or plane respectively comes from the detector calibration step (4.4.6).

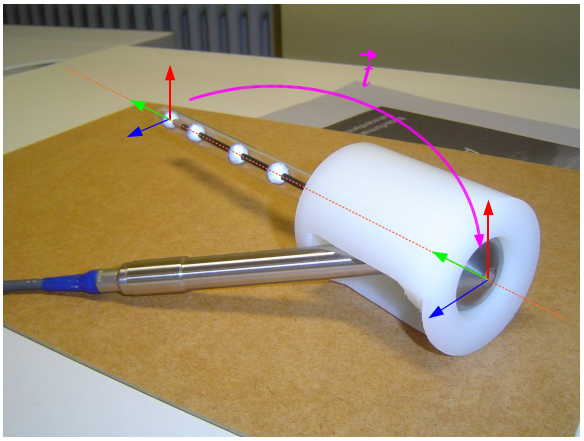

Figure 4.17.: High-energy-gamma-probe with attached tracking target. The configuration of the markers is on a line which matches per construction the axis of the sensor. Due to this geometric trick it is sufficient to calculate the distance from the tracking to the sensor in order to derive the complete transformation.

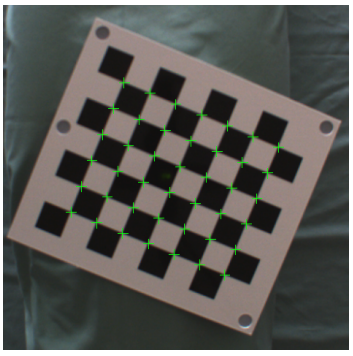

Figure 4.18.: Calibration board image during calibration. Image processing algorithm detects corners of board tiles and given the known dimensions of it estimates the focal length of the camera, as well as it principal point.

In the second step, based on the same frames, the rigid transformation between the camera target coordinate system and one at the camera center (image) can be computed. This is done by applying hand eye calibration [78] using corresponding poses of the camera in the chessboard coordinate system and poses of the tracking target in the tracking coordinate system. Any known point in coordinate system can thus be projected into the image plane.

For systems like ultrasound the calibration normally consists also in an optimization procedure, based on images of known geometries. One typical example is the single-wall calibration method of Prager et al. [263]. Several positions and orientations of the ultrasound probe's tracking target as well as corresponding images of a wall inside a water bath are acquired synchronously. The lines corresponding to the planar wall can be automatically segmented and used for the computation of all calibration parameters. As suggested by Treece et al. [336] the temporal offset between US acquisition and tracking for better data synchronization can be determined too. Here, like in the camera calibration, the use of a calibration protocol to ensure numeric stability for all degrees of freedom of the transformation is important.

4.4.7. Synchronization of signals

Given that the detector to be used in the architecture proposed here is not triggered, it is important to count with a good synchronization between the positioning information and the readings of the detector. In order to offer such a synchronization a good alternative is to use ring buffers and time-stamp matching.

In that approach, on arrival on the computer in charge of synchronization, the packages of information from the different sources are parsed and a time-stamp is added to them and stored in a ring buffer. Starting then from the slower data-stream, the synchronization succeeds on arrival of each package of the said stream to the computer. In this step the closest time-stamp of the faster signals to the latest time-stamp of the slowest one is selected as corresponding one. If a fixed delay is known in any of the data-stream it can be subtracted from the time stamp.

4.4.8. Summary

As noted in the last sections, several issues have to be completely rethought when doing 3D functional imaging without a gantry and in the operating room. The aspects mentioned here are only among the most relevant examples, but do not cover them all.

The key issues are:

- System architecture
- Dimensionality
- Definition of region to be reconstructed
- Calculation of the system matrix
- Positioning of detector to patient
- Calibration of detector
- Synchronization of signals

In order to validate the approach and confirm that the proposed solution is at all possible, in the coming chapters an implementation for 3D nuclear imaging in the OR is described in detail.

Chapter 5

Overview of Used Technology and Methods

In the last chapter a new approach for 3D functional intraoperative imaging was presented and its difference to the conventional approach for image reconstruction in a preoperative setup highlighted. The present chapter summarizes the technology and methods used in this work to design and implement such a 3D functional imaging system in the particular case of the freehand SPECT system to be described in detail in part III.

5.1. Tracking Systems and Navigation

As discussed in chapter 1, the application of imaging systems during surgery, such as the growing intra-operative use of mobile C-Arms [44, 92, 106, 217, 279], interventional MRI (magnetic resonance imaging) [17, 192, 382], and hand-held or catheter ultrasound devices [274, 305, 333] is defining advanced medical procedures [255, 378]. However, one particular aspect not mentioned in the last chapters is the fact that visualization of this immense amount of data in the proper position and orientation, as well as in an appropriate way, is a major issue if the surgeon wants to take advantage of them.

As a solution for this, in advanced operation theaters spatial localization systems (tracking systems) have been introduced to estimate the position and orientation of instruments and the patient, and thus provide a reference for guidance in a common coordinate sys-

tem [40, 43, 182]. Such integrated systems display the basic anatomical structure and the relative position of the instruments, thus making the information of one image modality visible in other ones. Furthermore, in case of the availability of a preoperative plan these systems may transfer these plans to the OR and keep track of the correct realization of the planned steps and thus guide the surgeon.

Commonly used tracking systems for intra-operative guidance are systems using electromagnetic tracking and optical tracking. Exemplary applications using electromagnetic tracking are realized by Cleary et al. [68] for navigation in radio-frequency-ablation of the liver, and Mori or Hautmann [223, 334] for bronchoscope navigation. Applications using optical tracking systems have been published for example by Shahidi et al. and Feuerstein et al. [96, 301] for laparoscope augmentation, by the group of Heining, Sauer, Traub et al. [135, 290, 335] for augmented reality in situ visualization, or by Birkfellner et al. [41] for navigation using a head-mounted operating microscopes. Some applications are proposed that use a combination of both systems [42, 229]. As long as the line of sight is available the external optical tracking system outperforms the electromagnetic tracking in terms of accuracy and robustness. Subjects of tracking are medical instruments [40, 182] and imaging devices like C-Arms [92, 216, 280], ultrasound probes [88], or endoscopes [223, 301] and the patient himself [280, 368].

Tracking and navigation also allow advanced visualization and thus an improved use of the available multi-modal data. Techniques that fuse the view of the real world with preoperative or intra-operative imaging data in real time in three dimensions [23, 24, 213] seem to be an upcoming technology. This is often referred to as augmented reality [360]. Azuma defines Augmented Reality as combination of the real and virtual world, which is interactive in real time, and is registered in three dimensions [23]. An example of such visualization can be seen in figure 5.1. This technique has been applied in medical prototypes for example in microscope surgery [41, 164], needle biopsy and therapy [97, 158, 207, 212, 290], or various laparoscopic interventions [96, 108, 226, 229, 238, 301] for sinus, spine, and abdominal surgery.

A tracking system provides the position (3D) and orientation (3D) of an object inside a certain tracking volume. In the case of optical tracking, the determination of the position is done by means of triangulation of objects detected in more than two cameras [19, 115,

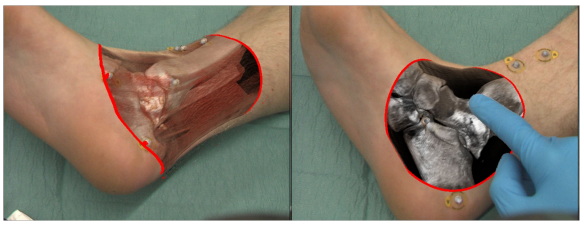

Figure 5.1.: Augmented reality visualization of a 3D rendered CT data set with different transfer functions and algorithm to avoid overlaying virtual data on surgical hand shoes. Image courtesy of Dr. Oliver Kutter from the Chair of Computer Aided Medical Procedures at TUM.

129]. To allow a robust tracking, the tracked objects are provided with tracking targets that present a big contrast to the background and can thus be easily segmented from the camera images. An example are infrared markers, which reflect infrared emissions very well in comparison to the rest of the objects in the operation room [46, 85, 355] (see figure 5.2).

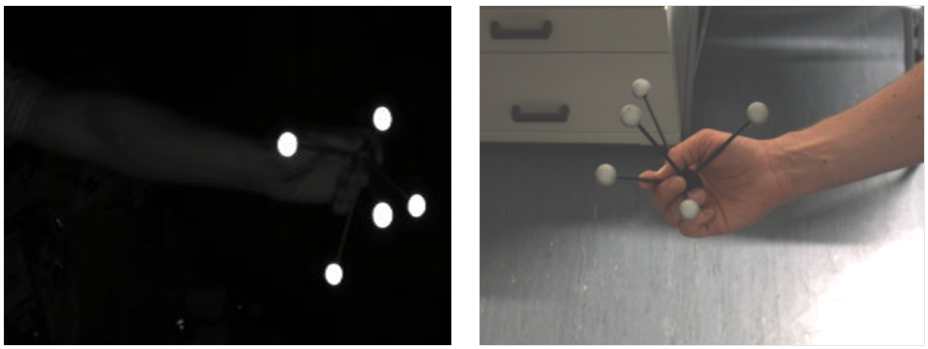

Figure 5.2.: Image of infrared camera used in a tracking system versus image of optical camera taken from a very close position and in the same direction. The retroflective spheres show an incredible contrast in relation to other structures around.

In figure 5.3, an example of the output of such a tracking system by A.R.T. GmbH (Weilheim, Germany) is shown.

Furthermore in order to be able to detect more than the 3D position of markers, fixed configurations in space are used [32, 265]. By comparing the relative distances of the de-

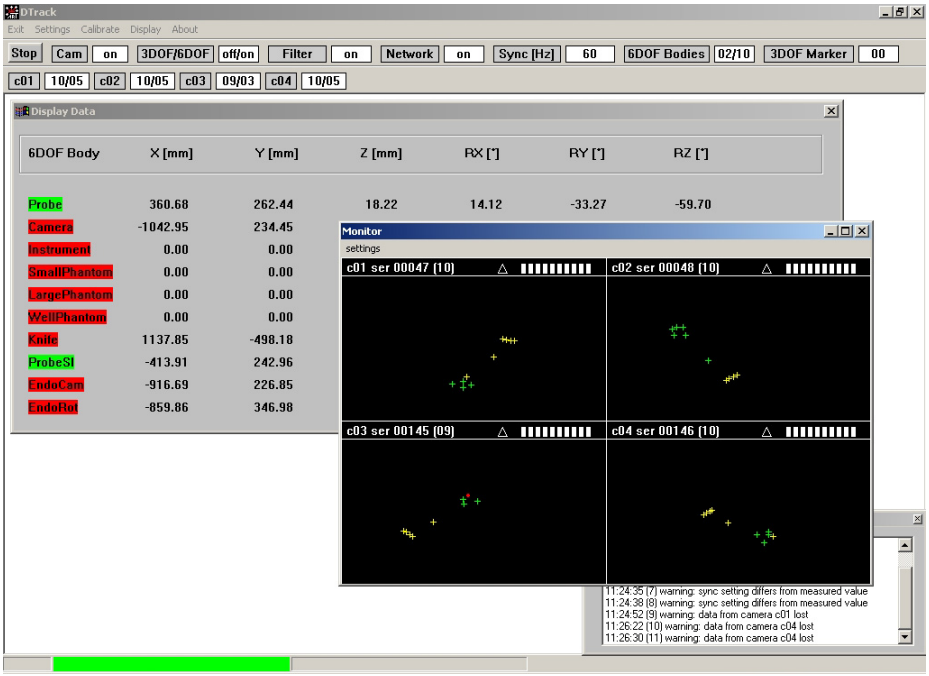

Figure 5.3.: Screenshot of software used by the optical tracking system of A.R.T. GmbH (Weilheim, Germany) to determine the 3D position and orientation of targets. In the 'Monitor' window, the images acquired by four used IR cameras are shown. The IR reflectors appear as green and yellow crosses and dots. The background window shows the position and the orientation of the different detected targets that were previously defined. Visit www.ar-tracking.de for further details.

tected 3D points these configurations can be found and their relative orientation to the reference coordinate system can be calculated. An example of a tracking target is included in figure 5.4.

Figure 5.4.: Exemplary IR marker target. The IR reflecting markers are distributed in a way, such that no ambiguities arise when calculating the pose based on the relative distances.

To include navigation, the tracked objects are also 'followed' by algorithms like Kalman or particle filters in order to include time information to make the calculation of the pose more robust. Indeed these algorithms are nothing but filters in the time domain that smooth the data using the expected dynamics. This makes their output robust for outliers [46, 85, 355, 384].

The present work will concentrate on infrared optical tracking. Details on the implementation and the different calibration procedures done are presented in chapter 7.

5.2. Gamma Probes

Hand-held probes are nowadays common diagnostic devices especially during surgery. As discussed in chapter 3 and shown by Povoski et al. in [262], intra-operative nuclear-assisted tumor localization is dominated by nuclear probes. The output of probes is just a one dimensional signal usually not constant in time. The main advantages of such devices lie in the portability, simplicity, and the possibility of miniaturizing them for the investigation of cavities for instance mounted on endoscopes. Moreover since each measurement is not restricted to be at a certain position with respect to the previous one, probes allow the

scan of arbitrary surfaces with a spatial accuracy only limited by the physical size of the detector.

Internally gamma probes commonly include scintillating crystals in which gamma rays interact and produce a proportional amount of light to the deposited energy (energy absorbed from the gamma ray). Such light can be then guided to a light sensor, like a photomultiplier tube, an avalanche photodiode or an array of those working in Geiger mode (so called Silicon photomultiplier). The resulting amplified pulses (one per detected ray and with energy-encoded amplitude) can then be digitized (see figure 5.5). Further approaches include the use of silicon detectors for direct detection of gamma rays where incoming radiation generates hole-electron pairs that can be detected and put in relation with the energy deposited by the gamma ray, like CdZnTe detectors.

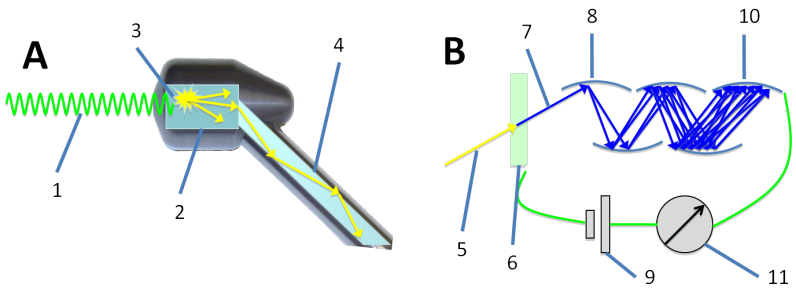

Figure 5.5.: Mock-up of gamma detection process. In (A) a gamma (1) hits the scintillator crystal (2) of the gamma probe. The energy absorbed produces a spark (3) whose light is guided over a light guide (4) to the control unit of the device. In (B) the incoming light (5) hits the photocathode of the photomultiplier (6) producing an electron in about 25% of the cases. That electron (7) is accelerated due to a potential difference to the first dynode (8) which on its own generates a multiple of electrons (for example 2). Those electrons are accelerated due to the potential (9) and hit a second dynode producing a multiple of them (for example four). After a cascade process several millions of electrons are generated (10). The resulting current can be measured (11) and digitized.

In the case of FDG-assisted tumor localization, gamma-probes detect the $511\ [keV]$ annihilation photons of the positrons within a small field of view. Thus based on the detection

rate the surgeon can be guided to the sources of radioactivity and obtain more information on the localization task [28, 60, 81, 122, 136, 174, 202, 210, 270].

A major difference (to standard gamma-probes) of these high-energy probes is the fact that at $511\ [keV]$ the detection of photons requires long trajectories through the sensor to guarantee detection. This does not only mean bigger detectors, but also the need of appropriate shielding. High-energy gamma-probes are restricted in terms of sensibility and suffer from an increased amount of scattering events in the shielding [116,210,297,380].

As an example, the high-energy gamma probe of Intra-Medical Imaging LLC (Los Angeles, USA) is shown in figure 5.6.

Figure 5.6.: High-energy and standard gamma-probes by Intra-Medical Imaging. The shielding of the high-energy gamma-probe is in this case $2.5\ [cm]$ of tungsten compared to the $2\ [mm]$ shielding of the standard probe. The conventional gamma-probe has been designed for $140\ [keV]$ ($140\ [keV]$ is the main energy emission peak of ^{99m}Tc, the standard radioactive label for SPECT and sentinel lymph-nodes applications.).

The disadvantage of gamma probes is that they are just point measurements. This makes the appreciation of the physical value on a surface difficult if it changes considerably with position and orientation. A further disadvantage is the need for many observations in order to interpolate a valid measurement map in big areas, which is not the best solution for detection of hot spots in scans of big body sections [91, 138].

In this work most of the development will take place using low-energy gamma probes, however an extension to high-energy probes may be possible.

5.3. Reconstruction Algorithms

In the last chapter abandoning the concept of using a gantry for imaging resulted in the need of constraining the reconstruction algorithms to iterative reconstruction algorithms. Those algorithms have been analysed extensively in the past. Here we explain the most important ones as they are implemented in the exemplary system realized to validate the feasibility of hand held 3D functional imaging.

The major representatives of this algorithm family can be divided in algebraic reconstruction techniques, one of which was explained briefly in chapter 4 and optimization based techniques.

5.3.1. Algebraic reconstruction techniques

The algebraic approach introduced above has several realizations used in emission tomography (see details in [153, 366]). The first one is the additive algebraic reconstruction technique (ART) in which the update of the solution is done by adding a term proportional to the substractive error for each projection in each iteration. One has

$$f_j^{(n+1)} = f_j^{(n)} + \eta H_{ij} \left(g_i - \sum_k H_{ik} f_k^{(n)} \right) \left(\sum_k H_{ik}^2 \right)^{-1}, \tag{5.1}$$

where H_{ij} is the entry at row i and column j of $\mathbf{H}$.

In this case, all voxels are update simultaneously with each projection. In every iteration n a new distribution $\vec{f}^{(n)}$ is computed. From it an estimated set of projections is calculated $\mathbf{H}\vec{f}^{(n)}$ and compared with the real measurements ($\vec{g}$) on an arithmetic basis (subtraction).

The major problem of ART is the fact that the weight of the projections on the image is not homogeneous. The last projection is best represented by the reconstructed image. In order to avoid this bias, people have included the use of a random order for the update, which increases the computation burden, but produces better images.

If the update is a multiplicative update (comparison on a geometric basis) and the error is the quotient error, one has the multiplicative algebraic reconstruction technique (MART), given by

$$f_j^{(n+1)} = f_j^{(n)} \left[g_i \left(\sum_k H_{ik} f_k^{(n)} \right)^{-1} \right]^{\eta(n)} . \tag{5.2}$$

This is valid only if H_{ij} is greater than zero.

A second variant of the above ART updates each voxel with every projection in each iteration. This technique is called simultaneous iterative reconstruction technique (SIRT) and is described by

$$f_j^{(n+1)} = f_j^{(n)} + \eta(n) \sum_i H_{ij} \left(g_i - \sum_k H_{ik} f_k^{(n)} \right) \left(\sum_k H_{ik}^2 \right)^{-1} . \tag{5.3}$$

In the case of SIRT, the convergence is slower than in the conventional ART case, as the changes in the reconstructed image $\vec{f}$ consider all projections before being updated, resulting in a very 'conservative' and slow approach. In contrast to ART, however, images look considerably nicer and are not biased towards the last updated projections. Here no randomization is needed.

Several other implementations and modifications have been proposed in the past, however, ART is still a standard algorithm mostly used as baseline for evaluation of higher complexity approaches.

5.3.2. Optimization based techniques

In contrast to the case of algebraic reconstruction techniques, in optimization based techniques a cost function is defined which is minimal when the reconstructed image fits the projections best. Thus the problem of solving the linear system of equation 4.6 is to find a vector $\vec{f}$ that minimizes this said cost function.

In emission tomography, several cost functions are available. The most popular is certainly the sum of square distances (SSD), in which case the reconstruction is given by:

$$\hat{\vec{f}} = \underset{\vec{f}}{\operatorname{argmin}} \left\{ \sum \left(\sum_j H_{ij} f_j - g_i \right)^2 \right\} . \tag{5.4}$$

The solution used in this case is the iterative update of each voxel additively based on the gradient information by

$$f_j^{(n+1)} = f_j^{(n)} + \eta(n)\Delta f_j^{(n)}. \tag{5.5}$$

For the case of SSD, the gradient shown can be calculated exactly. For the emission problem, it is given by

$$\Delta\vec{f} = -\mathbf{H}^T(\vec{g} - \mathbf{H}\vec{f}) \tag{5.6}$$

In the case of the steepest descent algorithm, t can be calculated to be optimal. In that case it is given by

$$\eta = \frac{\Delta\vec{f}^T\mathbf{H}^T(\vec{g} - \mathbf{H}\vec{f})}{\vec{f}^T\mathbf{H}^T\mathbf{H}\vec{f}}. \tag{5.7}$$

Similar to SSD, functions like SAD or in general any power of the absolute difference between projection ($\mathbf{H}\vec{f}^{(n)}$) and readings ($\vec{g}$) can be used.

Further cost functions usually used are the maximum likelihood (ML) functions. The likelihood L of a set of projections $\vec{g}$ being a result of a distribution $\vec{f}$ can be stated as

$$L(F = \vec{f}) = P(F = \vec{f}|G = \vec{g}) = \prod_i P(F = \vec{f}|G_i = g_i) \tag{5.8}$$

where it is assumed that there is independence between measurements. Due to the complexity of handling products, commonly a logarithmic likelihood Λ is used:

$$\Lambda(F = \vec{f}) = \sum_i \log P(F = \vec{f}|G_i = g_i) \tag{5.9}$$

In the case for emission tomography, the MAP (maximum a posteriori probability) algorithm has been applied as common reconstruction technique. Within this the values of the distribution $\vec{f}$ are moved so that the a posteriori probability of them being the cause of the readings $\vec{g}$ is maximized.

$$\hat{\vec{f}} = \underset{\vec{f}}{\operatorname{argmax}} \left\{ P(G = \vec{g}|F = \vec{f})P(F = \vec{f}) \right\}. \tag{5.10}$$

where the $P(F = \vec{f})$ is the probability of a given distribution of f. There a priori information can be incorporated. $P(G = \vec{g}|F = \vec{f})$ can be commonly derived from models like the one used for the system matrix. In this case the $P(G = \vec{g})$ is assumed constant.

Far more successful in terms of the frequence it is used in commercial solutions is the maximum likelihood estimation maximization algorithm. On one hand this algorithm takes logarithmic likelihood and tries to maximize the difference $\Lambda(F = \vec{f}^{n+1}$ and $\Lambda(F = \vec{f}^{n}$. On the other it considers the fact that information is missing, which is for example the case of emision tomography. In order words the probability is assumed to be:

$$P(G = \vec{g}|F = \vec{f}) = \sum_{\vec{z}} P(G_i = g_i|F = \vec{f}, Z = \vec{z})P(Z = \vec{z}|F = \vec{f}) \tag{5.11}$$

where

With some mathematical modifications the maximization mentioned above results in:

$$\vec{f} = \underset{\vec{f}}{\text{argmax}} \left\{ E_{Z|G=\vec{g},F=\vec{f}^{n}} \left(\log P(G = \vec{g}, Z = \vec{z}|F = \vec{f}) \right) \right\} = \underset{\vec{f}}{\text{argmax}} E_{cond} \tag{5.12}$$

Thus, the optimal solution for $\vec{f}$ arises from a two step procedure:

1. Estimation step: Determine the conditional expectation E_{cond}
2. Maximization step: Maximize this expression with respect to $\vec{f}$.

In practice, the described algorithm can be then stated in simpler terms depending on the underlying model between F, G and Z. For emission tomography for example one has:

$$f_j^{(n+1)} = f_j^{(n)} \left(\sum_l H_{l,j} \right)^{-1} \left(\sum_i H_{i,j} \frac{g_i}{\sum_k H_{i,k} f_k^{(n)}} \right). \tag{5.13}$$

where $H_{i,j}$ are the entries of the system matrix of the system.

This algorithm has proven to be extremely powerful in particular in emission tomography where it has also evolved to algorithms like the ordered subset estimation maximization (OSEM) algorithm among others. An generalization of the approach of the algorithm is also known as Generalized Expectation Maximization (GEM).

5.3.3. Summary

In the last pages a short overview over conventional iterative algorithms was presented. All of them result being a sort of black box trying to minimize the distance of measured projections ($\vec{g}$) and estimated ones ($\mathbf{H}\vec{f}^{(n)}$).

In general the importance of the image representation and accuracy of the projection computation (i.e. the accuracy of the system matrix and the validity of the assumption that 4.6 is true) can be very simply made evident. As all iterative techniques stop once the projections $\mathbf{H}\vec{f}^{(n)}$ are close to the measurements $\vec{g}$, the accuracy of the resulting reconstruction will depend to a major extent on how precisely the calculation of the projections matches the physical projection process.

Moreover, the convergence has not been mentioned, but can be proved for almost all the mentioned algorithms. Nevertheless the convergence speed plays a dramatical role. Defining how many iterations are needed for a reconstruction is thus in most cases rather an empiric selection than a scientific one.

As summary, iterative reconstruction algorithms should be definitely adapted to the problem to be solved. However there is enough performance already in the standard versions. Such potential is tested and extended to an extent in the implementation of freehand SPECT (see part III).

Part III.

Freehand SPECT: exemplary implementation for gamma-ray imaging

Chapter 6

Requirements of freehand SPECT

6.1. Introduction

I still remember a meeting in the office of Dr. Stefan Paepke of the Women's Hospital at TUM with him and Dr. Joerg Traub back in 2008. The objective was clear. We needed to fix the requirements we would consider to reimplement the first version of our 3D gamma reconstruction software into something that the expert surgeon sitting in front of us could use to accomplish his daily routine.

For Dr. Paepke things were clear. We had a technology capable of detecting radioactivity and making images out of it. Those images were in 3D and potentially in future could be combined with ultrasound.

'What I need is the following', he said. 'The axilla is a tetrahedron. The base of that tetrahedron is the axillary plane. What I need is to know where in that plane is located the sentinel node. And further how deep it is in respect to that plane'. When we asked what could be our maximum error he said 5mm, that should also be our voxel size. The maximum time we had to do such an image was 5min.

So I wrote down as requirements a short list:

1. Localize SLNs in the axilla with an accuracy of 5mm within 5min
2. Show position of SLNs in axillary plane
3. Show depth of SLN in axilla

Of course we were far from getting to the solution nor specifying it. Before many things

had to be defined. This chapter gives a brief overview of the steps needed to set up all information in order to create a new intraoperative imaging system for computer-aided SLNB. Such a system eventually was renamed from its original '3D gamma reconstruction' to 'freehand SPECT'.

6.2. Definition of constraints for freehand SPECT

An example of a more complete lists of constraints imposed for a system like the one Dr. Paepke was thinking of is the short study made within the scope of this work between November 2008 and January 2009. The aim of that study was to define the requirements for what later would be called freehand SPECT. A group of German breast cancer centers was selected and surgeons as well as technical personnel was posed a set of questions after a short presentations about the technology of intraoperative nuclear imaging that had been developed at TUM until that point in time. The tabulated results for intraoperative lymphatic mapping in breast cancer can be seen in table 6.1.

Within that study, the instance of the points mentioned by Prof. Aarsvold (chapter 2) would be the following:

Context The context is breast cancer surgery. In particular the target population are patients with low probability of metastatic spread - generally patients with large ductal carcinoma in situ (DCIS), clinically staged T1 - T2 tumors (with diameter below 2 cm) of invasive breast carcinoma with clinically and sonographically negative axillary nodes (N0, N0 (i+) or N0 (mic)) (i.e. patients for whom the sentinel lymph node procedure (SLNB) procedure is indicated according to German guideline [176])

Task The tasks to be solved are the following: (a) first the intraoperative 3D in vivo localization of preoperatively marked lymph nodes using standard of care ^{99m}Tc-colloids over a wide area of interest; (b) secondly once the region surveillance is complete, and if necessary, the localization of particular nodes in a smaller region of interest; (c) finally the post-excision confirmation of complete excision of relevant nodes within a wide area.

	Institution					
Question	1	2	3	4	5	6
Minimal resolution in [mm]	5	2	5	5	n/a	5
Maximal error in [mm]	5	2	5	5	n/a	5
Maximal extension in [min]	5	5	3	5	n/a	5
Maximal investment in [kEUR]	100	n/a	50	50	50	n/a
Maximal running costs in [EUR/a]	100	n/a	n/a	150	50	n/a

Table 6.1.: Results of questionnaire on 3D functional imaging for intraoperative lymphatic mapping in breast cancer. The minimal spatial resolution refers to the distance below which two different structures (marked tumor tissue, lymphatic vessels or lymph nodes) can be considered one entity. The maximal error refers to the maximal error in localizing a structure between image and reality. The maximal extension is the maximum time a normal procedure can be extended relative to the current procedure given the expected advantages of using 3D functional imaging in the OR. The cost points refer as stated to the maximum costs the institution would pay for having a 3D functional imaging system for guidance during oncologic operations in breast and axilla. The institutions considered were (1) Klinikum rechts der Isar, Munich, (2) Universitätsklinikum Köln, Cologne, (3) HSK Klinikum, Wiesbaden, (4) Universitätsklinikum Bayreuth, Bayreuth, (5) Klinikum Deggendorf, Deggendorf, (6) Universitätsklinikum Tübingen, Tübingen.

Technology The technology to be used is small flexible detectors for the specific standard tracer (in general ^{99m}Tc-colloids) in doses stated in the German guideline (i.e. 10-50 MBq for 1-day protocol and 150-250 MBq in the 2-day protocol - protocols will be explained below) [176]. The dose is expected to be applied by injecting it directly to the region of interest in 3 to 4 deposits of 0.2 to 1 ml. The injection technique is not fixed in the guideline, so the imaging system has to be capable of dealing with all 4 possible techniques: peritumoral, subdermal, intratumoral and periareolar injection.

The required sensitivity has to be sufficient to detect uptakes as low as 0.1 % of the total dose [31] within up to 8 hours and 16 hours for each protocol respectively. The guideline recommends at least 5 cps/kBq and ideally over 10 cps/kBq for one-dimensional gamma probes. The energy resolution on the one hand has to be as high as possible to avoid a too high contribution of scattered radiation. Separation of Compton and photoelectic peak must be clear [365]. Conventional probes are in the range 5-20 %. On the other hand the spatial resolution can be extracted directly from table 6.1 and the recommended field of view of the system as stated by the interviewed surgeons had to cover the complete breast and axillary areas, i.e. a volume of interest of at least 30x30x30 cm^3.

Positioning in this case, as in general for functional imaging in the OR, is complicated. In most hospitals, the access of the sentinel lymph nodes is with the patient in supine position the relevant arm(s) extended (see figure 6.1). Access for imaging can accordingly be only in anterior-posterior direction (AP direction) or along the curvature of the axilla in medial direction.

Protocol The overall protocol has to be in this case not dramatically different than the one stated in the guideline and consists of the steps indicated in the flow chart in figure 6.2. As learned from the discussions with the specialists, the SLNB protocol presents different divisions depending on the patient, the surgeon and the SOP used in the hospital. An example is the fact that the injection of the radionuclide can be done the day of surgery (so called 1-day protocol) or the day before (2-day protocol). The difference in that case is evidently the fact that for a 2-day protocol the injection dose has to be higher resulting in a higher radiation burden for the patient and the personnel, but with the logistic advantage of being able to operate the patient very early in the next morning and erasing completely

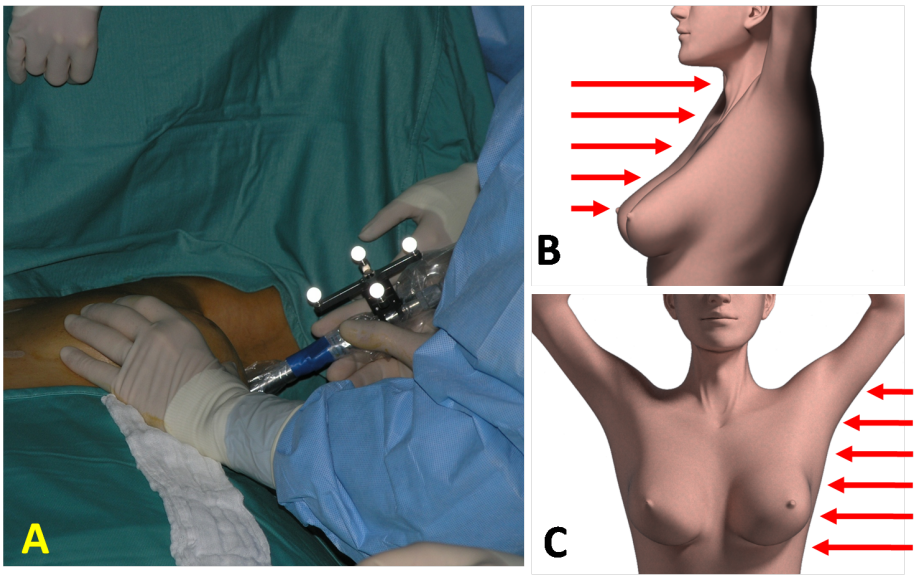

Figure 6.1.: (A) Exemplary positioning of physicians during SLNB procedure in breast cancer. Surgeon holds breast with the left hand while measuring radiation using a gamma probe with the right hand. The patient's head is covered by the separation sheet on the back between anesthesia and surgical field. (B) AP and (C) medial direction for scanning breast and axillary area.

the uncertainty of the duration of the lymphatic mapping. The duration of the lymphatic mapping is extremely dependent on the injection technique, being between a few minutes for periareolar injection [285] and a couple of hours for intratumoral injection [341].

Similarly the access to the axilla for the SLNB can be either done with a separated incision (most common procedure) or directly opening it from the breast according to the so called axillary dissection with access minimized (ADAM) technique [245]. A another difference in possible treatment is the way to approach a positive sentinel lymph node (lymph node with solid metastasis). There the German guideline leaves the option open to go for an axillary lymph node dissection (ALND), where all lymph nodes of levels I and II are resected or to go for a radiation therapy (RT) of the regional lymph node. The second is not recommended, but it is applicable in special cases.

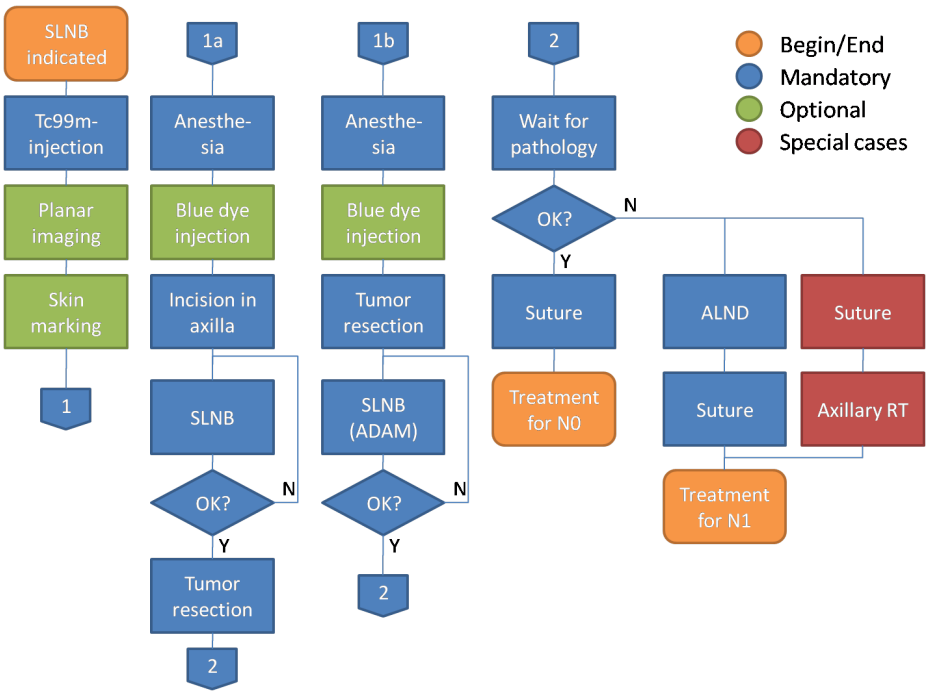

Figure 6.2.: Protocol for the SLNB according to the German guideline for SLNB in breast cancer.

The detailed protocol for the SLNB (using the ADAM technique or not) is shown in figure 6.3.

Part of the protocol has also to do with the logistics. If a functional imaging system is

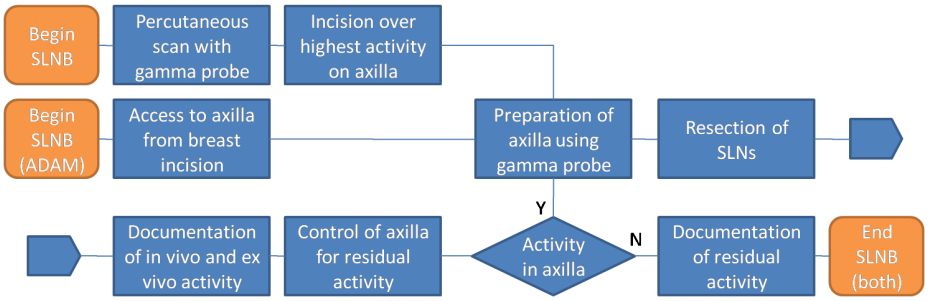

Figure 6.3.: Detailed steps in the SLNB starting from both the standard and the ADAM technique according to the German guideline for SLNB in breast cancer.

meant to be used in the OR, considerations have to be made of the available infrastructure. Further conditions like lighting and temperature may play a relevant role. In order to consider this, several breast-surgery operating rooms have been analyzed within this work (Klinikum rechts der Isar, Munich, Germany, Klinikum Augsburg, Augsburg, Germany, Universitätsklinikum Würzburg, Würzburg, Germany, Ospedale Santa Chiara, Pisa, Italy, Policlinico S. Orsola-Malpighi, Bologna, Italy, St. Joseph's Hospital, Los Angeles, CA, USA and St. John's Hospital, Los Angeles, CA, USA). Those with the most strict space constraints are to be considered as design inputs. The most restrictive example found was one of the operating rooms at Klinikum rechts der Isar. A layout of the smallest one is shown in figure 6.4.

With clear constraints, the next step was to define users, goals and scenarios.

6.3. Definition of users and their goals

Although for Dr. Paepke the image was clear: the user would be him, following the workflow of SLNB, there were more involved persons. In a first brain-storming session, the following list could be identified (see 6.2). They were on their own characterized by their affiliation, their knowledge and their goals.

Why would a circulator get in contact with the system? As part of the team during surgery he or she would be most probably involved in the main function of the system, generate images in the OR. According to his or her standard tasks, he or she would probably place the system, clean it, prepare it for use, potentially even interact with the software

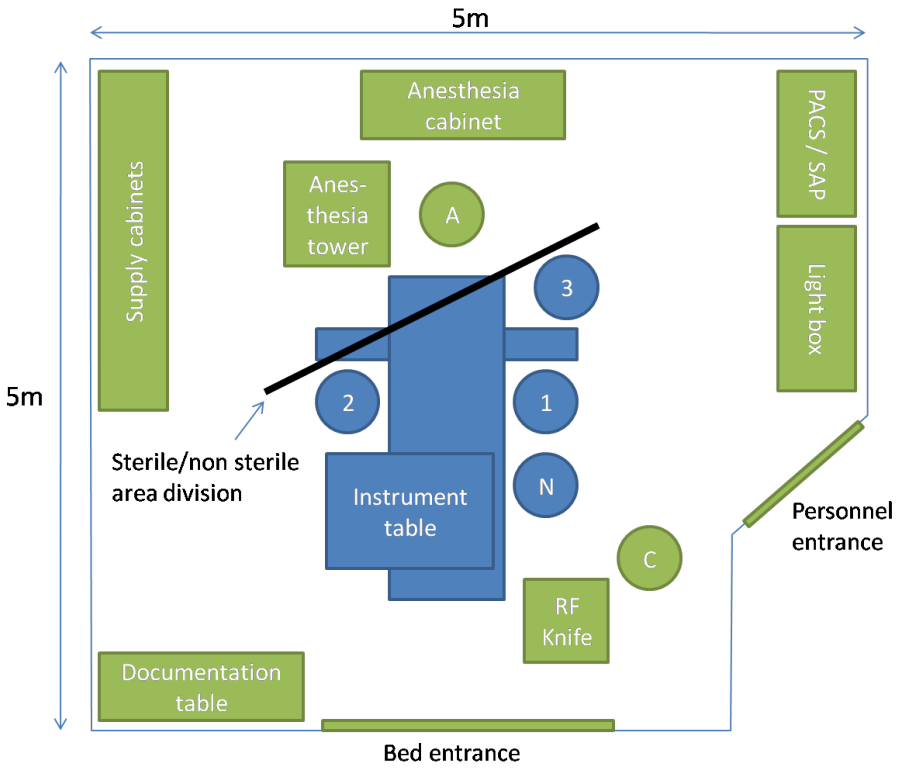

Figure 6.4.: Schematic layout of smallest OR in the breast cancer division at Klinikum rechts der Isar. Exemplary setup during a SLNB procedure for a patient with breast cancer on the left breast. The circles indicate the typical position of the involved personnel: A stands for anesthetist, 1 for main surgeon, 2 for assistant surgeon, 3 for additional assistant surgeon - commonly a student, N for OR nurse and C for circulator. The colors indicate the level of sterility, blue means sterile personnel and equipment, green only disinfected personnel and equipment. The patient bed is in the center of the room. Commonly extensions for both arms are appended to the bed. A separation sheet divides sterile and non-sterile area towards the head of the patient, which lies on the side of the anesthetist.

			Knowledge		
Description	**Affiliation**	**Authorized**	**Anatomy**	**Nuclear Medicine**	**Nuclear Technology**
Nuclear Medicine physician	Nuclear Medicine	Yes	High	High	Average
Surgeon Specialist in Senology	Gynaecology	Yes	High	Average	Low
Scrub nurse	Gynaecology	Yes	Average	Low	Low
Circulating nurse	Gynaecology	Yes	Average	Low	Low
Assistant medical technician	Nuclear Medicine	Yes	Average	Average	Low
Cleaning personal	Both	No	Low	Low	Low

Table 6.2.: Table with potential people that would come in contact with the imaging system meant to be developed.

during use and download the documentation created on it during surgery. Such a reasoning could be then applied to any of the persons mentioned in table 6.2.

6.4. Definition of workflow and scenarios

Ideally the procedure for SLNB for imaging the marked lymph nodes in the OR would result in minimal changes in the standard procedure. The reason is obviously the need of maximizing the experience gained in the standard procedure and allow thus a smooth integration in the clinical routine. Exemplary solutions from the discussions with the mentioned specialists are shown in figures 6.5 and 6.6.

The main differences from the normal procedure are essentially the simplification of the preoperative steps by eliminating the planar scintigraphy and the skin marking. These two steps are done in the Nuclear Medicine facility of the surgical unit in order to have a survey image of the lymphatic drain and give a rough indication of the localization of the SLNs over the skin. These steps are not necessary in case of the use of intraoperative imaging since an equivalent scintigraphy is available and localization in the OR can be achieved by the intraoperative imaging itself. Thus the imaging has to be at least equivalent in performance as compared to the planar scintigraphy: a wide area (breast, clavicula, sternum and axilla) has to be scanned, a relation to anatomy has to be established and an equivalent sensitivity has to be achieved (i.e. possibility of detecting hot spots of only 10-100 kBq in up to 4-6 cm depth) within a similar time frame for acquisition and visualization (i.e. only a couple of minutes).

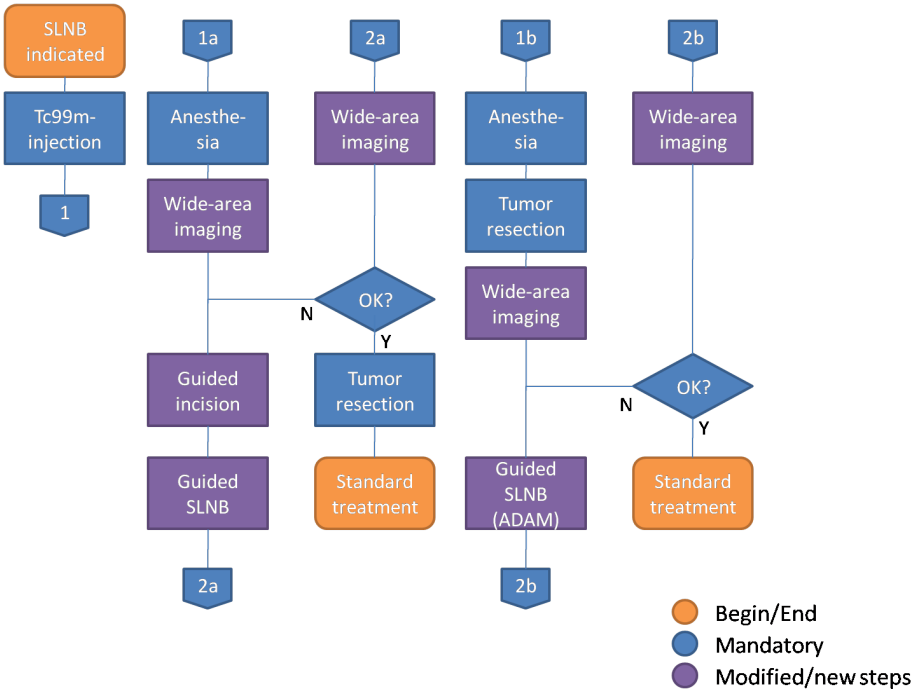

Figure 6.5.: Proposed SLNB protocol for breast cancer from discussions with specialists. First, the planar scintigraphy and skin marking steps the day before surgery are not necessary. Similarly the blue dye injection is avoided. In the standard procedure before the axilla incision a wide-area image is generated. This image gives an idea to the surgeon, how many nodes are present uptake and where they are located replacing the optimal planar scintigraphy. Based on this image the surgeon many perform an image-guided incision and a guided SLNB step. In the case of the ADAM technique, the wide-range image is generated before entering the axilla and it allows a guided SLNB. In both approaches a wide-area image at the end of the procedure allows verifying the complete resection of all lymph nodes meant to be extracted and the image documentation of the results of the procedure.

Further modifications have to do with the use of the imaging information for a guided incision and guided SLNB step, as well as finally control of residual activity in the region of interest. In the case of the standard SLNB the incision could be planned using the images. The resection of the lymph nodes is meant to benefit from the depth information made available by the 3D imaging. Ideally the imaging system would allow to document the radioactivity in the SLN in vivo and ex vivo, as well as permit comparisons between images acquired before the resection and after. All of this goes towards the (semi-)automatic generation of documentation of the procedure.

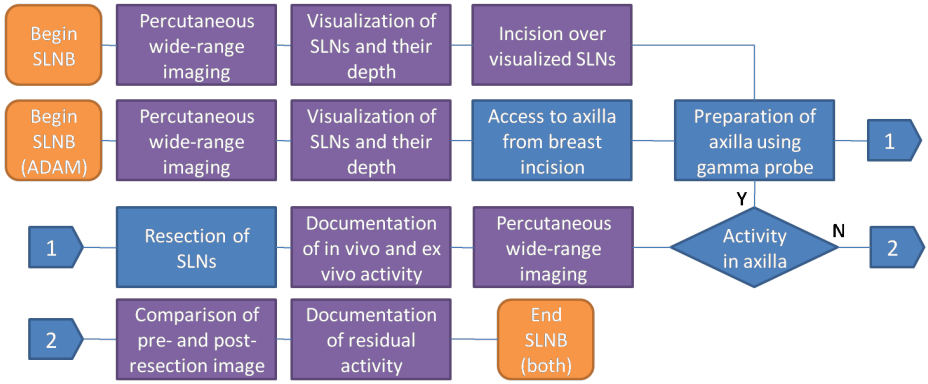

Figure 6.6.: Detailed protocol of SLNB step during the SLNB procedure according to the proposal from the interviewed surgeons. The use of functional imaging before entering the axilla would allow determining the depth of the lymph nodes to be extracted and thus provide valuable information for the resection. The documentation of the in-vivo and ex-vivo uptake would be done automatically. The control of residual activity would be done in this case using the imaging modality and would allow thus semi-automatic documentation.

With defined workflows the next step is the generation of scenarios. Scenarios tell how the different users would interact with the system. The scenarios for the use of our free-hand SPECT in the OR were then developed from the workflows of figures 6.5 and 6.6.

As example of how such a scenario is displayed in table 6.3.

Step	Description	User commands	Actions
1	Turn on cart	Press on button	Boot system
			Cart application starts automatically
2	Input password of AMT or Circulator	Enter text	Check password
			If password ok
			Go to 3
			Else
			Restart step
			End if
		Close	Save log
			Shut down system
3	Select workflow ”Download documentation”	Select from workflow list	Load workflow
			Go to 4
		Close	Save log
			Shut down system
4	Define patient	Select from patient list	Load patient data from database
			Go to 5
		Close	Save log
			Shut down system
5	Select data to upload	Select from available data list	Continue to 6
		Close	Save log
			Shut down system
6	Visualize information to upload	Proceed	If connection to PACS
			Upload information to PACS
			Else
			If transfer medica connected
			Copy information in transfer media
			Else
			Prompt user to connect transfer media
			End if
			End if
		Annotate image	Store image annotation
			Stay in step
		More data	Go to 5
		Close	Save log
			Shut down system

Table 6.3.: Example of simple scenario as developed for the specifications of requirements.

6.5. Functional and workflow requirements

When designing a complete system as in the case of freehand SPECT system requirements have to be broken down from high level requirements to concrete low level requirements on software and hardware, which can generate proper tasks to be worked up.

To exemplarize this point the first requirement for freehand SPECT would be analyzed in detail and in the light of the proposed architecture of 3D functional imaging systems.

In order to 'localize SLNs in the axilla with an accuracy of 5mm within 5min' several issues have to be addressed.

Localization : When using the word localization, Dr. Paepke meant the determination of a position in space of a particular structure. In order to do so essentially two approaches are possible. On the one hand the 3 particular coordinates of the structure can be estimated from information gathered from different sensors. That strategy is quite well-posed if sufficient information is available, however takes for granted that (a) the structure of interest is present in a certain volume and some high level information of it is known, like size, its properties in relation with the sensors to be used, etc. On the contrary, the second approach does not require much of that, as it leaves most of the intelligence on the side of the user. That approach is the one of 3D imaging. By creating an image from the information of the sensors and displaying it to a user - provided that the sensors are capable of detecting a distinguishable property of the structure of interest - the localization is on the hands of the user. This approach suffers however from the fact, that generating images is an ill-posed problem.

SLNs : SLNs are lymph nodes that are marked by substances injected at the related anatomy of interest, e.g. the breast, the location of a melanoma, etc. As described in details in chapter 3, there are several options to go for the hunt of SLNs. However, the only standard markations are radiotracers and blue-dye. Accordingly, unless allowing major changes in the workflow and approach, the SLN had to be detected with one of the two mentioned labelings.

Axilla : The axilla is a three dimensional region that extends over an area of 5x5cm^2 on the axillary plane reaching up to 6cm in depth in normal patients. If considering a solution for any sized patients, the volume can be extended to 10x10x10cm^3. In particular if SLNs are to be localized in the axilla, they may be located even beyond it, below the pectoralis minor deep below the clavicula. Under such conditions, the only possible conventional way of detecting such structures is by using a radioactive tracer. Accordingly the detectors should be gamma detectors like gamma probes or gamma cameras.

The list of the resulting requirements on the system can be extended almost ad nauseam. For freehand SPECT an excerpt of the initial requirements of early 2008 is listed below:

- Acquire radiation of Tc99m in case of SLN
- Acquire radiation from direction at least 2 perpendicular planes that enclose axilla
- Define a volume of reconstruction including the axilla
- Define for each acquisition the relative pose between volume of interest and axilla
- Define for each acquisition its relative position to the volume of reconstruction
- Integrate the acquisitions in a image
- Calculation of distance between marked structure and axillar plane
- Calculation of distance between marked structure and media-lateral axis
- Allow control by sterile personnel
- Allow contact with patient only of sterile parts
- Fit in the logistics of the OR
- Acquire sufficient data and integrate acquisition in less than 5 min
- Generate images of at least 5 mm voxels
- Have a spatial bias of at most 5mm in all directions
- Enable to stop acquisition

6.6. Regulatory and safety requirements for freehand SPECT

All previous sections went deep into the discussion of functional requirements. However, not much was said on the side of the regulatory issues. The design of freehand SPECT included a thorough analysis on the risks involved in the lifecycle of such a system.

Following the list of essential requirements on safety detailed in chapter 2 the first step is to define an intended use. The declared use of freehand SPECT can be for example:

'Freehand SPECT is meant to be used for imaging the distribution of radionuclides in the human body by means of photon detection. Freehand SPECT is intended to produce

both planar and tomographic images of a radio-marked source. Freehand SPECT may also be used intraoperatively or on pathological specimens if a protective sheath is used. Freehand SPECT may be used at the patient's bedside, or in an Emergency Room or Intensive Care Unit. The generated images can be used also for documentation and reporting. The interpretation and use of the images generated is intended to be done by trained personnel.'

Such an intended use is conform with the requirements specified in chapter 2.

Now in terms of expected border conditions, the easiest way of dealing with potential sources of harm is using the checklists given in the guidelines themselves. An excerpt of such a list of potential border conditions, as evaluated for freehand SPECT is shown in table 6.7.

In freehand SPECT the combination of products is a relevant issue as the gamma probe used can be used independently and is not integrated to the complete system (the latter follows from the necessity of counting on the gamma probe easily and portably in case of necessity).

In the case of freehand SPECT the sole relevant part to consider in terms of biocompatibility are the tracking targets used on the probe and on the patient. The reason for this is that the gamma probe is already used under a sterile cover. For the remaining materials non-toxicity has to be assured if a user can come into contact with them during the use stated in the intended use.

From a point of view of measuring devices, freehand SPECT measures distances (depth of radioactive structures) and count rate of radiation. As a result the display of such values has to be according to the requirements (size, units, accuracy, constancy over time, repeatability, etc).

Tests of electromagnetical compatibility as well as test of electrical safety according to EN 60601-1-2 and EN 60601-1 respectively have to be also performed for a freehand SPECT device as it is an electronic device. The requirements resulting from the standards have thus be considered from the first day. Similar is the case of mechanical risks in particular in relation with the tracking system to be placed at a high place over the OR table and thus suceptible to other constraints with respect to a standard PC.

An excerpt of the final list of requirements resulting from safety issues is listed below:

A = Applicable N = Not Applicable	Potential Risk EN ISO 14971 E.1. / List of Risks from Clinics and Technicians	Justification of non-applicability	Initiating Event(s)	Potential Implications	Applicable Standards	Patient	User	3rd Party	Construction	Production	Information	Software Development	System	Application	Measure of Damage	Probability	Risk Index	Procedure, Responsibilities, Schedule	Taken Measures	Measure of Damage	Probability	Risk Index
	EN ISO 14971																					
	Hardware CSS300																					
	Electricity																					
A	Earth leak		Protective earth connection has too high impedance	electrical hazzard on user/3rd party	EC 60601-1		X	X	X	X		X	X		2	9	18	Use of isolating transformer, use of proper protective earth conductors, test of impedance of conductors	Transformer according to IEC 60601-1 used, tests of complete system succeeded according to IEC 60601-1	2	2	4
A			Protective earth is not connected (connection broken)	electrical hazzard on user/3rd party	EC 60601-1		X	X	X	X		X	X		2	9	18	Use of isolating transformer, inclusion of proper isolation of accessible parts, test of earth leak	Transformer according to IEC 60601-1 used, tests of complete system succeeded according to IEC 60601-1	2	2	4
A	Contact current		Housing is not properly connected to earth	electrical hazzard on user/3rd party	EC 60601-1		X	X	X	X		X	X		2	9	18	Use of isolating materials for housing or well connected conducting housing, test of contact current	Materials selected to be good isolated, tests of complete system successful according to IEC 60601-1	2	2	4
A			Different housing parts have different potentials	electrical hazzard on user/3rd party	EC 60601-1		X	X	X	X		X	X		2	9	18	Use of isolating materials for housing or well connected conducting housing, test of contact current	Materials selected to be good isolated, tests of complete system successful according to IEC 60601-1	2	2	4
A			Protective earth is not connected (connection broken)	electrical hazzard on user/3rd party	EC 60601-1		X	X	X	X		X	X		2	9	18	Use of isolating transformer, inclusion of proper isolation of housing, test of contact current	Transformer according to IEC 60601-1 used, tests of complete system succeeded according to IEC 60601-1	2	2	4
A			Remaining charge in device	electrical hazzard on user/3rd party	EC 60601-1		X	X	X			X	X		2	9	18	Inclusion of circuitry for discharge of capacitors, not inclusion of capacitors, tests according to IEC 60601-1	Tests of complete system succeeded according to IEC 60601-1	2	2	4
A			Cable is broken and user/3rd party makes as bridge	electrical hazzard on user/3rd party	EC 60601-1		X	X	X	X		X	X		2	9	18	Use of cable according to IEC 60601-1	Cable according to IEC 60601-1	2	2	4
A	electromagnetic fields from other devices		other medical device emits electromagnetic fields	can distort aquired data from gamma probe and tracking system	EC 60601-1-2	X			X			X	X		2	5	10	add EMV shielding to sensitive parts (PC, cameras, cables); test according to IEC 60601-1-2	EMV shielding added to PC, AVH and cart housing; IEC 60601-1-2 test passed	2	2	4
A			other medical device emits electromagnetic fields	wrong reconstruction	EC 60601-1-2	X			X			X			2	5	10	add EMV shielding to sensitive parts (PC, cameras, cables); test according to IEC 60601-1-2	EMV shielding added to PC, AVH and cart housing; IEC 60601-1-2 test passed	2	2	4

Figure 6.7.: Analysis of risks for definition of requirements on safety for freehand SPECT (excerpt). Table shows the risks proposed in the guidelines and the way of processing them: (1) define if applicable or not, (2) if not applicable, explain why, (3) if applicable, determine initiative effects, potential developments and applicable standards, (4) analyse the involved users and development stages, (5) quantify probability and harm in order to calculate from the product of both the risk, (6) define approach for considering the risk and means to minimize it and (7) finally evaluate remaining risk after correction means.

- Perform automatic verification of system components at start
- Passing EMV Test must be plausible
- Ensure tracking camera signal through interface
- Ensure gamma probe signal and its validity
- Visual instructions for the patient target placement
- Ensure minimum amount of scan data / time
- Ensure time constraints after injection of activity
- Ensure that enough activity is injected
- Adequate instruction for each step in the workflow is needed
- Consider electrical system to pass STK
- Cart Provider must ensure 60601 - 1 mechanical stability - official protocol must be available
- Ensure that all surface material has no chemical reaction with OR environment and cleaning
- Add decription about the proper usage of device and its risks for wrong reconstruction to user manual
- Proper placement, positioning and movement of Cart in OR must be documented in user manual
- Description of intereference and side effects must be documented in user manual
- Ensure no data is lost when when system crashes
- Cleaning and storage instructions must be available

6.7. Economic constraints

As stated in chapter 2 economic constraints have to be taken into consideration before starting any development in order to generate solutions that could turn into plausible approaches on a general basis.

In order to define constraints on the economic side for the freehand SPECT device to be developed, the application to be considered has to be analysed in detail. For SLNB the costs related to the imaging part are essentially the running costs of the radionuclide, the price of the blue dye, the price of the planar scintigraphy and the price of the protective sheath of the probe. Those costs have to be covered with the DRG unless additional money flows into the procedure (e.g. due to a NUB). On the investment side, the costs reduce to the one of the gamma probe, and on service and maintenance to the costs required for quality assurance of the probe and occasional maintenance. Those costs are tabulated in table 6.4.

Item	Cost (EUR)	Frequency	Mean yearly cost (EUR)
Radionuclide	20	per operation	2.000
Blue dye	10	per operation	1.000
Protective sheath	5	per operation	500
Scintigraphy	80	per operation	8.000
Quality assurance	500	once every 3 years	170
Repair	1.000	once every 6 years, 20 % chance	30
Gamma probe	15.000	once every 6 years	2.500
Total	n/a	n/a	14.200

Table 6.4.: Estimated costs for SLNB for a breast surgery center. Assuming 100 patients per year, the average cost per year is calculated. For repairs, the costs are estimated and weighted with the probability of a failure.

Assuming the realization of the proposed protocols and based on the estimated costs in table 6.4, the use of intraoperative imaging only would sustain approximately 9.000 EUR per year (assuming a similar repair and service cost structure). Accordingly the constraint on the economic side is very restrictive.

The only way of loosening such constraint is to generate additional value. Which advantages would functional imaging have for SLNB in breast cancer which can result in reduction of costs and/or improvement of patient treatment? From figures 6.5 and 6.6 the following potential improvements are considered:

1. **Guided incision**: The use of a guided incision, minimizes the trauma and reduces the time in looking for the SLNs. However, in the axilla, most SLNs are located in a 'standard' location and even those placed deeper or further away are accessed from essentially the same incision. As a result, incision guidance results in no practical reduction of costs and thus only in a minimal contribution. This can be however different in applications like melanoma and ROLL (see here chapter 9).

2. **Guided SLNB**: More interesting than guidance for placing the incision is the avail-

ability of depth information during the SLNB. In up to 15 % of the patients the SLNs are located in level II and III [363]. If this information was known a priori in the OR, the procedure could be performed faster and with less trauma. This point can be definitely used as an argument for including freehand SPECT in the OR, however a deeper analysis of the cost reduction should be considered. Here also the applications of melanoma and ROLL can profit significantly.

3. **Control of resection**: Current control of remaining SLNs fails to detect remaining SLNs in up to 20 % of the patients according to internal numbers at Klinikum rechts der Isar. The question is if detecting these structures would result in a change in the diagnostic value of SLNB and at the end in the survival of the patients. Currently SLNB has a false negative rate of 5 % [160]. In an optimistic calculation, given that approximately 20 % of all SLNs are positive, the improvement in the false negative rate could go up to 4 %. This aspect should be considered.

4. **Documentation of procedure**: The last change in the procedure has to do with the possibility of documenting the procedure completely and in a semi-automatic way. Currently documentation is based on a short report including the amount of resected nodes, their count rate and the residual count rate in the axilla. The possibility of reducing time in this step seems negligible. Nevertheless, it may be a factor if the system is used in a country were performance of surgical procedures is usually put into question, as it is the case in the USA.

As a result, the only potential cost reductions would come from the depth information and the control of the resection. These numbers are however hard to quantify.

SLNB procedures take in mean less than an hour, the SLNB resection itself being only in the range of 9 min [64]. Accordingly even a reduction in the range of 5 min would result in almost no difference, as from the functional constraints the imaging time is meant to be in the range of 5 min. The reduction of costs then has to come from a reduced morbidity. The preciser information of freehand SPECT including depth information can result in such a reduction of morbidity, i.e. less damage in the tissue surrounding the SLN. Assuming that the reduced tissue damage due to the use of freehand SPECT results in the reduction of 1

day of hospitalization (faster healing) for the 15 % of the patients with deep lying SLNs, the reduction in costs would be in mean 3.000 EUR per year (1 day hospitalization can be estimated in 200 EUR).

From the side of non-resected SLNs, the cost must be calculated from the resulting costs of diagnosing a patient as N0 although being N1 or N1(mic). This cost is very hard to estimate as it is dependent on the patient. Assuming only an improvement of 2 % on the false-negative rate and a conservative reduction of 7.000 EUR due to a delayed treatment, the improvement for a center dealing with 100 patients a year would result in approximately 14.000 EUR per year.

Summing up all reductions, the available money for a functional imaging system for SLNB in breast cancer alone is reduced to 20.000 EUR per year, i.e. 120.000 EUR including running costs over 6 years. This of course does not include in any form the soft advantages like better patient treatment, increased security, etc.

This small budget reflects the overwhelming importance of a strong clinical impact of the solution proposed and soft advantages. In particular in the frame of freehand SPECT, the economic constraint was estimated for a system used in a hospital performing at least 100 breast cancer SLNBs and 20 melanoma SLNBs, i.e. a device that would have a maximum budget in the range of 150.000 EUR over 6 years. Unfortunately this value poses a limitation to the efforts in development and the costs of the resulting solution. It does not mean that the mentioned 'soft' advantages do not count, but it gives a taste of the hard truth that even the health system has a good component of economics and that increasing costs is only tolerated if there is a big improvement in patient care.

Chapter 7

Implementation of freehand SPECT

Commonly one of the hardest part of any development is to set up proper requirements. Proper requirements are however almost never available and this becomes evident during the implementation part as the devil hides in the details.

For freehand SPECT the implementation included a big part of hardware and more than 20,000 lines of code in 20 modules and almost 100 classes. Here we present the details for the final (and current) implementation in terms of hardware and software. Such implementation is the base of CSS300, the commercial instance of freehand SPECT by SurgicEye GmbH.

7.1. Hardware

Freehand SPECT started in 2005 as fundamentally a software project based on the framework of the Chair for Computer Aided Medical Procedures at TUM. Nevertheless the first major step was to implement proper interfaces for the gamma probe, the tracking system and the camera, all of them hardware components that provided the data needed for the 3D reconstruction and the subsequent visualization. During the development was necessary to give a support to such components, define the specifications for the data processing unit to be used and clarify the sterility of targets and covers for proper user interfaces.

Once the system requirements were fixed many of the degrees of freedom of the beginning were gone. However there is much to do in terms of specifying components and

architecture. For freehand SPECT the implementation of the architecture proposed in figure 4.10 was realized and extended in order to include additional features like augmented reality visualization, etc. The resulting connection plan for the hardware can be seen in figure 7.1.

7.1.1. Gamma probe

The first component to be considered was the gamma detecting probe. Such devices as detailed in chapter 5 provide a one dimensional signal proportional to the count rate detected over a fixed time interval. The requirements for the gamma probe were extracted from the requirement specification described in chapter 6. For the particular case of the gamma probe an excerpt of such requirements can be seen in table 7.1.

Gamma detector has to provide count rate in real time	Count rate input rate $>$ 15 Hz
Gamma detector to provide count rate output	Output to be acquired by PC
Gamma detector has to work linearly up to a high activity at close distance	Linear response up to 20.000 cps (1MBq at 2mm)
Gamma detector has to work for Tc99m	Energy range includes peak close at 140keV
Gamma detector has to hand held	Weight $<$ 500g
Gamma detector has to have a proper radiation shielding from side and back	Shielding $>$ 95% at side and back
Gamma detector has to have a high sensitivity	Sensitivity of at least 0.001 cps/Bq, at 10mm
Gamma detector control unit must be light	$<$ 10kg
Gamma detector control unit must be small	$<$ 50x50x50 cm^3
Gamma detector has to be usable in the OR	certification for probe
Collimator to be narrow	opening angle $<$ 50 degrees
Collimator to allow a minimal sensitivity	opening angle $>$ 10 degrees

Table 7.1.: Example of requirements and resulting specifications for case of gamma probe.

In the implementation of freehand SPECT several devices were evaluated in terms of performance (sensitivity, spatial resolution, sampling rate, weight, etc) in order to fit the requirements posed. From preliminary tests and theoretical consideration the highest priority had to be given to the sampling rate and the spatial resolution. Table 7.2 shows an excerpt of a thorough investigation of the performance of different gamma probe systems available in the market.

Gamma probes do not always provide an output for real-time reading of the count rate data. In the first implementations of freehand SPECT this resulted in the need of working together with the gamma probe manufacturers and defining protocols for data transfer.

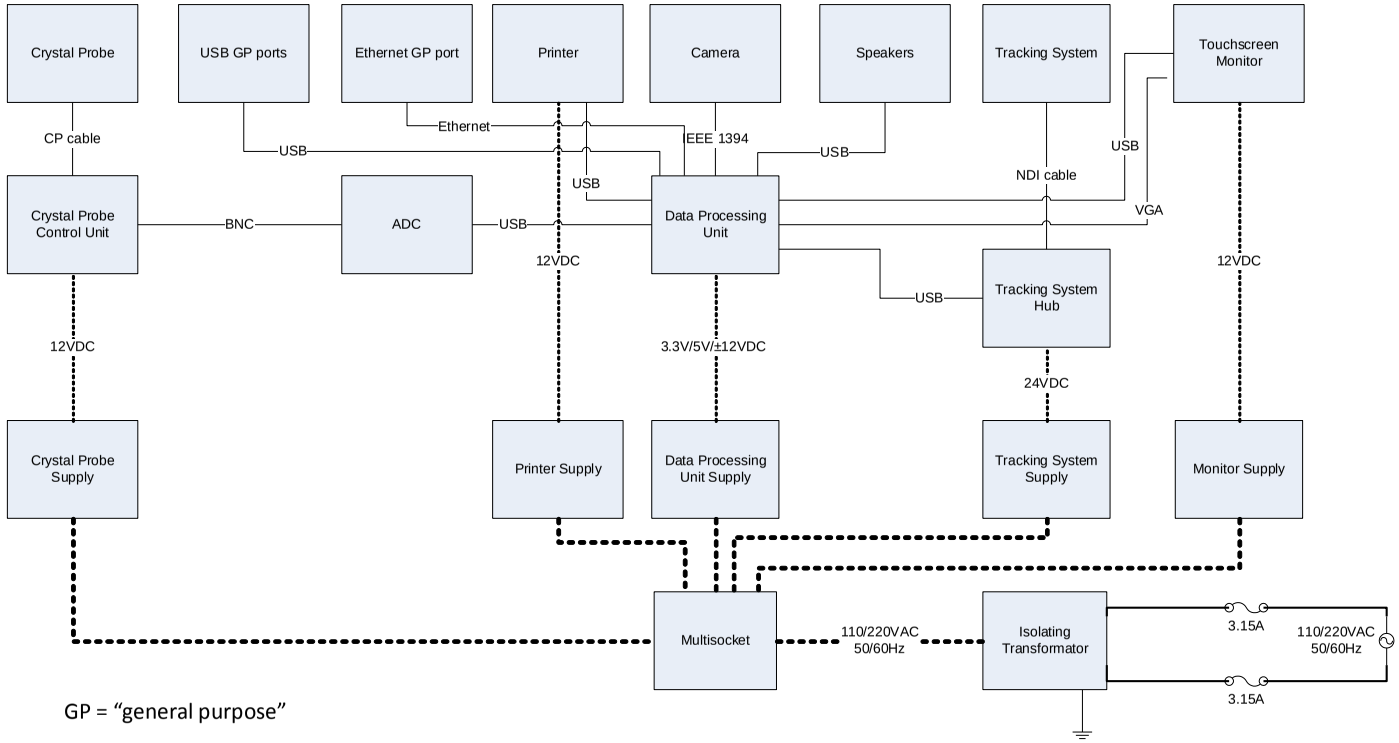

Figure 7.1.: Final hardware connection diagram for the freehand SPECT system. Several features are included for proper use in the OR and exploiting the best of it. Examples are the inclusion of a printer, transfer interfaces, a camera, etc.

Company	Name	Sensitivity, cps/Bq at 1cm	Weight, g	Bending of tip, deg	Technology	Tip diameter, mm	FHWM
Silicon Instruments	SI Gamma Probe	0.005	160	0	Plastic + Si	11	34 deg
Silicon Instruments	SI-Endoscope Gamma Probe	0.003	240	0	Plastic + Si	10	34 deg
Neoprobe	Model 1017	0.0049	80	0	CdZnTe (dia. 7mm, 4mm)	14	26mm at 1cm
Neoprobe	Model 1100 straight	0.0122	240	0	CdZnTe	14	26mm at 1cm
Neoprobe	Model 1100 angled	0.0122	240	30	CdZnTe	14	26mm at 1cm
Neoprobe	Model 2059	0.003	240	90	CdZnTe	10	30 deg at 1cm
Crystal Probe	Standard (Straight) Probe CXS-OPSZB	0.005	400	0	CsI:Tl (dia. 6mm, 8mm)	20	17mm at 1cm
Crystal Probe	Flexible Gamma Probe CXS-OPSZF	0.003	400	0-30	CsI:Tl (dia. 6mm, 8mm)	20	17mm at 1cm

Table 7.2.: Excerpt of comparison of different gamma probes.

Three of such protocols were implemented:

Silicon Instruments' Gamma Control Unit : The first implementation of a communication between gamma probe and data processing unit was implemented for the Gamma Control Unit of Silicon Instruments (Berlin, Germany). That system was based on a Windows 95 computer restricted to have only the minimally required services running on it. The acquisition of the gamma probe information was acquired using a National Instruments digital counter that counted events and was reset to zero by the application running on the system. Given those constraints a software was implemented to read the stack of the digital counter and keep track of the time being able to calculate a count rate at any time. The software ran thus in parallel to the standard software on the system and sent packages over Ethernet containing the count rate for a predefined time window (100ms for example). On the side of the PC collecting all signals, a time-stamp was assigned to each incoming package and added to a ring buffer later used for synchronization.

IntraMedical Imaging's Node Seeker : Another implementation was used in the case of the IntraMedical Imaging (Los Angeles, California, USA) system. There the producer modified his software in order to send a package with count rate and time stamp per Ethernet every 100ms (i.e. the refresh rate of the screen of the gamma probe system). The gamma probe system and the collecting PC were synchronized using the NTP protocol and thus the time stamps included in the package were essentially in the same time as the ones of the collecting computer, making it possible to store the packages as done in the previous case in the ring buffer.

Nucleomed's MR100V : Even best results were obtained using the implementation of

Nucleomed. There the producer modified the firmware of the probe in order to send a single 8-bit character asynchronously over the serial port every time an even was detected. The value of the character was used to encode the energy of the event. On the side of the collecting computer, the serial inputs were filtered using a predefined energy window for each radio-isotope and accumulated in intervals of 5ms, i.e. to have an identical sampling rate as the tracking system.

From all three systems, the best results in terms of synchronization took place with the Nucleomed protocol. The reason for this was the fact that there were not considered delays in the Ethernet communication and in the sampling of the gamma probe. Such effects could be made visible by comparing the count rates obtained with the tracking data. In the case of the Nucleomed device, the delays in the serial port ended up being negligible and the asynchronic character of the transmission enabled practical sampling rates higher than the 100ms set for the Silicon Instrument and the IntraMedical Imaging devices.

There was however a further improvement possible. This came to light by considering that the processing required for displaying the visual count rate and calculating the acoustic feedback did not have to be the same as the one for transferring data meant to be used for tomographic reconstruction using hand held devices. There the constraint was rather to have a proper synchronization between tracking and count rate instead of having a statistically stable value.

In that sense the analog output of the gamma probe was considered. Most gamma probes include such an output used to define energy windows and thus perform calibration. Acquiring such a signal would then also enable counting on the energy information and if proper triggering was possible optimal synchronization with the tracking.

As data acquisition card a PicoScope (Pico Technology Ltd., Cambridgeshire, United Kingdom) was selected and a sampling window of $1\mu s$ was used to sample the analogue signal of the photomultiplier. An example of such a signal can be seen in figure 7.2.

In order to have counts out of the analogue signal a simple peak detector algorithm was implemented to detect peaks over 1V by analyzing the signal once it passed the 1V threshold and then dropped that threshold. This algorithm was not able to tell apart two events if the resulting pulse in the photomultiplier did not fall below 1V, however in practice for

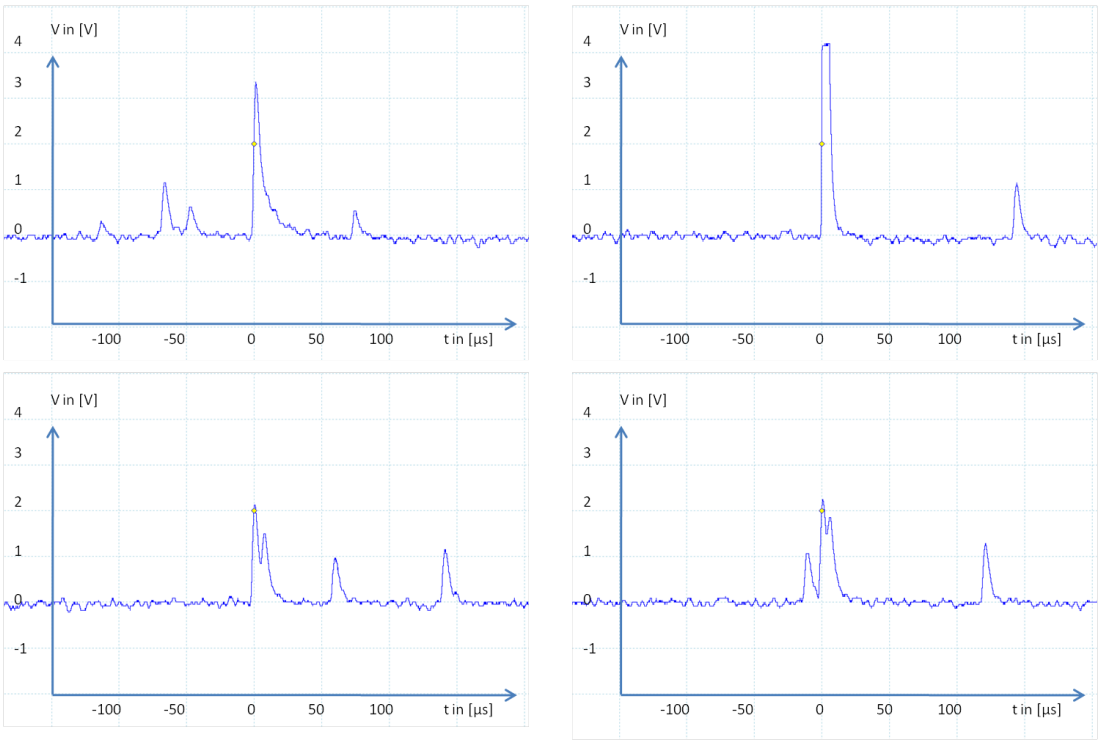

Figure 7.2.: Screenshots of data acquired using PicoScope. Sampling time is set to $1\mu s$ and sampling range from -5V to 5V. Triggering for visualization of curves is set at 2V with rising slope (yellow dot). On the image of the left top a standard waveform is shown. 5 different events can be seen, all of them with different energies. Energy is encoded in the height of the peak, which is proportional to the amount of light the photomultiplier amplified. On the image of the right top a saturated event is seen. The peak has a higher voltage than 5V which results in a saturation and an error in the energy assigned to the peak. On the bottom two examples of events that came too close are seen. On the left both events can be separated while on the right side not. This is due to the fact that a peak is considered to be 'over' if it drops below a voltage. In the implementation of freehand SPECT that threshold was set to 1V.

the count rates used in the target clinical application, this almost never happened. See also here figure 7.3.

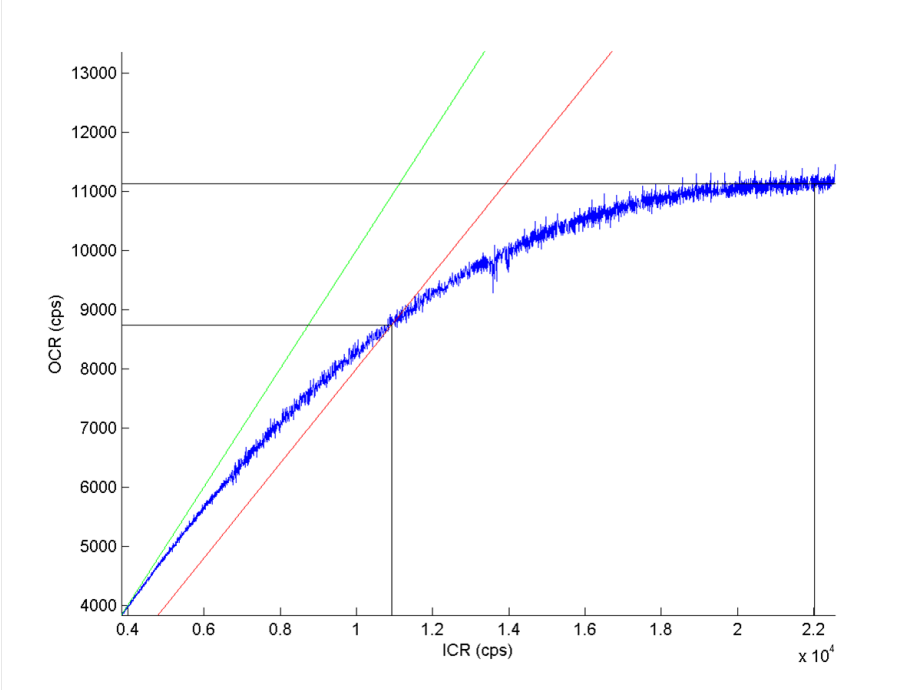

Figure 7.3.: Input count rate versus observed count rate for gamma probe used in freehand SPECT. For count rates over 10,000 cps the probe starts departing from linearity with a percentage of lost counts as high as 20% (difference between red and green line). Such count rates are almost impossible in real situations making mistakes due to saturation effects are minimal.

The digitalization of the analogue signal delivered then digital values for the height of the incoming peaks. In order to set then a proper energy window a discriminator based on two thresholds was implemented. In order to calibrate such a discriminator a graphical interface was programmed and used to visualize the energy spectra of the output of the gamma probe. In figure 7.4 an exemplary spectrum used for selection of energy thresholds can be seen.

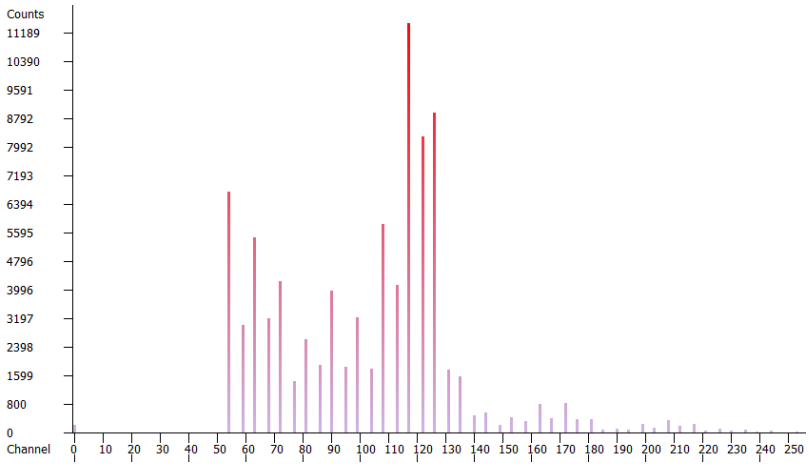

Figure 7.4.: Energy spectrum of gamma probe for ^{131}I. Channel 50 represents approximately the threshold of 1V under which no peak detection is ran. Peak in the range of channels 110 to 130 is the 364keV peak of iodine. The counts in the lower area are essentially scattered gamma rays as well as lower energy emissions of ^{131}I, like the 6% of the decays at 284keV.

7.1.2. Optical camera and tracking

One of the early decisions in the project was to go for optical tracking. Optical tracking was presented and discussed in details in chapter 5. However, beyond the advantages discussed then came from the fact that most gamma probes base on photomultiplier tubes. As a result they generate magnetic field that could disturb an electromagnetic tracking system. Electromagnetic tracking systems are the only alternative to optical tracking that has been successfully applied in medical devices.

Initial results showed that depending on the probe used and the distance between probe and electromagnetic tracking sensor, tracking errors would be in the range 1-3cm. As a result optical tracking was essentially the obvious solution.

In order to fix the required tracking system to be taken the workflow of the target procedures (SLNB) was considered. The specification for the tracking volume was defined from the volume in which the surgeon works. Figure 7.5 shows a tracking volume of sufficient size to cover the region to be reconstructed in almost any SLNB procedure.

Regarding the required frame rate the scanning behavior of several users was considered

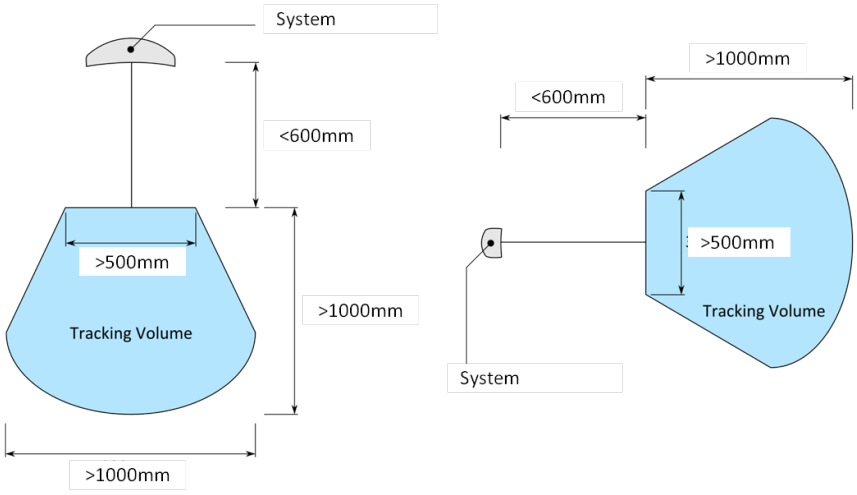

Figure 7.5.: Tracking volume specification for tracking system based on the working volume for SLNB procedures. The selected tracking system, the NDI Vicra system (Ontario, Canada) almost fulfilled such specification in all values.

when handling gamma probes by adding a tracking target to a probe. Results showed that the mean scanning speed was in the range of 0.64mm/s with a standard deviation of up to 2.77mm/s. The maximum speed was reported to be 20.61mm/s. In order to avoid blurring in the ideal case the sampling time should permit a cross talk of less than 20% of the voxel size, i.e. 1mm. As a result, the slowest possible sampling period should be 50ms in order to still catch the 20mm/s movements properly.

Regarding accuracy the maximum expected distance was considered together with a feasible construction of a tracked gamma probe. Given a target accuracy of 1mm at 20cm distance, the maximum error was calculated to be 0.12mm (approximate error amplification in the range of 7). The angular accuracy was calculated in a similar way yielding a maximum error of 0.8deg.

The selected system was then the NDI Vicra system which specifications can be found in table 7.1.2.

Related to the selection of the tracking components was the selection of the camera. The idea was to take an optical camera that could be mounted in direct proximity to the tracking system rigidly. If the camera was positioned to point essentially in the same di-

Accuracy	0.25mm RMS
Update rate	20Hz
Minimal operating distance	557mm
Maximal operating distance	1336mm
Tracking area at MOD	491x392mm2

Table 7.3.: Specifications for selected tracking system. Performance is slightly below the requirements, but within a sufficient range for the target applications.

rection than the tracking system, one could use it not only for displaying the reconstructed radioactive distribution overlaid on the real time video stream, but also to give an intuitive feedback on the position of the different instruments in regard to the tracking system. Ideally such a camera would cover the aperture of the tracking system, so that only instruments seen by the camera would be tracked. Moreover such a combination would enable easy determination of occlusions and even error correction if the images of the optical camera were processed.

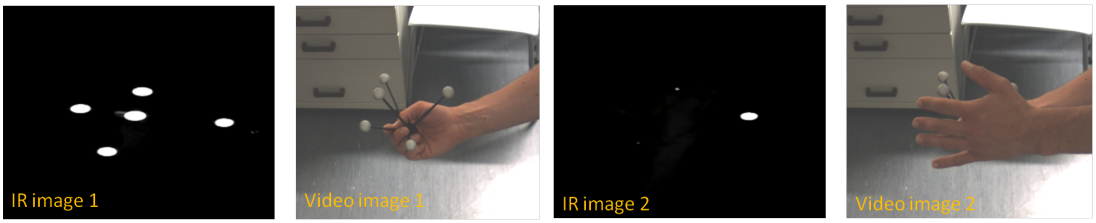

Figure 7.6.: Example of advantage of configuration where optical camera and tracking volume overlap. In images 1 no occlusion is present and optical image and tracking image (IR image) show all balls of the tracking target. In the second image the IR image shows only one ball, but it is impossible to know what is occluding the rest of the tracking markers. This can be easily seen in the optical image taken from almost the same perspective.

Following the specifications of table 7.1.2, a lens of 4mm was selected for a 1/3inch camera. Such focal length would allow the field of view of tracking and camera almost to overlap. In terms of performance parameters table 7.1.2 show the requirement specifi-

cations and the parameters of the selected camera. Particularly important was the frame rate of the camera, as well as its interface in order to enable proper synchronization with tracking and gamma probe readings.

7.1.3. Cart, arm and housing

From preliminary experiences with freehand SPECT it was clear that a proper support for all components was needed. Inspired in navigation solutions for neurosurgery, as well as ultrasound devices, a structure based on a cart with an arm was selected. The arm was meant to carry the tracking system and the camera, and pose them over the operation situs minimizing space requirements in the OR. The data processing unit was meant to be carried by the cart and used as weight on the lower part of it for better stability. The gamma probe control unit, if available, could also be placed in the cart making the transport of the system easy (see figure 7.7).

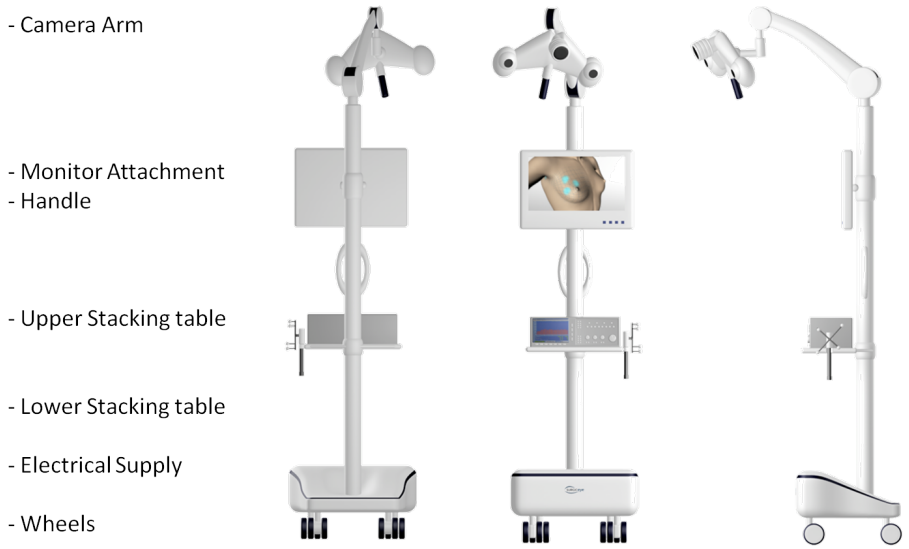

Figure 7.7.: Original target configuration of cart for freehand SPECT as shown with a mock up. Stacking tables were thought to place gamma probe and PC. The cart was meant to include a insulating transformator in order to be compliant with the safety regulations mentioned in chapters 2 and 11.

The specifications for the cart and arm were thus summarized and based on them a cart

Requirements of hardware	**Specifications of hardware**	**Specification of currently selected hardware**
Image size has to be a big part of screen	image size $>$ 800x600	1034x778
Image size has to allow fast processing (not too big)	image size $<$ 1200x800	1034x778
Refresh rate should be similar to the one of the tracking system	close to 20 fps	30 fps
Refresh rate sufficient for video "feeling" for normal humans	$>$ 15 fps	30 fps
Image has to be color image	RGB at least	RGB
Camera may not see IR light	IR filter must be included if not part of camera or lens	IR filter
Camera has to be small	$<$ 7x7x7 cm^3	48.2 x 30 x 30 mm^3
Camera has to be light	$<$ 200 g	50g
Camera has to work without interference of the surgical theatre	EMV shielding if not part of housing	industrial shielding

Table 7.4.: Requirements, specifications and technical details of selected camera for system.

was configured using catalogue parts of a cart supplier for medical devices. For each of the components a list of requirements was specified. For example for the arm the list included the following constraints:

- Arm has to be movable from head with one hand
- Arm should remain at a position once released
- Arm should move easily
- Cables have to be attached to arm
- Cables have to be covered
- Movement of arm should not interfere with cables
- Arm should enable disinfection
- Arm should fixable for transportation
- 3 cables to be considered (1x firewire 6-poles and IIDC V1.3 for single camera, 1x custom cable for tracking system), approximately each below 4mm diameter, min. bending radius 2cm

The final solution for the cart and arm can be seen in figure 7.8.

Figure 7.8.: Cart solution from original idea on the (left) to design from available components (center) and final realization (right). Besides the base components, also a proper housing for the PC was developed and used. In the current version the camera head has also been replaced for a finer design to be seen throughout this work.

Special care had to be taken regarding the power supply as it had to be chosen to be compliant with the standards EN 60601-1 and EN 60601-1-2 as explained in chapter 2 and in the appendix of chapter 11.

7.1.4. Data-processing unit

The selection of a proper data processing unit was also an important task. Essentially there are two components which play the most important role: the memory and the processor. In the current implementation of freehand SPECT the graphic card is not yet exploited completely, however if the porting of calculations to it is desired it will gain in importance.

In order to estimate the required memory the requirements of the system were considered. There the system was meant to be able to reconstruct volumina of up to 30x30x30 cm^3 with a resolution of $5mm$, resulting in a matrix of 216,000 voxels. Following the proposed solution of chapter 4, each line of the system matrix would require thus 200,000 floating point elements (16bit). For an expected amount of readings of up to 4,000, the memory requirements are 1,600,000,000Byte. Including thus a minimal buffer for the operating system a minimal requirement of 4GByte seems feasible. Current implementations of the system have 6GByte in order to minimize the risk of memory lack.

The processor was estimated from the computational burden for the reconstruction and the different threads running in parallel. The software was programmed to deal in different threads with (a) data-acquisition, (b) data synchronization, (c) data visualization, (d) user interaction, (e) image reconstruction. In this way ideally the architecture of the processor would have at least 4 cores. For the reconstruction a time limit of 1min was set which for 20 iterations of MLEM implies 16,000,000,000 updates in 60 seconds or in the range of 4GFLOP/s. The used PC had 4 cores and a clock of 2.67GHz (approx. 10GFLOP/s per core).

7.1.5. Tracking targets

In order to be able to track the gamma probe a proper tracking target had to be designed and constructed. The challenge here was to come to a solution that could be used sterile yet that would not need to calibrate the device in every use. The boundary conditions

were the following:

- Gamma probe has to be covered for sterile use.
- Optical tracking through sterile cover drops accuracy by a factor of 5 to 10.
- Calibration of gamma probe tip relative to tracking target should be a one time calibration and cannot be performed before each use.

Such constraints led to a solution where a non-sterile part (called probe base) was fixed rigidly to the gamma probe. A second sterile part (called probe target) was developed in a way that it would be able to grab the non-sterile probe base at a unique position through the sterile cover. See also figure 7.9.

Figure 7.9.: Proposed solution for probe target including a fixed base that enables to keep the calibration between probe tip and tracking target constant while making possible the use of a sterile target over the sterile cover.

The selection of the material here was important. In order to guarantee biocompatibility, mechanical stability and no deformations over hundreds of sterilization cycles only three materials came into evaluation: surgical steel, titan and PEEK. Due however to the inclusion of moving parts in the mechanism for fixing the probe target in relation to the probe base, the metals were preferred and due to to cost reasons the steel selected. This solution was further developed in terms of ergonomics and proper mechanics in cooperation with the design company Oxxid GbR resulting in the prototype of figure 5.4.

Evaluations on repositioning of the tracking target relative to the probe tip shown a repositioning error below 0.1mm matching a good solution. The sterile part was also suc-

cessfully evaluated in terms of cleaning and sterilization.

Not only the gamma probe had to be tracked but also the patient. The reason for this was the requirement on flexible movement of the tracking system and the patient during the operation. As in the case of the probe target the requirements on biocompatibility and re sterilization are also applicable. Here, however, no need of moving parts makes the development of a target easier.

The final solution consisted on a base part that is taped to the patient's skin (applied part according to the EN 60601-1). The design included posts in order to clip infrared marker spheres to it easily as in the case of the probe target.

In order to minimize running costs the base structure was made of a re sterilizable material (medical PEEK) and surgical steel pins. PEEK has excellent mechanical properties in terms of deformability and thermal stability. In this way there is no problem in using it for hundreds of sterilization cycles without detectable deformations.

The result can be seen in figure 7.10.

Figure 7.10.: Final version of patient target/reference. Three tracking markers are sufficient for tracking a 3D body. Dimensions are minimized in order to enable flexible positioning. Feet can be used to fix it to the patient with sterile tape.

7.1.6. Sterile covers

If meant to be used in the OR, as described in the previous version, care show be taken to cover all non sterile structures that may come into contact with the sterile area. If the freehand SPECT system essentially two components were considered: one of the handles and the monitor.

Ideally the touchscreen monitor would be operated solely by the surgeon and the OR

nurse. Accordingly a proper cover had to be designed. As constraint the cover had to extend way behind the monitor in order to be able to grab it on the sides in order to tilt it. Also reflections had to be taken into account. If the visibility of the images was jeopardized, the cover would end up making more problems than helping a proper use. The monitor itself had also to be chosen to have a resistance based touchscreen, rather than a capacitive one in order to be able to use a cover.

For the handle, several iterations had to be performed in order to obtain a proper result. In the case of OR lamps, most of the handles are clipped to the lamps with a fast clipping mechanism. The handles are thus made of sterilizable materials. Another alternative is to use a one-time cover that fits easily on the grip. Such was the selected solution in the current implementation of freehand SPECT. The handle of the device had to be adapted for such means. See figure 7.11 for solution.

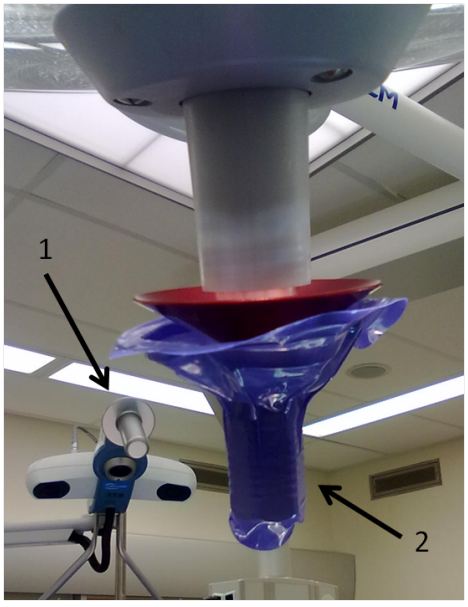

Figure 7.11.: Example of implementation of sterile handle with sterile cover. (1) shows the handle of the freehand SPECT device without cover and (2) shows a lamp with the selected cover.

7.2. Software

7.2.1. Synchronization

Synchronization is one of the key points in hand held imaging. The reason for this is the fact that any error in synchronization would result in improper information on the projection and thus inconsistencies in the data sets which result in blurring of the reconstructed image.

There are different strategies for proper synchronization. All of them however require the availability of a common clock. In order to do so essentially two approaches are available: the use of a single clock and hardware synchronization or the use of systems for clock synchronization like the NTP protocol.

Once a common clock is available timestamps can be used for each signal involved and synchronization can be used based on them. A good approach is the use of the closest timestamps rather than taking the last one. Accordingly all incoming signals can be stored in a ring buffer with the timestamps of their income. If synchronized data is needed, the latest closest signals can be selected based on the timestamps. See also figure 7.12.

Such an approach was implemented in freehand SPECT. There the input signals buffered are tracking data (for probe and patient), gamma probe data and video data from optical camera.

7.2.2. Pre-processing

Once the data is digitalized and synchronized, the reconstruction may being. Nevertheless there are initial filtering steps that can be taken in advance, which on their own have shown to have a big impact on the quality of the resulting imaging. This pre-processing steps are divided in filtering and carving procedures depending on the type of data they act. Filtering means act on the incoming measurements, i.e. on the 7-tuple that describes count rate and 6D position/orientation. Carving acts on the system matrix by eliminating voxels that either cannot be reconstructed or which value is know before hand.

In this work, filtering is performed in two steps. First, all rows i of the system matrix H where $\sum_i H_{i,j} \leq t_r$ are discarded. t_r is a threshold in cps/Bq under which the contribution

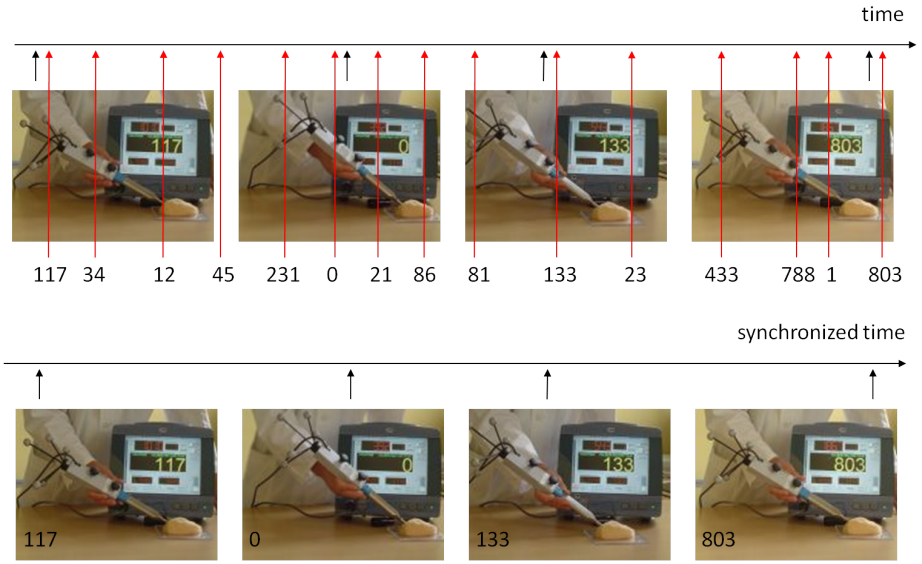

Figure 7.12.: Synchronization of signals with different refresh rates based on the comparison of timestamps and selection of the closest inputs. Here signal of a gamma probe is synchronized to the video signal of the camera.

of a measurement to the overall reconstruction is considered negligible. Since the acquisition is performed freehand, this situation frequently occurs: low value rows correspond to measurements that did not "looked" into the region to be reconstructed according to the model used. In a second step, readings that were acquired during too fast movement are rejected. The speed is estimated from the angular and linear displacement relative to the previous reading.

The next step is to eliminate voxels with too little information. Here also the sum over the system matrix H can be done, however now over each column j. All columns i with $\sum_j H_{i,j} \leq t_c$ are discarded. Low value columns are voxels for which the scanning was incomplete, again a common situation in freehand scanning.

The second carving step removes all voxels x_i that intersect with the detector during the scan, meaning those voxels are not located inside the object of interest but in the air, and can thus be discarded for reconstruction. This filtering is performed by geometric intersection of the region to be reconstructed with the detector modeled as a cylinder for all measurements $j = 1, \ldots, m$. An example of such a carving can be seen in figure 7.13.

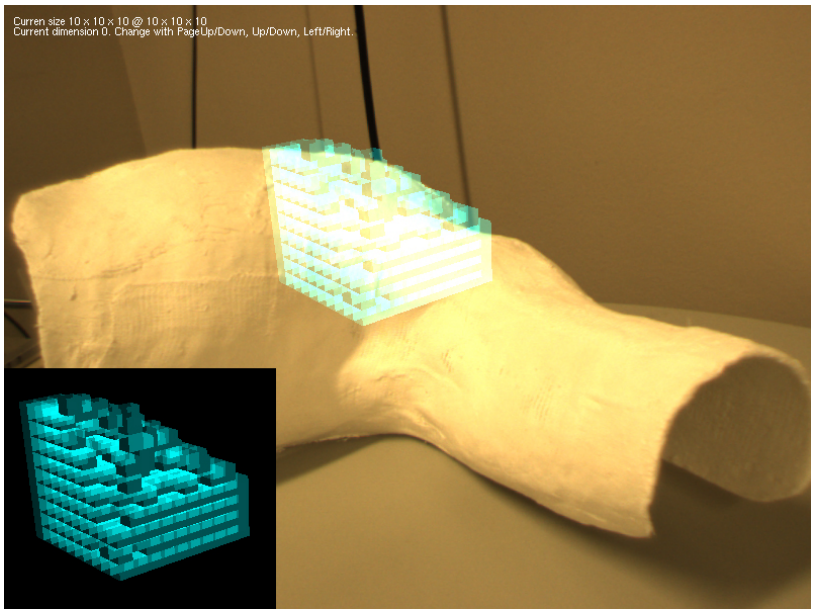

Figure 7.13.: Example of performance of carving algorithm based on the contact of the gamma probe with the volume of interest (left lower corner) and augmented reality visualization over model for plausibility evaluation.

7.2.3. Models

In chapter 4 the image reconstruction proposed required. During the development of this work several models for gamma radiation were developed from the initial work by Alexander Hartl from the Chair for Computer Aided Medical Procedures [128].

In all of them the response of a gamma probe in presence of a point source at a particular distance d and the angle α between it and the axis of the detector was modeled (see figure 4.15 for reference).

As example, a very first approach is consider the detector as a pure active area. If a gamma ray passes this area then the detector would count an event. In such a configuration the amount of gamma rays detected in average from a 1Bq source at a distance d subtending an angle α is given by:

$$m_{SA}(d,\alpha) = \frac{1}{2\pi}\int_0^R \int_0^{2\pi} \frac{r}{\sqrt{(d\cos\alpha - r\cos\theta)^2 + r^2\sin^2\theta + d^2\sin^2\alpha}} d\theta dr \qquad (7.1)$$

where R is the radius of the detector.

If further a collimator is added and modeled as a perfect absorber, the model can be corrected slightly:

$$m_{SA2}(d,\alpha) = \begin{cases} m_{SA}(d,\alpha) & \alpha < \beta \\ 0 & \alpha > \beta \end{cases}, \tag{7.2}$$

where $\tan\beta = R/L$. L is here the length of the collimator.

The two upper models can be also seen graphically in figure 7.14.

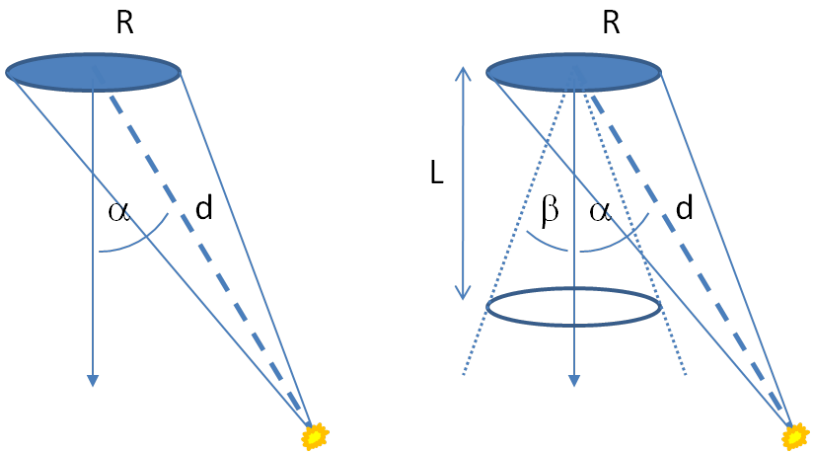

Figure 7.14.: Two simple models for gamma probe detection process. Solid angle between point source and detecting area is calculated in order to determine average gamma ray flow through the detector. R is the radius of the detector, L the length of the collimator. β is the aperture angle of the collimator. The independent variables here are the distance between the center of the detector d and the angle α.

For this final implementation of freehand SPECT several further models of different complexity were considered. As biggest dicotomy the models developed are divided in area, volume and ray-tracing models. The first ones propose that the acquisition process can be modeled by considering the detector as an area. As such the amount of detected gamma-photons could be expressed as a fraction of the gamma-rays passing through the detector area. In a second approach, the detector was considered as a detecting volume. In this case the shielding of the sensor was also considered. The third case was a more realistic

view of the acquisition in which the detected rays were followed from their emission point and the different events on the ray were considered. Table 7.5 summarizes the effects considered in each type and version of the model implemented up to date.

For further details on the modeling process, please refer to the report of the project by Alexander Hartl [128].

Model	Version	Effects considered
Area	1	Distance attenuation
	2	Distance attenuation, Background noise
	3	Geometric attenuation
	4	Geometric attenuation, Background noise
	5	Geometric attenuation, Length of interaction
	6	Geometric attenuation, Length of interaction, Background noise
Volume	1	Geometric attenuation, Length of interaction, Shielding
	2	Geometric attenuation, Length of interaction, Shielding, Background noise
	3	Geometric attenuation, Length of interaction, Shielding, Scattering in Shielding
	4	Geometric attenuation, Length of interaction, Shielding, Scattering in Shielding, Background noise
Ray tracer	1	Geometric attenuation, Length of interaction, Shielding
	2	Geometric attenuation, Length of interaction, Shielding, Background noise
	3	Geometric attenuation, Length of interaction, Shielding, Scattering in Shielding
	4	Geometric attenuation, Length of interaction, Shielding, Scattering in Shielding, Background noise
	5	Geometric attenuation, Length of interaction, Shielding, Scattering in Shielding, Absorption in patient
	6	Geometric attenuation, Length of interaction, Shielding, Scattering in Shielding, Absorption in patient, Background noise

Table 7.5.: Implemented models for the acquisition of gamma-probe readings as proposed in the work of Alexander Hartl.

Chapter 8

Preoperative evaluation of freehand SPECT

After successful evaluation in a preclinical setup during the implementation steps, phase I and II studies were planned in humans. Both studies were done for the particular case of lymphatic mapping in breast cancer. The major reason for this was the fact that SLNB in breast cancer was one of the first target indications and moreover, it was an indication were the big throughput of patients in most hospitals would allow a rapid evaluation. Technically imaging SLNs in the axilla was also not considered to be the most difficult task that freehand SPECT was targeting.

8.1. Pilot study on scan protocol and validation

The first step for evaluating the freehand SPECT technology clinically was to check the feasibility of it for imaging radioactive deposits in human bodies. Unknowns were at that time, what would be a proper scan duration and if the uptake of target structures in the case of living organisms, as well as its position would make it possible for freehand SPECT to detect them or not. In the first stage, the feasibility in the case of sentinel lymph node (SLN) mapping in breast cancer was evaluated.

8.1.1. Aim

Aim of the pilot study was the determination of optimal parameters for freehand SPECT imaging. The study was on its own divided in a one pilot study with 50 patients and further a validation study with 35 patients. The pilot study was considered as a phase I study, in order to clarify the parameters needed for proper imaging. In particular, as the acquisition protocol strongly affects the performance of freehand SPECT, the goal was to define thresholds and quality criteria that allow determination of an appropriate freehand SPECT image quality. The second part was meant to obtain a first grasp of the potential performance of the system given the optimized parameters from the first study.

The results of this study were published in [363] and are adapted here to the thesis.

8.1.2. Methods

Inclusion and exclusion criteria

This first study was planned as a prospective study. The inclusion and exclusion criteria were the same as used for routine SLN biopsy in breast cancer patients, as described in the guidelines for SLN diagnosis of the 'Deutsche Gesellschaft für Senologie' (German Association for Senology) [176]. Criteria therein are essentially equivalent to those of the American Society of Clinical Oncology [196]. Among these, the key inclusion criteria were the initial diagnosis of invasive breast cancer or advanced ductal carcinoma in situ (size $>$50mm, confirmed by core needle biopsy), the lack of prior anticancer treatment, and age over 18 years. Key exclusion criteria were preoperatively confirmed multicentric tumor growth, clinically suspicious axillary lymph nodes, and pregnancy.

Ethical considerations

The acquisition of the data required for the studies did not required any additional radioactivity nor any invasive procedure. All patients undergoing conventional lymphatic mapping of breast cancer were asked if they agreed to stay for 15 minutes longer for a freehand SPECT acquisition. Details of the procedure were explained to the recruited patients. The patients also received an information sheet. This procedure was approved by both the

directors of the Nuclear Medicine Department and the director of the Women's Hospital at Klinikum rechts der Isar after discussion with the representative for the Ethical Committee of the hospital.

Clinical and histopathological characteristics of patients

A total of 85 consecutive patients (age 29-88 years, mean 59.5 years, Sept. 2008 - Sept. 2009) undergoing conventional SLN biopsy were additionally scanned using freehand SPECT and SPECT/CT serving as reference. Six patients were not included during the final evaluation, due to missing information for a proper comparison (3 during the pilot study and 3 during the validation study). According to the preoperative clinical staging procedures, 71 out of 76 patients (93%) had a core needle biopsy confirming cT1 or cT2 invasive-ductal or invasive-lobular breast cancer (size 4-44 mm) and no clinical suspicion of axillary lymph node involvement. Five patients had a locally advanced ductal carcinoma in situ (size 50-140 mm). No metastatic disease was evident at the time of surgery. Fifty-eight patients (78%) received breast-conserving surgery; in 18 patients (24%) radical or subcutaneous mastectomy was performed owing to an unfavorable ratio of tumor and normal breast tissue. A single patient underwent a primary standard axillary dissection, due to the intraoperative presence of suspicious axillary lymph nodes. In fifteen patients (20%), the SLN showed tumor cells in the frozen section and a standard axillary dissection of lymph nodes (levels I and II) was performed. Five patients had a tumor-free SLN in the histological frozen section but micrometastases were described in the final pathology report following secondary axillary dissection (levels I and II).

Planar scintigraphy

For lymphatic mapping, patients received a ^{99m}Tc-Nanocoll injection of approximately 0.2ml, distributed equally in four spots, either periareolar (76 cases) or peritumoral (9 cases). The amount of radioactivity was 57.9MBq (SD, 5.5MBq). All but one patient underwent a 2-day protocol, which is the standard procedure at our institution. The injected activity was in the range of 10-20MBq for the 1-day protocol and 50-90 MBq for the 2-day protocol. In all patients, dynamic planar lymphoscintigraphy representing the standard

imaging protocol for lymphatic mapping at TUM was performed (see figure 8.1). Delayed planar images were used only in case of a negative early scan. For intraoperative identification of sentinel nodes, planar scintigraphy was used as reference method. A flood phantom with 1MBq was used to give an anatomical context.

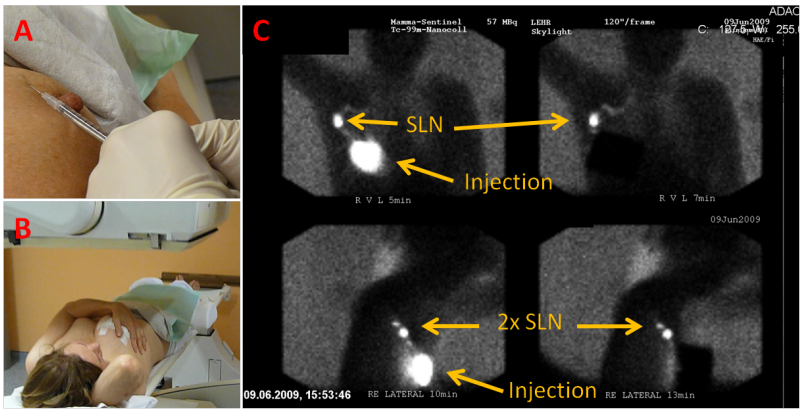

Figure 8.1.: Preoperative planar scintigraphy procedure at TUM. (A) after injection, time starts running. (B) planar images at taken with 2 head camera in AP direction, as well as lateral projection. During acquisition patient holds breast in contra lateral direction and has arm up. Camera is placed as close as possible to patient, in (B) camera is not yet finally placed. (C) shows the result for one exemplary patient with an excellent uptake and 2 clear SLNs.

SPECT/CT

The SPECT/CT protocol consisted of 45 projections (180 degrees of rotating using two opposing heads for acquisition) of 7s each using a Symbia T6 hybrid scanner and LEHR collimators (Siemens Healthcare, Erlangen, Germany). For image reconstruction, an OSEM reconstruction algorithm with 16 subsets, 8 iterations, collimator blur, and attenuation and scatter correction (Flash3D software, Siemens Healthcare, Erlangen, Germany) was used. Postprocessing was performed using an 8.4mm Gaussian filter; attenuation correction was performed using CT data. The reconstruction volume included the injection site and the axilla and neck region. The reconstruction voxel size was 4.7mm in each direction. For CT scanning, a low-dose procedure was used with a 3mm slice thickness (20-40mA tube cur-

rent, 130keV tube voltage, shallow breathing, and expected absorbed dose of 0.2-0.4mSv, depending on patient size). In all patients, SPECT/CT was performed within 15 min after planar scintigraphy. The level assignment (levels I - III) of SLNs was determined using the SPECT/CT images according to the current guidelines [196] (see also figure 8.2).

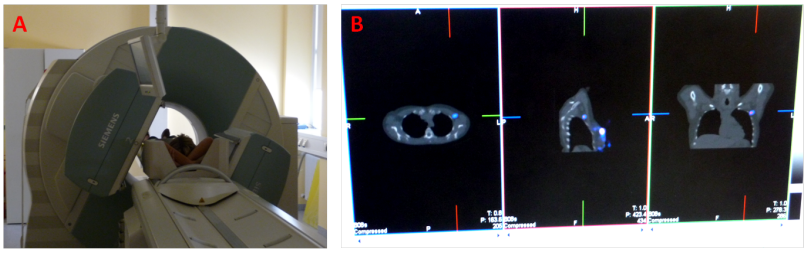

Figure 8.2.: Preoperative SPECT/CT at TUM. (A) SPECT/CT is acquired with arms behind head. (B) Reconstructed 3D images are then visualized in all three slices.

Freehand SPECT

For the freehand SPECT acquisition (performed shortly before or after SPECT/CT), the gamma probe system by IntraMedical Imaging (NodeSeeker, Los Angeles, CA, USA) and the optical tracking system by Northern Digital (Polaris Vicra, Waterloo, ON, Canada) were used. The gamma probe was connected over Ethernet and was modified to send the count rate at a frame rate of 10fps. Furthermore, a PC was included in order to: (a) acquire the readouts of the probe and the position synchronously, (b) process the readings into a 3D image, and (c) display it for visualization. Infrared markers were attached to the gamma probe in order to acquire its position. To reference a common coordinate system, a patient target (as described in the chapter 7) was used to determine the position of the patient (Figure 1A). The hardware was designed and adapted to be completely mobile so as to be suitable for application in the OR. The gamma probe was calibrated to include the 140keV peak of ^{99m}Tc with an energy window of 50keV. The collimator opening of the probe was measured using a point source and yielded approximately 50 degrees.

The freehand SPECT acquisition consisted of three steps. Initially, a volume of interest (VOI) was defined interactively by putting the tip of the tracked gamma probe over predefined anatomical landmarks (as described in chapter 7). Subsequently, the region to be

reconstructed (axillary region) was scanned. Finally, visualization of reconstructed images was performed. The reconstruction was done using a version of the MLEM algorithm adapted for the particular case of freehand SPECT. For the determination of the system matrix, the solid angle model considering only distance and angle was used. The probe carving was turned on during all acquisitions. After 20 iterations (value empirically determined from preliminary experiments during preclinical phase), the output was filtered with a 6-mm 3D Gaussian filter and visualized. In the event of node localization in close proximity to the injection site, the filter was set down to 4 mm to determine whether there was a clear separation between node and injection site. Additional voxels were added in the required direction a posteriori if the volume of reconstruction did not cover the complete VOI as indicated by SPECT/CT imaging.

Due to the freehand nature of the new technology, a scanning protocol had to be defined, in particular regarding the duration of the scan and the orientation of the probe relative to the anatomy. The protocol consisted of a scan of the injection site and the axillary area (see figure 8.3). The scanning protocol was validated by several phantom acquisitions.

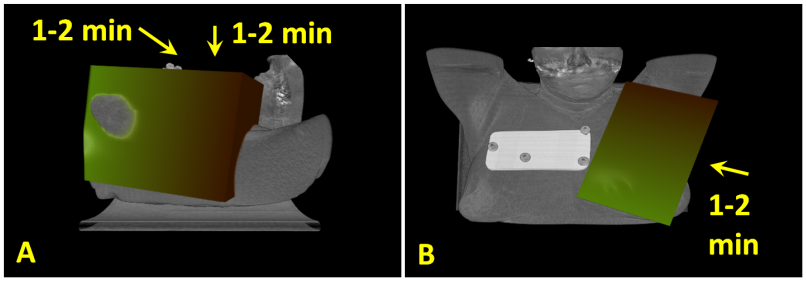

Figure 8.3.: Scan protocol of freehand SPECT during pilot study. The protocol was divided into 1-2min acquisitions in the medial direction, 1-2min pointing in the dorsal direction, and 1-2 min in a craniodorsal direction.

For the first 50 patients (pilot study), no feedback on the quality of the acquisition was given during the scan. For the second group of 35 patients (validation study), the information density accumulated in each single voxel of the VOI was displayed during the acquisition as well the position of each acquisition (see figure 8.4). The scan was only stopped when the complete volume reached a sufficient information density and thus a sufficient quality. The used quality threshold was the average value of the column sum for the par-

ticular voxel (see next subsections). Quantitative thresholds on this quality measure were derived from the data of the pilot study with 50 patients.

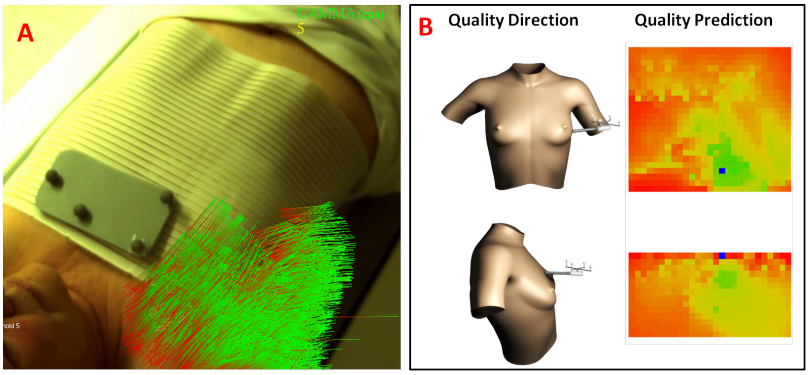

Figure 8.4.: Quality visualization for freehand SPECT during protocol. (A) shows the display of the acquisition lines over the patient. Red shows the tip of the probe and green the distal end of it. Simultaneously the quality was displayed using a visualization similar to the one in (B). Both images start in red and turn greener and greener the more quality is collected. The blue point shows the voxel that currently is 'touched' by the gamma probe.

Comparison of freehand SPECT and SPECT/CT

In order to compare SPECT/CT and freehand SPECT images in an identical coordinate system, a tracking target was attached to the patient. The target consisted of a fixed configuration of optical markers (1 cm diameter) that could be easily identified on CT images, enabling a point-based registration of the coordinate system of the optical positioning system and CT. SPECT images were co-registered with CT images according to the information in the DICOM tag. The freehand SPECT images were generated in the coordinate system of the optical markers of the patient target. The registration error of the target was calculated to be 0.6-3.1mm (average 1.1mm).

Data analysis

Each anonymized SPECT/CT image was reviewed by two expert nuclear medicine physicians in random order. The number of detected SLNs or lymph node conglomerates and

their position were documented. Lymph node conglomerates were considered as a single entity. This information was used to calculate the uptake in each node/conglomerate using attenuation-corrected SPECT data. The uptake was expressed as percentage of total activity in the reconstruction area and calculated from the counts inside the manually segmented lymph node and the total counts in the attenuation-corrected SPECT image. The complete injection site and the drainage area of the breast were included in all SPECT images in order to obtain the true relative uptake. The segmentation was done directly in the 3D images to avoid errors resulting from projections. Subsequently, two nuclear medicine physicians evaluated freehand SPECT images in random order and in a combined visualization together with the video stream of the procedure or CT data in order to correlate functional data with anatomy (see figure 8.5). The number of lymph nodes and lymph node conglomerates was recorded together with their respective anatomic position.

Statistical evaluation

The results of the blinded analyses of SPECT/CT and freehand SPECT were considered together with the uptake calculated from attenuation-corrected SPECT. In addition, for the first 50 patients, the quality of the scan was assessed using the positions and orientations measured and the position of the lymph nodes as segmented manually by the physicians.

For each position and orientation of the gamma probe during a scan, the expected count rate (expressed in cps/kBq) was calculated as if a point source of 1kBq was located in the position of the segmented SLN, according to a model based on the geometric information (see figure 8.6). This count rate was averaged over all measurements which included the lymph node in the corresponding scan. This value was used as information density and consequently used for the calculation of different quality values of the scan for the lymph node.

A small value of quality should mean that the scan did not fully cover the position of the SLN, such that the average information acquired coming from its position was very low. A high value of quality mean that the position of the SLN was inside the field of view of the probe in several of the measurements, leading to accumulation of a higher amount of information.

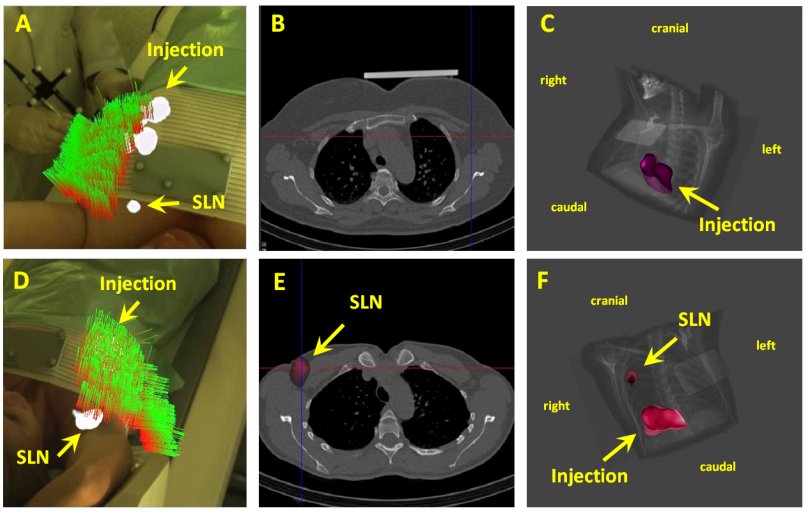

Figure 8.5.: Examples of a poor quality (A-C) and one good quality scan (D-F). The lines shown in A and D represent the positions and orientations of the gamma probe during the scan. In A and D, the injection site and the SLNs as seen in the SPECT image are also shown, co-registered in the correct position. In B and E, the freehand SPECT images are co-registered with CT data derived from SPECT/CT data. In C and F, co-registered visualization is rendered from an arbitrary point of view. One SLN can be seen in 3D fused visualization for the good scan (F) together with the injection site. In the poor quality scan, only the injection site is visible (C). The poor scan clearly misses the SLN (A), while several readings cover the SLN in the case of the good scan (D).

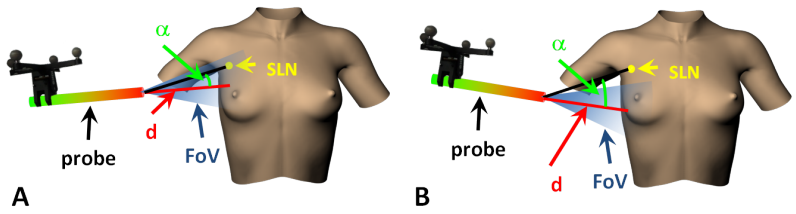

Figure 8.6.: Mock-up of the methodology used to calculate the quality measures analyzed of a scan. In (A) the tracked gamma probe (tip, red; back, green) receives information from the radioactivity in its field of view (FoV). Using the position of the SLN segmented manually by the physician and the position and orientation of the gamma probe, the distance d and the angle α can be calculated. Subsequently, these values are used to calculate the expected count rate measured by the probe assuming 1kBq at the position of the SLN, this value is then used to calculate the different quality measures. For calculation, the solid angle and the parameters of the gamma probe are also used. In (B), a measurement is shown where the probe does not include the SLN in its FoV. Accordingly, there is no contribution with respect to the quality of the scan in none of the measures.

Several quality values were calculated from the expected count rate $E[g_i]$. They are listed below:

$$Q_{count} = \sum_{E[g_i]>0} 1 \tag{8.1}$$

$$Q_{average} = \sum_{i} E[g_i] \tag{8.2}$$

$$Q_{sum} = \sum_{i} E[g_i] \times N_{meas} \tag{8.3}$$

$$Q_{non-zero\ count} = \sum_{i} E[g_i] \times \frac{N_{meas}}{Q_{count}} \tag{8.4}$$

$$Q_{count\ 0.0001} = \sum_{E[g_i]>0.0001} 1 \tag{8.5}$$

$$Q_{0.0001\ count} = \sum_{i} E[g_i] \times \frac{N_{meas}}{Q_{count\ 0.0001}} \tag{8.6}$$

Accuracy was calculated using SPECT/CT findings as reference. It was calculated for the overall patient group, as well as for each scan quality level and also with respect to the relative and absolute tracer uptake in the SLNs.

In order to give a measure for the available information for the reconstruction, the mean number of readings per voxel was calculated from the quotient of the total amount of readings and the total amount of voxels.

8.1.3. Results

Findings of SPECT/CT

A total of 125 SLNs were detected on SPECT/CT (83 and 42 in each part of the examination, respectively). At least one SLN was detected in 96.2% of the patients (76/79); see details in table 8.1.

The average relative uptake in the SLNs was 0.86% (SD, 1.3%, range 0.003-14.1%) of the total radioactivity administered at attenuation-corrected SPECT. The absolute uptake presented a similar distribution, being in the range of 1.3-7,882.3kBq (mean, 499.5kBq, SD, 741.0kBq). No radioactivity beyond the injection site and lymphatic draining region could be detected in all of the patients. Out of 125 SLNs, 64 nodes were located in level I, 15 in level II and 4 in level III, respectively (pilot study). In the validation study, 34,

	Pilot study (n=50)		Validation study (n=35)	
	SPECT/CT	fhSPECT	SPECT/CT	fhSPECT
Patient drop outs	3	3	3	3
Patients without SLNs	3	27	0	4
Patients with 1 SLN	23	17	23	20
Patients with 2 SLNs	12	2	8	7
Patients with 3 SLNs	4	1	1	1
Patients with 4 SLNs	3	0	0	0
Patients with 5 SLNs	0	0	0	0
Patients with 6 SLNs	2	0	0	0
SLNs in level I	64	21	34	29
SLNs in level II	15	2	5	3
SLNs in level III	4	1	3	3

Table 8.1.: Detection of SLNs in the pilot and validation studies. fhSPECT stands for freehand SPECT.

5 and 3 SLN were located in levels I, II and III, respectively. SPECT/CT images were acquired approximately 78min (SD, 37 min) (pilot study) or 66 min (SD, 15 min, validation study) after injection of the radiopharmaceutical. The dynamic imaging protocol started approximately 7.8 or 7.7min (range, 1-32min or 2-29min) after injection and was completed 29.6 or 26.3min (range, 15-57min or 15-59min) after injection, respectively.

Acquisition parameters for freehand SPECT

The mean VOI defined for reconstructing freehand SPECT images had 27,349 voxels (range 15,200-65,664) with a standardized voxel size of 5x5x5mm^3 for most patients. In 22 patients, the voxel size had to be increased to 6x6x6mm^3 owing to the large VOI needed to cover the injection site and axilla. The dimensions of the volume were on average 39 x 26 x 27 voxels in the longitudinal, medial, and transverse axis, respectively. The scan duration was documented to be 4.3 min on average (range, 0.9-11.5min, SD, 1.2min) and the mean number of data acquired during the scan was 3,004 (range, 542-7,078, SD, 701). The average number of readings per voxel was calculated to be 0.126 (i.e. 126 readings per 1000 voxels), ranging from 0.024 to 0.408 readings/voxel, with a standard deviation of 0.038 readings/voxel. The time interval for the overall procedure (including patient positioning, volume definition, scanning, and visualization) ranged from 3 to 12min (mean, 6.5min). This time frame was considered acceptable with respect to an application in the OR.

The requirement of acquiring data in such a way that the complete VOI had a minimum quality resulted in an increased scanning time. While for the first patient group (pilot study) the mean time interval was 3.5min (range, 0.9-7.4min), in the validation study, scan time ranged from 1.9 to 11.5 min with an average of 5.5 min. This also entailed a higher amount of readings per voxel of 0.187 versus 0.126 for the first patient group, respectively.

On average, freehand SPECT images were acquired 72 min (SD, 40 min) after injection in the pilot study and 62min (SD, 26min) in the validation study. Freehand SPECT images were acquired within 14.4min (range, 2-26 min) or 15min (range, 4-29 min) prior to or after SPECT/CT acquisition (before SPECT/CT, 21% and 35% of freehand SPECT acquisitions, respectively).

Definition of quality thresholds

For evaluation of the scan quality (pilot study), the quality measures mentioned above based on each detected node were calculated. The best separation of mapped and missed nodes was found for $Q_{average}$ (see figure 8.7). For that value, the average was 1.37cps/kBq, ranging from 0.31 to 8.25cps/kBq (SD, 1.12cps/kBq). Taking only those measurements into account yielding $Q_{average}$ values higher than 2cps/kBq, an accuracy that was similar to that of conventional SLN mapping was achieved ('good quality' group). The lower threshold was selected to divide the low-quality range equally. Thus, the quality of scan Q was ranked in three levels: good ($Q_{average} >$ 2cps/kBq), intermediate (1cps/kBq $< Q_{average} <$ 2cps/kBq), or poor ($Q_{average} <$ 1cps/kBq). According to this quality assessment, nine nodes in the pilot study were scanned with a quality that fulfilled the criteria of a good scan. In 35 nodes the scans were rated as intermediate and in 39 as poor quality.

Mapping performance of freehand SPECT

Pilot study : In the subgroup of SLNs with a good scan quality, freehand SPECT detected 77.8% of the SLNs (7/9), while for intermediate and poor quality scans, 34.3% (12/35) and 12.8% (5/39) of the nodes were detected, respectively. No false positive findings were reported, making sensitivity and accuracy equal in the pilot study. Accordingly, the positive predictive value was 100%. As seen in figure 8.7, both relative and absolute uptake affected the accuracy of freehand SPECT. In general, the results showed that the higher the uptake, the lower the required quality of scan needed to map the SLN. For example, three of the five nodes which were scanned with a poor quality but were correctly mapped had an absolute uptake above 600kBq corresponding to 1% of relative uptake. On the other hand, with a good quality of scan, freehand SPECT was able to map two nodes with an uptake of below 50kBq corresponding to 0.1% of relative uptake. Freehand SPECT mapped successfully 21/64 level I nodes, 2/15 level II nodes and 1/4 level III nodes.

Validation study : In a total of 35 patients, three patients dropped out of the study. In the remaining 32 patients, freehand SPECT detected 83.3% of the nodes (35/42). There were seven false negative findings in five patients and two false positive findings in two

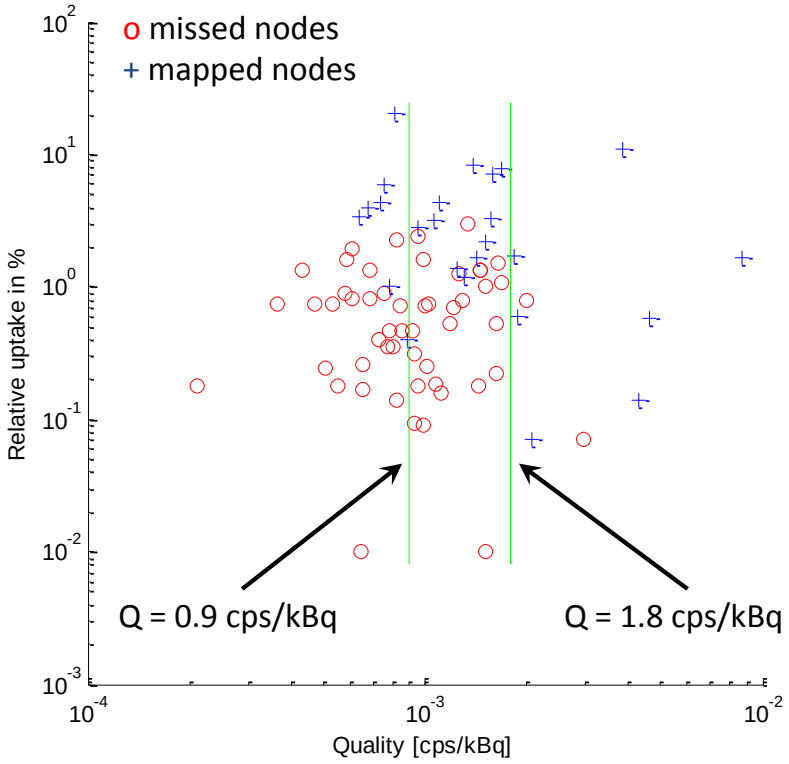

Figure 8.7.: Scatter plot of the results for the first patient group (pilot study) for quality measure $Q_{average}$. Nodes mapped with freehand SPECT (blue) and nodes missed (red) are placed according to respective quality of scan (x-axis) and relative or absolute uptake (y-axis). Two vertical lines separating good, intermediate and poor scan qualities are also shown ($Q_{average}$ = 1cps/kBq and $Q_{average}$ = 2cps/kBq). Both axes are logarithmic and nodes with a quality of scan equal to zero are not displayed. The higher the uptake, the lower is the required quality of scan in order to map a node correctly.

patients. Thus the accuracy was 80%, the sensitivity 83%, and the positive predictive value 95%. As expected, the accuracy for the validation study was in the range of the 77.8% obtained for the good quality scans of the pilot study. The influence of the uptake was also consistent with the results in this group of patients (see figure 8.8). Here, the seven nodes missed by freehand SPECT had a small relative uptake (mean 0.19%, range 0.07-0.49%), as well as absolute uptake (mean 107kBq, range 38-285kBq). For the correctly mapped SLNs, the mean uptake was 0.9% or 522kBq, respectively. There were, however, cases where nodes with uptake as low as 0.003% and 1.33kBq were correctly mapped. Regarding the level assignment, freehand SPECT managed to map 29/34 level I nodes, 3/5 level II nodes and 3/3 level III nodes.

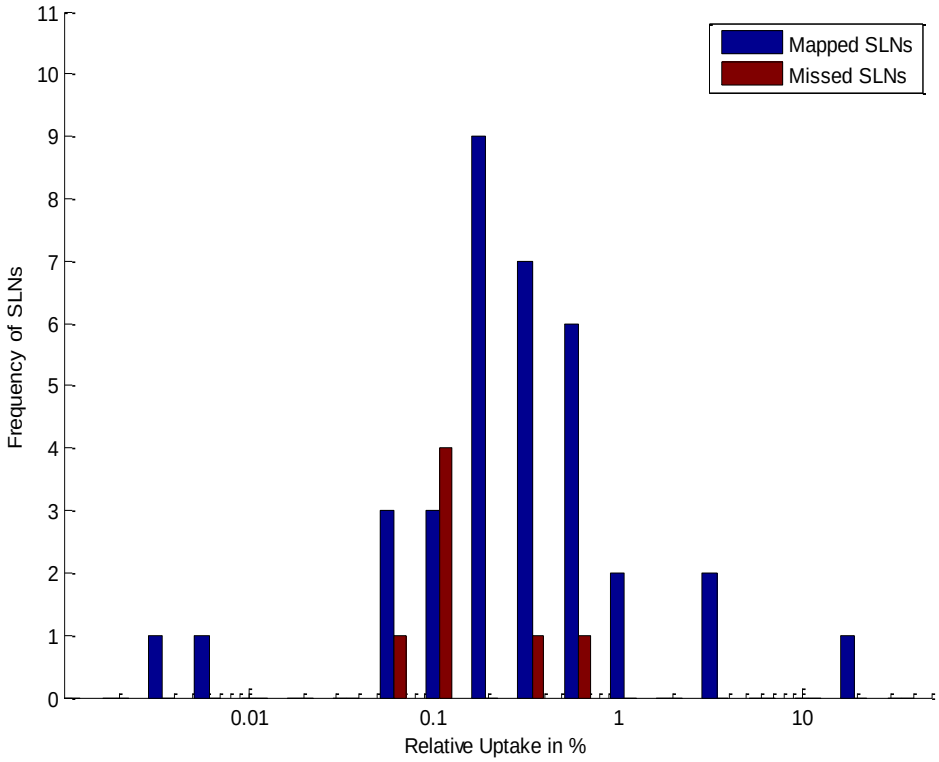

Figure 8.8.: Histograms of nodal uptake in the validation study. Nodes that were not mapped are indicated in red and successfully mapped nodes in blue. Although the average uptake in missed nodes is lower than in detected nodes, there is a significant overlap. This demonstrates that uptake and scan quality do not sufficiently explain the ability to detect the SLN.

8.1.4. Conclusions

This first experience could show that freehand SPECT is feasible for lymphatic mapping in breast cancer. A sensitivity of 83.3% and a positive predictive value of 95% with respect to the gold standard (SPECT/CT) as reported in the validation study are at least within one standard deviation of the average values of gamma probe-based intraoperative detection [160]. Thus, given a sufficient quality of scan, the accuracy of SLN detection may approach levels of clinical applicability.

Several technical aspects, however, remained to be addressed in this study. Despite the considerable improvements shown by using an online feedback during the acquisition, freehand SPECT still yields false negative and false positive findings. Accordingly, further research should be directed at optimizing methods to classify good and bad acquisitions and thus provide better feedback on the quality of the scan.

The proximity to the injection site clearly played an important role in the false negative findings of the validation study. In particular, in three patients with peritumoral injection, the injection site extended to the position of the SLN in the freehand SPECT images. Unfortunately, neither changing the thresholds nor altering the defined filter range made it possible to separate the SLN from the injection site.

Further issues to be considered were automatic quality control and improved quality criteria, denser scan of the axillary and subclavicular regions, and optimization of reconstruction parameters, such as number of iterations, postprocessing filter, etc. Another important issue is the relative uptake of the radiopharmaceutical within the SLN. Scans with only intermediate or even poor quality yielded good results if SLNs presented high uptake. Quantification in attenuation-corrected SPECT has not generally been validated, but our results are in accordance with uptake values reported in the literature. Although absolute uptake behaved very similar to the relative uptake, one issue to be addressed in future is to test if freehand SPECT performs better using a one-day protocol. The influence of timing regarding diffusion of the radiotracer was considered to be minimal, as the average difference between SPECT/CT and freehand SPECT acquisitions was in the range of 15min and after approximately 1h after injection.

8.2. Clinical usability study

With the promising results obtained during the pilot study and in particular during its validation, the next step was to confirm the clinical usability of the generated images. For such means, the University Hospital of Bologna accepted to realize a study on 50 patients, where freehand SPECT images would be generated and evaluated in terms of their potential use in the OR.

This work is currently under review by a major journal.

8.2.1. Aim

The aim of the Bolognese study was thus to evaluate freehand SPECT's accuracy in the detection and localization of sentinel lymph-nodes in patients with breast cancer with the particular goal of evaluating the quality of the images for use in image-guidance during SLNB. The study served also as first phase II study for freehand SPECT in comparison with planar scintigraphy, the standard mapping method in most hospitals. As secondary goal, the study was meant to validate further improvements on the system learned from the Munich experience.

8.2.2. Methods

Inclusion and exclusion criteria

This study was also planned as a prospective study since the inclusion and exclusion criteria were the essentially same as in the Munich experience with the difference that also patients undergoing a combined SLNB and a radio-guided occult lesion localization (combined SLNB and ROLL are commonly called SNOLL) were included. In practical terms, this changes the imaging minimally, as a further injection site is placed deeper (intratumoral injection). Due to internal regulations only patients having signed a consent were recruited.

Ethical considerations

The ethical committee at the University of Bologna required the signed consent of the patient. Here also no changes in the amount of injected radioactivity were done. The dose received by the patient due to the lymphatic mapping was also in the range of 0.2-0.4mSv. The additional burden in time was slightly less in this study, as the freehand SPECT acquisition was done directly in the gamma camera used for planar scintigraphy avoiding the delay of Munich between planar scintigraphy and SPECT/CT.

Patient group and planar scintigraphy

50 consecutive patients affected by invasive breast cancer cT1-cT2, already scheduled for surgery, underwent lymphatic mapping. The standard procedure in Bologna includes an intradermal administration of 60-80MBq of ^{99m}Tc Nanocoll in contrast to the subareolar injection used at TUM. Acquisitions were done during 2min from the side (lateral) as well as obliquely (AP-medial direction). The gamma camera used was a Picker Prism 2000 XP (Picker International, Cleveland, USA, currently property of Philips, Hamburg, Germany). Imaging was done 15-20min after injection and it was repeated if no uptake was reported. In contrast to Munich no flood phantom was used. Skin marking was done using a $^{5}7Co$ pen. All patients scanned underwent a 2-day protocol.

Freehand SPECT

The freehand SPECT system of Munich was cloned and modified on the software to incorporate a faster acquisition (20fps instead of 10fps as used in the Munich system). The gamma probe used in this case was a modified Nucleomed MR100 (Rome, Italy) with a variable collimator probe (probe model 15V). For scanning the collimation was fixed to the maximum collimation resulting in an opening angle of approximately 30 degrees. Connection with the gamma probe was over the serial port of the device and asynchronously. Energy discrimination was done by the freehand SPECT software (energy window at 140keV with 10keV width).

The acquisition was performed immediately after the planar scintigraphy (2-5min delay) in order to avoid echelon lymph nodes to appear in freehand SPECT that were not seen in

planar scintigraphy. The acquisition of freehand SPECT was performed in the same bed of the gamma camera (see figure 8.9) and took in mean 5.49min (SD, 2.37min) resulting in 3658 measurements pro acquisition (SD, 1290 measurements). 28 of the acquisitions were performed by a first physician while 22 by a second one.

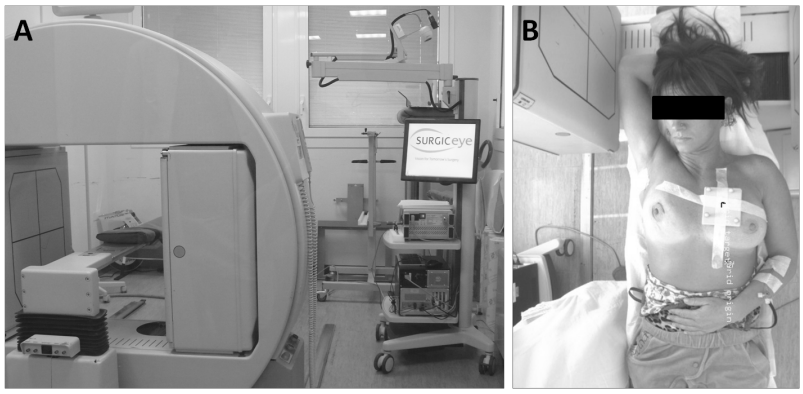

Figure 8.9.: (A) setup of phase II study at University of Bologna. Gamma camera (on the left) and freehand SPECT (on the right) are acquired in the same bed. (B) shows image of freehand SPECT system a few instants before starting acquisition.

For image reconstruction the ML-EM algorithm was used with 20 iterations. The probe carving and the quality carving were active in all acquisitions. The threshold selected for the quality carving was 0.1cps/kBq. For visualization also the quality filter was applied with a threshold of 0.4cps/kBq.

Statistical evaluation

For evaluation of the datasets, two expert physicians evaluated correspondingly blindly the planar scintigraphy and the freehand SPECT images. The number and approximate location of the SLNs were reported. For freehand SPECT the possibility was to visualize the images using an overlaid of the 3D radioactivity reconstruction on top of the video of the optical camera. Further there was the possibility to adjust the threshold and to visualize the image in 3D on a virtual reality window (see figure 8.10).

Each physician had to evaluate the clinical usability of the images for surgical planning and grade it in a scale of 1 to 5 being 1 unusable, 3 equivalent to planar what scintigraphy

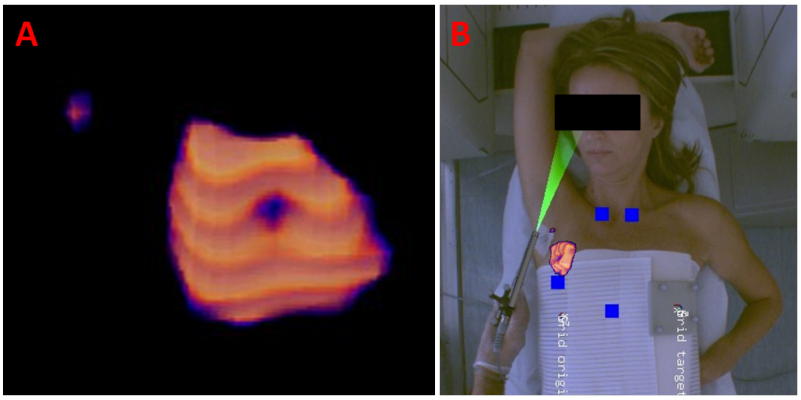

Figure 8.10.: (A) 3D view of radioactivity distribution in one patient in virtual reality mode. (B) same patient in augmented reality mode, next to the radioactivity reconstruction, overlaid on the video, the anatomical landmarks used for definition of the VOI can be seen as blue spots together with the green cone showing the direction of the FoV of the gamma probe.

would offer and 5 considerably better than planar scintigraphy.

8.2.3. Results

Performance of detection of nodes

In all patients planar scintigraphy mapped at least one SLN in the axilla, while freehand SPECT managed to identify at least one SLN in 49 out of 50 patients resulting in 98% sensitivity on a patient base.

Overall planar scintigraphy detected 91 SLNs, while freehand SPECT identified 76/91 SLN. This resulted on a SLN basis, on both sensitivity and accuracy resulted in 84%. In 10 patients freehand SPECT detected fewer SLNs than in planar scintigraphy resulting in 15/91 false negative SLNs. In 1 patient freehand SPECT was able to detect one SLN more than planar scintigraphy, which was validated with the gamma probe.

False negative results (15 SLNs) were probably due to low tracer migration to sentinel SLNs (low uptake in planar scintigraphy), insufficient freehand SPECT scanning of the axillary area or in 3 cases SLNs which were located too close to the injection site which ended up merging with it in a bigger blob (see figure 8.11A).

Freehand SPECT showed 1 additional spot in 6 patients and 2 additional spots in 2 patients easily recognized as artifacts with no risk of misunderstanding (see figure 8.11B).

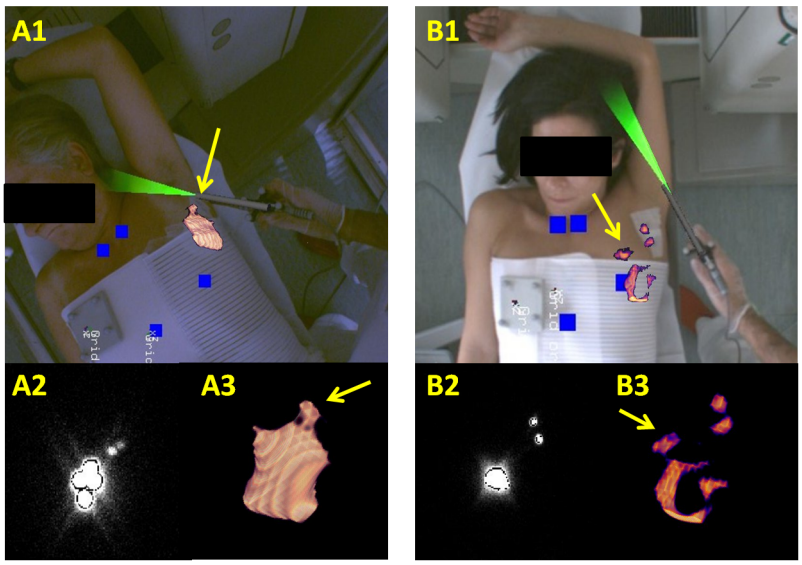

Figure 8.11.: (A) Case were freehand SPECT was unable to tell apart between SLN (arrow) and injection site. In (A1) the augmented reality view shows however that despite the proximity of the node and the injection site, the image is clinically usable. Image (A2) confirms the proximity in the planar scintigraphy. (A3) shows how the node can be to some extend be distinguished. In (B) a case of an evident artifact is shown. Near the two true SLNs a hot spot (arrow) is seen medially in close proximity to the injection site. Such artifact is clearly not an SLN, however cannot be really attributed to the injection site as seen in the planar scintigraphy (B2) and the 3D view (B3).

Clinical usability

The results of the usability evaluation showed that in average freehand SPECT was better than planar scintigraphy (average 4.22, SD 1.28). In 34 patients freehand SPECT provided a considerably better image for surgical planning than planar scintigraphy, whereas in 3 cases, the image of freehand SPECT was unusable and in 4 cases the image of freehand SPECT was not better than planar scintigraphy.

Among the reasons for the dispersion the physicians complained about the artifacts, which could confuse an inexperienced physician, but mostly the missing nodes in case of low uptake. Cases were the lymph node merged with the injection site were given grade 3 and 4 (equivalent to planar scintigraphy or better), as commonly the topology was good enough to give a good localization. The 3D nature of freehand SPECT played the most relevant role in the qualitative evaluation.

8.2.4. Conclusions

As first phase II study of freehand SPECT the results were promising. The improvements in the software (inclusion of quality filter for visualization and increased sample rate) as well as the change in the gamma detector yielded significantly better quantitative results and also qualitative images. Problems, like lack of proper scanning and uptake could be however still seen in the series. Evaluation of the quality was quite satisfactory with a mean of 4.22/5, however with up to 14% cases with bad grades leaves still place for improvement.

In summary, the preliminary data of the study showed that freehand SPECT technology is able to localize sentinel SLN in the axilla adding 3D information that could be potentially useful in the operating room. Although not optimal the results opened the door to initiate intraoperative evaluations.

Chapter 9

Intraoperative evaluation of freehand SPECT

The good results in the preoperative phase led the group in Munich to obtain an ethical approval to start the evaluation of the system in the OR. Two different trials ran in parallel at Klinikum rechts der Isar, one going for SLNB in breast cancer and one in melanoma.

9.1. SLNB in breast cancer

After the successful preliminary study in a preoperative setup, a first intraoperative study was launched at the Women's Hospital of TUM (Prof. Kiechle, Dr. Schnelzer). Essential requirements for safety were evaluated before allowing the start of the study.

On the side of clinical motivation, freehand SPECT was considered to have a potential in solving several practical issues in SLNB in breast cancer. Among those one can mention the criteria for definition of sentinel node [295], the value of dynamic information [86] as well as the value of preoperative lymphoscintigraphy [285]. The problem behind some of these questions rely on the impracticability to implement the preoperative imaging information into the intraoperative procedure of SLNB using a hand-held gamma probe. Intraoperative lymphoscintigraphy by freehand SPECT had the potential of solving at least some of these problems and shed light over the mentioned controversies.

This study resulted in a publication which is currently under review by a major journal.

9.1.1. Aim

The objective of the study was to test feasibility of freehand SPECT imaging for lymphatic mapping in the OR in the particular case of breast cancer. In concrete terms, the end points of the study would determine:

1. The feasibility of localizing radioactively marked lymph nodes in axilla with freehand SPECT in comparison to preoperative planar scintigraphy and the gamma probe alone.
2. The correct localization of the lymph nodes in freehand SPECT images as compared with the position located by the gamma probe (in case the gamma probe detects radioactive LNs).
3. The feasibility of localizing remaining radioactivity in the axilla after LN excision with freehand SPECT.
4. The amount of radioactive nodes detected by freehand SPECT not detected with gamma probe after excision.
5. The amount of metastasic LNs detected with freehand SPECT and not detected with gamma probe. (This would probably not be possible to show in such a small setup as the one planned here).

Beyond the performance analysis, a risk and ergonomics analysis was performed in parallel to the study.

9.1.2. Methods

Inclusion and exclusion criteria

For this study the inclusion and exclusion criteria were again the same as for routine sentinel lymph node biopsy in breast cancer patients (refer to guidelines of the DGS [176]). Accordingly the study had as key inclusion criteria an age above 18 years, a core needle biopsy confirmed invasive breast cancer and the eligibility for sentinel lymph node biopsy and breast conserving surgery. As key exclusion criteria the study had pregnancy, clinically suspicious axillary lymph nodes, ductal or lobular carcinoma in situ only, multifocal tumor growth, the need for breast amputation or clinical considerations (risk of complications due to age or particular condition of the patient).

Ethical considerations

The Women's Hospital and the Nuclear Medicine Department at TUM posed a joint Ethic Proposal for the use of freehand SPECT for intraoperative marking sentinel lymph nodes combined with sonography [296]. The proposal was required as the setup includes the use of a further marking wire only for validation of the position of the SLN as detected with freehand SPECT. The proposal was approved on April 8, 2009.

As in the preoperative experiences, the amount of radioactivity used was the same compared to the gold standard method (gamma probe based SLNB). Only the additional time of about 15-20 min (pessimistic time needed for sentinel identification with freehand SPECT including post-excision control) had to be accepted by the patients. The advantage for the patient was stated to be that the sentinel lymph node gets specifically localized with freehand SPECT and can get dissected precisely out of the axilla region without destroying adjacent tissue.

Regarding the quality of the received treatment, all patients were planned to obtain the gold standard preoperative procedure for localization of the axillary sentinel lymph node. After identifying the sentinel with freehand SPECT the gold standard method for identification was required to confirm the located lymph node as the sentinel. If the sentinel lymph nodes identified by freehand SPECT and by gold standard method did not match both lymph nodes were to be removed and histologically tested for metastases, unless the operator decided intraoperatively not to go for those nodes, due to clinical reasons.

On the side of increased morbidity due to harvest of additional nodes, the patient would not have a disadvantage from removal of more than one sentinel lymph node as very often up to 7 sentinel lymph nodes get removed in the standard procedure if they are located next to each other. In general the harvest of small amount of additional nodes does not have an impact in morbidity.

For further verification a freehand SPECT image would be acquired after removal in order to guarantee that no radioactive lymph nodes are left behind. This would ensure the quality of a complete resection of affected lymph nodes.

Patient group and lymphatic mapping

The study was planned to be a prospective study and 30 patients were recruited. The patient age was in mean 57.6 (range 39-84). All had a clinically confirmed invasive breast cancer and received a breast conserving procedure.

The protocol for lymphatic mapping using planar scintigraphy was essentially the same of the preoperative study at TUM. The mean injected activity was 91.9MBq (SD, 20.9MBq). The injection technique was in all cases a periareolar injection in 4 deposits of approximately 0.05ml each. These images were available to the surgeon in order to allow proper planning according to the guidelines.

Freehand SPECT and procedure in the OR

An improved version of the freehand SPECT system used in the preoperative trials was used during the intraoperative studies. The major changes were the use of a new gamma probe, a Crystal Probe straight with 60 degrees of opening by the company Crystal Photonics GmbH (Berlin, Germany). The signal acquisition was in this case done directly from the analog output of the photomultiplier of the probe. The signal was thresholded in the way to get an energy window of 40keV centered at 140keV. The gamma probe control unit was active during the procedure and worked independently of freehand SPECT. Additionally a wireless gamma probe (Gamma Finder) by Silicon Instruments GmbH (Berlin, Germany, currently rights for Gamma Finder are property of World of Medicine, Hamburg, Germany) was used for validation.

The software used included probe carving, quality carving (threshold 0.001cps/kBq) and quality filtering of the visualization (threshold 0.4cps/kBq). For smoothing a Gaussian filter with 6mm was used on the raw output of the reconstruction. Iteration number was increased to 25; the algorithm used was still ML-EM and the model used for the gamma probe included the solid angle effect and angle dependency.

For sterile cover of the probe the interface developed in collaboration with SurgicEye GmbH (Munich, Germany) was used, such that the tracking target was not covered and the probe was. The tracking target was sterilized together with the patient target using 135 degrees steam sterilization. The tracking markers were provided sterile by SurgicEye.

On the day of the operation and according to the guidelines blue dye (patent blue) will be also injected in the breast. The patient was then covered with the sterile covers used in the standard procedure and the patient target was fixed using to the sterile target on the sternum of the patient. The freehand SPECT device was then placed in a way that the patient target was properly seen and that the screen was on the opposite side of the main surgeon (see figure 9.1).

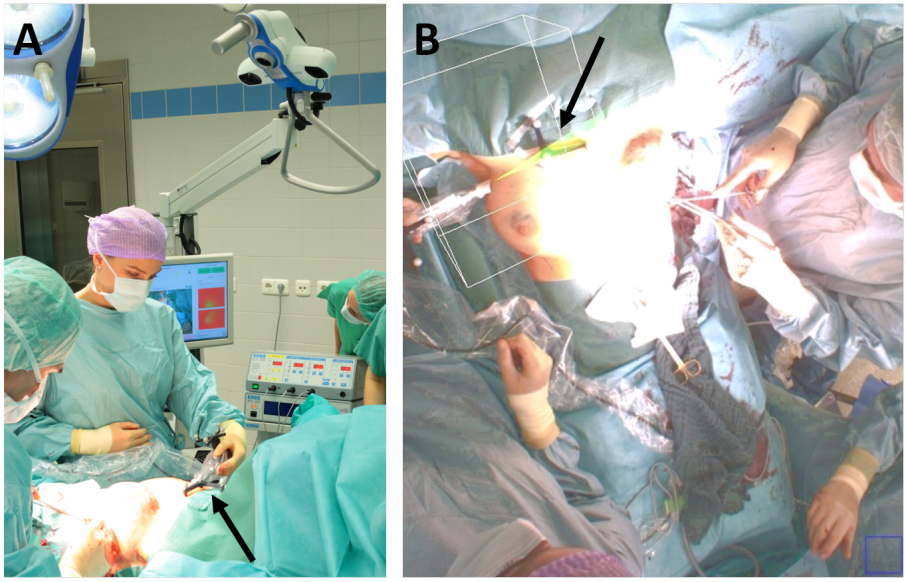

Figure 9.1.: (A) outside view of freehand SPECT system looking at operating situs while doctor is scanning the right breast. In this particular case, the patient underwent an SLNB procedure with breast conserving surgery on the right breast and a mastectomy on the left side. Main surgeon started with the mastectomy during freehand SPECT scan. The arrow shows the position of the patient tracking target. (B) shows the same situation from the freehand SPECT camera. The wire-box overlaid on the patient shows the VOI for that particular image.

Shortly before the first incision of the axilla or shortly before the SLNB part in case of the use of the ADAM procedure [245] the conventional gamma probes (both the Gamma Finder and Crystal Probe used independently from the freehand SPECT device) were used to localize the SLNs percutaneously. The amount of detected nodes was reported in the

protocol. Then the first freehand SPECT scanning was performed . The scanning protocol was shortened to be 3min after a new improvement on the software that allowed even shorter acquisitions. The directions of scan were 1min in AP direction over the axilla, 1min in medial direction in the axillary area and 1min on the breast (AP and medial direction).

The generated images were then visualized in the augmented reality mode as well as in the probe view mode explained in chapter 7 (see also figure 9.2). The threshold for visualization was set such that the visualized images did not contain artifacts and still allowed seeing low uptake SLNs. The distance calculation was available too.

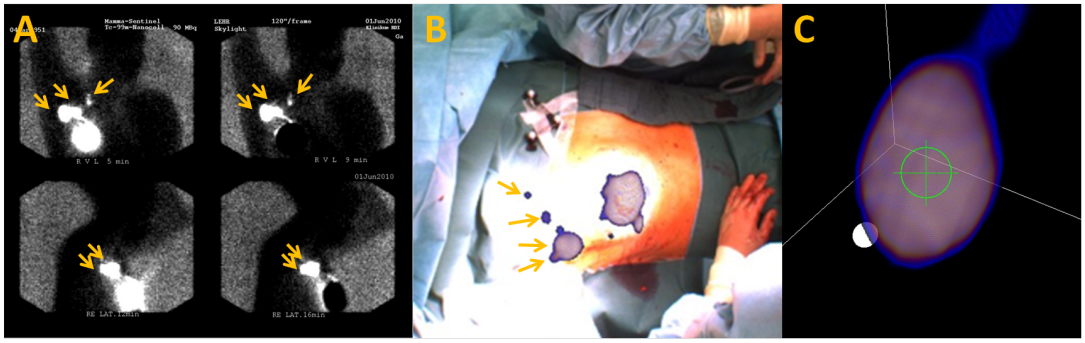

Figure 9.2.: (A) Planar scintigraphy of patient showing several SLNs up to subclavicular area. (B) Augmented reality visualization of freehand SPECT image of same patient. (C) 'Probe view' of the major hot spot used for 3D navigation.

Following the visualization of the SLNs with freehand SPECT, the surgeon proceeded to prepare the axilla, using the selected conventional procedure. At the point the SLNs were found the surgeon was asked to validate if the location the SLNs were found matched the one indicated by the freehand SPECT. The 'conventional' method considered as sentinel lymph nodes, any lymph node presenting uptake of blue dye and radioactive emission verified with any of the hand held gamma probes.

The SLNs were then removed in any case (blue coloring or radioactive uptake) and sent for frozen section. The axilla was then controlled with the gamma probes first and in case no further activity was found, a second acquisition of freehand SPECT took place. That second acquisition was meant to guarantee that no radioactive lymph node was left behind.

In the case additional SLNs were detected with freehand SPECT they were assessed with the gamma probe in order to confirm radioactive uptake. The decision to take them out or not was given to the surgeon based on the amount of already resected SLNs and the clinical situation of the patient. According to the German guideline [176], resecting more than 3 SLNs does not bring a significant improvement in the false negative rate of the procedure. Accordingly it is left to the operator whether to resect those nodes or not.

Statistical evaluation

Based on the number of lymph nodes detected and later resected using the different information, the sensitivity of the freehand SPECT system can be assessed (primary end-point). Of particular interest are following criteria:

- Sensitivity of gamma probe to scintigraphy: SLNs seen with percutaneously vs. those seen preoperatively
- Sensitivity of freehand SPECT to scintigraphy: SLNs seen with percutaneously vs. those seen preoperatively
- False positive rate of freehand SPECT: artifacts seen that could confuse operator
- Rate of correctly additional detected SLNs with freehand SPECT: SLNs seen after control with gamma probe, that gamma probe proved to be radioactive
- Rate of potential additional detected SLNs with freehand SPECT: SLNs seen after control with gamma probe, that gamma probe could not to be radioactive
- Histology of resected SLNs in concordance: histology of nodes seen by both techniques
- Histology of additionally resected SLNs: histology of nodes resected due to freehand SPECT

The final histological results for each lymph node and the duration of the different steps were documented (base for calculation of further secondary endpoints).

9.1.3. Results

Planar scintigraphy

Planar scintigraphy detected a total of 50 primary SLN and 11 secondary SLNs. Lymphatic mapping of at least one SLN was possible in all 30 patients. In mean each patient had thus

1.67 primary SLNs and 0.37 secondary ones. Mean time for visualization of the first SLN was 10min and the examinations had a last acquisition in mean after 20min of injection. According to the protocol of the hospital, although dynamic information is available, commonly both primary and secondary SLNs are resected due to the impossibility of mapping them in the OR without any imaging technology.

Intraoperative detection with gamma probe and freehand SPECT

Pre-incision freehand SPECT images were generated in average 19.6h after injection (SD, 4.7h), while post-excision freehand SPECT images where performed 20.4h after injection (SD, 4.6h). This resulted in an effective activity of 10.6MBq (SD, 7.0MBq) at time of operation for pre-incision scans and 9.6MBq (SD, 6.4MBq) for post-excision scans. The duration of freehand SPECT acquisitions was 2.7min (SD, 1.1min) and 2.5min (SD, 1.0min) for pre-incision and post-excision scans respectively.

In 28 of the 30 patients a pre-incision freehand SPECT scan was performed. For those patients the conventional hand held probe detected 41 SLNs in 26 patients in contrast to the 57 SLNs visualized in those 28 patients by planar scintigraphy (SLN sensitivity 71.9% - 41/57, patient sensitivity 92.9% - 26/28). Freehand SPECT, on the other hand detected 52 SLNs in 27 patients, while one additional SLN was detected in 1 patient (SLN sensitivity 91.2% - 52/57, patient sensitivity 96.4% - 27/28). Both freehand SPECT and gamma probe failed to detect SLNs in the same patient.

In 27 of the 30 patients a post-excision freehand SPECT scan was performed. There freehand SPECT detected 17 SLNs not previously detected with the gamma probe in 15 patients out of 27 (55.5%). From those 10 SLNs were left behind on purpose due to either a sufficient harvest, a too low uptake or clinical considerations on the patient's health. 7 from them were additionally resected and sent separately to histology. Radioactivity was confirmed with the gamma probe in all cases. Images before and after were compared in the OR to validate complete resection (see figure 9.3).

Artifacts were observed in 5 patients, in 3 of which, they could have confused an unexperienced physician, resulting in 26 of 29 cases where freehand SPECT could produce clinically usable images (89.6%).

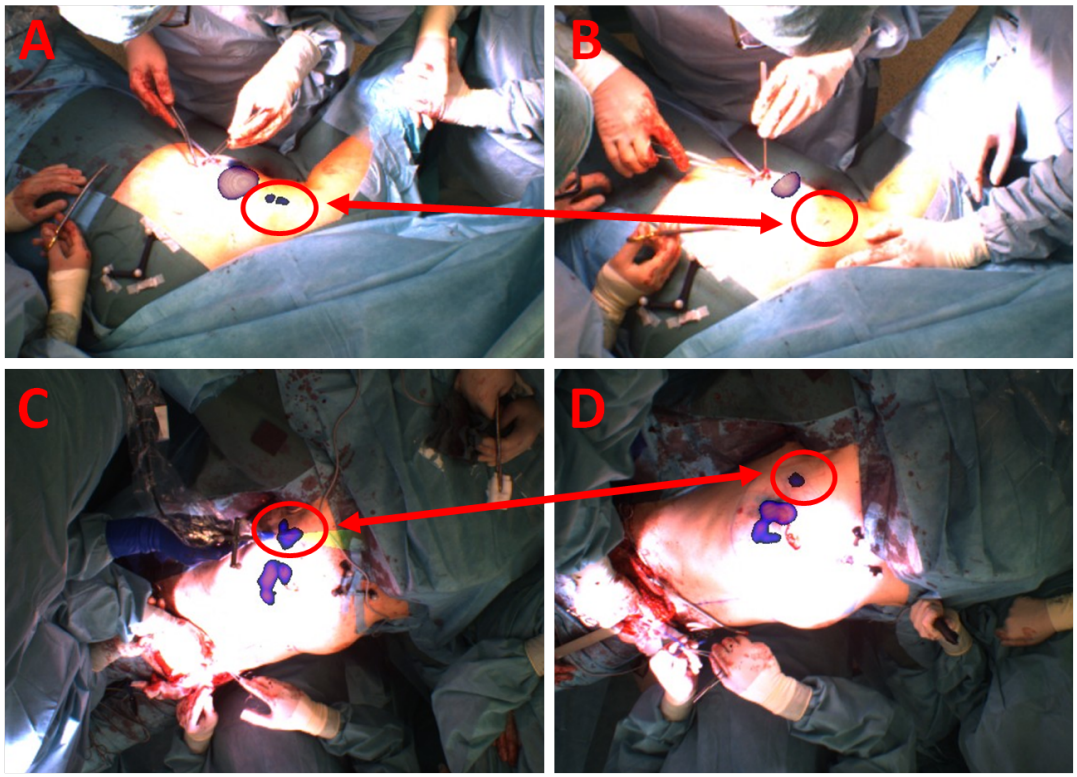

Figure 9.3.: (A) Pre-incision freehand SPECT overlaid on post-excision situs to be able to compare with current situation as seen in (B). Here the two SLNs were removed cleanly. On the other hand in (C) and (D) part of the radioactivity is still inside the axilla. Freehand SPECT allows an impartial comparison before and after resection.

Histological evaluation

Unfortunately to date it has not been possible to collect all histology data for the 30 patients. This part was not included consequently in the submitted paper. Due to the fact that most of the additional nodes detected by freehand SPECT were not resected, however it is highly probable that there will not be a significant statement. At least at a frozen section level, no difference in the final staging of the axilla could be observed.

9.1.4. Conclusions

The preliminary experience in the OR showed already some of the advantages of freehand SPECT, however also pointed out issues still to be treated. In regard to the objectives, freehand SPECT could probe to be feasible to detect SLNs after 19-20h of injection with almost the same performance of planar scintigraphy. Moreover freehand SPECT was capable of detecting more than the gamma probe alone. The position the SLNs were detected with freehand SPECT did match the approximate position estimated with planar scintigraphy and the one detected invasively with the gamma probe.

In another dimension freehand SPECT was able to detect additional lymph nodes in up to 50% of the patients. This opens rather the medical question of the amount of nodes to be excised and where to stop after some SLNs were already resected. In that sense freehand SPECT poses an optimal tool for such means. The impact on the management of the patients due to the additionally resected nodes remained however restricted as the information on the histology is still pending.

The qualitative feedback of the surgeons using the system was positive and gathered wishes in the direction of allowing a robust distance measurement as well as real time imaging. In 3 cases the artifacts present in the reconstructed images shadowed the results showing also better ways to determine the conditions for a good quality freehand SPECT image.

9.2. SLNB in melanoma

Like in breast cancer, SLNB in melanoma using one dimensional gamma probes is a standard of care worldwide (e.g. [69]). Reports on the performance are claimed by most groups to successfully detect the SLNs during the surgical procedure in almost 100% of the patients. In clinical practice, however, several issues remain which are usually not addressed: the difficulty of intraoperative detection of deep located nodes, SLN detection in heavy weight patients or in the groin [190]. Moreover, the fact that often a ”dissection” is performed rather a ”biopsy” involving far more nodes than needed and the impossibility to make a scan of the entire wound after SLN resection probably results in a higher false negative rate [325]. These aspects could be addressed with proper intraoperative imaging and navigation. Accordingly freehand SPECT could open new alternatives.

These results are currently under review by a major journal for publication.

9.2.1. Aim

The aim of this study was to gain a first experience of using freehand SPECT for navigated SLNB towards making SLNB a minimally invasive and highly successful procedure also in complicated clinical scenarios. Endpoints of the study were to obtain an idea of how the promised advantages of freehand SPECT could turn into real clinical advantages. Issues like incision guidance, depth calculation, quality assessment and image-guidance in general were to be analyzed.

Issues to be analyzed were the possibility of detecting SLNs several hours after injection, the usability of the fused 3D functional information with the anatomical image, the additional time burden and the rate of SLNs left behind by a gamma probe alone.

9.2.2. Methods

Inclusion and exclusion criteria

The inclusion and exclusion criteria used in this study, were the combined ones of the European Organization for Research and Treatment of Cancer (EORTC) and the European Association of Nuclear Medicine (EANM) [62] which are essentially the same as the ones of

the National Comprehensive Cancer Network of USA (NCCN) [69]. According to the those guidelines, SLNB is indicated for melanoma patients with tumor thickness between 1 and 4mm. Individual factors towards a higher level of malignancy (e.g. deep margins, lymphovascular invasion, etc) leaves the option of SLNB also for lower thickness melanomas. Further inclusion criteria are age over 18 years and patient preference if tumor thickness is above 4mm. Exclusion criteria are pregnancy and signals of clinical involvement of regional lymph nodes.

Ethical considerations

The study for melanoma SLNB ran under the umbrella of the breast cancer ethical approval [296] as the Ethical Committee at TUM did not consider any increased risk, on the other hand, the melanoma evaluation was expected to be simpler due to the higher uptake of SLNs in melanoma and the minimized influence of the injection site which is commonly far from the lymph basins.

Patient group

To date 14 patients with indicated SLNB due to a melanoma were recruited. The average age was 60.4y (range 30-72y). The location of the melanoma was 4 times in the foot or lower leg, 3 on the back, 4 in the lower arm or elbow, 1 in the breast, 1 on the belly, 1 in the shoulder.

Planar scintigraphy

The protocol for the melanoma patients was with minimal modifications the same as the one of the breast cancer patients. The injection in this case was 0.2ml of ^{99m}Tc in four deposits around the tumor or around the scar of the tumor resection as some patients' tumor thickness was determined only after resection of the primary tumor.

The acquisition was done also with the Philips Skylight gamma camera (Hamburg, Germany) and according to the 2min two side acquisition scheme using lead to cover the injection site in case of melanomas too close to the axilla, the neck or the groin. In order to

minimize the risk of imaging the wrong lymphatic basin, a full body 2D scintigraphy was acquired in patients with the melanoma in the torso.

Surgical protocol

Similarly to the breast cancer case, the entire protocol consisted of 6 steps: (1) anesthesia, (2) pre-incision gamma probe scanning, freehand SPECT acquisition and visualization of 3D data, (3) skin incision and SLN biopsy, (4) post-resection freehand SPECT acquisition and visualization, (5) biopsy of additionally detected SLNs using the information derived from freehand SPECT and confirmed by gamma probe, (6) suture. Steps (4) and (5) were repeated, as long as SLNs were detected in post-resection scans.

The freehand SPECT acquisition was dependent of the lymphatic drain scanned. The axillary case was exactly as done for the breast cancer patients. On the other hand for drain to the groin the scan was performed in AP direction trying to incline the probe in direction medial and lateral in order to obtain at least 90 degrees of projections. Abdominal SLNs were scanned like the axilla. Drain to the neck was planned to be scanned also in AP direction and in medial direction. In total scans were meant to be 1-3min depending on the extent of the are of interest.

The patient target was also fixed according to the lymphatic basin drained. For axillary drain, the target was placed over the sternum. For inguinal drain, the target was

For the freehand SPECT image reconstruction, the system and software was one to one the used for the intraoperative breast cancer study. On the side of the probe, besides the Crystal Probe integrated to the freehand SPECT device, a SI gamma probe probe (Silicon Instrument GmbH, Berlin, Germany, nowadays Silicon Sensor AG) was used.

The amount of SLNs detected by percutaneously with the gamma probe, as well as the ones detected by freehand SPECT were documented. After resection and verification with the gamma probe, the number of SLNs further detected with freehand SPECT was also recorded.

9.2.3. Results

Planar scintigraphy

All 14 patients underwent planar scintigraphy in mean 18.8h before the surgical operation (range 16.4-22.2h). 8 patients showed drain only to the axilla (4 arm patients, 3 back patients, breast patient), 4 patients only to the groin (4 lower leg patients), 1 patients to the lateral side of the abdomen and the axilla (belly patient), 1 patients to the lateral side of the abdomen, the axilla and the groin (1 back patient), and 1 to the axilla and the neck (shoulder patient). Planar scintigraphy could image, 10 nodes in the groin, 14 SLNs in the axilla, 6 to the side abdomen and 2 to the neck area.

Freehand SPECT and gamma probe findings

Axillary drain From the 10 patients showing axillary drain, 2 were discarded due to missing data or similar. In the remaining 8 freehand SPECT managed to map 13 nodes from 13 nodes seen in scintigraphy, while gamma probe missed 1 during the pre-incision acquisition. The post-excision acquisition revealed 1 SLN, which could be verified by the gamma probe. Freehand SPECT images showed artifacts which could be a potential interpretation risk in 2 cases at pre-incision only. Freehand SPECT scan duration was in mean 3.2min (SD, 1.1min) at pre-incision, while it was 2.9min (SD, 0.6min) at post-excision. For exemplary performance see figure 9.4.

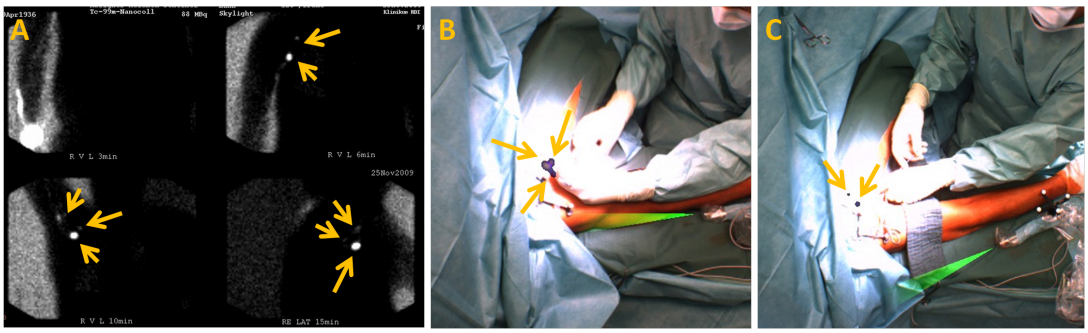

Figure 9.4.: Example of results with in axilla. (A) shows the scintigraphy were 3 SLNs are visible in a triangular configuration. (B) shows the pre-incision image were the 3 SLNs are visible too. (C) is an aquisition after the resection of the first SLN.

Inguinal drain In the 5 patients showing axillary drain freehand SPECT managed to map 11 nodes from 10 nodes seen in scintigraphy, while gamma probe showed the same nodes seen in scintigraphy during the pre-incision acquisition. The additional node seen in freehand SPECT was confirmed with the gamma probe. The post-excision acquisition revealed 2 SLNs, which could be verified by the gamma probe. Freehand SPECT images showed artifacts which could be a potential interpretation risk in 2 cases at pre-incision and in 3 cases at post-excision. Freehand SPECT scan duration was in mean 2.6min (SD, 0.3min) at pre-incision, while it was 2.8min (SD, 0.3min) at post-excision. An example of the type of images generated can be seen in figure 9.5.

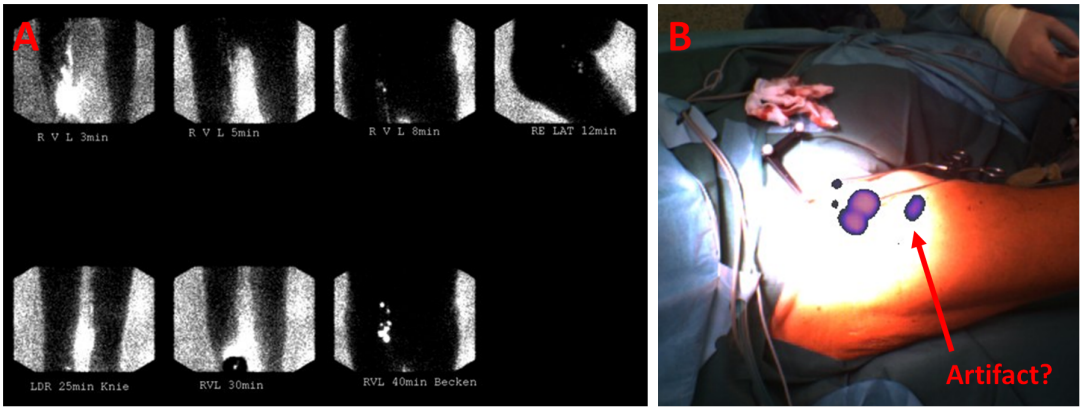

Figure 9.5.: Example of groin case. In (A) planar scintigraphy shows a complex drain to the groin with several nodes. Freehand SPECT image reconstructs correctly the lower SLNs, however a spot appears in direction caudal which is not seen in scintigraphy. Confirmation with gamma probe shows that the spot is an error of sampling.

Abdominal drain In the 2 patients showing axillary drain both freehand SPECT and the gamma probe could map all 6 nodes seen in scintigraphy. No SLNs was found in the post-excision acquisition. In 1 of those particular cases several artifacts in pre-incision and post-excision images were seen, which made interpretation complicated. Acquisition times were here similar to the procedures in the groin.

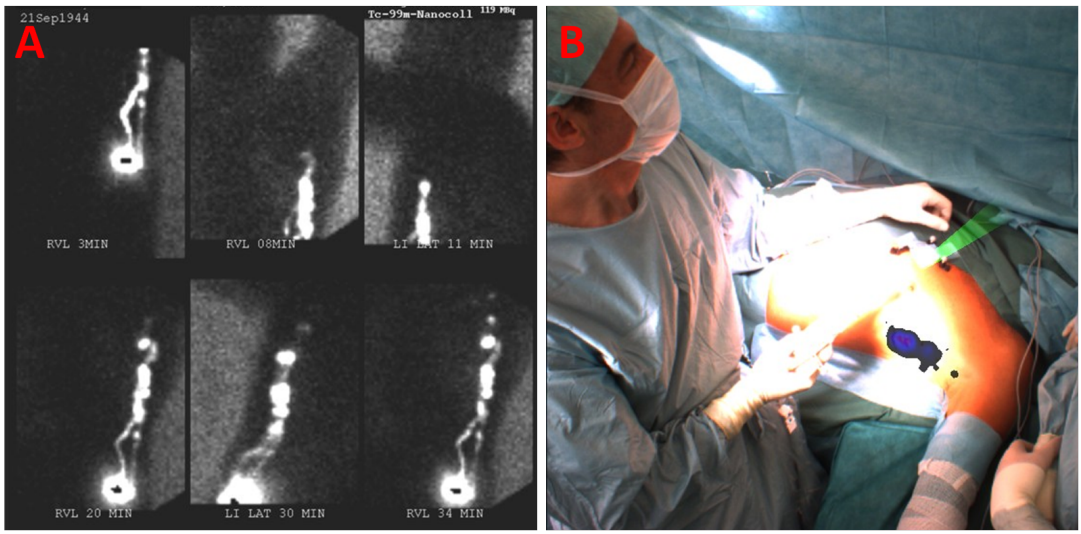

Figure 9.6.: (A) Dynamic planar scintigraphy of melanoma patient showing at chain of lymph nodes on the abdominal wall from the injection site into the axilla. Injection consisted in 4 spots placed periareolarly. Acquisitions at 3 min, 8 min, 20 min and 34 min are frontal projections while acquisitions at 11 min and 30 min are lateral projections. (B) Overlay of freehand SPECT 3D image on the video image of the same patient for easier anatomical correlation. The same chain structure seen in planar scintigraphy can be seen in intraoperative images allowing a proper incision planning.

9.2.4. Results

With a sensitivity of 100%, freehand SPECT showed very good results in melanoma patients. The presence of artifacts however was considerably higher than in the case of breast cancer. Incorporation of the acquisition in the workflow was very smooth in this case. It must be considered that here, as in the case of breast cancer the interval between injection and operation was in the range of 20h with a resulting practical activity of 9.5MBq (SD, 3MBq) at the time of surgery. This factor did not seen to make the detection rate sink.

The 3D information provided by freehand SPECT was used mainly for the definition of incisions, which are not trivial as in the case of breast cancer (see figure 9.7). Depth information was not used as an aid mostly because of the fact that the time of imaging was inappropriate. The use of a second acquisition after opening of the skin may result in an improvement.

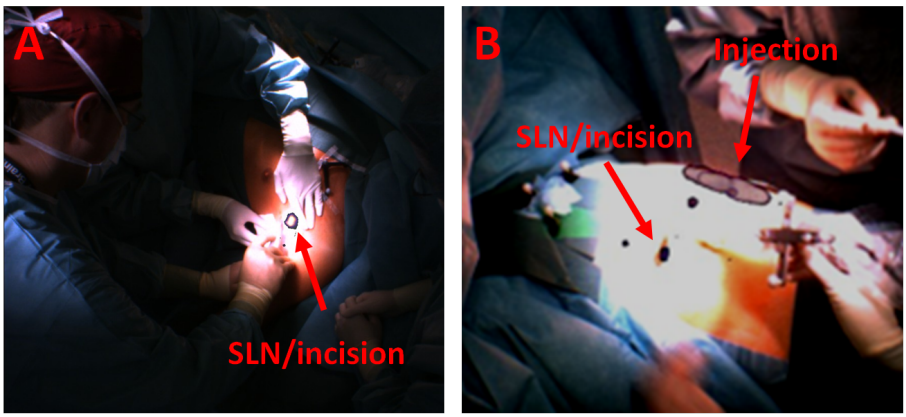

Figure 9.7.: Two examples how incision planning works. In (A) opening of axilla is guided by freehand SPECT image. In (B) the same is done for a node in the side of the abdomen for a patient with melanoma in the back.

In contrast to the case of breast cancer, the rate of SLNs left behind was considerably lower in melanoma. Also the time burden for the procedure was almost minimal. On the contrary for cases like the one of figure 9.6 freehand SPECT speeded up the procedure.

Part IV.

Conclusion

Chapter 10

Conclusions

It was back in a sunny day of 2005 that I joined the trip that brought me here. Much has happened since then and of one thing I can be sure is that this trip is not over yet. In this moment of pause there is however an opportunity to look back to the last years and draw some lessons learned and conclusions on the work done.

In the last chapters, the problem of providing 3D intraoperative imaging was presented and a particular solution was proposed based on tracked hand held detectors and reconstruction algorithms capable of 3D imaging from sparse, limited–angle and irregularly sampled data. In order to validate this solution, freehand SPECT, one particular implementation of the concept proposed within this thesis was explained in details from its requirements over its implementation to its evaluation both in a preoperative as well as in a intraoperative setup.

10.1. Lessons learnt

Beyond the enthusiasm, the frustration and the infinite days of programming, constructing and calibrating there are many things that can be learned from this experience. Those lessons can be later used for further implementations of the concept of 3D imaging using tracked hand held detectors, but also in general for the development of intraoperative systems.

Importance of the clinical benefit : By the current date I must have visited at least 50 hospitals in search of interest to bring freehand SPECT into standard clinical use and I have not met a single physician that has not discussed on the clinical benefit of our system. It does not matter if you are standing in front of a young-in-spirit enthusiastic surgeon or a wise prudent physician. It does not matter if they model the process themselves or if they ask directly what the clinical benefit is, that is one of the first points in the list of things to evaluate on a new technology.

I still do not have an answer that convinces everyone. The current procedures of SLNB in breast cancer and melanoma are already too successful. Any improvement on them is accordingly hard to prove and even harder to make it evident enough so that the community realises there is still an improvement. Most surgeons are simply satisfied with detection rates of 95% and false negative rates of 5% on paper. At the end all is a thing of interpretation and numbers can be always be interpreted in a positive way. So even unexperienced surgeons with lower performance than the one required by the guidelines would argument that there is little clinical benefit behind freehand SPECT. The reason is clear, the problem of harvesting SLNs is not anymore a problem in their minds.

In breast cancer, incision planing, availability of depth information, less invasiveness through preciser localization may sound good and as shown in the studies are possible with the developed system, but they will not convince the physician to change their procedure. The clinical benefit is here the quality assurance. However the advantage of having this said quality assurance is hard to prove. The current estimations tell us that in order to prove that freehand SPECT enables to detect more tumor affected SLNs is going to take in the range of few thousant patients.

In melanoma things may be different. There two applications may play a significant role: melanomas in the head and neck and melanomas with drain to the groin. There the situation changes as many open questions are still presen. As an example Ling et al. [190] published a work lately where they shown a complication rate of 10% (mostly seromas and infection) in melanoma SLNB patients. They looked at the case closer and realised that the morbidity correlated with the body index of the patient and that the probability of complications was 3 times higher for procedures involving SLNs in the groin. The lack of 3D information and in particular depth may explain to a good extent this problem.

Currently the use of a hand-held gamma probe requires mobilization of tissue for proper localization. This could be minimized if depth information was available before. SLNs in the groin area can also be located as deep as parailiacal, which further contributes to the difficulty of the procedure and the need of proper information. As Prof. Lutz Kretschmer, head of the Melanoma Surgery Division at the University of Göttingen, explains 'the SLNB procedure in the groin is not a solved problem. Many people ignore it, but there is considerable place for improvement.' Interestingly such comments are common from experts on the field like Prof. Kretschmer, but the clinical benefit is not clear to everyone.

A completely different situation arises when freehand SPECT is presented for other indications where this clinical benefit is evident not only for the experts. In such cases the problem has not been solved in the mind of the common surgeon. That is the case for SLNB procedures in gynecological and urological malignancies. Finding SLNs there is simply hard. Anatomy is complex, probes do not deliver a clear signal due to scattering and the target volume is far bigger than the tetrahedron of Dr. Paepke. It is not a surprise that in these fields mini-gamma cameras have been successful (e.g. [349]). 3D information would solve a problem that is evident for almost anyone and the impact on the success of the procedure could be major.

Importance of understanding the workflow : As stated in the introductory chapters, the workflow has to be considered in details. While introducing freehand SPECT this asseveration can be extended to say, the particular workflow of each hospital is extremely important. Workflows change dramatically between hospitals and even between operators without any regard on guidelines. I have been in operations where freehand SPECT is used almost as a non-intraoperative imaging tool, as images are taken before the start of any step in surgery and also after suturing all wounds. I have been in hospitals where up to 4 images are generated while looking of SLNs.

The workflow is a good representation of the inner processes of a hospital. From workflow it is possible to read where the main focus is placed, and implicitely detect the real necessities. If a hospital does not want to include a freehand SPECT acquisition at the end of the procedure, they certainly do not believe that it brings an improvement on quality. Those cases have to be convinces by other advantages.

The best way to introduce freehand SPECT into the setup of a hospital is then to discuss with the involved surgeons before hand and explain them when they could have an advantage from the system. It is also recommendable to remind them continuosly during the first operations when freehand SPECT could help them. Surprisingly the 'aha' effect, i.e. the instant when a surgeon realises why freehand SPECT is useful comes only when they have it available in the right moment of the operation. Of course, this requires a deep understanding of the procedure for the person training the surgeon.

For example for SLNB in breast cancer it is recommendable for the first two to three cases to push the surgeon to use the system in the following steps:

1. Once the patient is washed and before any incision or plan on the incisions is made. An image in such a step could help the surgeon make a better idea of the incision for the SLNs, the incision for the tumor and even decide the order of these steps. For example, if the SLNs are close the injection site and the surgeon gets this information through the freehand SPECT images, he or she will most probably start resecting the tumor to minimize shadowing and shine-through and perhaps even go for the SLNs then using the same incision. This is valid of course only if for both tumor and SLN a frozen section is done or no frozen section is planned. If only one of the entities is to be analysed with frozen section, then most probably that structure will be first removed.
2. Once the SLNB procedure is about to start. This is of particular importance in case the tumor was resected first, as during the tumor resection deformation is major and also commonly a part of the injection site is removed.
3. Directly after the resection of an SLN. Immediately after an SLN is removed freehand SPECT images can provide a fast control of complete resection and thus enable a prompt decision if further SLNs are to be extracted or if the axilla can be sutured.
4. During the wait for frozen section. A longer acquisition, capable of providing higher sensitivity is recommendable if a wait is given. This image may show additional SLNs not seen during a faster confirmation image and could thus even result in extending the biopsy by a couple of nodes.

It is important to mention that any decision whether an image has to be generated or not, have to be taken in the light of the boundary conditions of the surgery. Patient general

health condition, disease prognosis, logistics of the OR, etc cannot be forgotten.

Importance of the cost structure : As long as a technique does not change the cost structure of a particular procedure, it has to bring considerable cost reductions. While presenting freehand SPECT in different hospitals to different specialists, this became extremely clear. Essentially there were completely different scenarios.

In the first scenario the specialist purchasing the device would be a Nuclear Medicine physician. He or she would then have a service to offer to the breast cancer surgeons. However it would be most likely that the budget for the new service would not be different from the one already existent for the preoperative lymphoscintigraphy and the injection of the yadioactive tracer. In this way any purchase by the Nuclear Medicine physician would be only justified if the surgeon would push him to offer freehand SPECT imaging, if he or she would get more patients due to the fact that he or she offers freehand SPECT or if he or she would reduce his or her costs using freehand SPECT.

In the second scenario the specialist purchasing the system would be a surgeon. Here he or she would be able to do the scintigrahy on his own and thus would not necessarily need to pay for preoperative imaging, but rather only for the injection of the radioactive tracer. In this case the cost structure changes dramatically enabling the surgeon to get reimbursement previously assigned to a Nuclear Medicine phyisician. As a result the investment would make sense if the cost of freehand SPECT would be lower than the cost of the preoperative imaging transdered to the Nuclear Medicine specialist.

In general the easiest calculations result from the second scenario and thus it is a rather favourable approach in order to integrate a new solution into the clinical routine.

Importance of usability and robustness : Although robustness and proper usability are given for granted in medical devices 'given for granted' does not mean always 'solved'. This was particularly made evident in the development and introduction of freehand SPECT into clinical use.

When following all development requirements one often forgets that the system to be developed will be used by people who have a completely different training as the people planing the system. Giving for granted that a user of the system will improvise or will

make obvius corrections if something is wrong is not really an option.

If a system is meant to be used in medicine it has to be available. Being available means that if the surgeon needs it at a point during the operation, it has to be there and ready to be used. A fast booting or initialization, a prompt possibility to be used without calibration steps or alike and a fast re-initialization if the device is unplugged are mandatory and can really affect the incorporation of the technology in the OR.

On the side of certification reproducibility is expected. A system can be robust enough for medical use if it is reproducible. It is not tolerable that results vary from patient to patient, or if yes only minimally. For freehand SPECT and in general for hand held imaging this was a great challenge that pushed the use of guidance systems for the scanning part of the imaging procedure. The results of the preoperative study performed in Munich are extremely clear on this point.

In order to be usable by any user, the experience with freehand SPECT showed that the system and in particular its user interface has to be easy to learn and easy to remember. Rotation in hospitals is common. Older physicians go, newer come, but also the indications assigned to physicians are rotated on a normal base to minimize the need of continously implementing training and to keep the team at a good level of practice. Due to this and as an example during the intraoperative studies at Klinikum rechts der Isar freehand SPECT has been in the hands of 8 leading surgeons and up to 14 assisting surgeons, as well as 6 different OR teams. This numbers apply only to approximately 30 surgeries in two Departments. The system has to be able to be taught to newbies easily and experienced users coming back to the system have to be able to use it again without starting the learning process from zero.

Related to the previous topic in order to guarantee proper usability, any system has to be forgiving. If a user makes a mistake while interacting with the system, he or she has to be able to correct it easily and fast. In the case of freehand SPECT the definition of the volume of interest with landmarks was a particular case, where this was solve unproperly during the first studies. Making mistakes while controlling software systems is possible and frequent, in particular during surgery. Adding more intelligence and minimizing user interactions help to reduce these problems as the inclusion of the automatic volume of interest calculation resulted in freehand SPECT.

Efficiency is also mandatory for medical devices. Originally freehand SPECT included seven different steps in order to produce and visualize images. In terms of user interactions this meant over 30 interactions and as a result a big amount of potential mistakes and failures. Currently the system used in the intraoperative studies has 3 steps and requires less than 7 interactions for essentially the same means. This has a huge impact on time and thus in the acceptance of the surgeons and the integration into the workflow in terms of changes in general and time.

Importance of time : As described in almost any marketing book, a fundamental factor in the success of a product is the proper timing.

Prof. John Aarsvold closed his talk at AIIR in Matinatta last year by trying to explain why he failed to introduce intraoperative imaging in the nineties and why he saw a chance now. He explained that the adoption of technologies like PET/CT and SPECT/CT started making structures visible that could not be seen before. If such structures were to be found during surgery only intraoperative imaging could have a chance. In the experience of freehand SPECT this was also clear, but yet there was a further dimension. The right time is not the same time everywhere.

While presenting freehand SPECT almost never a negative feedback was obtained. All surgeons asked spoke of the way to the future. Interestingly only a hand full of them thought however that the future was now.

Clinical applications have also a time and this is the first fact that plays a role. If freehand SPECT helps in an application, it only makes sense if that application is being done or if it is about to start.

Trends also have an influence. In breast cancer surgery the SLNB procedure has been accussed lately of being inncessary. The inclusion of new technology would there not make any sense. On the other hand the introduction of the ROLL procedures in more and more countries (i.e. in Italy [221], Spain [204], France [16], Turkey [22], etc.) or the inclusion of vulva cancer as indication for SLNB (e.g. [56]) speak for freehand SPECT.

Time has to do also with people. Trying to recruit a newly hired Head of a Department to test freehand SPECT was consoderably easier than convincing an older Head of Department with a fixed portofolio of research and patient services. This has to do with

the different challenges posed to each of them and with their motivation. Including new technology and innovation sounds simply excellent for a shortly hired physician to gain a place in his or her hospital.

The place of luck : No matter how well planned everything is, no matter how good things work on the paper, at the bitter end in every success there is always a non-negligible component of luck.

I still do not know if we would have managed to convince our colleagues of Bologna to push freehand SPECT if we did not have such a good patient the first time we were together in the OR. It was a case of SNOLL. The images were simply beautiful: the injection site, the ROLL marked tumor and the SLN were visible. Even an intramammarian lymph node could be guessed. The specimen imaging was even better. The borders were too close to one side. Prof. Mario Taffurelli made an act of faith an extended the borders in the direction our system was showing. Some minutes later the radiologist called and confirmed: the microcalcifications were indeed too close.

Luck cannot be underestimated. Even a good solution can fail if there is no luck. In the introduction of freehand SPECT into the clinic we have had luck. Many of the results presented here could not have been possible without it.

10.2. Closing words

Freehand SPECT was the first implementation of an intraoperative 3D imaging system based on the combination of hand-held devices and tracking technologies. As sumary and conclusion of the process of design, implementation and evaluation of the system the first statement that can be given is that the approach is feasible. With almost 200 cases and systems installed in a hand full of sites the images generated by freehand SPECT are valid and within the requirements accurate and precise. This has to be considered in the light of the type of data available to generate such images. The algorithms developed here and the correction methods have shown to be able to deal with sparsity, limited angularity and asymmetry in order to extract from them the best estimation for a radioactivity distribution.

Further the implementation of the system although not necessarily optimal is sufficient for intraoperative use. Obstacles in terms of usability, safety issues, workflow integration and economic requirements. The resulting design has been evaluated successfully in over 20 centers all over Europe and the USA showing sufficient performance, proper size and flexibility. No major issues haasve arisen from the sterility requirements and the designed hardware has been succesfully tested for sterilization and usability.

The generated images have also not only been valid and the resulting system being suitable for intraoperative use, but the proposed changes in the clinical procedure have been shown and to some extent proven to contribute to the treatment of the patient. Disregarding the impact on survival freehand SPECT has been able to detect radioactive nodes in breast cancer and melanoma SLNB procedures that would otherwise not have been found. Depth information has been made available and it has been incorporated by physicians in the treatment changing it in more than 10% of the cases.

The indication selected as initial for freehand SPECT, the SLNB procedure in breast cancer was shown to be good in terms of allowing fast evaluation due to the availability of it in most hospitals, but showed also not to be optimal. If freehand SPECT is become a standard of care in that application there is still major work to be done in terms of evaluation. Nevertheless indications like SLNB in melanoma for tumors with drain in groin and neck, SLNB in vulvar and head and neck cancer, ROLL, etc are very promising and initial data supports its further development in those directions.

From the technical side the major challenge was related with the scan quality. The detailed analysis on it during the Munich preoperative study may this evident. The reason is however quite intuitive. If an image of a certain area is to be generated this is only possible if there is sufficient information of that specific area. This is very important in 3D imaging, where the lack of projections from at least two direction makes it impossible to make proper depth reconstructions. The methods developed in this work enable attacking that problem in a rather intuitive way. Specially the latest implementation were the 3D information is quantified and overlaid on the video image of the patient has potential.

The next step in this trip will not be short nor easy. Many issues remain open not only for freehand SPECT, but in general for the approach introduced in this work. Looking back however the distance left behind is not minor and many things nobody would have

thought to be possible were shown to be indeed. The concept was good. The indication was clear. The clinical benefits for patient, surgeon and hospital were feasible. But mostly perseverance was kept by the team over long nights and endless hard headed attempts to make from a taped prototype a real medical device.

Part V.

Appendices

Chapter 11

Appendix I: Essential requirements for medical electrical devices

On the following the most important points of the list of essential requirements will be explicitly in the view of a functional imaging system for use in the operating room. The motivation for such extended analysis comes from the fact that during development in research institutions these issues are almost left aside although they may play a fundamental.

11.1. General requirements

In essence medical products and in particular functional imaging systems have to have a clear intended use (see example in figure 11.1). This intended use has to be related to a diagnostic procedure. Any risk or side effect of the use of the device has to be minimized and considered in relation to the supposed advantage for the patient. Accordingly, in imaging systems, the information gained by the use of the imaging has to be considerably above the potential dangers it may involve including risks for the user (medical doctors, technicians, etc.).

The design of medical devices has to consider all expected border conditions. If for example meant to be used in the OR, the system to be developed has to consider the magnetic fields, electromagnetic radiation, electrostatic discharges, pressure, temperature and

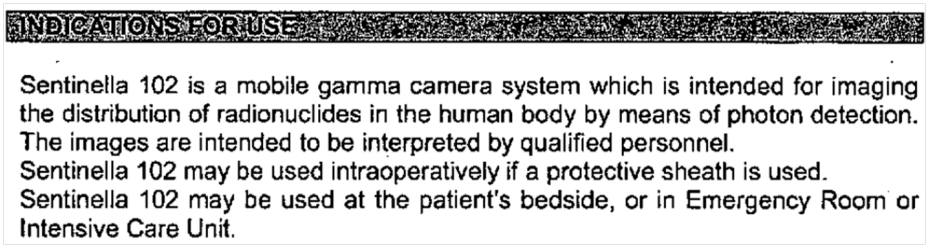
INDICATIONS FOR USE

Sentinella 102 is a mobile gamma camera system which is intended for imaging the distribution of radionuclides in the human body by means of photon detection.
The images are intended to be interpreted by qualified personnel.
Sentinella 102 may be used intraoperatively if a protective sheath is used.
Sentinella 102 may be used at the patient's bedside, or in Emergency Room or Intensive Care Unit.

Figure 11.1.: Example of intended use of intraoperative medical device (gamma camera by Oncovision/GEM Imaging). Text taken from Summary of Substantial Equivalence from FDA's file K092471.

acceleration that may take place in the OR, i.e. consider all possible devices and situations where these may result to be harmful to the patient and user given the operation of the device being designed. Typical pitfalls here are not considering fluids like blood, cleaning liquids, etc. that may be spilled over devices or enter them causing problems (see here the definition of the IP class of a device).

Similarly possible interactions with other devices in the OR have to be considered and if applicable interfaces have to be analyzed in terms of possible risks that would only be probable if the interface exists. If there is a possibility that an electro cautery is used simultaneously with the device be designed, then the high electromagnetic disturbance such electro cauteries generate in the electrical network must be considered (see figure 11.2).

The latter argumentation is also valid for so called 'combination products': at the end, the combination of products must not change the performance and risk of the separated parts, nor create further dangers due to interfaces. For example the combination of tracking and functional probes can only be accepted if the probes would work essentially equally if the tracking was absent (see figure 11.3).

11.2. Requirements on materials

Functional imaging systems have to consider in particular the materials they are built of. In general materials should not be inflammable nor explosive. If any part of the device is meant to be in contact with patient or user, it is not allowed to be toxic given the intended

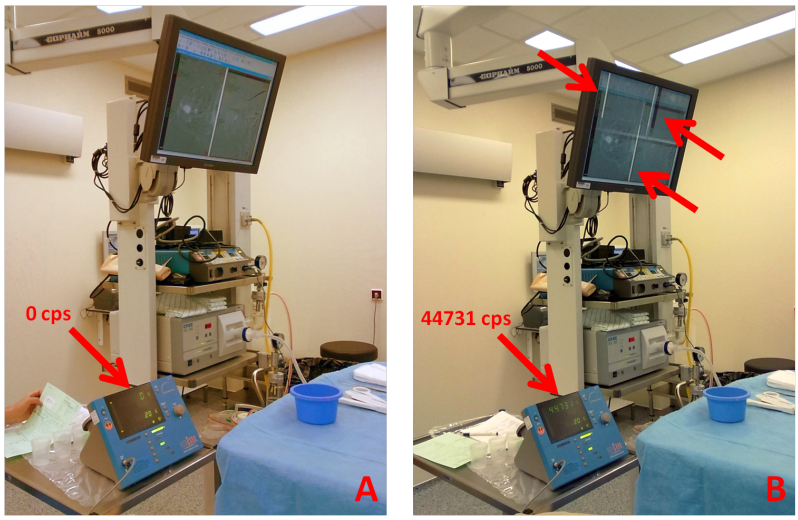

Figure 11.2.: Example of interference between medical devices in OR. In (A) the electro cautery is in use, but is not in contact with other metalic instruments. Gamma probe shows no counts (as it is not pointing to patient and monitor shows image without artifacts). In (B) some seconds later, the surgeon touches metallic forceps with electro cautery. This generates electromagnetic fields in a frequency range that disturb probe and monitor. Probe display shows over 40,000 cps although probe was pointing in direction to a wall where no radioactivity was found. Simultaneously the monitor image flickers.

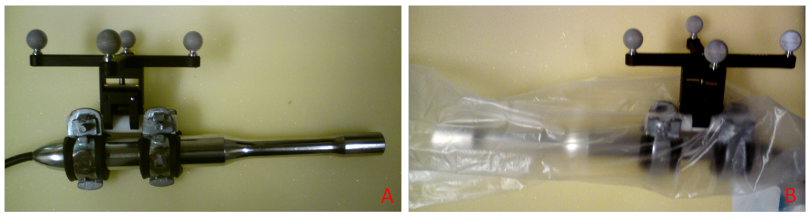

Figure 11.3.: Example of violation of requirement on combination of medical products and possible solution: In (A) a gamma probe is combined with tracking target. The gamma probe cannot be sterilized, so it must be covered with a sterile cover for intended used. This however would not allow proper optical tracking as tracking through cover increases tracking error at least 5 times. On the other hand, not covering the probe disables it to be used in the OR. (B) shows a solution, where probe is covered by sterile sheath and tracking target (sterile) is placed on top of it. Both, probe use and tracking are possible with proper performance.

use and the expected advantage for the patient. Possible uses outside the intended use must be also considered and risks minimized. In the particular case of imaging, the use of devices for clinical applications, for which they were not designed, is a typical source of risks in terms of the materials used.

If the imaging system requires parts of it to be in contact with the patient or the user, biocompatibility has to be taken care of. In general, biocompatibility is to be considered in the light of the exposure time and frequency. This can be of relevance for example when using imaging devices that require contact like ultrasound or references on the patient, like tracking targets in navigated systems.

Aging of materials has to be considered also, deformation and degradation over time may result in the need of establishing time frames for validation or recalibration, like in the case of energy windows in nuclear detectors, geometry in tracking targets, homogeneity in X-ray systems, etc.

In particular for housings, the risks of materials, like gases or fluids, penetrating inside must be avoided in the case they may generate dysfunctions or further dangers. Contamination of the operating field through housings is also to be minimized. For example, in

case of using functional probes like gamma probes, the possibility of carrying microorganisms into the OR field on its surface them must be minimized.

Dangers of harm due to ergonomic issues are also relevant when designing housings, sharp borders have to minimized and the design has to avoid grabbing or coming into contact with the housing in a way a harm to the user could happen (see figure 11.4).

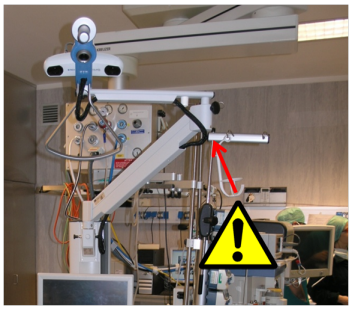

Figure 11.4.: Example of warning sign in housing of intraoperative device (arrow). Arm of CSS300 (implementation of freehand SPECT technology by spin-off company SurgicEye) is too low and can be a danger to users. Accordingly a warning has to be added to it.

Requirements related to sterility

As functional imaging systems working in the OR may come into contact with the open wounds of the patient, it is quite likely that many parts of it must be sterile. Starting from the housings, if they cannot be sterilized, it must be possible to cover them with sterile sheaths or equivalent (see figure 11.3B). An interesting example is for example the case of handles. If a handle is to be used it has to be designed in a way, that if the user tries to grab it without looking he/she cannot by mistake touch a non-sterile part of the housing (see figure 11.5).

Sterile parts have to guarantee that they can be sterilized with validated sterilization methods. They must be packaged in a way that they cannot lose their sterility under normal transport, storage, etc. Finally they have to be manufactured under controlled conditions.

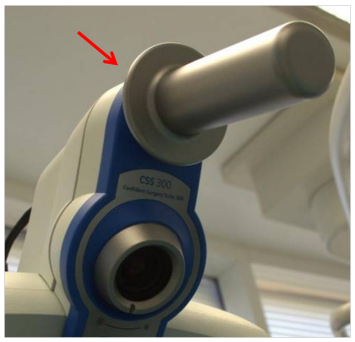

Figure 11.5.: Example of sterile handle in CSS300. The handle is wider towards the cameras in order to avoid sterile personnel to unintentionally touch non-sterile cameras.

11.3. Requirements related to measuring devices

Measuring devices, which could be the case of functional imaging devices have special requirements according to the regulations of EN 60601-1. They have to guarantee a minimal accuracy within the intended use. In the case of soft tissue probably a 5mm value for distance measurements (derived from the images) is appropriate. This is radically different in neurosurgery applications, where any distance displayed should be at least 2mm accurate. The accuracy has to be guaranteed to be held constant over a period and the time frame for recalibration must be made explicit.

Ergonomic issues play also a role in measuring devices. The display has to be suitable (readable from far, see figure 11.6) and the units used have to be according to the country it is used.

11.4. Requirements for devices emitting radiation

Radiation of any type has to be taken seriously. The exposure of patient and users of a medical device have to be in the range permitted for the particular application. In functional imaging devices, this is of importance for devices including X-ray sources, radioactive materials, illumination, lasers, but also electromagnetic fields.

Radiation has to be reproducible, within an acceptable tolerance and include automatic

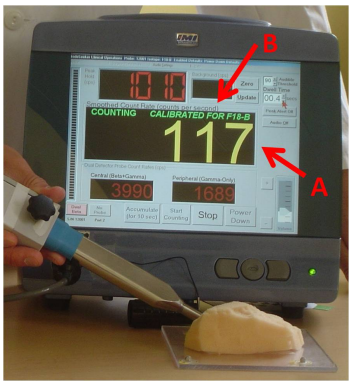

Figure 11.6.: Example of display of measure. Beta probe device shows count rate (A), the most important value according to intended use, in big letters (4-5 cm) in order to allow easy reading of it from distance. Other values may be smaller, as they are needed only for setting additional functions. Units are shown also on screen to avoid confusion (B).

limits to avoid over exposure per mistake. Also invisible radiation has to be made visible or acoustically detectable by the user and/or the patient to avoid harm (see figure 11.7). X-rays, gamma-rays, infrared light, etc. usually part of functional imaging systems are considered among them.

Figure 11.7.: Example of way of warning the presence of invisible radiation. Sign on door turns on when radiation is been applied. Also sound is made to make personnel aware of danger.

In particular scattered radiation (both elastic and inelastic scattering) must be also considered, as it may result in additional exposure to patient and user.

Devices like X-ray devices have to include ways to control the type, geometry and dose of the administered radiation.

For imaging it has to be optimized the quality of the generated images in relation to the dangers involved for patient and user in the light of the advantages of using the system.

In the case of X-ray based imaging, the benefit-risk relation has to be considered. Commonly the quality of the images improves with increasing dose, so that the exposure has to be as high as necessary to obtain clinically good images and as low as possible to avoid a potential harm due to the effect of the used ionizing radiation for the patient.

11.5. Requirements for devices that deliver energy to the patient

As in the case of radiation emitting devices there are constraints for devices that in general deliver energy to the patient.

Electronic devices (which is the case of almost all imaging devices) must behave with proper reproducibility, reliability and performance. Errors that may occur must be caught to avoid risks. Electromagnetic compatibility according for example the standard EN 60601-1-2 must be guaranteed in order to avoid disturbing other devices and on the other hand working properly in the presence of electromagnetic disturbances. Finally, electrical discharges have to be controlled (see figure 11.8) in case they take place and properly designed fuses and transformers have to be included (see here in particular [10]).

On the side of mechanical risks, issues like stability (see figure 11.9) and potential risks due to moving parts must be considered. Mechanical vibrations are of particular relevance, which must for example be taken into account in ultrasound devices. Acoustic energy is also to be considered, beyond dangers in the sound itself. For example if due to sound a phyisician is annoyed and cannot concentrate or in general if the device developed may result in attention deviation from important devices or physiological processes, special care has to be taken of.

On the side of heat, to avoid burnings, temperature must be kept in general below 310 K (37 $^{\circ}C$), unless explicitly needed.

In general if energy is delivered to the patient alarms have to be included if changes in the said energy delivered turn to a risk. This also refers to unintentional energy delivery. In X-ray systems or laser systems this is has to be considered as potential risk.

A particular risk is the potential reactions of contrast media with the delivered image, as

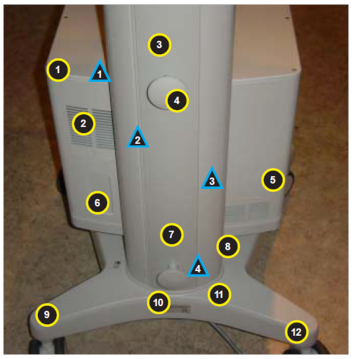

Figure 11.8.: Example of points tested on electrical discharges (air discharges marked with yellow circles, contact discharges marked with blue triangles) on a medical device. Tests have to be repeated with device running and only connected to network, as well as in case of a disconnected earth connection. Image taken from protocol of EN 60601-1-2:2007 compliance of CSS300 by spin-off SurgicEye.

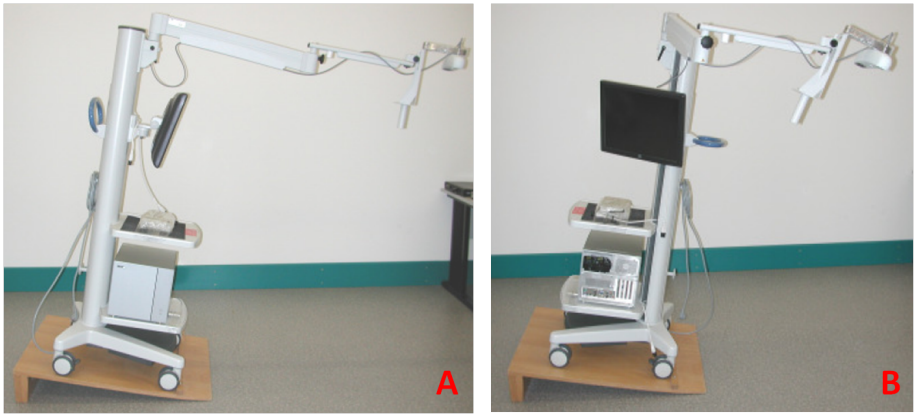

Figure 11.9.: Example of stability test according to EN 60601-1. Medical device is placed on a 10 degrees inclined ramp in the most unfortunate position possible from a stability point of view (here A and B are exemplary unfortunate positions). A small force is applied in vertical direction down (here by pushing arm down). If device comes back to its position, it passed the test. Otherwise stability is not guaranteed according to the said standard and either additional warnings have to be included or other corrective measures implemented.

it is the case in light activated contrast media. Any reaction of the light activated contrast media has to be analyzed.

11.6. Further requirements

The list of essential requirements of EN 60601-1 includes a complete chapter on user documentation which will be omitted here.

Chapter 12

Appendix II: List of Abbreviations

Medical Terms

AP	Anterior-posterior
OR	Operating room
SOP	Standard operating procedure
SLN	Sentinel lymph node
SLNB	SLN biopsy
ADAM	Axillary Dissection with Access Minimized
ALND	Axillary Lymph Node Dissection
WGL	Wire-Guide Localization
ROLL	Radio-guided Occult Lesion Localization
RULL	Radio-guided Ultrasound Lymph node Localization
RT	Radiotherapy
DCIS	Ductal Carcinoma In Situ
DRG	Diagnosis Related Group
ICD	International Classification of Disease
NUB	Neue Untersuchungs- und Behandlungsmethode

Mathematical terms

ART	Algebraic Reconstruction Technique
MART	Multiplicative Algebraic Reconstruction Technique
SIRT	Simultaneous Iterative Reconstruction Technique
ML-EM	Maximum Likelihood - Expectation Maximization
BN	Best Neighbor Optimizer
GN	Gauss-Newton Optimizer
LM	Levenberg Marquandt Optimizer
SSD	Sum of Square Differences
MSSD	Mean Sum of Square Differences
CC	Cross Correlation
CR	Correlation Ratio
MI	Mutual Information
GS	Gauss-Seidel method (iterative solver)
SOR	Successive Over-Relaxation method (iterative solver)
CG	Conjugate Gradient (iterative solver)
SD	Standard Deviation

Medical Imaging Modalities & related topics

CT	(X-ray) Computed Tomography
MR	Magnetic Resonance (also MRI for Imaging or MRT for Tomography)
MRS	MR Spectroscopy (also MRSI for Imaging)
fMRI	functional MRI (also BOLD MRI, BOLD stands for blood oxygenation level dependency)
PET	Positron Emission Tomography
SPECT	Single Photon Emission Computed Tomography
US	Ultrasound
CE	Contrast-enhanced, e.g. CEUS is contrasted-enhanced US
IO	Intraoperative, e.g. IOMRI is intraoperative MRI
PACS	Picture Archiving and Communication System
VOI	Volume of Interest
FoV	Field of View

Pharmaceuticals and biomolecules

5-ALA	5-aminolevulinic acid
Cu-ATSM	^{64}Cu-Cu(II)-diacetyl-bis(N4-methylthiosemicarbazone)
DOTA	1,4,7,10-tetraazacyclododecane-1,4,7,10-tetraacetic acid
DOTATOC	(DOTA(0)-Phe(1)-Tyr(3))octreotid
FAZA	^{18}F-fluoroazomycin arabinoside
FDG	^{18}F-2-fluoro-2-deoxy-D-glucose
FDOPA	^{18}F-L-Dihydroxyphenylalanine
FET	O-(2-^{18}F-fluoroethyl)-L-tyrosine
FLT	3-^{18}F-fluoro-3-deoxy-thymidine
FMISO	^{18}F-fluoromisonidazole
Gd-DTPA	Gadopentetate Dimeglumine
GLUT	Glucose active transport proteins
I-MIBG	I-meta-iodobenzylguanidine
ICG	Indocyanin green
In-octreotid	^{111}In-diethylenetriamine pentaacetic acid-D-[Phe1]-octreotid
MET	^{11}C-methyl-L-methionine
MIBI	^{99m}Tc-2-methoxy-2-methylpropylisonitrile
PPIX	Protoporphyrin IX

Regulatory terms

CDMR	Canadian Medical Device Regulation
CFR	Code of Federal Regulations
FDA	U.S. Federal Drug Administration
MDD	Medical Device Directive
MPG	Medizinproduktegesetz
MPBetreibV	Medizinprodukte-Betreiberverordnung

Chapter 13

Appendix III: List of own publications

A long list of publications appeared during the last years. Here a list of them is given up to June 2010.

13.1. Journals

- T. Wendler, K. Herrmann, A. Schnelzer, T. Lasser, J. Traub, O. Kutter, A. Ehlerding, K. Scheidhauer, T. Schuster, M. Kiechle, M. Schwaiger, N. Navab, S. I. Ziegler, A. K. Buck; First demonstration of 3-D lymphatic mapping in breast cancer using freehand SPECT; European Journal of Nuclear Medicine and Molecular Imaging, Springer Berlin/Heidelberg, March 2010

13.2. Full papers

- N. Navab, J. Traub, A. K. Buck, S. I. Ziegler, T. Wendler; Navigated nuclear probes for intra-operative functional imaging; Proceedings of 5th IEEE International Symposium on Biomedical Imaging (ISBI 2008), Paris, France, May 14 - 17 2008, pp. 1395-1398

- T. Wendler, M. Feuerstein, J. Traub, T. Lasser, J. Vogel, S. I. Ziegler, N. Navab; Real-time fusion of ultrasound and gamma probe for navigated localization of liver metastases; Proceedings of Medical Image Computing and Computer-Assisted Interven-

tion (MICCAI 2007), Brisbane, Australia, October 29 - November 2007, LNCS 4792 (2), pp. 909-917

- T. Wendler, A. Hartl, T. Lasser, J. Traub, S. I. Ziegler, N. Navab; Towards intra-operative 3D nuclear imaging: reconstruction of 3D radioactive distributions using tracked gamma probes; Proceedings of Medical Image Computing and Computer-Assisted Intervention (MICCAI 2007), Brisbane, Australia, October 29 - November 2 2007, LCNS 4792 (2), pp. 252-260

- T. Wendler, J. Traub, S. I. Ziegler, N. Navab; Navigated three dimensional beta probe for optimal cancer resection; Proceedings of Medical Image Computing and Computer-Assisted Intervention (MICCAI 2006), Copenhagen, Denmark, October 1-6 2006, LNCS 4190 (1), pp. 565-569

13.3. Short papers

- T. Wendler, T. Lasser, S. I. Ziegler, N. Navab; Towards Confident 3D Tomographic Reconstruction for Asymmetric, Sparse Detector Geometries; Proceedings of IEEE Medical Imaging Conference (IEEE MIC 2008), Dresden, Germany, October 2008

- T. Lasser, T. Wendler, S. I. Ziegler, N. Navab; Towards Reproducibility of Freehand 3D Tomographic Nuclear Imaging; Proceedings of IEEE Medical Imaging Conference (IEEE MIC 2008), Dresden, Germany, October 2008

13.4. Abstracts

- Ehlerding, A. Schnelzer, T. Wendler, K. Herrmann, T. Lasser, K. Scheidhauer, O. Kutter, T. Schuster, M. Schwaiger, A. K. Buck, S. I. Ziegler, N. Navab, S. Paepke, M. Kiechle; Vorstellung der Pilotstudie zur 3D-Darstellung des Wächterlymphknotens bei Brustkrebspatientinnen mittels Freehand-SPECT; Proceedings of Annual Meeting of the German Society of Senology (DGS), Hamburg, Germany, Jul. 2010

- Santi, L. Fantini, K. Herrmann, Ch. Fuccio, T. Wendler, Paola Caroli, P. Castellucci, A. K. Buck, M. Schwaiger, S. Fanti; Freehand SPECT for sentinel lymph node biopsy:

first clinical experience; Proceedings of the Annual Meeting of the Society of Nuclear Medicine (SNM), Salt Lake City, Utah, USA, June 2010

- D. I. Shakir, J. Bieniarz, , T. Wendler, N. Navab, S. I. Ziegler; A first study on biological feasibility of intraoperative control of tumor resection borders with navigated beta-probe surface imaging; Proceedings of the Annual Meeting of the Society of Nuclear Medicine (SNM), Salt Lake City, Utah, USA, June 2010

- M. C. Kreissl, A. Okur, M. Chen, A. Bartel, T. Wendler, K. Scheidhauer; Pilot study of freehand SPECT for lymphatic mapping in melanoma in upper body; Proceedings of the Annual Meeting of the Society of Nuclear Medicine (SNM), Salt Lake City, Utah, USA, June 2010

- K. Herrmann, A. Schnelzer, M. E. Martignoni, T. Wendler, A. K. Buck; Evaluation of feasibility of freehand SPECT in the operating room; Proceedings of the Annual Meeting of the Society of Nuclear Medicine (SNM), Salt Lake City, Utah, USA, June 2010

- J. Saeckl, A. Ehlerding, K. Herrmann, T. Wendler, M. Schwaiger, M. Kiechle, H. Friess, A. K. Buck, A. Schnelzer, M. E. Martignoni; Evaluation of feasibility of freehand SPECT in the operating room; Proceedings of the International Conference on Sentinel Node Biopsy and Radio-Guided Head and Neck Surgery (SNB), Copenhagen, Denmark, May 2010

- K. Herrmann, T. Wendler, A. Schnelzer, T. Lasser, J. Traub, O. Kutter, A. Ehlerding, K. Scheidhauer, T. Schuster, M. Kiechle, M. Schwaiger, N. Navab, S. I. Ziegler, A. K. Buck; First demonstration of 3D lymphatic mapping using freehand SPECT; Proceedings of the International Conference on Sentinel Node Biopsy and Radio-Guided Head and Neck Surgery (SNB), Copenhagen, Denmark, May 2010

- A. K. Buck, A. Schnelzer, T. Wendler, K. Herrmann, T. Lasser, J. Traub, O. Kutter, T. Schuster, A. Ehlerding, K. Scheidhauer, M. Kiechle, N. Navab, S. I. Ziegler, M. Schwaiger; First demonstration of 3D lymphatic mapping in breast cancer using freehand SPECT; Proceedings of DGN Nuklearmedizin 2010, Leipzig, Germany, April

2010

- K. Herrmann, A. Schnelzer, T. Wendler, M. Hoyer, D. Weisgerber, T. Lasser, S. Paepke, M. E. Martignoni, M. Kiechle, N. Navab, S. I. Ziegler, M. Schwaiger; Evaluation of feasibility of freehand SPECT in the operating room; Proceedings of DGN Nuklearmedizin 2010, Leipzig, Germany, April 2010

- A. Duliu, T. Lasser, T. Wendler, A. Safi, S. I. Ziegler, N. Navab; Navigated Tracking of Skin Lesion Progression with Optical Spectroscopy; SPIE Medical Imaging, San Diego, California, USA, 13-18 February 2010

- T. Wendler, K. Herrmann, A. Schnelzer, T. Lasser, J. Traub, O. Kutter, T. Schuster, M. Kiechle, M. Schwaiger, N. Navab, S. I. Ziegler, A. K. Buck; Clinical introduction of freehand SPECT for image-guided sentinel lymph node biopsy; Proceedings of Annual Congress of the European Association of of Nuclear Medicine (EANM 2009), Barcelona, Spain, October 2009

- T. Wendler, X. Feng, K. Herrmann, T. Lasser, J. Traub, S. I. Ziegler, N. Navab, A. K. Buck; 2D/3D registration of freehand SPECT and planar scintigraphy for clinical evaluation of 3D thyroid scintigraphy; Proceedings of Annual Congress of the European Association of of Nuclear Medicine (EANM 2009), Barcelona, Spain, October 2009

- T. Wendler, K. Herrmann, T. Lasser, J. Traub, M. Schwaiger, N. Navab, S. I. Ziegler, A. K. Buck; First experience with freehand SPECT for lymphatic mapping in melanoma in upper body Proceedings of Annual Congress of the European Association of of Nuclear Medicine (EANM 2009), Barcelona, Spain, October 2009

- T. Wendler, T. Lasser, J. Traub, S. I. Ziegler, N. Navab; Freehand SPECT / ultrasound fusion for hybrid image-guided resection; Proceedings of Annual Congress of the European Association of of Nuclear Medicine (EANM 2009), Barcelona, Spain, October 2009

- T. Lasser, A. Duliu, T. Wendler, S. I. Ziegler, N. Navab; Interactive Reconstruction for Freehand SPECT: An Approach to Acquisition Guidance?; Proceedings of An-

nual Congress of the European Association of of Nuclear Medicine (EANM 2009), Barcelona, Spain, October 2009

- Özgür, J. Bieniarz, T. Lasser, S. I. Ziegler, N. Navab, T. Wendler; Phenomenological Models for intraoperative Positron Emission Surface Imaging using Handheld Probes; Proceedings of World Congress in Medical Physics and Biomedical Engineering (WC 2009), Munich, Germany, September 2009

- J. Traub, K. Herrmann, T. Wendler, T. Lasser, M. Schwaiger, N. Navab, S. I. Ziegler, A. K. Buck; First clinical results of freehand SPECT for lymphatic mapping in breast cancer; Proceedings of the Molekulare Bildgebung (MOBI), Berlin, Germany, Jun. 2009

- T. Wendler, K. Herrmann, T. Lasser, J. Traub, M. Schwaiger, S. I. Ziegler, N. Navab, A. K. Buck; Freehand SPECT: first in-vivo evaluation and comparison to conventional lymphatic mapping; Proceedings of Annual Meeting of Society of Nuclear Medicine (SNM 2009), Toronto, USA, June 2009

- T. Wendler, X. Feng, T. Lasser, K. Herrmann, J. Traub, K. Scheidhauer, S. I. Ziegler, D. Lenhart, J. Grahneis, M. Schwaiger, N. Navab, A. K. Buck; Freehand SPECT for 3D thyroid scintigraphy: first patient report; Proceedings of DGN Nuklearmedizin 2009, Leipzig, Germany, April 2009

- K. Herrmann, T. Wendler, M. Chen, A. Bartel, T. Lasser, K. Scheidhauer, J. Traub, T. Schuster, S. I. Ziegler, M. Schwaiger, A. K. Buck, N. Navab; Freehand SPECT: first in-vivo use for lymphatic mapping and comparison to conventional imaging; Proceedings of DGN Nuklearmedizin 2009, Leipzig, Germany, April 2009

- T. Wendler, T. Lasser, A. K. Buck, C. Özgür, M. Schwaiger, S. I. Ziegler, N. Navab; First in Vivo Use of a Fused Gamma Ultrasound System; Proceedings of RSNA 2008, Chicago, USA, December 2008

- T. Lasser, T. Wendler, J. Traub, S. I. Ziegler, N. Navab; Definition of optimal collimator geometries for 3D tomographic thyroid scintigraphy using navigated gamma probes;

Proceedings of Annual Congress of the European Association of Nuclear Medicine (EANM 2008), Munich, Germany, October 2008

- T. Wendler, T. Lasser, A. K. Buck, J. Traub, M. Schwaiger, S. I. Ziegler, N. Navab; First case report of 3D tomographic thyroid scintigraphy with tracked gamma probes; Proceedings of Annual Congress of the European Association of Nuclear Medicine (EANM 2008), Munich, Germany, October 2008, Eur J Nuc Med Mol Imaging, vol. 35 (Suppl. 2), S129

- T. Wendler, A. Hartl, T. Lasser, J. Traub, S. I. Ziegler, N. Navab; Tracking-based statistical correction for radio-guided cancer surgery; Proceedings of World Molecular Imaging Congress (WMIC 2008), Nice, France, September 2008

- T. Lasser, A. Duliu, T. Wendler, J. Becker, S. I. Ziegler, N. Navab; Computer-assisted spectral quantification of disease progression in CTCL; Proceedings of World Molecular Imaging Congress (WMIC 2008), Nice, France, September 2008

- T. Wendler, J. Traub, T. Lasser, M. Feuerstein, J. Vogel, S. I. Ziegler, N. Navab; Combined ultrasound and gamma probe imaging for examination of thyroid nodules; Proceedings of Annual Meeting of Society of Nuclear Medicine (SNM 2008), New Orleans, USA, June 2008

- T. Wendler, A. Hartl, T. Lasser, J. Traub, S. I. Ziegler, N. Navab; 3D Intra-operative nuclear imaging for SLNB in neck; Proceedings of Annual Meeting of Society of Nuclear Medicine (SNM 2008), New Orleans, USA, June 2008

- T. Lasser, A. Duliu, T. Wendler, S. I. Ziegler, N. Navab; Navigated tracking of skin lesion progression with optical spectroscopy; Proceedings of Annual Meeting of Society of Nuclear Medicine (SNM 2008), New Orleans, USA, June 2008

- A. Hartl, T. Wendler, J. Traub, T. Lasser, S. I. Ziegler, N. Navab; Confident radioactivity surface reconstruction for control of resection borders; Proceedings of Annual Meeting of Society of Nuclear Medicine (SNM 2008), New Orleans, USA, June 2008

- T. Wendler, I. Faure de Pebeyre, T. Lasser, N. Navab; Integrated Surface Acquisition

for Hand-Held Probes; Proceedings of OSA Biomedical Optics (BIOMED 2008), St. Petersburg, USA, March 2008

- T. Wendler, J. Traub, A. Hartl, T. Lasser, M. Burian, A. K. Buck, F. Daghighian, M. Schwaiger, S. I. Ziegler, N. Navab; Adding navigation to radio-guided surgery: new possibilities, new problems, new solutions; Proceedings of Russian Bavarian Conference on Biomedical Engineering (RBC Biomed 2007), Erlangen, Germany, July 2-3, 2007, pp. 96-100

- T. Wendler, A. Hartl, J. Traub, S. I. Ziegler, N. Navab; Intraoperative nuclear imaging using navigated gamma-probes for tumor localization; Proceedings of Annual Meeting of Society of Nuclear Medicine (SNM 2007), Washington D.C., USA, June 2007

- T. Wendler, J. Traub, S. I. Ziegler, N. Navab; Validation of navigated beta-probe imaging with PET/CT-generated activity surfaces. New approach in radio-guided resection for FDG-positive tumors; Proceedings of Annual Meeting of Society of Nuclear Medicine (SNM 2007), Washington D.C., USA, June 2007; Meeting Abstracts 48: 46P-b

- O. Kishenkov, T. Wendler, J. Traub, S. I. Ziegler, N. Navab; Method for projecting functional 3D information onto anatomic surfaces: Accuracy improvement for navigated 3D beta-probes; Proceedings of Bildverarbeitung fuer die Medizin (BVM 2007), Munich, Germany, March 2007, pp.66-70

Bibliography

[1] *IP Guardian 2*.

[2] *Minicam I and Minicam II*.

[3] *SensiMag*.

[4] *Sentinella 102*.

[5] *Gesetz zur wirtschaftlichen Sicherung der Krankenhaeuser und zur Regelung der Krankenhauspflegesaeze (Krankenhausfinanzierungsgesetz - KHG)*, Jun. 1972.

[6] *CFR - Code of Federal Regulations Title 21 - Food and Drugs*, Mar. 1977.

[7] *Council Directive 93/42/EEC of 14 June 1993 concerning medical devices*, Jun. 1993.

[8] *Gesetz ueber Medizinprodukte (Medizinproduktegesetz - MPG)*, Aug. 1994.

[9] *Verordnung ueber das Errichten, Betreiben und Anwenden von Medizinprodukten (Medizinprodukte-Betreiberverordnung - MPBetreibV)*, Jun. 1998.

[10] *Medical electrical equipment - Part 1: General requirements for basic safety and essential performance*, Nov. 2006.

[11] *Siemens' Artis zeego brings surgery and industry together.*, Cardiovasc J Afr, 20(4), 2009, p. 258.

[12] J. N. AARSVOLD, *Anyone can find a hot node*, in Proceedings of the Symposium "Advanced Intra-operative Imaging of Radioisotopes", F. Garibaldi, J. N. Aarsvold,

J. N. Aarsvold, E. Auffray, M.-A. Duval, P. Lecoq, S. Majewski, and M. B. Williams, eds., vol. 1, Centre Europeen de la Recherche en Imagerie Medicale (CERIMED), Sep. 2009.

[13] J. N. AARSVOLD, *Commercial Devices for possible use for Intraoperative Nuclear Medicine*, in Proceedings of the Advanced Intraoperative Imaging of Radioisotopes Symposium, J. N. Aarsvold and F. Garibaldi, eds., September 2009.

[14] S. ABE, M. MEGURO, Y. TAKEISHI, I. TONO-OKA, J. CHIBA, I. MASAKANE, K. TSUIKI, H. TOMOIKE, A. KOMATANI, and K. TAKAHASHI, *[Evaluation of non-circular orbit in thallium-201 myocardial SPECT]*, Kaku Igaku, 28(9), Sep 1991, pp. 1105–1109.

[15] T. E. AHLERING, D. WOO, L. EICHEL, D. I. LEE, R. EDWARDS, and D. W. SKARECKY, *Robot-assisted versus open radical prostatectomy: a comparison of one surgeon's outcomes.*, Urology, 63(5), May 2004, pp. 819–822.

[16] G. AKERMAN, L. TULPIN, C. M. DE MALARTIC, O. MOREL, P. DESFEUX, and E. BARRANGER, *[Radioguided occult lesion localization in breast cancer (ROLL): new techniques?]*, Gynecol Obstet Fertil, 37(1), Jan 2009, pp. 45–49.

[17] B. ALBAYRAK, A. SAMDANI, and P. BLACK, *Intra-operative magnetic resonance imaging in neurosurgery.*, Acta Neurochir. (Wien), 146(6), June 2004, pp. 543–556.

[18] P. L. ALO', P. VISCA, A. MARCI, A. MANGONI, C. BOTTI, and U. D. TONDO, *Expression of fatty acid synthase (FAS) as a predictor of recurrence in stage I breast carcinoma patients.*, Cancer, 77(3), Feb 1996, pp. 474–482.

[19] M. APPEL and N. NAVAB, *3D Reconstruction from Co-Registered Orthographic and Perspective Images: Theoretical Framework and Applications*, in IEEE International Conference on Pattern Recognition, Quebec City, Canada, August 2002, 2002.

[20] D. G. ASSIMOS and K. J. HANSEN, *Role of intraoperative ultrasonography in urology.*, Semin Urol, 12(4), Nov 1994, pp. 283–291.

[21] M. AYAD, A. J. ULM, T. YAO, E. ESKIOGLU, and R. A. MERICLE, *Real-time image guidance for open vascular neurosurgery using digital angiographic roadmapping.*, Neurosurgery, 61(3 Suppl), Sep 2007, pp. 55–61; discussion 61–2.

[22] F. AYDOGAN, V. OZBEN, V. CELIK, C. URAS, G. TAHAN, E. GAZIOGLU, A. CENGIZ, M. FERAHMAN, A. CERCEL, M. H. YILMAZ, M. HALAC, and H. UNAL, *Radioguided occult lesion localization (ROLL) for non-palpable breast cancer: a comparison between day-before and same-day protocols.*, Breast, 19(3), Jun 2010, pp. 226–230.

[23] R. T. AZUMA, *A Survey of Augmented Reality*, Presence: Teleoperators and Virtual Environments, 6(4), 1997, pp. 355–385.

[24] R. T. AZUMA, Y. BAILLOT, R. BEHRINGER, S. FEINER, S. JULIER, and B. MACINTYRE, *Recent Advances in Augmented Reality*, IEEE Computer Graphics and Applications, 2001.

[25] M. BABJUK, W. OOSTERLINCK, R. SYLVESTER, E. KAASINEN, A. BOEHLE, and J. PALOU, *Guidelines on TaT1 (Non-muscle invasive) Bladder Cancer*, 2009.

[26] S. BALDARI, G. R. PECORELLA, S. COSENTINO, and F. MINUTOLI, *Investigation of brain tumours with (99m)Tc-MIBI SPET.*, Q J Nucl Med, 46(4), Dec 2002, pp. 336–345.

[27] J. K. BANERJEE, *Conventional operation versus keyhole surgery.*, J Indian Med Assoc, 91(11), Nov 1993, p. 297.

[28] E. BARRANGER, K. KERROU, Y. PETEGNIEF, E. DAVID-MONTEFIORE, A. CORTEZ, and E. DARAI, *Laparoscopic resection of occult metastasis using the combination of FDG-positron emission tomography/computed tomography image fusion with intraoperative probe guidance in a woman with recurrent ovarian cancer.*, Gynecol Oncol, 96(1), Jan 2005, pp. 241–244.

[29] E. BARRANGER, K. KERROU, S. PITRE, M.-A. DUVAL, Y. CHARON, and S. UZAN, *Place of a hand-held gamma camera (POCI) in the breast cancer sentinel node biopsy.*, Breast, 16(5), Oct 2007, pp. 443–444.

[30] H. H. BARRETT, *Limited-angle tomography for the nineties.*, J Nucl Med, 31(10), Oct 1990, pp. 1688–1692.

[31] A. BARTEL, T. WENDLER, K. HERRMANN, and A. K. BUCK, *Uptake quantification of Sentinel Lymph Nodes in breast cancer using SPECT/CT*, in Proceedings of the 2009 Annual Meeting of the Society of Nuclear Medicine, Society of Nuclear Medicine, Jun. 2009.

[32] M. BAUER, M. SCHLEGEL, D. PUSTKA, N. NAVAB, and G. KLINKER, *Predicting and Estimating the Accuracy of Vision-Based Optical Tracking Systems*, in Proc. IEEE International Symposium on Mixed and Augmented Reality (ISMAR'06), Santa Barbara (CA), USA, October 2006.

[33] M. BAUMHAUER, M. FEUERSTEIN, H.-P. MEINZER, and J. RASSWEILER, *Navigation in endoscopic soft tissue surgery: perspectives and limitations.*, J Endourol, 22(4), Apr 2008, pp. 751–766.

[34] E. BEENEN and D. B. W. DE ROY VAN ZUIDEWIJN, *Patients blue on patent blue: an adverse reaction during four sentinel node procedures.*, Surg Oncol, 14(4), Dec 2005, pp. 151–154.

[35] A. J. BEER, A.-L. GROSU, J. CARLSEN, A. KOLK, M. SARBIA, I. STANGIER, P. WATZLOWIK, H.-J. WESTER, R. HAUBNER, and M. SCHWAIGER, *[18F]galacto-RGD positron emission tomography for imaging of alphavbeta3 expression on the neovasculature in patients with squamous cell carcinoma of the head and neck.*, Clin Cancer Res, 13(22 Pt 1), Nov 2007, pp. 6610–6616.

[36] A. J. BEER, M. NIEMEYER, J. CARLSEN, M. SARBIA, J. NAEHRIG, P. WATZLOWIK, H.-J. WESTER, N. HARBECK, and M. SCHWAIGER, *Patterns of alphavbeta3 expression in primary and metastatic human breast cancer as shown by 18F-Galacto-RGD PET.*, J Nucl Med, 49(2), Feb 2008, pp. 255–259.

[37] A. J. BEER and M. SCHWAIGER, *Imaging of integrin alphavbeta3 expression.*, Cancer Metastasis Rev, 27(4), Dec 2008, pp. 631–644.

[38] W. H. BEIERWALTES, J. C. SISSON, and B. SHAPIRO, *Diagnosis of adrenal tumors with radionuclide imaging.*, Spec Top Endocrinol Metab, 6, 1984, pp. 1–54.

[39] J. M. BENLLOCH, M. ALCANIZ, B. ESCAT, M. M. FERNANDEZ, M. GIMENEZ, R. GOMEZ, V. GRAU, C. LERCHE, J. L. PALMERO, N. PAVON, M. RAFECAS, F. SANCHEZ, and D. VERA, *The Gamma Functional Navigator*, IEEE Trans. on Nuclear Science, 51(3), June 2004, pp. 682–689.

[40] W. BIRKFELLNER, *Tracking Systems in Sugical Navigation*, PhD thesis, Department of Biomedical Engineering and Physics, General Hospital, University of Vienna, 2000.

[41] W. BIRKFELLNER, M. FIGL, K. HUBER, F. WATZINGER, F. WANSCHITZ, J. HUMMEL, R. HANEL, W. GREIMEL, P. HOMOLKA, R. EWERS, and H. BERGMANN, *A Head-Mounted Operating Binocular for Augmented Reality Visualization in Medicine-Design and Initial Evaluation*, IEEE Transactions on Medical Imaging, 21(8), 2002, pp. 991–997.

[42] W. BIRKFELLNER, F. WATZINGER, F. WANSCHITZ, R. EWERS, and H. BERGMANN, *Calibration of Tracking Systems in a Surgical Environment*, IEEE Transactions on Medical Imaging, 17(5), Oct. 1998.

[43] G. BISHOP, G. WELCH, and B. D. ALLEN, *Course 11-Tracking: Beyond 15 Minutes of Thought*, 2001.

[44] J. BONATTI, M. DANZMAYR, T. SCHACHNER, and G. FRIEDRICH, *Intraoperative angiography for quality control in MIDCAB and OPCAB.*, Eur J Cardiothorac Surg., 24(4), October 2003, pp. 647–649.

[45] C. BONETI, S. KOROURIAN, Z. DIAZ, C. SANTIAGO, S. MUMFORD, L. ADKINS, and V. S. KLIMBERG, *Scientific Impact Award: Axillary reverse mapping (ARM) to identify and protect lymphatics draining the arm during axillary lymphadenectomy.*, Am J Surg, 198(4), Oct 2009, pp. 482–487.

[46] S. BORTHWICK, M. STEVENS, and H. DURRANT-WHYTE, *Position estimation and tracking using optical range data*, in Intelligent Robots and Systems '93, IROS '93.

Proceedings of the 1993 IEEE/RSJ International Conference on, vol. 3, 26-30 July 1993, pp. 2172–2177vol.3.

[47] J. A. T. BOSCH, E. V. ROUWET, C. T. H. PETERS, L. JANSEN, H. J. M. VERHAGEN, M. H. PRINS, and J. A. W. TEIJINK, *Contrast-enhanced ultrasound versus computed tomographic angiography for surveillance of endovascular abdominal aortic aneurysm repair.*, J Vasc Interv Radiol, 21(5), May 2010, pp. 638–643.

[48] R. A. BOWERMAN, S. MCCRACKEN, T. M. SILVER, and J. E. KNAKE, *Abdominal and miscellaneous applications of intraoperative ultrasound.*, Radiol Clin North Am, 23(1), Mar 1985, pp. 107–119.

[49] C. E. BREDENBERG, M. IANNETTONI, M. ROSENBLOOM, C. J. HODGE, G. K. LITVIN, J. C. AUST, and E. CACAYORIN, *Operative angiography by intraarterial digital subtraction angiography: a new technique for quality control of carotid endarterectomy.*, J Vasc Surg, 9(4), Apr 1989, pp. 530–534.

[50] P. BRUECKE and F. PIZA, *[On the criticism of preoperative and on the indication of intraoperative angiography of peripheral arterial stenosis]*, Wien Klin Wochenschr, 79(1), Jan 1967, pp. 21–23.

[51] A. K. BUCK, M. BOMMER, S. STILGENBAUER, M. JUWEID, G. GLATTING, H. SCHIRRMEISTER, T. MATTFELDT, D. TEPSIC, D. BUNJES, F. M. MOTTAGHY, B. J. KRAUSE, B. NEUMAIER, H. DOEHNER, P. MOELLER, and S. N. RESKE, *Molecular imaging of proliferation in malignant lymphoma.*, Cancer Res, 66(22), Nov 2006, pp. 11055–11061.

[52] A. K. BUCK, M. HETZEL, H. SCHIRRMEISTER, G. HALTER, P. MOELLER, C. KRATOCHWIL, A. WAHL, G. GLATTING, F. M. MOTTAGHY, T. MATTFELDT, B. NEUMAIER, and S. N. RESKE, *Clinical relevance of imaging proliferative activity in lung nodules.*, Eur J Nucl Med Mol Imaging, 32(5), May 2005, pp. 525–533.

[53] A. K. BUCK and S. N. RESKE, *Cellular origin and molecular mechanisms of 18F-FDG uptake: is there a contribution of the endothelium?*, J Nucl Med, 45(3), Mar 2004, pp. 461–463.

[54] A. K. BUCK, H. SCHIRRMEISTER, M. HETZEL, M. V. D. HEIDE, G. HALTER, G. GLATTING, T. MATTFELDT, F. LIEWALD, S. N. RESKE, and B. NEUMAIER, *3-deoxy-3-[(18)F]fluorothymidine-positron emission tomography for noninvasive assessment of proliferation in pulmonary nodules.*, Cancer Res, 62(12), Jun 2002, pp. 3331–3334.

[55] R. M. CABANAS, *An approach for the treatment of penile carcinoma.*, Cancer, 39(2), Feb 1977, pp. 456–466.

[56] O. CAMARA, H. GONNERT, J. HERRMANN, A. EGBE, H. DIEBOLDER, M. GAJDA, W. MICHELS, and I. B. RUNNEBAUM, *Sentinel lymph node biopsy in vulvar cancer: a pilot study.*, Eur J Gynaecol Oncol, 30(6), 2009, pp. 622–624.

[57] R. W. CARISON, D. C. ALLRED, B. O. ANDERSON, H. J. BURSTEIN, W. B. CARTER, S. B. EDGE, J. K. ERBAN, W. B. FARRAR, S. H. GIORDANO, L. J. GOLDSTEIN, W. J. GRADISHAR, D. F. HAYES, C. A. HUDIS, M. JAHANZEB, B.-M. LJUNG, P. K. MARCOM, I. A. MAYER, B. MCCORMICK, L. M. NABELL, L. J. PIERCE, E. C. REED, M. L. SMITH, G. SOMIO, N. S. TOPHAM, J. H. WARD, E. P. WINER, and A. C. WOLFF, *NCCN Clinical Practice Guidelines in Oncology: Breast Cancer*, 2010.

[58] S. CARLSSON, A. E. NILSSON, M. C. SCHUMACHER, M. N. JONSSON, D. S. VOLZ, G. STEINECK, and N. P. WIKLUND, *Surgery-related Complications in 1253 Robot-assisted and 485 Open Retropubic Radical Prostatectomies at the Karolinska University Hospital, Sweden.*, Urology, Dec 2009.

[59] A. CARPENTIER, S. JEANNOTTE, J. VERREAULT, B. LEFEBVRE, G. BISSON, C. J. MONGEAU, and P. MAHEUX, *Preoperative localization of parathyroid lesions in hyperparathyroidism: relationship between technetium-99m-MIBI uptake and oxyphil cell content.*, J Nucl Med, 39(8), Aug 1998, pp. 1441–1444.

[60] D. CARRERA, A. FERNANDEZ, J. ESTRADA, J. MARTIN-COMIN, and C. GOMEZ, *Detection of occult malignant melanoma by 18F-FDG PET-CT and gamma probe*, Rev Esp Med Nucl, 24(6), 2005, pp. 410–413.

[61] E. C. C. CAUBERG, S. KLOEN, M. VISSER, J. J. M. C. H. DE LA ROSETTE, M. BABJUK, V. SOUKUP, M. PESL, J. DUSKOVA, and T. M. DE REIJKE, *Narrow Band Imaging Cystoscopy Improves the Detection of Non-muscle-invasive Bladder Cancer.*, Urology, Mar 2010.

[62] A. H. CHAKERA, B. HESSE, Z. BURAK, J. R. BALLINGER, A. BRITTEN, C. CARACO, A. J. COCHRAN, M. G. COOK, K. T. DRZEWIECKI, R. ESSNER, E. EVEN-SAPIR, A. M. M. EGGERMONT, T. G. STOPAR, C. INGVAR, M. C. MIHM, S. W. MCCARTHY, N. MOZZILLO, O. E. NIEWEG, R. A. SCOLYER, H. STARZ, J. F. THOMPSON, G. TRIFIRO, G. VIALE, S. VIDAL-SICART, R. UREN, W. WADDINGTON, A. CHITI, A. SPATZ, A. TESTORI, and E. A. OF NUCLEAR MEDICINE-EUROPEAN ORGANISATION FOR RESEARCH, *EANM-EORTC general recommendations for sentinel node diagnostics in melanoma.*, Eur J Nucl Med Mol Imaging, 36(10), Oct 2009, pp. 1713–1742.

[63] R. B. CHATTERJI, *Conventional operation versus keyhole surgery.*, J Indian Med Assoc, 91(1), Jan 1993, pp. 2–3.

[64] M.-C. CHEN, *Clinical evaluation of freehand SPECT for sentinel lymph node biopsy in breast carcinoma*, tech. rep., Technische Universität München, Mar. 2009.

[65] Z. CHENG, J. LEVI, Z. XIONG, O. GHEYSENS, S. KEREN, X. CHEN, and S. S. GAMBHIR, *Near-infrared fluorescent deoxyglucose analogue for tumor optical imaging in cell culture and living mice.*, Bioconjug Chem, 17(3), 2006, pp. 662–669.

[66] Z. CHO, J. CHAN, L. ERIKSSON, M. SINGH, S. GRAHAM, N. MACDONALD, and Y. YANO, *Positron ranges obtained for biomedical important positron-emitting radionucleotides*, Journal of Nuclear Medicine, 16, 1975, pp. 1174–1176.

[67] R. CITRO, E. BOSSONE, B. KUERSTEN, G. GREGORIO, and A. SALUSTRI, *Tissue Doppler and strain imaging: anything left in the echo-lab?*, Cardiovasc Ultrasound, 6, 2008, p. 54.

[68] K. R. CLEARY, F. BANOVAC, E. LEVY, and D. TANAKA, *Development of a liver respiratory motion simulator to investigate magnetic tracking for abdominal interventions*,

in Proc. SPIE Vol. 4681, p. 25-29, Medical Imaging 2002: Visualization, Image-Guided Procedures, and Display, Seong K. Mun; Ed., May 2002, pp. 25–29.

[69] D. G. COIT, R. ANDTBACKA, C. K. BICHAKJIAN, W. E. CARSON, R. A. DILAWARI, D. DIMAIO, V. GUILD, A. C. HALPERN, F. S. HODI, M. KASHANI-SABET, M. C. KELLEY, J. R. LANGE, A. LIND, L. MARTIN, M. C. MARTINI, S. K. PRUITT, M. I. ROSS, S. M. SWETTER, K. K. TANABE, J. A. THOMPSON, V. TRISAL, M. M. URIST, J. WEBER, and M. K. WONG, *NCCN Clinical Practice Guidelines in Oncology: Melanoma*, 2010.

[70] D. COLUCCIA, J. FANDINO, M. FUJIOKA, S. CORDOVI, C. MUROI, and H. LANDOLT, *Intraoperative 5-aminolevulinic-acid-induced fluorescence in meningiomas.*, Acta Neurochir (Wien), Jun 2010.

[71] O. D. A. COMMITTEE, *FDA Advisory Committee Briefing Document*, tech. rep., U.S. Food and Drug Administration, 2009.

[72] C. E. COX, E. DUPONT, G. F. WHITEHEAD, M. D. EBERT, K. NGUYEN, E. S. PELTZ, D. PECKHAM, A. CANTOR, and D. S. REINTGEN, *Age and body mass index may increase the chance of failure in sentinel lymph node biopsy for women with breast cancer.*, Breast J, 8(2), 2002, pp. 88–91.

[73] C. E. COX, S. PENDAS, J. M. COX, E. JOSEPH, A. R. SHONS, T. YEATMAN, N. N. KU, G. H. LYMAN, C. BERMAN, F. HADDAD, and D. S. REINTGEN, *Guidelines for sentinel node biopsy and lymphatic mapping of patients with breast cancer.*, Ann Surg, 227(5), May 1998, pp. 645–51; discussion 651–3.

[74] H. CRAMER and A. KARPATI, *Lymphography*, Munch Med Wochenschr, 93(7), Feb 1951, pp. 309–314.

[75] F. DAGHIGHIAN, J. C. MAZZIOTTA, E. J. HOFFMAN, P. SHENDEROV, B. ESHAGHIAN, S. SIEGEL, and M. E. PHELPS, *Intraoperative beta probe: A device for detecting tissue labeled with positron or electron emitting isotopes during surgery*, Medical Physics, 21(1), 1994, pp. 153–157.

[76] M. J. DALY, J. H. SIEWERDSEN, D. J. MOSELEY, D. A. JAFFRAY, and J. C. IRISH, *Intraoperative cone-beam CT for guidance of head and neck surgery: Assessment of dose and image quality using a C-arm prototype.*, Med Phys, 33(10), Oct 2006, pp. 3767–3780.

[77] R. DAMADIAN, M. GOLDSMITH, and L. MINKOFF, *NMR in cancer: XVI. FONAR image of the live human body.*, Physiol Chem Phys, 9(1), 1977, pp. 97–100, 108.

[78] K. DANIILIDIS, *Hand-eye calibration using dual quaternions*, Journal of Robotics Research, 18, 1999, pp. 286–298.

[79] T. R. DEGRADO, R. E. COLEMAN, S. WANG, S. W. BALDWIN, M. D. ORR, C. N. ROBERTSON, T. J. POLASCIK, and D. T. PRICE, *Synthesis and evaluation of 18F-labeled choline as an oncologic tracer for positron emission tomography: initial findings in prostate cancer.*, Cancer Res, 61(1), Jan 2001, pp. 110–117.

[80] D. DELBEKE, H. SCHOEDER, W. H. MARTIN, and R. L. WAHL, *Hybrid imaging (SPECT/CT and PET/CT): improving therapeutic decisions.*, Semin Nucl Med, 39(5), Sep 2009, pp. 308–340.

[81] D. DESAI, M. ARNOLD, S. SAHA, G. HINKLE, D. SOBLE, J. FRY, L. DEPALATIS, J. MANTIL, M. SATTER, and E. MARTIN, *Correlative Whole-Body FDG-PET and Intraoperative Gamma Detection of FDG Distribution in Colorectal Cancer.*, Clin Positron Imaging, 3(5), Sep 2000, pp. 189–196.

[82] A. J. DICK, V. K. RAMAN, A. N. RAVAL, M. A. GUTTMAN, R. B. THOMPSON, C. OZTURK, D. C. PETERS, A. M. STINE, V. J. WRIGHT, W. H. SCHENKE, and R. J. LEDERMAN, *Invasive human magnetic resonance imaging: feasibility during revascularization in a combined XMR suite.*, Catheter Cardiovasc Interv, 64(3), Mar 2005, pp. 265–274.

[83] S. K. DINESH, J. THOMAS, and I. NG, *Intraoperative computed tomographic angiography in cerebral aneurysm surgery: a pilot feasibility study.*, Neurosurgery, 66(2), Feb 2010, pp. 349–52; discussion 352–3.

[84] T. DOBY, *Cerebral angiography and Egas Moniz.*, AJR Am J Roentgenol, 159(2), Aug 1992, p. 364.

[85] K. DORFMUELLER-ULHAAS, *Robust Optical User Motion Tracking Using a Kalman Filter*, Tech. Rep. TR-2003-06, Augsburg University, 2003.

[86] M. H. E. DOTING, H. M. A. STIEKEMA, J. DE VRIES, C. LEMSTRA, H. J. HOEKSTRA, M. VRIELING, L. RIETMAN, and P. L. JAGER, *Immediate dynamic lymphoscintigraphy delivers no additional value to lymphoscintigraphy 3 hr after tracer injection in sentinel lymph node biopsy in breast cancer patients.*, J Surg Oncol, 95(6), May 2007, pp. 469–475.

[87] A. N. EBERLE, G. MILD, and S. FROIDEVAUX, *Receptor-mediated tumor targeting with radiopeptides. Part 1. General concepts and methods: applications to somatostatin receptor-expressing tumors.*, J Recept Signal Transduct Res, 24(4), 2004, pp. 319–455.

[88] J. ELLSMERE, J. STOLL, D. W. RATTNER, D. BROOKS, R. KANE, W. M. WELLS, III, R. KIKINIS, and K. VOSBURGH, *A Navigation System for Augmenting Laparoscopic Ultrasound*, in Medical Image Computing and Computer-Assisted Intervention – MICCAI 2003, 2003, pp. 184–191.

[89] E. T. ENDICOTT, *Peritoneoscopy*, J Am Med Womens Assoc, 3(5), May 1948, pp. 192–194.

[90] J. I. EPSTEIN, M. CARMICHAEL, and A. W. PARTIN, *OA-519 (fatty acid synthase) as an independent predictor of pathologic state in adenocarcinoma of the prostate.*, Urology, 45(1), Jan 1995, pp. 81–86.

[91] R. ESSNER, E. C. HSUEH, P. I. HAIGH, E. C. GLASS, Y. HUYNH, and F. DAGHIGHIAN, *Application of an F18-Fluorodeoxyglucose-Sensitive Probe for the Intraoperative Detection of Malignancy*, Journal of Surgical Research, 96, January 2001, pp. 120—126.

[92] E. EULER, S. WIRTH, U. LINSENMAIER, W. MUTSCHLER, K. PFEIFER, and A. HEBECKER, *Comparative study of the quality of C-arm based 3D imaging of the talus*, Unfallchirurg., 104(9), September 2001, pp. 839–846.

[93] D. H. EVANS, *Colour flow and motion imaging.*, Proc Inst Mech Eng H, 224(2), 2010, pp. 241–253.

[94] M. G. FELDMAN, J. C. RUSSELL, J. T. LYNCH, and A. MATTIE, *Comparison of mortality rates for open and closed cholecystectomy in the elderly: Connecticut statewide survey.*, J Laparoendosc Surg, 4(3), Jun 1994, pp. 165–172.

[95] J. FERRER-REBOLLEDA, P. S. NOVALES, P. E. NAVAS, F. G. DOMENECH, M. D. R. OJEDA, E. C. CALABUIG, and J. D. GALOFRE, *[Contribution of a portable hand-held miniature gamma camera in surgical treatment of primary hyperparathyroidism]*, Rev Esp Med Nucl, 27(2), 2008, pp. 124–127.

[96] M. FEUERSTEIN, S. M. WILDHIRT, R. BAUERNSCHMITT, and N. NAVAB, *Automatic Patient Registration for Port Placement in Minimally Invasive Endoscopic Surgery*, in Proceedings MICCAI 2005, Palm Springs, USA, October 2005, pp. 287–294.

[97] G. FICHTINGER, A. DEGUET, K. MASAMUNE, E. BALOGH, G. FISCHER, H. MATHIEU, R. H. TAYLOR, L. M. FAYAD, and S. J. ZINREICH, *Needle Insertion in CT Scanner with Image Overlay - Cadaver Studies*, in Medical Image Computing and Computer-Assisted Intervention – MICCAI 2004, C. Barillot, D. R. Haynor, and P. Hellier, eds., vol. 3217 of LNCS, Springer, 2004, pp. 795–803.

[98] K. S. FISHER, E. J. REDDICK, and D. O. OLSEN, *Laparoscopic cholecystectomy: cost analysis.*, Surg Laparosc Endosc, 1(2), Jun 1991, pp. 77–81.

[99] P. FLORENTIN, J. ROUSSEL, and P. SCHOUMACHER, *[Histopathologic significance of radiologically viewed calcifications in breast cancer.]*, Rev Med Nancy, 80, Dec 1955, pp. 987–992.

[100] D. FONTAINE, H. DUFFAU, and S. LITRICO, *[New surgical techniques for brain tumors]*, Rev Neurol (Paris), 162(8-9), Sep 2006, pp. 801–811.

[101] N. FOROGLOU, A. ZAMANI, and P. BLACK, *Intra-operative MRI (iop-MR) for brain tumour surgery.*, Br J Neurosurg, 23(1), Feb 2009, pp. 14–22.

[102] D. L. FRANKLIN, W. SCHLEGEL, and R. F. RUSHMER, *Blood flow measured by Doppler frequency shift of back-scattered ultrasound.*, Science, 134, Aug 1961, pp. 564–565.

[103] S. M. FRAYNE, *Windbelt Presentation at Google TechTalk*. online, Dec. 2007.

[104] S. M. FRAYNE, *Generator utilizing fluid-induced oscillations*, 8 2009.

[105] M. P. FRIED, L. HSU, and F. A. JOLESZ, *Interactive magnetic resonance imaging-guided biopsy in the head and neck: initial patient experience.*, Laryngoscope, 108(4 Pt 1), Apr 1998, pp. 488–493.

[106] G. FRIEDRICH, P. JONETZKO, N. BONAROS, T. SCHACHNER, M. DANZMAYR, J. BONATTI, G. LAUFER, O. PACHINGER, and J. BONATTI, *Hybrid coronary artery revascularization: logistics and program development.*, Heart Surg Forum., 8(4), 2005, pp. 258–261.

[107] J. FRUEHLING, A. VERBIST, and D. BALIKDJIAN, *Which diphosphonate for routine bone scintigraphy (MDP, HDP or DPD)?*, Nucl Med Commun, 7(6), Jun 1986, pp. 415–425.

[108] H. FUCHS, M. A. LIVINGSTON, R. RASKAR, D. COLUCCI, K. KELLER, A. STATE, J. R. CRAWFORD, P. RADEMACHER, S. H. DRAKE, and A. A. MEYER, *Augmented Reality Visualization for Laparoscopic Surgery*, in Medical Image Computing and Computer-Assisted Intervention – MICCAI 1998, 1998, pp. 934–943.

[109] Y. FUJIBAYASHI, H. TANIUCHI, Y. YONEKURA, H. OHTANI, J. KONISHI, and A. YOKOYAMA, *Copper-62-ATSM: a new hypoxia imaging agent with high membrane permeability and low redox potential.*, J Nucl Med, 38(7), Jul 1997, pp. 1155–1160.

[110] M. FUJII and T. WAKABAYASHI, *[Image-guided neurosurgery using intraoperative MRI]*, Brain Nerve, 61(7), Jul 2009, pp. 823–834.

[111] B. FURLOW, *Contrast-enhanced ultrasound.*, Radiol Technol, 80(6), 2009, pp. 547S–561S.

[112] B. GAGEL, P. REINARTZ, C. DEMIREL, H. J. KAISER, M. ZIMNY, M. PIROTH, M. PINKAWA, S. STANZEL, B. ASADPOUR, K. HAMACHER, H. H. COENEN, U. BUELL, and M. J. EBLE, *[18F] fluoromisonidazole and [18F] fluorodeoxyglucose positron emission tomography in response evaluation after chemo-/radiotherapy of non-small-cell lung cancer: a feasibility study.*, BMC Cancer, 6, 2006, p. 51.

[113] S. S. GAMBHIR, *Molecular imaging of cancer with positron emission tomography.*, Nat Rev Cancer, 2(9), Sep 2002, pp. 683–693.

[114] T. GASSER, O. GANSLANDT, E. SANDALCIOGLU, D. STOLKE, R. FAHLBUSCH, and C. NIMSKY, *Intraoperative functional MRI: implementation and preliminary experience.*, Neuroimage, 26(3), Jul 2005, pp. 685–693.

[115] Y. GENC, S. RIEDEL, F. SOUVANNAVONG, C. AKINLAR, and N. NAVAB, *Marker-less Tracking for AR: A Learning-Based Approach*, in IEEE International Symposium on Mixed and Augmented Reality (ISMAR'02), October 2002, 2002.

[116] J. GERL, I. KOJOUHAROV, F. AMEIL, and A. SUROWIEC, *High energy gamma probe with position sensing capability*, Tech. Rep. EP 1,596,223 A1, European Patent Office, May 2004.

[117] E. GITSCH, K. PHILIPP, and N. PATEISKY, *Intraoperative lymph scintigraphy during radical surgery for cervical cancer.*, J Nucl Med, 25(4), Apr 1984, pp. 486–489.

[118] B. B. GOLDBERG, D. A. MERTON, J.-B. LIU, G. MURPHY, and F. FORSBERG, *Contrast-enhanced sonographic imaging of lymphatic channels and sentinel lymph nodes.*, J Ultrasound Med, 24(7), Jul 2005, pp. 953–965.

[119] G. M. M. GOMMANS, E. GOMMANS, F. M. VAN DER ZANT, G. J. J. TEULE, T. G. VAN DER SCHORS, and J. W. D. DE WAARD, *99mTc Nanocoll: a radiopharmaceutical for sentinel node localisation in breast cancer–in vitro and in vivo results.*, Appl Radiat Isot, 67(9), Sep 2009, pp. 1550–1558.

[120] E. A. GOULD, T. WINSHIP, P. H. PHILBIN, and H. H. KERR, *Observations on a "sentinel node" in cancer of the parotid.*, Cancer, 13, 1960, pp. 77–78.

[121] M. GROHER, T. F. JAKOBS, N. PADOY, and N. NAVAB, *Planning and Intraoperative Visualization of Liver Catheterizations: New CTA Protocol and 2D-3D Registration Method*, Academic Radiology, 14(11), 2007, pp. 1324–1339. Special issue of MICCAI 2006.

[122] S. GULEC, F. DAGHIGHIAN, and R. ESSNER, *PET-Probe: Evaluation of Technical Performance and Clinical Utility of a Handheld High-Energy Gamma Probe in Oncologic Surgery.*, Ann Surg Oncol, Jul 2006.

[123] S. A. GULEC, *PET probe-guided surgery.*, J Surg Oncol, 96(4), Sep 2007, pp. 353–357.

[124] S. A. GULEC and R. BAUM, *Radio-guided surgery in neuroendocrine tumors.*, J Surg Oncol, 96(4), Sep 2007, pp. 309–315.

[125] W. A. HALL, H. LIU, R. E. MAXWELL, and C. L. TRUWIT, *Influence of 1.5-Tesla intraoperative MR imaging on surgical decision making.*, Acta Neurochir Suppl, 85, 2003, pp. 29–37.

[126] J. G. HAMILTON and M. H. SOLEY, *A Comparison of the Metabolism of Iodine and of Element 85 (Eka-Iodine).*, Proc Natl Acad Sci U S A, 26(8), Aug 1940, pp. 483–489.

[127] R. A. HANEL, P. NAKAJI, and R. F. SPETZLER, *Use of microscope-integrated near-infrared indocyanine green videoangiography in the surgical treatment of spinal dural arteriovenous fistulae.*, Neurosurgery, 66(5), May 2010, pp. 978–84; discussion 984–5.

[128] A. HARTL, tech. rep., Chair for Computer-Aided Medical Procedures, Faculty of Computer Science, Technische Universität München, 2007.

[129] R. HARTLEY and A. ZISSERMAN, *Multiple View Geometry in Computer Vision*, Cambridge University Press, 2nd ed., 2003.

[130] N. E. HARTSOUGH, H. B. BARBER, J. M. WOOLFENDEN, H. H. BARRETT, T. S. HICKERNELL, and D. P. KWO, *Probes containing gamma radiation detectors for in vivo tumor detection and imaging*, in Proceedings of SPIE Medical Imaging Conference, no. 1068, 1989, pp. 92–99.

[131] P. HASTREITER, C. REZK-SALAMA, G. SOZA, M. BAUER, G. GREINER, R. FAHLBUSCH, O. GANSLANDT, and C. NIMSKY, *Strategies for brain shift evaluation.*, Med Image Anal, 8(4), Dec 2004, pp. 447–464.

[132] B. HAVEKES, E. W. LAI, E. P. M. CORSSMIT, J. A. ROMIJN, H. J. L. M. TIMMERS, and K. PACAK, *Detection and treatment of pheochromocytomas and paragangliomas:*

current standing of MIBG scintigraphy and future role of PET imaging., Q J Nucl Med Mol Imaging, 52(4), Dec 2008, pp. 419–429.

[133] A. HEERSCHAP, G. J. JAGER, M. VAN DER GRAAF, J. O. BARENTSZ, J. J. DE LA ROSETTE, G. O. OOSTERHOF, E. T. RUIJTER, and S. H. RUIJS, *In vivo proton MR spectroscopy reveals altered metabolite content in malignant prostate tissue.*, Anticancer Res, 17(3A), 1997, pp. 1455–1460.

[134] P. HEIDENREICH, R. BARES, W. BRENNER, F. GRUENWALD, J. KOPP, G. LOTTES, D. L. MUNZ, C. REINERS, J. H. RISSE, O. SCHOBER, C. SCHUEMICHEN, H. VOGT, H. WENGENMAIR, and E. WERNER, *Verfahrensanweisung fuer die nuklearmedizinische Waechter-Lymphknoten (sentinel lymph node; SLN) - Diagnostik*, 2003.

[135] S.-M. M. HEINING, P. STEFAN, F. SAUER, E. EULER, N. NAVAB, and J. TRAUB, *Evaluation of an in-situ visualization system for navigated trauma surgery*, in Proceedings of The 6th Computer Assisted Orthopaedic Surgery (CAOS 2006), Montreal, Canada, June 2006.

[136] T. HIGASHI, T. SAGA, T. ISHIMORI, M. MAMEDE, K. ISHIZU, T. FUJITA, T. MUKAI, S. SATO, H. KATO, Y. YAMAOKA, K. MATSUMOTO, M. SENDA, and J. KONISHI, *What is the most appropriate scan timing for intraoperative detection of malignancy using 18F-FDG-sensitive gamma probe? Preliminary phantom and preoperative patient study.*, Ann Nucl Med, 18(2), Apr 2004, pp. 105–114.

[137] C. HIRCHE, S. DRESEL, R. KREMPIEN, and M. HUENERBEIN, *Sentinel Node Biopsy by Indocyanine Green Retention Fluorescence Detection for Inguinal Lymph Node Staging of Anal Cancer: Preliminary Experience.*, Ann Surg Oncol, Mar 2010.

[138] E. J. HOFFMAN, M. P. TORNAI, M. JANECEK, B. E. PATT, and J. S. IWANCZYK, *Intraoperative probes and imaging probes.*, Eur J Nucl Med, 26(8), Aug 1999, pp. 913–935.

[139] L. HOHWUE, O. AKRE, K. V. PEDERSEN, M. JONSSON, C. V. NIELSEN, and O. GUSTAFSSON, *Open retropubic prostatectomy versus robot-assisted laparoscopic*

prostatectomy: a comparison of length of sick leave., Scand J Urol Nephrol, 43(4), 2009, pp. 259–264.

[140] J. P. HOLLAND, J. S. LEWIS, and F. DEHDASHTI, *Assessing tumor hypoxia by positron emission tomography with Cu-ATSM.*, Q J Nucl Med Mol Imaging, 53(2), Apr 2009, pp. 193–200.

[141] W. J. HOLLIS and W. H. BROWN, *Peritoneoscopy, an analysis of its use in 69 cases.*, New Orleans Med Surg J, 100(11), May 1948, pp. 498–504.

[142] L. HUWART and B. E. VAN BEERS, *MR elastography.*, Gastroenterol Clin Biol, 32(6 Suppl 1), Sep 2008, pp. 68–72.

[143] A. IAGARU, D. PETERSON, A. QUON, S. DUTTA, C. TWIST, F. DAGHIGHIAN, S. S. GAMBHIR, and C. ALBANESE, *123I MIBG mapping with intraoperative gamma probe for recurrent neuroblastoma.*, Mol Imaging Biol, 10(1), 2008, pp. 19–23.

[144] W. IARED, D. C. SHIGUEOKA, J. C. CRISTOFOLI, R. ANDRIOLO, A. N. ATALLAH, S. A. AJZEN, and O. VALENTE, *Use of color Doppler ultrasonography for the prediction of malignancy in follicular thyroid neoplasms: systematic review and meta-analysis.*, J Ultrasound Med, 29(3), Mar 2010, pp. 419–425.

[145] D. INNOCENZI, P. L. ALO', A. BALZANI, V. SEBASTIANI, V. SILIPO, G. L. TORRE, G. RICCIARDI, C. BOSMAN, and S. CALVIERI, *Fatty acid synthase expression in melanoma.*, J Cutan Pathol, 30(1), Jan 2003, pp. 23–28.

[146] J. M. JACOBSON and N. NEGROPONTE, *Low cost portable computing device*, 1 2006.

[147] J. S. JAFFE, *Limited angle reconstruction using stabilized algorithms.*, IEEE Trans Med Imaging, 9(3), 1990, pp. 338–344.

[148] R. JAIN, P. DANDEKAR, and V. PATRAVALE, *Diagnostic nanocarriers for sentinel lymph node imaging.*, J Control Release, 138(2), Sep 2009, pp. 90–102.

[149] S. JAIN and R. C. KOCKELBERGH, *The role of photodynamic diagnosis in the contemporary management of superficial bladder cancer.*, BJU Int, 96(1), Jul 2005, pp. 17–21.

[150] P. A. JERABEK, T. B. PATRICK, M. R. KILBOURN, D. D. DISCHINO, and M. J. WELCH, *Synthesis and biodistribution of 18F-labeled fluoronitroimidazoles: potential in vivo markers of hypoxic tissue.*, Int J Rad Appl Instrum A, 37(7), 1986, pp. 599–605.

[151] P. JICHLINSKI, L. GUILLOU, S. J. KARLSEN, P.-U. MALMSTROEM, D. JOCHAM, B. BRENNHOVD, E. JOHANSSON, T. GAERTNER, N. LANGE, H. VAN DEN BERGH, and H.-J. LEISINGER, *Hexyl aminolevulinate fluorescence cystoscopy: new diagnostic tool for photodiagnosis of superficial bladder cancer–a multicenter study.*, J Urol, 170(1), Jul 2003, pp. 226–229.

[152] H. KALAFAT, I. MIHMANLI, K. SARIBEYOGLU, and A. BELLI, *Intraoperative doppler ultrasound: a reliable diagnostic method in insulinoma.*, Hepatogastroenterology, 54(76), Jun 2007, pp. 1256–1258.

[153] W. A. KALENDER, *Computed Tomography. Fundamentals, System Technology, Image Quality, Applications*, Publicis Corporate Publishing, 2005.

[154] B. KATEB, V. YAMAMOTO, C. YU, W. GRUNDFEST, and J. P. GRUEN, *Infrared thermal imaging: a review of the literature and case report.*, Neuroimage, 47 Suppl 2, Aug 2009, pp. T154–T162.

[155] K. KATO, H. SUGIMOTO, N. KANAZUMI, S. NOMOTO, S. TAKEDA, and A. NAKAO, *Intra-operative application of real-time tissue elastography for the diagnosis of liver tumours.*, Liver Int, 28(9), Nov 2008, pp. 1264–1271.

[156] G. E. KELES and M. S. BERGER, *Advances in neurosurgical technique in the current management of brain tumors.*, Semin Oncol, 31(5), Oct 2004, pp. 659–665.

[157] D. KENDOFF, T. HUEFNER, M. CITAK, J. GEERLING, E. MOESSINGER, L. BASTIAN, and C. KRETTEK, *Navigated Iso-C3D-based percutaneous osteoid osteoma resection: a preliminary clinical report.*, Comput Aided Surg, 10(3), May 2005, pp. 157–163.

[158] A. KHAMENE, S. VOGT, F. AZAR, T. SIELHORST, and F. SAUER, *Local 3D reconstruction and augmented reality visualization of freehand ultrasound for needle biopsy procedures*, in Medical Image Computing and Computer-Assisted Intervention – MICCAI 2003, 2003, pp. 344–355.

[159] S. KHANDELWAL, S. F. SENER, L. PURDY, and R. M. PERLMAN, *I-123-guided excision of metastatic papillary thyroid cancer.*, J Surg Oncol, 96(2), Aug 2007, pp. 173–175.

[160] T. KIM, A. E. GIULIANO, and G. H. LYMAN, *Lymphatic mapping and sentinel lymph node biopsy in early-stage breast carcinoma: a metaanalysis.*, Cancer, 106(1), Jan 2006, pp. 4–16.

[161] W. J. KIM, J. Y. CHO, S. W. JEONG, K. M. KIM, I. S. CHOI, J. H. HAM, B. Y. LEE, J. O. KIM, J. S. LEE, and S. Y. JIN, *Comparison of autofluorescence imaging endoscopic findings with pathologic findings after endoscopic submucosal dissection of gastric neoplasms.*, Gut Liver, 2(3), Dec 2008, pp. 186–192.

[162] K. KIMURA, N. TANIGAWA, M. MATSUKI, T. NOHARA, M. IWAMOTO, K. SUMIYOSHI, S. TANAKA, Y. TAKAHASHI, and Y. NARUMI, *High-resolution MR lymphography using ultrasmall superparamagnetic iron oxide (USPIO) in the evaluation of axillary lymph nodes in patients with early stage breast cancer: preliminary results.*, Breast Cancer, Jul 2009.

[163] P. E. KINAHAN, D. W. TOWNSEND, T. BEYER, and D. SASHIN, *Attenuation correction for a combined 3D PET/CT scanner.*, Med Phys, 25(10), Oct 1998, pp. 2046–2053.

[164] A. P. KING, P. J. EDWARDS, C. R. MAURER, JR., D. A. DE CUNHA, D. J. HAWKES, D. L. G. HILL, R. P. GASTON, M. R. FENLON, A. J. STRONG, C. L. CHANDLER, A. RICHARDS, and M. J. GLEESON, *A System for Microscope-Assisted Guided Interventions*, IEEE Transactions on Medical Imaging, 19(2), 2000, pp. 94–102.

[165] T. A. KING, J. V. FEY, K. J. V. ZEE, A. S. HEERDT, M. L. GEMIGNANI, E. R. PORT, L. SCLAFANI, V. SACCHINI, J. A. PETREK, H. S. CODY, P. I. BORGEN, and L. L. MONTGOMERY, *A prospective analysis of the effect of blue-dye volume on sentinel lymph node mapping success and incidence of allergic reaction in patients with breast cancer.*, Ann Surg Oncol, 11(5), May 2004, pp. 535–541.

[166] T. KITAI, T. INOMOTO, M. MIWA, and T. SHIKAYAMA, *Fluorescence navigation with indocyanine green for detecting sentinel lymph nodes in breast cancer.*, Breast Cancer, 12(3), 2005, pp. 211–215.

[167] J. E. KNAKE, R. A. BOWERMAN, T. M. SILVER, and S. MCCRACKEN, *Neurosurgical applications of intraoperative ultrasound.*, Radiol Clin North Am, 23(1), Mar 1985, pp. 73–90.

[168] H. KOBAYASHI, S. KAWAMOTO, M. BERNARDO, M. W. BRECHBIEL, M. V. KNOPP, and P. L. CHOYKE, *Delivery of gadolinium-labeled nanoparticles to the sentinel lymph node: comparison of the sentinel node visualization and estimations of intra-nodal gadolinium concentration by the magnetic resonance imaging.*, J Control Release, 111(3), Apr 2006, pp. 343–351.

[169] H. KOBAYASHI, S. KAWAMOTO, Y. SAKAI, P. L. CHOYKE, R. A. STAR, M. W. BRECHBIEL, N. SATO, Y. TAGAYA, J. C. MORRIS, and T. A. WALDMANN, *Lymphatic drainage imaging of breast cancer in mice by micro-magnetic resonance lymphangiography using a nano-size paramagnetic contrast agent.*, J Natl Cancer Inst, 96(9), May 2004, pp. 703–708.

[170] T. KOJIMA, S.-I. KUMITA, F. YAMAGUCHI, S. MIZUMURA, T. KITAMURA, T. KUMAZAKI, and A. TERAMOTO, *Radio-guided brain tumorectomy using a gamma detecting probe and a mobile solid-state gamma camera.*, Surg Neurol, 61(3), Mar 2004, pp. 229–38; discussion 238.

[171] D. B. KOPANS, J. E. MEYER, K. K. LINDFORS, and S. S. BUCCHIANERI, *Breast sonography to guide cyst aspiration and wire localization of occult solid lesions.*, AJR Am J Roentgenol, 143(3), Sep 1984, pp. 489–492.

[172] R. KOPP, W. ZUERN, R. WEIDENHAGEN, G. MEIMARAKIS, and D. A. CLEVERT, *First experience using intraoperative contrast-enhanced ultrasound during endovascular aneurysm repair for infrarenal aortic aneurysms.*, J Vasc Surg, 51(5), May 2010, pp. 1103–1110.

[173] Y. KOYAMA, V. S. TALANOV, M. BERNARDO, Y. HAMA, C. A. S. REGINO, M. W. BRECHBIEL, P. L. CHOYKE, and H. KOBAYASHI, *A dendrimer-based nanosized contrast agent dual-labeled for magnetic resonance and optical fluorescence imaging to localize the sentinel lymph node in mice.*, J Magn Reson Imaging, 25(4), Apr 2007, pp. 866–871.

[174] F. KRAEBER-BODERE, B. CARIOU, C. CURTET, B. BRIDJI, C. ROUSSEAU, F. DRAVET, B. CHARBONNEL, B. CARNAILLE, J. C. L. NOEL, and E. MIRALLIE, *Feasibility and benefit of fluorine 18-fluoro-2-deoxyglucose-guided surgery in the management of radioiodine-negative differentiated thyroid carcinoma metastases.*, Surgery, 138(6), Dec 2005, pp. 1176–82; discussion 1182.

[175] K. A. KROHN and B. YEUH, *Novel imaging approaches to head and neck cancer.*, Semin Oncol, 35(3), Jun 2008, pp. 262–273.

[176] T. KUEHN, A. BEMBENEK, T. DECKER, D. L. MUNZ, M.-L. SAUTTER-BIHL, M. UNTCH, D. WALLWIENER, and C. C. OF THE GERMAN SOCIETY OF SENOLOGY, *A concept for the clinical implementation of sentinel lymph node biopsy in patients with breast carcinoma with special regard to quality assurance.*, Cancer, 103(3), Feb 2005, pp. 451–461.

[177] D. E. KUHL, J. HALE, and W. L. EATON, *Transmission scanning: a useful adjunct to conventional emission scanning for accurately keying isotope deposition to radiographic anatomy.*, Radiology, 87(2), Aug 1966, pp. 278–284.

[178] R. KUMAR, A. MAVI, G. BURAL, and A. ALAVI, *Fluorodeoxyglucose-PET in the management of malignant melanoma.*, Radiol Clin North Am, 43(1), Jan 2005, pp. 23–33.

[179] M. KUSANO, Y. TAJIMA, K. YAMAZAKI, M. KATO, M. WATANABE, and M. MIWA, *Sentinel node mapping guided by indocyanine green fluorescence imaging: a new method for sentinel node navigation surgery in gastrointestinal cancer.*, Dig Surg, 25(2), 2008, pp. 103–108.

[180] B. LAMPRECHT, P. PORSCH, C. PIRICH, and M. STUDNICKA, *Electromagnetic navigation bronchoscopy in combination with PET-CT and rapid on-site cytopathologic examination for diagnosis of peripheral lung lesions.*, Lung, 187(1), 2009, pp. 55–59.

[181] R. J. LANE, *Intraoperative B-mode scanning.*, J Clin Ultrasound, 8(5), Oct 1980, pp. 427–434.

[182] S. LAVEALLE, G. C. BURDEA, and R. TAYLOR, *Computer-Integrated Surgery: Technology and Clinical Applications*, MIT Press, 1996.

[183] M. LAW, K. C. CHENG, P. M. WU, W. Y. HO, and L. W. C. CHOW, *Patient effective dose from sentinel lymph node lymphoscintigraphy in breast cancer: a study using a female humanoid phantom and thermoluminescent dosemeters.*, Br J Radiol, 76(911), Nov 2003, pp. 818–823.

[184] R. LAWSON, *Thermography; a new tool in the investigation of breast lesions.*, Can Serv Med J, 8(8), Sep 1957, pp. 517–524.

[185] R. N. LAWSON and L. L. ALT, *SKIN TEMPERATURE RECORDING WITH PHOSPHORS: A NEW TECHNIQUE.*, Can Med Assoc J, 92, Feb 1965, pp. 255–260.

[186] C. P. LEBLOND, G. W. WILKINSON, L. F. BELANGER, and J. ROBICHON, *Radio-autographic visualization of bone formation in the rat.*, Am J Anat, 86(2), Mar 1950, pp. 289–341.

[187] M. S. LENHARD, A. BURGES, T. R. C. JOHNSON, P. STIEBER, C. KUEMPER, N. DITSCH, R. LINKE, and K. FRIESE, *PET-CT in recurrent ovarian cancer: impact on treatment planning.*, Anticancer Res, 28(4C), 2008, pp. 2303–2308.

[188] S. P. LEONG, E. DONEGAN, W. HEFFERNON, S. DEAN, and J. A. KATZ, *Adverse reactions to isosulfan blue during selective sentinel lymph node dissection in melanoma.*, Ann Surg Oncol, 7(5), Jun 2000, pp. 361–366.

[189] R. LEVKOVITZ, D. FALIKMAN, M. ZIBULEVSKY, A. BEN-TAL, and A. NEMIROVSKI, *The design and implementation of COSEM, an iterative algorithm for fully 3-D listmode data.*, IEEE Trans Med Imaging, 20(7), Jul 2001, pp. 633–642.

[190] A. LING, R. DAWKINS, M. BAILEY, M. LEUNG, H. CLELAND, J. SERPELL, and J. KELLY, *Short-term morbidity associated with sentinel lymph node biopsy in cutaneous malignant melanoma.*, Australas J Dermatol, 51(1), Feb 2010, pp. 13–17.

[191] E. C. LIPSITZ, F. J. VEITH, and R. A. WAIN, *Digital fluoroscopy as a valuable adjunct to open vascular operations.*, Semin Vasc Surg, 16(4), Dec 2003, pp. 280–290.

[192] A. LIPSON, P. GARGOLLO, and P. BLACK, *Intraoperative magnetic resonance imaging: considerations for the operating room of the future*, J Clin Neurosci., 8(4), July 2001, pp. 305–310.

[193] F. LIU, J. SAFFER, F. NEWCOMER, J. KARP, N. LOCKYER, and W. KONONENKO, *Performance of a dual-layer positron-sensitive surgical probe*, Nuclear Science Symposium Conference Record, 2001 IEEE, 1, November 2001, pp. 53—57.

[194] H. LIU, W. A. HALL, and C. L. TRUWIT, *The roles of functional MRI in MR-guided neurosurgery in a combined 1.5 Tesla MR-operating room.*, Acta Neurochir Suppl, 85, 2003, pp. 127–135.

[195] A. LUXEN, M. GUILLAUME, W. P. MELEGA, V. W. PIKE, O. SOLIN, and R. WAGNER, *Production of 6-[18F]fluoro-L-dopa and its metabolism in vivo–a critical review.*, Int J Rad Appl Instrum B, 19(2), Feb 1992, pp. 149–158.

[196] G. H. LYMAN, A. E. GIULIANO, M. R. SOMERFIELD, A. B. BENSON, D. C. BODURKA, H. J. BURSTEIN, A. J. COCHRAN, H. S. CODY, S. B. EDGE, S. GALPER, J. A. HAYMAN, T. Y. KIM, C. L. PERKINS, D. A. PODOLOFF, V. H. SIVASUBRAMANIAM, R. R. TURNER, R. WAHL, D. L. WEAVER, A. C. WOLFF, E. P. WINER, and A. S. OF CLINICAL ONCOLOGY, *American Society of Clinical Oncology guideline recommendations for sentinel lymph node biopsy in early-stage breast cancer.*, J Clin Oncol, 23(30), Oct 2005, pp. 7703–7720.

[197] M. J. MACK, *Intraoperative coronary graft assessment.*, Curr Opin Cardiol, 23(6), Nov 2008, pp. 568–572.

[198] J. MAEURER, C. WILLAM, H. J. STEINKAMP, F. D. KNOLLMANN, and R. FELIX, *Keratinization and necrosis. Morphologic aspects of lymphatic metastases in ultrasound.*, Invest Radiol, 31(9), Sep 1996, pp. 545–549.

[199] I. MAIER, *Bestimmung der Fluoreszenzkinetik von 5-Aminolaevulinsaeureinduziertem Protoporphyrin-IX an dreidimensionalen Organkulturen menschlicher Bronchialschleimhaut*, PhD thesis, Ludwig-Maximilians-Universitaet Muenchen, 2005.

[200] L. MAIER-HEIN, A. TEKBAS, A. SEITEL, F. PIANKA, S. A. MUELLER, S. SATZL, S. SCHAWO, B. RADELEFF, R. TETZLAFF, A. M. FRANZ, B. P. MUELLER-STICH, I. WOLF, H.-U. KAUCZOR, B. M. SCHMIED, and H.-P. MEINZER, *In vivo accuracy assessment of a needle-based navigation system for CT-guided radiofrequency ablation of the liver.*, Med Phys, 35(12), Dec 2008, pp. 5385–5396.

[201] J. A. MALDJIAN, M. SCHULDER, W. C. LIU, I. K. MUN, D. HIRSCHORN, R. MURTHY, P. CARMEL, and A. KALNIN, *Intraoperative functional MRI using a real-time neurosurgical navigation system.*, J Comput Assist Tomogr, 21(6), 1997, pp. 910–912.

[202] G. MARIANI, S. A. GULEC, D. RUBELLO, G. BONI, M. PUCCINI, M. R. PELIZZO, G. MANCA, D. CASARA, G. SOTTI, P. ERBA, D. VOLTERRANI, and A. E. GIULIANO, *Preoperative localization and radioguided parathyroid surgery.*, J Nucl Med, 44(9), Sep 2003, pp. 1443–1458.

[203] R. C. G. MARTIN, S. HUSHECK, C. R. SCOGGINS, and K. M. MCMASTERS, *Intraoperative magnetic resonance imaging for ablation of hepatic tumors.*, Surg Endosc, 20(10), Oct 2006, pp. 1536–1542.

[204] A. M. MARTINEZ, M. SOLA, A. P. DE TUDELA, J. F. JULIAN, M. FRAILE, S. VIZCAYA, and J. FERNANDEZ, *Radioguided localization of nonpalpable breast cancer lesions: randomized comparison with wire localization in patients undergoing conservative surgery and sentinel node biopsy.*, AJR Am J Roentgenol, 193(4), Oct 2009, pp. 1001–1009.

[205] D. A. MARTINEZ, D. R. KING, C. ROMSHE, R. A. LOZANO, J. D. MORRIS, M. S. O'DORISIO, and E. MARTIN, *Intraoperative identification of parathyroid gland pathology: a new approach.*, J Pediatr Surg, 30(9), Sep 1995, pp. 1306–1309.

[206] M. C. MARTINEZ-BISBAL and B. CELDA, *Proton magnetic resonance spectroscopy imaging in the study of human brain cancer.*, Q J Nucl Med Mol Imaging, 53(6), Dec 2009, pp. 618–630.

[207] K. MASAMUNE, G. FICHTINGER, A. DEGUET, D. MATSUKA, and R. TAYLOR, *An Image Overlay System with Enhanced Reality for Percutaneous Therapy Performed Inside CT Scanner*, in Medical Image Computing and Computer-Assisted Intervention – MICCAI 2002, 2002.

[208] C. MATHELIN, S. SALVADOR, S. CROCE, N. ANDRIAMISANDRATSOA, D. HUSS, and J.-L. GUYONNET, *Optimization of sentinel lymph node biopsy in breast cancer using an operative gamma camera.*, World J Surg Oncol, 5, 2007, p. 132.

[209] J. M. MCGREEVY, M. J. CANNON, and C. B. GRISSOM, *Minimally invasive lymphatic mapping using fluorescently labeled vitamin B12.*, J Surg Res, 111(1), May 2003, pp. 38–44.

[210] B. MELLER, K. SOMMER, J. GERL, K. VON HOF, A. SUROWIEC, E. RICHTER, B. WOLLENBERG, and M. BAEHRE, *High energy probe for detecting lymph node metastases with 18F-FDG in patients with head and neck cancer.*, Nuklearmedizin, 45(4), 2006, pp. 153–159.

[211] N. W. MERRALL, R. PLEVIN, and G. W. GOULD, *Growth factors, mitogens, oncogenes and the regulation of glucose transport.*, Cell Signal, 5(6), Nov 1993, pp. 667–675.

[212] R. MICU, T. JAKOBS, M. URSCHLER, and N. NAVAB, *A new registration/visualization paradigm for CT-Fluoroscopy guided RF liver ablation*, in Proc. Int'l Conf. Medical Image Computing and Computer Assisted Intervention (MICCAI), Lecture Notes in Computer Science, Springer, 2006.

[213] P. MILGRAM, H. TAKEMURA, A. UTSUMI, and F. KISHINO, *Augmented reality: a class of displays on the reality-virtuality continuum*, Proc. SPIE, Telemanipulator and Telepresence Technologies, 2351, 1995.

[214] M. MINATO, C. HIROSE, M. SASA, H. NISHITANI, Y. HIROSE, and T. MORIMOTO, *3-dimensional computed tomography lymphography-guided identification of sentinel lymph nodes in breast cancer patients using subcutaneous injection of nonionic contrast medium: a clinical trial.*, J Comput Assist Tomogr, 28(1), 2004, pp. 46–51.

[215] T. J. MINER, C. D. SHRIVER, P. R. FLICEK, F. C. MINER, D. P. JAQUES, M. E. MANISCALCO-THEBERGE, and D. N. KRAG, *Guidelines for the safe use of radioactive materials during localization and resection of the sentinel lymph node.*, Ann Surg Oncol, 6(1), 1999, pp. 75–82.

[216] M. MITSCHKE and N. NAVAB, *Recovering the X-ray projection geometry for three-dimensional tomographic reconstruction with additional sensors: attached camera versus external navigation system.*, Med Image Anal., 7(1), March 2003, pp. 65–78.

[217] M. MITSCHKE, O. SCHUETZ, N. NAVAB, K. WIESENT, and R. GRAUMANN, *Intra-operative three-dimentional X-ray imaging of high contrast objects with a mobile C-arm system*, in SURGETICA CAS 2002, Grenoble, September 2002, 2002.

[218] S.-I. MIYATAKE, Y. KAJIMOTO, and T. KUROIWA, *[Intraoperative photo-dynamic diagnosis of brain tumors]*, Brain Nerve, 61(7), Jul 2009, pp. 835–842.

[219] S. MOEHRS, M. DEFRISE, N. BELCARI, A. D. GUERRA, A. BARTOLI, S. FABBRI, and G. ZANETTI, *Multi-ray-based system matrix generation for 3D PET reconstruction.*, Phys Med Biol, 53(23), Dec 2008, pp. 6925–6945.

[220] M. MONICI, *Cell and tissue autofluorescence research and diagnostic applications.*, Biotechnol Annu Rev, 11, 2005, pp. 227–256.

[221] S. MONTI, V. GALIMBERTI, G. TRIFIRO, C. D. CICCO, N. PERADZE, F. BRENELLI, J. FERNANDEZ-RODRIGUEZ, N. ROTMENSZ, A. LATRONICO, A. BERRETTINI, M. MAURI, L. MACHADO, A. LUINI, and G. PAGANELLI, *Occult breast lesion*

localization plus sentinel node biopsy (SNOLL): experience with 959 patients at the European Institute of Oncology., Ann Surg Oncol, 14(10), Oct 2007, pp. 2928–2931.

[222] I. MOORE, *Demonstration of some New Instruments recently designed for the Removal of Foreign Bodies from the Lungs by Per-oral Endoscopy.*, Proc R Soc Med, 12(Laryngol Sect), 1919, p. 20.

[223] K. MORI, D. DEGUCHI, K. AKIYAMA, T. KITASAKA, C. R. M. JR., Y. SUENAGA, H. TAKABATAKE, M. MORI, , and H. NATORI, *Hybrid Bronchoscope Tracking Using a Magnetic Tracking Sensor and Image Registration*, in Medical Image Computing and Computer-Assisted Intervention – MICCAI 2005, Springer-Verlag, 2005, pp. 543–550.

[224] D. L. MORTON, D. R. WEN, J. H. WONG, J. S. ECONOMOU, L. A. CAGLE, F. K. STORM, L. J. FOSHAG, and A. J. COCHRAN, *Technical details of intraoperative lymphatic mapping for early stage melanoma.*, Arch Surg, 127(4), Apr 1992, pp. 392–399.

[225] K. MOTOMURA, H. INAJI, Y. KOMOIKE, T. KASUGAI, S. NOGUCHI, and H. KOYAMA, *Sentinel node biopsy guided by indocyanine green dye in breast cancer patients.*, Jpn J Clin Oncol, 29(12), Dec 1999, pp. 604–607.

[226] F. MOURGUES and E. COSTE-MANIERE, *Flexible Calibration of Actuated Stereoscopic Endoscope for Overlay in Robot Assisted Surgery*, in Medical Image Computing and Computer-Assisted Intervention – MICCAI 2002, 2002, pp. 25–34.

[227] D. MURAWA, C. HIRCHE, S. DRESEL, and M. HUENERBEIN, *Sentinel lymph node biopsy in breast cancer guided by indocyanine green fluorescence.*, Br J Surg, 96(11), Nov 2009, pp. 1289–1294.

[228] Z. NAHAS, D. GOLDENBERG, C. FAKHRY, M. EWERTZ, M. ZEIGER, P. W. LADENSON, R. WAHL, and R. P. TUFANO, *The role of positron emission tomography/computed tomography in the management of recurrent papillary thyroid carcinoma.*, Laryngoscope, 115(2), Feb 2005, pp. 237–243.

[229] M. NAKAMOTO, Y. SATO, M. MIYAMOTO, Y. NAKAMJIMA, K. KONISHI, M. SHIMADA, M. HASHIZUME, and S. TAMURA, *3D Ultrasound System Using a*

Magneto-optic Hybrid Tracker for Augmented Reality Visualization in Laparoscopic Liver Surgery, in Medical Image Computing and Computer-Assisted Intervention – MICCAI 2002, 2002, pp. 148–155.

[230] T. NEGELE, G. MEISETSCHLAEGER, T. BRUECKNER, K. SCHEIDHAUER, M. SCHWAIGER, and H. VOGELSANG, *Radio-guided surgery for persistent differentiated papillary thyroid cancer: case presentations and review of the literature.*, Langenbecks Arch Surg, 391(3), Jun 2006, pp. 178–186.

[231] I. M. NORDON, R. J. HINCHLIFFE, A. H. MALKAWI, J. TAYLOR, P. J. HOLT, R. MORGAN, I. M. LOFTUS, and M. M. THOMPSON, *Validation of DynaCT in the morphological assessment of abdominal aortic aneurysm for endovascular repair.*, J Endovasc Ther, 17(2), Apr 2010, pp. 183–189.

[232] J. NORMAN and H. CHHEDA, *Minimally invasive parathyroidectomy facilitated by intraoperative nuclear mapping.*, Surgery, 122(6), Dec 1997, pp. 998–1003; discussion 1003–4.

[233] S. NOURA, M. OHUE, Y. SEKI, K. TANAKA, M. MOTOORI, K. KISHI, I. MIYASHIRO, H. OHIGASHI, M. YANO, O. ISHIKAWA, and Y. MIYAMOTO, *Feasibility of a lateral region sentinel node biopsy of lower rectal cancer guided by indocyanine green using a near-infrared camera system.*, Ann Surg Oncol, 17(1), Jan 2010, pp. 144–151.

[234] U. OEHRVALL, J. E. WESTLIN, S. NILSSON, C. JUHLIN, J. RASTAD, H. LUNDQVIST, and G. AKERSTROEM, *Intraoperative gamma detection reveals abdominal endocrine tumors more efficiently than somatostatin receptor scintigraphy.*, Cancer, 80(12 Suppl), Dec 1997, pp. 2490–2494.

[235] A. OF BREAST SURGERY AT BASO 2009, *Surgical guidelines for the management of breast cancer.*, Eur J Surg Oncol, 35 Suppl 1, 2009, pp. 1–22.

[236] S. OGAWA, T. M. LEE, A. R. KAY, and D. W. TANK, *Brain magnetic resonance imaging with contrast dependent on blood oxygenation.*, Proc Natl Acad Sci U S A, 87(24), Dec 1990, pp. 9868–9872.

[237] S. OHNISHI, E. S. GARFEIN, S. J. KARP, and J. V. FRANGIONI, *Radiolabeled and near-infrared fluorescent fibrinogen derivatives create a system for the identification and repair of obscure gastrointestinal bleeding.*, Surgery, 140(5), Nov 2006, pp. 785–792.

[238] B. OLBRICH, J. TRAUB, S. WIESNER, A. WIECHERT, H. FEUSSNER, and N. NAVAB, *Respiratory Motion Analysis: Towards Gated Augmentation of the Liver*, in Proceedings of Computer Assisted Radiology and Surgery (CARS 2005), Berlin, Germany, June 2005, pp. 248–253.

[239] J. OPHIR, I. CESPEDES, H. PONNEKANTI, Y. YAZDI, and X. LI, *Elastography: a quantitative method for imaging the elasticity of biological tissues.*, Ultrason Imaging, 13(2), Apr 1991, pp. 111–134.

[240] J. E. ORTUNO, G. KONTAXAKIS, J. L. RUBIO, P. GUERRA, and A. SANTOS, *Efficient methodologies for system matrix modelling in iterative image reconstruction for rotating high-resolution PET.*, Phys Med Biol, 55(7), Apr 2010, pp. 1833–1861.

[241] W. R. OSEBOLD, E. L. LESTER, J. H. HURLEY, and R. L. VINCENT, *Intraoperative use of the mobile gamma camera in localizing and excising osteoid osteomas of the spine.*, Spine (Phila Pa 1976), 18(13), Oct 1993, pp. 1816–1828.

[242] N. OYAMA, H. AKINO, H. KANAMARU, Y. SUZUKI, S. MURAMOTO, Y. YONEKURA, N. SADATO, K. YAMAMOTO, and K. OKADA, *11C-acetate PET imaging of prostate cancer.*, J Nucl Med, 43(2), Feb 2002, pp. 181–186.

[243] A. R. PADHANI, *Where are we with imaging oxygenation in human tumours?*, Cancer Imaging, 5, 2005, pp. 128–130.

[244] A. R. PADHANI, K. A. KROHN, J. S. LEWIS, and M. ALBER, *Imaging oxygenation of human tumours.*, Eur Radiol, 17(4), Apr 2007, pp. 861–872.

[245] S. PAEPKE, U. SCHWARZ-BOEGER, M. KIECHLE, and V. R. JACOBS, *Axillary Dissection with Access Minimized (ADAM): a new technique for lymph node dissection in conservative surgery for breast cancer.*, Int J Fertil Womens Med, 48(5), 2003, pp. 232–237.

[246] G. PAGANELLI, C. DECICCO, A. LUINI, E. CASSANO, M. PIZZAMIGLIO, M. FIORENZA, V. GALIMBERTI, S. ZURRIDA, and U. VERONESI, *Radioguided surgery in non-palpable breast lesions*, Eur J Nucl Med, 24, 1997, p. 893.

[247] M. N. PAMIR, K. OZDUMAN, A. DINCER, E. YILDIZ, S. PEKER, and M. M. OZEK, *First intraoperative, shared-resource, ultrahigh-field 3-Tesla magnetic resonance imaging system and its application in low-grade glioma resection.*, J Neurosurg, 112(1), Jan 2010, pp. 57–69.

[248] P. V. PANDHARIPANDE, M. G. HARISINGHANI, E. M. OZANNE, M. C. SPECHT, C. HUR, J. M. LEE, and G. S. GAZELLE, *Staging MR lymphangiography of the axilla for early breast cancer: cost-effectiveness analysis.*, AJR Am J Roentgenol, 191(5), Nov 2008, pp. 1308–1319.

[249] V. Y. PANIN, F. KEHREN, C. MICHEL, and M. CASEY, *Fully 3-D PET reconstruction with system matrix derived from point source measurements.*, IEEE Trans Med Imaging, 25(7), Jul 2006, pp. 907–921.

[250] P. PAREDES, S. VIDAL-SICART, G. ZANON, N. ROE, S. RUBI, S. LAFUENTE, J. PAVIA, and F. PONS, *Radioguided occult lesion localisation in breast cancer using an intraoperative portable gamma camera: first results.*, Eur J Nucl Med Mol Imaging, 35(2), Feb 2008, pp. 230–235.

[251] D. PAULEIT, A. ZIMMERMANN, G. STOFFELS, D. BAUER, J. RISSE, M. O. FLUESS, K. HAMACHER, H. H. COENEN, and K.-J. LANGEN, *18F-FET PET compared with 18F-FDG PET and CT in patients with head and neck cancer.*, J Nucl Med, 47(2), Feb 2006, pp. 256–261.

[252] E. K. PAUWELS, M. J. RIBEIRO, J. H. STOOT, V. R. MCCREADY, M. BOURGUIGNON, and B. MAZIERE, *FDG accumulation and tumor biology.*, Nucl Med Biol, 25(4), May 1998, pp. 317–322.

[253] J. PERSLIDEN, *Patient and staff doses in interventional X-ray procedures in Sweden.*, Radiat Prot Dosimetry, 114(1-3), 2005, pp. 150–157.

[254] M. D. PESHAVE and N. D. DHARKAR, *An integrated shaft for twin cylinder internal combustion inline common rail diesel engine*, 10 2008.

[255] T. PETERS, *Image-guidance for surgical procedures*, Phys Med Biol, 51(14), 2006, pp. R505–40.

[256] T. M. PETERS, *Image-guidance for surgical procedures.*, Phys Med Biol, 51(14), Jul 2006, pp. R505–R540.

[257] M. E. PHELPS, *PET: The Merging of Biology and Imaging into Molecular Imaging*, The Journal of Nuclear Medicine, 41(4), April 2000, pp. 661—681.

[258] M. E. PHELPS and S. R. CHERRY, *The Changing Design of Positron Imaging Systems.*, Clin Positron Imaging, 1(1), Dec 1998, pp. 31–45.

[259] M. PICCHIO, R. BECK, R. HAUBNER, S. SEIDL, H.-J. MACHULLA, T. D. JOHNSON, H.-J. WESTER, G. REISCHL, M. SCHWAIGER, and M. PIERT, *Intratumoral spatial distribution of hypoxia and angiogenesis assessed by 18F-FAZA and 125I-Gluco-RGD autoradiography.*, J Nucl Med, 49(4), Apr 2008, pp. 597–605.

[260] M. PICCHIO, U. TREIBER, A. J. BEER, S. METZ, P. BOESSNER, H. VAN RANDENBORGH, R. PAUL, G. WEIRICH, M. SOUVATZOGLOU, R. HARTUNG, M. SCHWAIGER, and M. PIERT, *Value of 11C-choline PET and contrast-enhanced CT for staging of bladder cancer: correlation with histopathologic findings.*, J Nucl Med, 47(6), Jun 2006, pp. 938–944.

[261] M. PIERT, H.-J. MACHULLA, M. PICCHIO, G. REISCHL, S. ZIEGLER, P. KUMAR, H.-J. WESTER, R. BECK, A. J. B. MCEWAN, L. I. WIEBE, and M. SCHWAIGER, *Hypoxia-specific tumor imaging with 18F-fluoroazomycin arabinoside.*, J Nucl Med, 46(1), Jan 2005, pp. 106–113.

[262] S. P. POVOSKI, R. L. NEFF, C. M. MOJZISIK, D. M. O'MALLEY, G. H. HINKLE, N. C. HALL, D. A. MURREY, M. V. KNOPP, and E. W. MARTIN, *A comprehensive overview of radioguided surgery using gamma detection probe technology.*, World J Surg Oncol, 7, 2009, p. 11.

[263] R. W. PRAGER, R. N. ROHLING, A. H. GEE, and L. BERMAN, *Rapid calibration for 3-D freehand ultrasound.*, Ultrasound Med Biol, 24(6), Jul 1998, pp. 855–869.

[264] D. T. PRICE, R. E. COLEMAN, R. P. LIAO, C. N. ROBERTSON, T. J. POLASCIK, and T. R. DEGRADO, *Comparison of [18 F]fluorocholine and [18 F]fluorodeoxyglucose for positron emission tomography of androgen dependent and androgen independent prostate cancer.*, J Urol, 168(1), Jul 2002, pp. 273–280.

[265] D. PUSTKA, M. HUBER, M. BAUER, and G. KLINKER, *Spatial Relationship Patterns: Elements of Reusable Tracking and Calibration Systems*, in Proc. IEEE International Symposium on Mixed and Augmented Reality (ISMAR'06), October 2006.

[266] J. QI and R. H. HUESMAN, *Effect of errors in the system matrix on maximum a posteriori image reconstruction.*, Phys Med Biol, 50(14), Jul 2005, pp. 3297–3312.

[267] J. QI, R. M. LEAHY, S. R. CHERRY, A. CHATZIIOANNOU, and T. H. FARQUHAR, *High-resolution 3D Bayesian image reconstruction using the microPET small-animal scanner.*, Phys Med Biol, 43(4), Apr 1998, pp. 1001–1013.

[268] S. RAJASEKARAN, K. KARTHIK, V. R. CHANDRA, N. RAJKUMAR, and J. DHEENADHAYALAN, *Role of intraoperative 3D C-arm-based navigation in percutaneous excision of osteoid osteoma of long bones in children.*, J Pediatr Orthop B, 19(2), Mar 2010, pp. 195–200.

[269] G. RAVIZZINI, B. TURKBEY, T. BARRETT, H. KOBAYASHI, and P. L. CHOYKE, *Nanoparticles in sentinel lymph node mapping.*, Wiley Interdiscip Rev Nanomed Nanobiotechnol, 1(6), Nov 2009, pp. 610–623.

[270] R. R. RAYLMAN, *Performance of a dual, solid-state intraoperative probe system with 18F, 99mTc, and (111)In.*, J Nucl Med, 42(2), Feb 2001, pp. 352–360.

[271] R. R. RAYLMAN, S. J. FISHER, S. P. E. RAYA S. BROWN, and R. L. WAHL, *Fluorine-18-Fluorodeoxyglucose-Guided Breast Cancer Surgery with a Positron-Sensitive Probe: Validation in Preclinical Studies*, J Nucl Med, 36(10), 1995, pp. 1869—1874.

[272] R. R. RAYLMAN and R. L. WAHL, *A Fiber-Optically Coupled Positron-Sensitive Surgical Probe*, Journal of Nuclear Medicine, 35(5), 1993, pp. 909–913.

[273] R. R. RAYLMAN and R. L. WAHL, *Evaluation of ion-implanted-silicon detectors for use in intraoperative positron-sensitive probes*, Medical Physics, 23(11), 1996, pp. 1889—1895.

[274] C. RENNER, D. LINDNER, J. SCHNEIDER, and J. MEIXENSBERGER, *Evaluation of intra-operative ultrasound imaging in brain tumor resection: a prospective study.*, Neurol Res., 27(4), June 2005, pp. 351–357.

[275] S. N. RESKE, N. M. BLUMSTEIN, B. NEUMAIER, H.-W. GOTTFRIED, F. FINSTERBUSCH, D. KOCOT, P. MOELLER, G. GLATTING, and S. PERNER, *Imaging prostate cancer with 11C-choline PET/CT.*, J Nucl Med, 47(8), Aug 2006, pp. 1249–1254.

[276] L. RETTENBACHER, *Protokolle - Waechterlymphknoten: Malignes Melanom*, February 2004.

[277] L. RETTENBACHER, *Protokolle - Waechterlymphknoten: Mammakarzinom*, February 2004.

[278] J. C. REUBI, *Peptide receptors as molecular targets for cancer diagnosis and therapy.*, Endocr Rev, 24(4), Aug 2003, pp. 389–427.

[279] M. RICHTER, J. GEERLING, S. ZECH, T. GOESLING, and C. KRETTEK, *Intraoperative three-dimensional imaging with a motorized mobile C-arm (SIREMOBIL ISO-C-3D) in foot and ankle trauma care: a preliminary report.*, J Orthop Trauma., 19(4), April 2005, pp. 259–266.

[280] D. RITTER, M. MITSCHKE, and R. GRAUMANN, *Markerless Navigation with the Intra-Operative Imaging Modality SIREMOBIL Iso-C3D*, electromedica, 70(1), 2002, pp. 31–36.

[281] D. L. L. ROBERTS, A. V. ANSTEY, R. J. BARLOW, N. H. COX, J. A. N. BISHOP, P. G. CORRIE, J. EVANS, M. E. GORE, P. N. HALL, N. KIRKHAM, B. A.

OF DERMATOLOGISTS, and M. S. GROUP, *U.K. guidelines for the management of cutaneous melanoma.*, Br J Dermatol, 146(1), Jan 2002, pp. 7–17.

[282] J. N. ROGART, H. R. ASLANIAN, and U. D. SIDDIQUI, *Narrow Band Imaging to Detect Residual or Recurrent Neoplastic Tissue During Surveillance Endoscopy.*, Dig Dis Sci, Jun 2010.

[283] S. ROSSI, W. OU, D. TANG, N. BHATTACHARYA, A. P. D. TOS, J. A. FLETCHER, and M. LODA, *Gastrointestinal stromal tumours overexpress fatty acid synthase.*, J Pathol, 209(3), Jul 2006, pp. 369–375.

[284] J. M. RUBIN, M. MIRFAKHRAEE, E. E. DUDA, G. J. DOHRMANN, and F. BROWN, *Intraoperative ultrasound examination of the brain.*, Radiology, 137(3), Dec 1980, pp. 831–832.

[285] R. SADEGHI, M. N. FORGHANI, B. MEMAR, M. T. R. MASHHADI, V. R. D. KAKHKI, A. ABDOLLAHI, and S. R. ZAKAVI, *How long the lymphoscintigraphy imaging should be continued for sentinel lymph node mapping?*, Ann Nucl Med, 23(6), Aug 2009, pp. 507–510.

[286] A. SAFTOIU and P. VILMAN, *Endoscopic ultrasound elastography– a new imaging technique for the visualization of tissue elasticity distribution.*, J Gastrointestin Liver Dis, 15(2), Jun 2006, pp. 161–165.

[287] M. SAPOVAL, O. PELLERIN, J.-L. REHEL, N. HOUDOUX, G. RAHMOUNE, B. AUBERT, and I. FITTON, *Uterine Artery Embolization for Leiomyomata: Optimization of the Radiation Dose to the Patient Using a Flat-Panel Detector Angiographic Suite.*, Cardiovasc Intervent Radiol, Jan 2010.

[288] L. SARLI, N. PIETRA, F. CARRERAS, E. LONGINOTTI, and A. PERACCHIA, *[Laparoscopic cholecystectomy as evolution of traditional cholecystec- tomy. Comparative evaluation.]*, Acta Biomed Ateneo Parmense, 62(5-6), 1991, pp. 139–146.

[289] T. F. SATTEL, T. KNOPP, S. BIEDERER, and T. M. BUZUG, *Open Coil Arrangement for Interventional Magnetic Particle Imaging*, in Proceedings of the International Society for Magnetic Resonance in Medicine, vol. 18, Stockholm, Mai 2010, p. 945.

[290] F. SAUER, A. KHAMENE, and S. VOGT, *An Augmented Reality Navigation System with a Single-Camera Tracker: System Design and Needle Biopsy Phantom Trial*, in Medical Image Computing and Computer-Assisted Intervention – MICCAI 2002, 2002.

[291] O. SCHNELL, B. KREBS, J. CARLSEN, I. MIEDERER, C. GOETZ, R. H. GOLDBRUNNER, H.-J. WESTER, R. HAUBNER, G. POEPPERL, M. HOLTMANNSPOETTER, H. A. KRETZSCHMAR, H. KESSLER, J.-C. TONN, M. SCHWAIGER, and A. J. BEER, *Imaging of integrin alpha(v)beta(3) expression in patients with malignant glioma by [18F] Galacto-RGD positron emission tomography.*, Neuro Oncol, 11(6), Dec 2009, pp. 861–870.

[292] O. SCHOBER, G. J. MEYER, D. STOLKE, and H. HUNDESHAGEN, *Brain tumor imaging using C-11-labeled L-methionine and D-methionine.*, J Nucl Med, 26(1), Jan 1985, pp. 98–99.

[293] M. SCHOLZ, V. NOACK, I. PECHLIVANIS, M. ENGELHARDT, B. FRICKE, U. LINSTEDT, B. BRENDEL, D. ING, K. SCHMIEDER, H. ERMERT, and A. HARDERS, *Vibrography during tumor neurosurgery.*, J Ultrasound Med, 24(7), Jul 2005, pp. 985–992.

[294] M. SCHULDER, J. A. MALDJIAN, W. C. LIU, I. K. MUN, and P. W. CARMEL, *Functional MRI-guided surgery of intracranial tumors.*, Stereotact Funct Neurosurg, 68(1-4 Pt 1), 1997, pp. 98–105.

[295] S. SCHUMAN, G. WALKER, and E. AVISAR, *Processing Sentinel Nodes: When and How Many?*, in Cancer Research Meeting Abstract Supplement, vol. 69, December 2009, p. 1007.

[296] M. SCHWAIGER, M. KIECHLE, A. K. BUCK, A. SCHNELZER, S. PAEPKE, and K. HERRMANN, *Validierung von Freehand SPECT zur intraoperativen Darstellung von Waechterlymphknoten des Mammakarzinoms*, ethical votum, Klinikum rechts der Isar, Technische Universitaet Muenchen, January 2009.

[297] G. SCIBILIA and A. SOLURI, *Surgical Probe for laparoscopy or intracavitary tumor localization*, Tech. Rep. US 6,021,341, US Patent Office, Feb. 2000.

[298] S. M. SEIDLIN, L. D. MARINELLI, and E. OSHRY, *Radioactive iodine therapy; effect on functioning metastases of adenocarcinoma of the thyroid.*, J Am Med Assoc, 132(14), Dec 1946, pp. 838–847.

[299] S. M. SEIDLIN, E. OSHRY, and A. A. YALOW, *Twelve cases of metastatic thyroid carcinoma studied with radioactive iodine.*, J Clin Endocrinol Metab, 7(6), Jun 1947, p. 467.

[300] A. SEVER, S. JONES, K. COX, J. WEEKS, P. MILLS, and P. JONES, *Preoperative localization of sentinel lymph nodes using intradermal microbubbles and contrast-enhanced ultrasonography in patients with breast cancer.*, Br J Surg, 96(11), Nov 2009, pp. 1295–1299.

[301] R. SHAHIDI, M. R. BAX, C. R. J. MAURER, J. A. JOHNSON, E. P. WILKINSON, B. WANG, J. B. WEST, M. J. CITARDI, K. H. MANWARING, and R. KHADEM, *Implementation, Calibration and Accuracy Testing of an Image-Enhanced Endoscopy System*, IEEE Transactions on Medical Imaging, 21(12), 2002, pp. 1524–1535.

[302] R. R. SHAMIR, L. JOSKOWICZ, S. SPEKTOR, and Y. SHOSHAN, *Localization and registration accuracy in image guided neurosurgery: a clinical study.*, Int J Comput Assist Radiol Surg, 4(1), Jan 2009, pp. 45–52.

[303] C. J. J. M. SIKKINK, M. M. P. J. REIJNEN, and C. J. ZEEBREGTS, *The creation of the optimal dedicated endovascular suite.*, Eur J Vasc Endovasc Surg, 35(2), Feb 2008, pp. 198–204.

[304] S. D. SILVA, M. AGOSTINI, I. N. NISHIMOTO, R. D. COLETTA, F. A. ALVES, M. A. LOPES, L. P. KOWALSKI, and E. GRANER, *Expression of fatty acid synthase, ErbB2 and Ki-67 in head and neck squamous cell carcinoma. A clinicopathological study.*, Oral Oncol, 40(7), Aug 2004, pp. 688–696.

[305] A. K. SIOSTEEN and A. ELVIN, *Intra-operative uses of contrast-enhanced ultrasound*, Eur. Radiol., 14(8), October 2004, pp. 87–95.

[306] H. SITTEK, C. PERLET, K. HERRMANN, E. LINSMEIER, H. KOLEM, M. UNTCH, M. KESSLER, and M. REISER, *[MR mammography. Preoperative marking of non-palpable*

breast lesions with the Magnetom open at 0.2 T], Radiologe, 37(9), Sep 1997, pp. 685–691.

[307] N. SKUBAS, *Intraoperative Doppler tissue imaging is a valuable addition to cardiac anesthesiologists' armamentarium: a core review.*, Anesth Analg, 108(1), Jan 2009, pp. 48–66.

[308] B. SOENMEZ, H. ARBATLI, S. TANSAL, N. YAGAN, M. UNAL, E. DEMIRSOY, F. TUEKENMEZ, and O. YILMAZ, *Real-time patency control with thermal coronary angiography in 1401 coronary artery bypass grafting patients.*, Eur J Cardiothorac Surg, 24(6), Dec 2003, pp. 961–966.

[309] P. SOM, H. L. ATKINS, D. BANDOYPADHYAY, J. S. FOWLER, R. R. MACGREGOR, K. MATSUI, Z. H. OSTER, D. F. SACKER, C. Y. SHIUE, H. TURNER, C. N. WAN, A. P. WOLF, and S. V. ZABINSKI, *A fluorinated glucose analog, 2-fluoro-2-deoxy-D-glucose (F-18): nontoxic tracer for rapid tumor detection.*, J Nucl Med, 21(7), Jul 1980, pp. 670–675.

[310] L. M. W. K. SONG, D. G. ADLER, J. D. CONWAY, D. L. DIEHL, F. A. FARRAYE, S. V. KANTSEVOY, R. KWON, P. MAMULA, B. RODRIGUEZ, R. J. SHAH, W. M. TIERNEY, and A. S. G. E. T. COMMITTEE, *Narrow band imaging and multiband imaging.*, Gastrointest Endosc, 67(4), Apr 2008, pp. 581–589.

[311] M. SOUVATZOGLOU, A. L. GROSU, B. ROEPER, B. J. KRAUSE, R. BECK, G. REISCHL, M. PICCHIO, H.-J. MACHULLA, H.-J. WESTER, and M. PIERT, *Tumour hypoxia imaging with [18F]FAZA PET in head and neck cancer patients: a pilot study.*, Eur J Nucl Med Mol Imaging, 34(10), Oct 2007, pp. 1566–1575.

[312] U. SPECK, B. BEHRENS-STEINS, and P. BLASZKIEWICZ, *X- Ray Contrast Media. Overview, Use and Pharmaceutical Aspects*, Springer-Verlag GmbH, 3rd edition ed., December 1991.

[313] S. STAELENS, Y. D'ASSELER, S. VANDENBERGHE, M. KOOLE, I. LEMAHIEU, and R. V. DE WALLE, *A three-dimensional theoretical model incorporating spatial detection*

uncertainty in continuous detector PET., Phys Med Biol, 49(11), Jun 2004, pp. 2337–2350.

[314] K. SUGA, N. OGASAWARA, M. OKADA, and N. MATSUNAGA, *Interstitial CT lymphography-guided localization of breast sentinel lymph node: preliminary results.*, Surgery, 133(2), Feb 2003, pp. 170–179.

[315] K. SUGA, Y. YUAN, N. OGASAWARA, M. OKADA, and N. MATSUNAGA, *Localization of breast sentinel lymph nodes by MR lymphography with a conventional gadolinium contrast agent. Preliminary observations in dogs and humans.*, Acta Radiol, 44(1), Jan 2003, pp. 35–42.

[316] K. SUGA, Y. YUAN, M. OKADA, N. MATSUNAGA, A. TANGOKU, S. YAMAMOTO, and M. OKA, *Breast sentinel lymph node mapping at CT lymphography with iopamidol: preliminary experience.*, Radiology, 230(2), Feb 2004, pp. 543–552.

[317] D. SUN, M. BLOOMSTON, G. HINKLE, O. H. AL-SAIF, N. C. HALL, S. P. POVOSKI, M. W. ARNOLD, and E. W. MARTIN, *Radioimmunoguided surgery (RIGS), PET/CT image-guided surgery, and fluorescence image-guided surgery: past, present, and future.*, J Surg Oncol, 96(4), Sep 2007, pp. 297–308.

[318] J. V. SWINNEN, P. P. V. VELDHOVEN, L. TIMMERMANS, E. D. SCHRIJVER, K. BRUSSELMANS, F. VANDERHOYDONC, T. V. DE SANDE, H. HEEMERS, W. HEYNS, and G. VERHOEVEN, *Fatty acid synthase drives the synthesis of phospholipids partitioning into detergent-resistant membrane microdomains.*, Biochem Biophys Res Commun, 302(4), Mar 2003, pp. 898–903.

[319] M. D. SZETO, G. CHAKRABORTY, J. HADLEY, R. ROCKNE, M. MUZI, E. C. ALVORD, K. A. KROHN, A. M. SPENCE, and K. R. SWANSON, *Quantitative metrics of net proliferation and invasion link biological aggressiveness assessed by MRI with hypoxia assessed by FMISO-PET in newly diagnosed glioblastomas.*, Cancer Res, 69(10), May 2009, pp. 4502–4509.

[320] Y. TAJIMA, M. MURAKAMI, K. YAMAZAKI, Y. MASUDA, M. KATO, A. SATO, S. GOTO, K. OTSUKA, T. KATO, and M. KUSANO, *Sentinel Node Mapping Guided by*

Indocyanine Green Fluorescence Imaging During Laparoscopic Surgery in Gastric Cancer., Ann Surg Oncol, Feb 2010.

[321] Y. TAJIMA, K. YAMAZAKI, Y. MASUDA, M. KATO, D. YASUDA, T. AOKI, T. KATO, M. MURAKAMI, M. MIWA, and M. KUSANO, *Sentinel node mapping guided by indocyanine green fluorescence imaging in gastric cancer.*, Ann Surg, 249(1), Jan 2009, pp. 58–62.

[322] E. TANAKA, F. Y. CHEN, R. FLAUMENHAFT, G. J. GRAHAM, R. G. LAURENCE, and J. V. FRANGIONI, *Real-time assessment of cardiac perfusion, coronary angiography, and acute intravascular thrombi using dual-channel near-infrared fluorescence imaging.*, J Thorac Cardiovasc Surg, 138(1), Jul 2009, pp. 133–140.

[323] G. A. TAYLOR, N. SHEA, T. O'BRIEN, J. E. HALL, and S. T. TREVES, *Osteoid osteoma: localization by intraoperative magnification scintigraphy.*, Pediatr Radiol, 16(4), 1986, pp. 313–316.

[324] A. TESTORI, M. RASTRELLI, E. D. FIORI, J. SOTELDO, P. D. VIGNA, G. TRIFIRO, G. MAZZAROL, L. L. TRAVAINI, F. VERRECCHIA, E. L. RATTO, and M. BELLOMI, *Radio-guided ultrasound lymph node localization: feasibility of a new technique for localizing and excising nonpalpable lymph nodes ultrasound suspicious for melanoma metastases.*, Melanoma Res, 20(3), Jun 2010, pp. 197–202.

[325] A. TESTORI, G. L. D. SALVO, M. C. MONTESCO, G. TRIFIRO, S. MOCELLIN, G. LANDI, G. MACRIPO, P. CARCOFORO, G. RICOTTI, G. GIUDICE, F. PICCIOTTO, D. DONNER, F. D. FILIPPO, J. SOTELDO, D. CASARA, M. SCHIAVON, A. VECCHIATO, S. PASQUALI, F. BALDINI, G. MAZZAROL, C. R. ROSSI, and I. M. INTERGROUP, *Clinical considerations on sentinel node biopsy in melanoma from an Italian multicentric study on 1,313 patients (SOLISM-IMI).*, Ann Surg Oncol, 16(7), Jul 2009, pp. 2018–2027.

[326] G. THEMELIS, J. S. YOO, K.-S. SOH, R. SCHULZ, and V. NTZIACHRISTOS, *Real-time intraoperative fluorescence imaging system using light-absorption correction.*, J Biomed Opt, 14(6), 2009, p. 064012.

[327] T. THOMAS, R. SINGH, and K. RAGUNATH, *Trimodal imaging-assisted endoscopic mucosal resection of early Barrett's neoplasia.*, Surg Endosc, 23(7), Jul 2009, pp. 1609–1613.

[328] J. F. THOMPSON, *Clinical Practice Guidelines for the Management of Melanoma in Australia and New Zealand*, October 2008.

[329] H. TILLEY, *A Surgical Contretemps, illustrating the Value of Endoscopy.*, Proc R Soc Med, 11(Laryngol Sect), 1918, pp. 73–74.

[330] A. TODD-POKROPEK, *Non-circular orbits for the reduction of uniformity artefacts in SPECT.*, Phys Med Biol, 28(3), Mar 1983, pp. 309–313.

[331] Y. TOMITA, T. SHIOGAI, M. HARA, and I. SAITO, *[3D-transcranial Doppler–transcranial Doppler blood flow mapping system]*, Nippon Rinsho, 51 Suppl, Nov 1993, pp. 146–153.

[332] M. P. TORNAI, B. E. PATT, J. S. IWANCZYK, C. R. TULL, L. R. MACDONALD, and E. J. HOFFMAN, *A novel silicon array designed for intraoperative charged particle imaging.*, Med Phys, 29(11), Nov 2002, pp. 2529–2540.

[333] C. TRANTAKIS, J. MEIXENSBERGER, D. LINDNER, G. STRAUSS, G. GRUNST, A. SCHMIDTGEN, and S. ARNOLD, *Iterative neuronavigation using 3D ultrasound. A feasibility study.*, Neurol Res., 24(7), October 2002, pp. 666–670.

[334] J. TRAUB, J. MUCH, A. SCHNEIDER, F. PELTZ, H. HAUTMANN, and N. NAVAB, *User interface for electromagnetic navigated bronchoscopy*, in 5. Jahrestagung der Deutschen Gesellschaft fuer Computer-und Roboter-Assistierte Chirurgie (CURAC 2006), Hannover, Germany, Oktober 2006.

[335] J. TRAUB, P. STEFAN, S.-M. M. HEINING, C. R. TOBIAS SIELHORST, E. EULER, and N. NAVAB, *Hybrid navigation interface for orthopedic and trauma surgery*, in Proceedings of MICCAI 2006, ???, ed., LNCS, Copenhagen, Denmark, Oct. 2006, MICCAI Society, Springer, p. ???

[336] G. M. TREECE, A. H. GEE, R. W. PRAGER, C. J. C. CASH, and L. H. BERMAN, *High-definition freehand 3-D ultrasound.*, Ultrasound Med Biol, 29(4), Apr 2003, pp. 529–546.

[337] S. L. TROYAN, V. KIANZAD, S. L. GIBBS-STRAUSS, S. GIOUX, A. MATSUI, R. OKETOKOUN, L. NGO, A. KHAMENE, F. AZAR, and J. V. FRANGIONI, *The FLARE intraoperative near-infrared fluorescence imaging system: a first-in-human clinical trial in breast cancer sentinel lymph node mapping.*, Ann Surg Oncol, 16(10), Oct 2009, pp. 2943–2952.

[338] G. M. TSE, P.-H. TAN, A. L. M. PANG, A. P. Y. TANG, and H. S. CHEUNG, *Calcification in breast lesions: pathologists' perspective.*, J Clin Pathol, 61(2), Feb 2008, pp. 145–151.

[339] Y. TSUJINO, K. MIZUMOTO, Y. MATSUZAKA, H. NIIHARA, and E. MORITA, *Fluorescence navigation with indocyanine green for detecting sentinel nodes in extramammary Paget's disease and squamous cell carcinoma.*, J Dermatol, 36(2), Feb 2009, pp. 90–94.

[340] C. S. UBHI, J. G. HARDY, and C. A. PEGG, *Mediastinal parathyroid adenoma: a new method of localization.*, Br J Surg, 71(11), Nov 1984, pp. 859–860.

[341] R. A. VALDES-OLMOS, L. JANSEN, C. A. HOEFNAGEL, O. E. NIEWEG, S. H. MULLER, E. J. RUTGERS, and B. B. KROON, *Evaluation of mammary lymphoscintigraphy by a single intratumoral injection for sentinel node identification.*, J Nucl Med, 41(9), Sep 2000, pp. 1500–1506.

[342] J. R. VALVO, R. MADEB, R. GILBERT, C. NICHOLSON, G. OLEYOURRYK, S. PERRAPATO, A. RICOTTONE, W. ROBERTS, and L. EICHEL, *Policy guidelines suggested for robot-assisted prostatectomy*, J Robotic Surg, 1, July 2007, pp. 173–176.

[343] S. VANDENBERGHE, S. STAELENS, C. L. BYRNE, E. J. SOARES, I. LEMAHIEU, and S. J. GLICK, *Reconstruction of 2D PET data with Monte Carlo generated system matrix for generalized natural pixels.*, Phys Med Biol, 51(12), Jun 2006, pp. 3105–3125.

[344] S. D. VECCHIO and M. SALVATORE, *99mTc-MIBI in the evaluation of breast cancer biology.*, Eur J Nucl Med Mol Imaging, 31 Suppl 1, Jun 2004, pp. S88–S96.

[345] S. VERMA, A. RAJESH, J. J. FUETTERER, B. TURKBEY, T. W. J. SCHEENEN, Y. PANG, P. L. CHOYKE, and J. KURHANEWICZ, *Prostate MRI and 3D MR spectroscopy: how we do it.*, AJR Am J Roentgenol, 194(6), Jun 2010, pp. 1414–1426.

[346] L. VERMEEREN, W. MEINHARDT, A. BEX, H. G. VAN DER POEL, W. V. VOGEL, C. A. HOEFNAGEL, S. HORENBLAS, and R. A. V. OLMOS, *Paraaortic sentinel lymph nodes: toward optimal detection and intraoperative localization using SPECT/CT and intraoperative real-time imaging.*, J Nucl Med, 51(3), Mar 2010, pp. 376–382.

[347] L. VERMEEREN, R. A. V. OLMOS, W. MEINHARDT, A. BEX, H. G. VAN DER POEL, W. V. VOGEL, F. SIVRO, C. A. HOEFNAGEL, and S. HORENBLAS, *Intraoperative radioguidance with a portable gamma camera: a novel technique for laparoscopic sentinel node localisation in urological malignancies.*, Eur J Nucl Med Mol Imaging, 36(7), Jul 2009, pp. 1029–1036.

[348] U. VERONESI, *The new frontiers of surgical oncology*, in Proceedings of the Annual Meeting of the Italian Society of Surgical Oncology, P. Veronesi, P. P. Bianchi, G. Campanelli, A. Testori, and G. Giugliano, eds., vol. 1, Societa Italiana di Chirurgia Oncologica, Jun. 2010.

[349] S. VIDAL-SICART, P. PAREDES, G. ZANON, J. PAHISA, S. MARTINEZ-ROMAN, X. CAPARROS, A. VILALTA, R. RULL, and F. PONS, *Added value of intraoperative real-time imaging in searches for difficult-to-locate sentinel nodes.*, J Nucl Med, 51(8), Aug 2010, pp. 1219–1225.

[350] W. R. VOGLER and R. W. POWELL, *A clinical evaluation of thermography and heptyl adehyde in breast cancer detection.*, Cancer Res, 19(2), Feb 1959, pp. 207–209.

[351] G. K. VONSCHULTHESS and J. HENNIG, *Functional Imaging*, Lippincott Williams & Wilkins, March 1998.

[352] L. VOSS, *[A new method for puncture and marking of non-palpable breast-lesions (author's transl)]*, Rontgenblatter, 35(2), Feb 1982, pp. 54–57.

[353] R. H. WACHSBERG, *B-flow imaging of the hepatic vasculature: correlation with color Doppler sonography.*, AJR Am J Roentgenol, 188(6), Jun 2007, pp. W522–W533.

[354] A. M. WALLACE, C. K. HOH, S. J. ELLNER, D. D. DARRAH, G. SCHULTEIS, and D. R. VERA, *Lymphoseek: a molecular imaging agent for melanoma sentinel lymph node mapping.*, Ann Surg Oncol, 14(2), Feb 2007, pp. 913–921.

[355] J. WANG and J. CHUN, *Multiple IR target tracking in clutter environment using the Viterbi algorithm*, in Proc. SPIE Vol. 4130, p. 710-717, Infrared Technology and Applications XXVI, Bjorn F. Andresen; Gabor F. Fulop; Marija Strojnik; Eds., B. F. Andresen, G. F. Fulop, and M. Strojnik, eds., Dec. 2000, pp. 710–717.

[356] G. WEBER, *Enzymology of cancer cells (first of two parts).*, N Engl J Med, 296(9), Mar 1977, pp. 486–492.

[357] W. A. WEBER, H. J. WESTER, A. L. GROSU, M. HERZ, B. DZEWAS, H. J. FELDMANN, M. MOLLS, G. STOECKLIN, and M. SCHWAIGER, *O-(2-[18F]fluoroethyl)-L-tyrosine and L-[methyl-11C]methionine uptake in brain tumours: initial results of a comparative study.*, Eur J Nucl Med, 27(5), May 2000, pp. 542–549.

[358] I. WEINBERG, *Hand held camera with tomographic capability*, 9 2003.

[359] A. G. WEISENBERG, *Gamma-ray blind beta probe*, Tech. Rep. US 6,317,622, US Patent Office, Nov. 2001.

[360] P. WELLNER, W. MACKAY, and R. GOLD, *Computer augmented environments: Back to the real world*, Communications of the ACM, 36(7), July 1993, pp. 24–26.

[361] T. WENDLER, *Beta and Gamma Probe Reconstruction and Registration with PET/CT*, Master's thesis, Technische Universität München, Dec. 2006.

[362] T. WENDLER, A. HARTL, T. LASSER, J. TRAUB, F. DAGHIGHIAN, S. ZIEGLER, and N. NAVAB, *Towards intra-operative 3D nuclear imaging: reconstruction of 3D radioactive distributions using tracked gamma probes*, in International Conference on Medical Image Computing and Computer-Assisted Intervention (MICCAI), N. Ayache,

S. Ourselin, and A. Maeder, eds., vol. 4792 of LNCS, Brisbane, Australia, October 2007, MICCAI Society, Springer-Verlag Berlin Heidelberg, pp. 909–917.

[363] T. WENDLER, K. HERRMANN, A. SCHNELZER, T. LASSER, J. TRAUB, O. KUTTER, A. EHLERDING, K. SCHEIDHAUER, T. SCHUSTER, M. KIECHLE, M. SCHWAIGER, N. NAVAB, S. I. ZIEGLER, and A. K. BUCK, *First demonstration of 3-D lymphatic mapping in breast cancer using freehand SPECT.*, Eur J Nucl Med Mol Imaging, Mar 2010.

[364] T. WENDLER, J. TRAUB, S. ZIEGLER, and N. NAVAB, *Navigated three dimensional beta probe for optimal cancer resection*, in Proceedings of MICCAI 2006, ???, ed., no. ??? in LNCS ????, Copenhagen, Denmark, Oct. 2006, MICCAI Society, Springer, p. ???

[365] H. WENGENMAIR, J. KOPP, H. VOGT, and J. SCIUK, *Gammasonden zur intraoperativen Lokalisierung von radioaktiv markierten Waechterlymphknoten, Tumoren und Metastasen*, tech. rep., Klinikum Augsburg, 2006.

[366] M. N. WERNICK and J. N. AARSVOLD, *Emission Tomography: The Fundamentals of PET and SPECT*, Academic Press, 2004.

[367] H. P. WESKOTT, *Emerging roles for contrast-enhanced ultrasound.*, Clin Hemorheol Microcirc, 40(1), 2008, pp. 51–71.

[368] J. B. WEST and J. M. FITZPATRICK, *Fiducial Point Placement and the Accuracy of Point-based, Rigid Body Registration*, Neurosurgery, 48(4), April 2001.

[369] H.-J. WESTER, *Nuclear imaging probes: from bench to bedside.*, Clin Cancer Res, 13(12), Jun 2007, pp. 3470–3481.

[370] H. J. WESTER, M. HERZ, W. WEBER, P. HEISS, R. SENEKOWITSCH-SCHMIDTKE, M. SCHWAIGER, and G. STOECKLIN, *Synthesis and radiopharmacology of O-(2-[18F]fluoroethyl)-L-tyrosine for tumor imaging.*, J Nucl Med, 40(1), Jan 1999, pp. 205–212.

[371] N. WETZIG, J. KOLLIAS, N. PATHMANATHAN, S. PENDLEBURY, L. PENTLAND, S. ROVELLI, and R. UREN, *Recommendations for use of Sentinel node biopsy in early (operable) breast cancer*, June 2008.

[372] G. WIDHALM, S. WOLFSBERGER, G. MINCHEV, A. WOEHRER, M. KRSSAK, T. CZECH, D. PRAYER, S. ASENBAUM, J. A. HAINFELLNER, and E. KNOSP, *5-Aminolevulinic acid is a promising marker for detection of anaplastic foci in diffusely infiltrating gliomas with nonsignificant contrast enhancement.*, Cancer, 116(6), Mar 2010, pp. 1545–1552.

[373] J. E. WILDBERGER, A. H. MAHNKEN, A. M. SINHA, A. STARGARDT, P. HAAGE, S. SCHALLER, and R. W. GUENTHER, *[A differentiated approach to the diagnosis of pulmonary embolism and deep venous thrombosis using multi-slice CT]*, Rofo, 174(3), Mar 2002, pp. 301–307.

[374] K. C. WONG, S. M. KUMTA, G. E. ANTONIO, and L. F. TSE, *Image fusion for computer-assisted bone tumor surgery.*, Clin Orthop Relat Res, 466(10), Oct 2008, pp. 2533–2541.

[375] X. XU, *Workflow analysis for tumor resection procedures and evaluation of potential applications for radio-guided surgery*, tech. rep., Technische Universität München, Jan. 2008.

[376] G.-P. YAN, W. XU, L. YANG, L. LI, F. LIU, and Q.-Z. GUO, *Dextran Gadolinium Complexes as Contrast Agents for Magnetic Resonance Imaging to Sentinel Lymph Nodes.*, Pharm Res, Jun 2010.

[377] D. J. YANG, C.-G. KIM, N. R. SCHECHTER, A. AZHDARINIA, D.-F. YU, C.-S. OH, J. L. BRYANT, J.-J. WON, E. E. KIM, and D. A. PODOLOFF, *Imaging with 99mTc ECDG targeted at the multifunctional glucose transport system: feasibility study with rodents.*, Radiology, 226(2), Feb 2003, pp. 465–473.

[378] Z. YANIV and K. CLEARY, *Image-Guided Procedures: A Review*, tech. rep., Computer Aided Interventions and Medical Robotics, Imaging Science and Information

Systems Center, Department of Radiology, Georgetown University Medical Center, Washington, DC, 20007, USA, April 2006.

[379] K. YASUDA, S. NAKAJIMA, A. WAKAYAMA, S. OSHINO, S. KUBO, and T. YOSHIMINE, *Intraoperative three-dimensional reconstruction of power Doppler vascular images.*, Minim Invasive Neurosurg, 46(6), Dec 2003, pp. 323–326.

[380] S. YASUDA, H. MAKUUCHI, H. FUJII, H. NAKASAKI, M. MUKAI, S. SADAHIRO, T. TAJIMA, M. IDE, A. SHOHTSU, and Y. SUZUKI, *Evaluation of a surgical gamma probe for detection of 18F-FDG.*, Tokai J Exp Clin Med, 25(3), Oct 2000, pp. 93–99.

[381] T. YOSHIDA, M. MORI, Y. NIMURA, G. HIKITA, S. T. GISHI, K. NAKANISHI, and S. SATOMURA, *Analysis of heart motion with ultrasonic Doppler method and its clinical application.*, Am Heart J, 61, Jan 1961, pp. 61–75.

[382] S. YRJANA, J. KATISKO, R. OJALA, O. TERVONEN, H. SCHIFFBAUER, and J. KOIVUKANGAS, *Versatile intraoperative MRI in neurosurgery and radiology.*, Acta Neurochir (Wien), 144(3), March 2002, pp. 271–278.

[383] F. ZARACA, C. STRINGARI, J. A. EBNER, and H. EBNER, *Routine versus Selective Use of Intraoperative Angiography During Thromboembolectomy for Acute Lower Limb Ischemia: Analysis of Outcomes.*, Ann Vasc Surg, Apr 2010.

[384] M. A. ZAVERI, S. N. MERCHANT, and U. B. DESAI, *Tracking of multiple-point targets using multiple-model-based particle filtering in infrared image sequence*, Optical Engineering, 45, May 2006, pp. 6404–+.

[385] E. E. ZERVOS, D. C. DESAI, L. R. DEPALATIS, D. SOBLE, and E. E. MARTIN, *F18-Labeled Fluorodeoxyglucose Positron Emission Tomography-Guided Surgery for Recurrent Colorectal Cancer: A Feasibility Study*, Journal of Surgical Research, 97, March 2001, pp. 9—13.

[386] R.-Q. ZHENG, R. MAO, J. REN, E.-J. XU, M. LIAO, P. WANG, M.-Q. LU, Y. YANG, C.-J. CAI, and G.-H. CHEN, *Contrast-enhanced ultrasound for the evaluation of hepatic artery stenosis after liver transplantation: potential role in changing the clinical algorithm.*, Liver Transpl, 16(6), Jun 2010, pp. 729–735.

[387] H. ZHOU, K. LUBY-PHELPS, B. E. MICKEY, A. A. HABIB, R. P. MASON, and D. ZHAO, *Dynamic near-infrared optical imaging of 2-deoxyglucose uptake by intracranial glioma of athymic mice.*, PLoS One, 4(11), 2009, p. e8051.